TECHNISCHE UNIVERSITÄT MÜNCHEN

TUM School of Life Sciences

Targeted Chemoprofiling and Bioactivity Screening of Willow Bark

Kyriaki Antoniadou

Vollständiger Abdruck der von der TUM School of Life Sciences der Technischen Universität München zur Erlangung des akademischen Grades einer

Doktorin der Naturwissenschaften
(Dr. rer. nat.)

genehmigten Dissertation.

Vorsitzende: Prof. Dr. Mirjana Minceva

Prüfer der Dissertation:

1.   Prof. Dr. Thomas F. Hofmann
2.   Prof. Dr. Wilfried Schwab

Die Dissertation wurde am 26.09.2022 bei der Technischen Universität München eingereicht und durch die TUM School of Life Sciences am 15.01.2023 angenommen.

"Medicine to produce health must examine disease;

and music, to create harmony must investigate discord."

~ Plutarch

ACKNOWLEDGMENTS

PRELIMINARY REMARK

The practical work was conducted from December 2017 to March 2021 at the Chair of Food Chemistry and Molecular Sensory Science at the Technical University of Munich under the supervision of Prof. Dr. Thomas Hofmann as head of the chair until September 2019 followed by Prof. Dr. Corinna Dawid as acting head of the chair.

LIST OF PUBLICATIONS

The thesis was partially published in the following articles and poster:

Chemoprofiling as Breeding Tool for Pharmaceutical Use of *Salix*.

Nadja Förster, Kyriaki Antoniadou, Matthias Zander, Sebastian Baur, Verena Karolin Mittermeier-Kleßinger, Corinna Dawid, Christian Ulrichs, Inga Mewis. 2021. *Front. Plant Sci.* 12:579820. doi.org/10.3389/fpls.2021.579820

Comparative Anti-Inflammatory Effects of *Salix* Cortex Extracts and Acetylsalicylic Acid in SARS-CoV-2 Peptide and LPS-Activated Human *In Vitro* Systems.

Nguyen Phan Khoi Le, Corinna Herz, João Victor Dutra Gomes, Nadja Förster, Kyriaki Antoniadou, Verena Karolin Mittermeier-Kleßinger, Inga Mewis, Corinna Dawid, Christian Ulrichs, Evelyn Lamy. 2021. *Int. J. Mol. Sci.* 22(13), 6766. doi.org/10.3390/ijms22136766

Identification of Salicylates in Willow Bark (*Salix* Cortex) for Targeting Peripheral Inflammation.

Kyriaki Antoniadou, Corinna Herz, Nguyen Phan Khoi Le, Verena Karolin Mittermeier-Kleßinger, Nadja Förster, Matthias Zander, Christian Ulrichs, Inga Mewis, Thomas Hofmann, Corinna Dawid, Evelyn Lamy. 2021. *Int. J. Mol. Sci.* 22(20), 11138. doi.org/10.3390/ijms222011138

Targeted *Salix* Chemoprofiling for Improved Medicinal Potential of Willow Bark.

Kyriaki Antoniadou, Corinna Herz, Evelyn Lamy, Nadja Förster, Inga Mewis, Christian Ulrichs, Matthias Zander, Nicole Mähler, Philipp Peterburs, Corinna Dawid. 2020. Wiley 74 (S1), S1-013-S1-013. 71st regional conference (Regionalverbandstagung) Bayern, 9th and 10th of March 2020 in Würzburg. doi.org/10.1002/lemi.202051013

CONTENT

ABBREVIATION INDEX

Δε	molar ellipticity
µg	Microgram
µL	Microliter
µM	Micromolar
µmol/L	micromole per liter
A	Absorbance
ARE	antioxidant responsive element
BEH	ethylene bridged hybrid
CE	collision energy
^{13}C-NMR	carbon-13 nuclear magnetic resonance
COSY	homonuclear (^{1}H,^{1}H) correlation spectroscopy
cum	Cumulative
CXP	collision cell exit potential
Da	Dalton
DAD	diode array detector
DMSO	dimethyl sulfoxide
DP	declustering potential
DW	dry weight
e.g.	*exempli gratia*
ELSD	evaporative light scattering detector
et al.	*et alii* (and other)
ESI	electrospray ionization
FAB-MS	fast atom bombardment mass spectrometry
FW	fresh weight
g	Gram
h	hour(s)
H$_2$O	Water
HCO$_2$H	formic acid
^{1}H-NMR	proton nuclear magnetic resonance
HDMS	high-definition mass spectrometry
HPLC	high performance liquid chromatography
HSQC	heteronuclear single quantum coherence spectroscopy

ICAM-1	intercellular adhesion molecule-1
Inc.	incorporation
IR	Infrared
kPa	Kilopascal
L.	Carolus Linnaeus
LC	liquid chromatography
min	minute(s)
mL	Milliliter
mM	Millimolar
mQ H$_2$O	ultrapure water (milliQ)
MRM	multiple reaction monitoring
MS	mass spectrometer/spectrometry
N$_2$	Nitrogen
n/a	not available
NCBI	national center for biotechnology information
n.d.	not determined
ng	Nanogram
NMR	nuclear magnetic resonance spectroscopy
n.o.	not obtained
no.	Number
Nrf2	nuclear erythroid 2-related factor 2
NSAID	nonsteroidal anti-inflammatory drug
P.	*Populus*
p.a.	pro analysis (high purity)
PG	prostaglandin(s)
ppm	parts per million
psi	pound-force per square inch
rel.	Relative
rpm	rounds per minute
RT	room temperature
S.	*Salix*
sec	second(s)
SEM	scanning electron microscope
Si	Silica

SPE	solid-phase extraction
spp.	species *pluralis*
SRP	short rotation plantation
ssp.	Subspecies
t	Time
TIC	total ion chromatogram
TNF-α	tumor necrosis factor-alpha
ToF	time-of-flight
U	unit
UGT	uridine 5'-diphospho-glucuronosyltransferase
UHPLC	ultra-high-performance liquid chromatography
UPLC	ultra-performance chromatography
UV	ultraviolet light
UV/Vis	ultra-violet visible
V	Volt
Var.	variety
XIC	extracted ion chromatogram

Symbols

$\boldsymbol{\delta}$	chemical shift [ppm]
$\boldsymbol{m/z}$	mass-to-charge ratio
$\boldsymbol{J}$	coupling constant [Hz]
$\boldsymbol{\lambda}$	wavelength [nm]
°C	degree Celsius

1 INTRODUCTION

1.1 *Salix* L. genus

The *Salicaceae* family contains the genera *Populus* and *Salix* (Woodson, Schery, and D'Arcy 1978), with *Salix* being the largest of the family with about 450 species worldwide (Lauron-Moreau et al. 2015, Argus 1997, Chen et al. 2010). In particular, willows (*Salix* spp.) can be found all over the world, including Europe, America, Africa, and Asia with a higher variety of species located in China (Argus 1997).

In the book "The willows of middle and north Europe" by Lautenschlager-Fleury and Lautenschlager-Fleury (1994a), *Salix* species have been anatomically identified and described, such as *S. alba* and *S. fragilis* growing as floodplain forest trees, and *S. elaeagnos*, *S. purpurea*, *S. triandra*, *S. viminalis*, and *S. cinerea* as bushes. Moreover, *S. aurita*, *S. repens*, and *S. myrtilloides* are found between reed meadows and moor, and the small tree or bush *S. pentandra* near wet land and mountainous areas (Lautenschlager-Fleury and Lautenschlager-Fleury 1994a). For example, the bay-leaved *S. pentandra* plant grows rapidly on nutrient-rich fields and banks (Ruuhola and Julkunen-Tiitto 2003), and has a dark grey stem, longitudinally cracked bark, and yellow to red-brown and bald shoots, as characterized by Lautenschlager-Fleury and Lautenschlager-Fleury (1994b) (Table 1). Moreover, *S. pentandra* species have stored only low amount of water in the tissue and are cold-resistant (Junttila and Kaurin 1990, Kacperska and Kulesza 1987).

Figure 1: *S. pentandra* L. anatomy (modified from i-flora (n.d.)).

Salix species are dioecious (individuals with both sexes), zoophilous (mainly entomophilous) and anemophilous due to their inflorescence (Hou et al. 2015, Tollsten and Knudsen 1992), and can undergo cross-pollination, which results in natural hybridization (Kuzovkina and Volk 2009, Dötterl et al. 2014). Furthermore, *Salicaceae* plant pollination may be triggered also by wind, although this technique is more common in *Populus* flowers (Faegri and Van Der Pijl 2013, Woodson, Schery, and D'Arcy 1978).

Specifically, entomophily promotes pollination if volatile compounds of willow plants are present attracting various insects, e.g. bees, flies, moths, beetles, and butterflies (Füssel et al. 2007, Karrenberg, Kollmann, and Edwards 2002, Tollsten and Knudsen 1992, Totland and Sottocornola 2001, Vroege and Stelleman 1990). Phenolic glucosides from willow leaves are attractive for herbivores, providing stimulatory and inhibitory signals for food selection purposes (Tahvanainen, Julkunen-Tiitto, and Kettunen 1985). For instance, *Phratora vitellinae* L. larva have developed a defensive mechanism, surviving on the plants due to the salicin (**1**, Figure 2) digestion and formation of the volatile salicylaldehyde (**2**, Figure 2) by *β*-glucosidase in their glands, acting as a repellent (Pasteels et al. 1983, Ruuhola 2001). Moreover, salicin hydrolysis provides the larva with glucose, which is essential for larval growth and as energy reservoir (Pasteels et al. 1983, Rowell-Rahier and Pasteels 1986). Volatile aglycones, such as **2** and 6-hydroxycyclohexenone (**3**, Figure 2), are being

2

released when plant material is damaged, acting as a repellent by producing even more volatiles against insects (Paré and Tumlinson 1999, Reichardt et al. 1990).
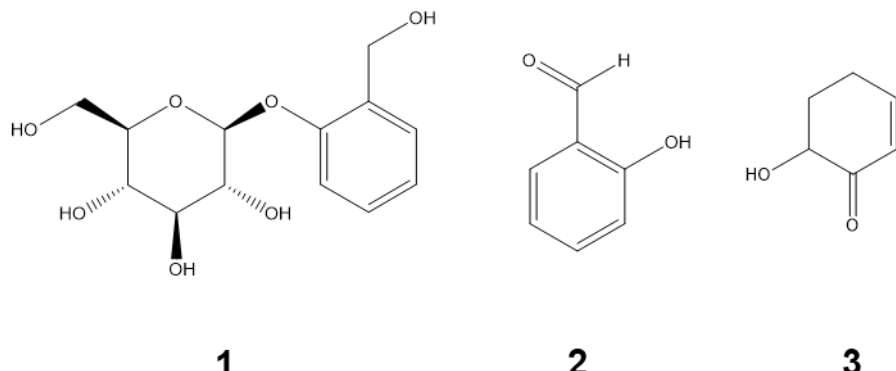
Figure 2: Chemical structures of salicin (**1**), salicylaldehyde (**2**), 6-hydroxycyclohexenone (6-HCH, **3**).

Thus, the relationship between *Salicaceae* plants and herbivores has shown that salicylates may act as defensive or feeding phytochemicals for some herbivores, however, also protect the plant itself from other insects (Ruuhola and Julkunen-Tiitto 2000). This plant defensive mechanism has a positive impact on the environmental (section 1.2) as well as pharmaceutical application (section 1.3) of *Salix.*

1.2 Environmental applications of *Salix* L.

Salix species contribute positively to fuel and fiber production by implementing environmental management, such as ecosystem restoration, phytoremediation, bioengineering, and biomass production due to the rapid tree growth without any need of soil condition optimization (Kuzovkina and Quigley 2005, Kuzovkina and Volk 2009, Palo 1984, Straškraba 1993). Furthermore, willow trees may even provide protection of the soil, and water or wind erosion, because of their strong root system (Hathaway and Penny 1975).

The fast-growing potential of *Salix* hardwoods has the advantage of using the woody part for renewable energy production, due to a higher biomass yield compared to *Populus* plants, and thus utilizing the plants for sustainable short-

rotation coppice (SRC) plantations (Aylott et al. 2008, Karp 2014, Lindegaard and Barker 1997, Dušek and Květ 2006). During the 20 year coppice cycle, the plant material is harvested, which can re-sprout, produce shoots, and after one to five years the stem can be chopped all over again (Fenning 2013, European Biomass Industry Association n.d.). The stem height and diameter, wood density, and bark concentration are important characteristics in order to acquire an increased biomass production (Kuzovkina and Volk 2009). The harvested biomass can be used in the heat and power production by converting wood chemical energy into renewable thermal energy (Table 3; Fellin et al. (2016)). Thus, in order to effectively produce energy, woody core (heartwood) is the preferred option compared to bark, due to a higher heating value preventing ash by-product and pollutant formation (Nosek, Holubcik, and Jandacka 2016, Shin 2014).
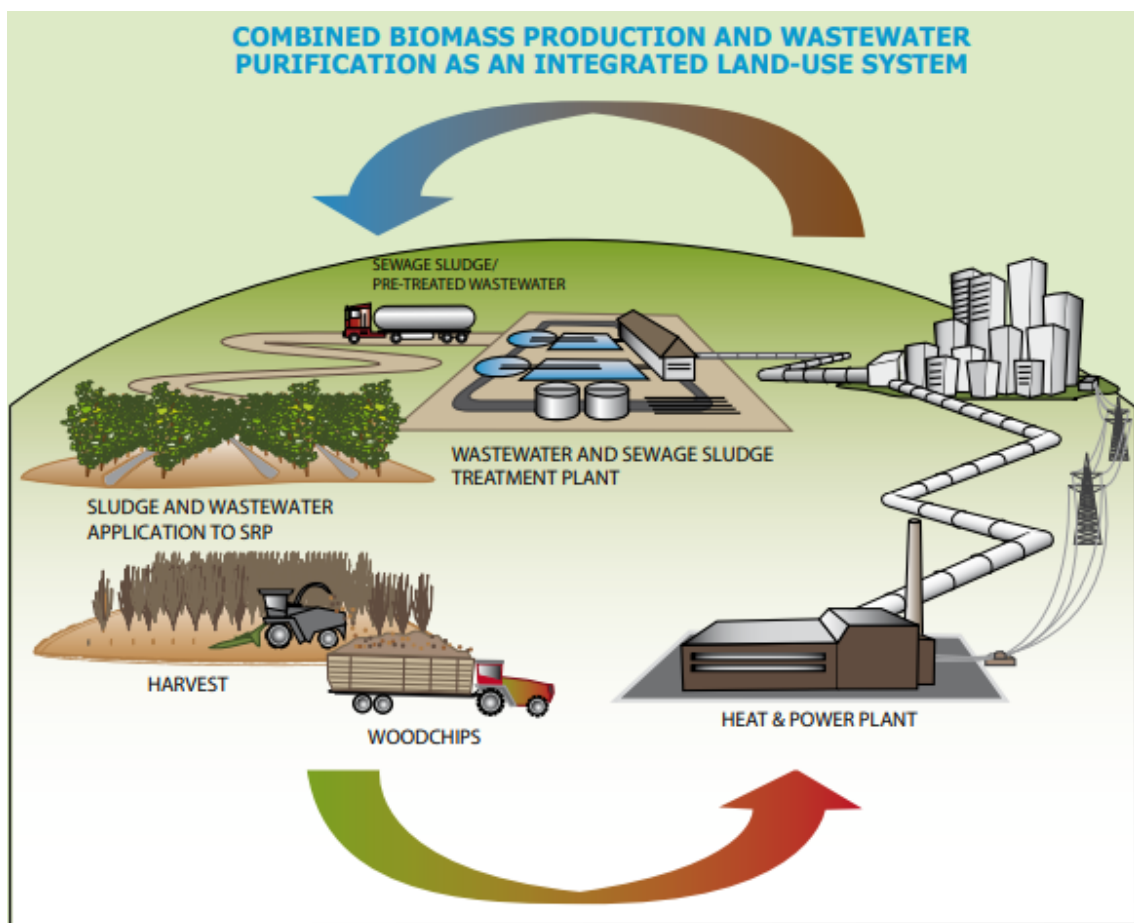
Figure 3: Short-rotation plantation (SRP) combining wastewater treatment with biomass production for energy production (acquired from European Biomass Industry Association (n.d.)).

Besides the important positive impact on the environment and ecosystem, it has to be ensured that *Salix* phytopharmaceutical production and food consumption

is safe and low in contaminants. For example, intense research showed that the concentration of the heavy metal cadmium was lower in the topsoil of SRC fields treated with or without sludge and/or ash than in the conventional annual crop of reference fields, whereas the chemical elements chromium, copper, nickel, lead, and zinc were contained in the same amounts in both fields (Dimitriou et al. 2012, Šyc et al. 2012). These analytes were investigated in *Salix* and other plants in order to highlight the need of further analysis of herbal medicinal drugs before consumption, ensuring limited amounts of heavy metals (Zeiner and Cindrić 2017). In a positive manner, accumulated contaminants in the plant system can be disposed by thermal processes, for example through a fluidized bed incineration (Šyc et al. 2012). Nevertheless, Mleczek et al. (2009) have postulated that *Salix* is not highly accumulative on heavy metals.

1.3 Pharmaceutical application of acetylsalicylic acid vs. *Salix* L.

Willows were used against inflammatory rheumatic disease, musculoskeletal joint pain, and fever since ancient times (Jack 1997, Mahdi 2010). Stone (1763) reported first clinical trials using the bitter tasting white willow bark, which successfully cured agues (malaria fever), however, its medicinal effect was never mentioned in any botanical book ever since then (Stone 1763, Vane 2000).

Later, in the 19th century, an antipyretic willow bark compound named "salicina" (salicin) was extracted from *S. alba* for the first time by two Italian pharmacists, Bartolommeo Rigatelli and Francesco Fontana (Marson and Pasero 2006, 2008, Rigatelli 1824). Piria (1838) converted salicin to *D*-glucose and saligenin by hydrolysis, and then to salicylic acid by oxidation for the first time in the 19th century (Figure 4). Later in the 1870s, patients with acute rheumatism were treated and cured with salicin (Maclagan 1876). In sections 1.3.1 and 1.3.2 it will be discussed in detail how the herbal medicinal plant heals inflammation and how acetylsalicylic acid (Aspirin[®]) was developed.
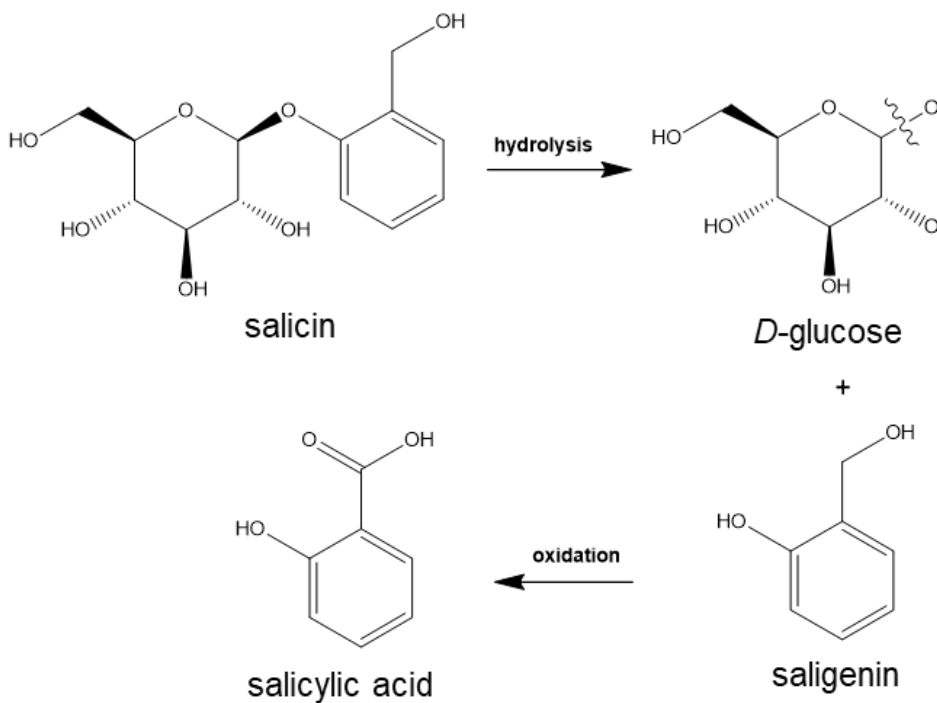
Figure 4: Salicin acid hydrolysis followed by oxidation of saligenin into salicylic acid (Klessig, Tian, and Choi 2016).

1.3.1 Acetylsalicylic acid

In the 19th century, salicin as a single compound had lost popularity due to gastritis side effect (Desborough and Keeling 2017), and salicylic acid was found to lead to irritations of the upper gastrointestinal tract, nausea, or tinnitus, which resulted in the development and production of an acetylated form of salicylic acid (acetylsalicylic acid), commercially named Aspirin® (Figure 5; Dempsey and Klessig (2017), Mahdi (2010), Sneader (2000)).
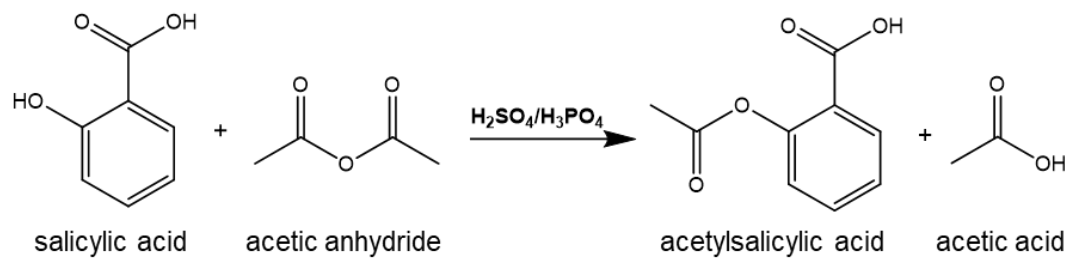
Figure 5: Acetylation reaction of salicylic acid into acetylsalicylic acid (Huremovic et al. 2016).

Acetylsalicylic acid has been investigated showing antithrombotic properties (Smith and Willis 1971) as well as preventive and anti-inflammatory effects against cardiovascular disease, colorectal cancer, and Alzheimer's disease (Ridker et al. 1997, Bosetti, Gallus, and La Vecchia 2002, Stewart et al. 1997).

Plasma membranes consist of phospholipids releasing arachidonic acid, a polyunsaturated fatty acid, which is responsible for the synthesis of prostaglandins by two cyclooxygenase isozymes (COX-1/COX-2; Figure 6; Ricciotti and FitzGerald (2011)). COX-1-derived prostaglandins can regulate homeostasis of the gastrointestinal tract and renal system (Morteau 2000, Vane and Botting 2003). However, upregulation of prostaglandins or disruption of homeostasis can lead to inflammation (e.g. rheumatoid- and osteoarthritis, fever, and pain; Adelizzi (1999), Vane and Botting (2003)). Thus, nonsteroidal anti-inflammatory drug (NSAID) Aspirin® can be administered, expressing a dose-dependent anionic drug character (Sheetz and Singer 1974, Sun et al. 2008) and inactivating irreversibly COX-1 activity by acetylating serine 530 of the prostaglandin-H_2 synthase, and acetylating COX-2 by releasing $15R$-hydroxy-eicosatetraenoic acid through enzymatic catalysis, which can act against platelet aggregation (Bala et al. 2008, Giménez-Bastida et al. 2019, Loll, Picot, and Garavito 1995).
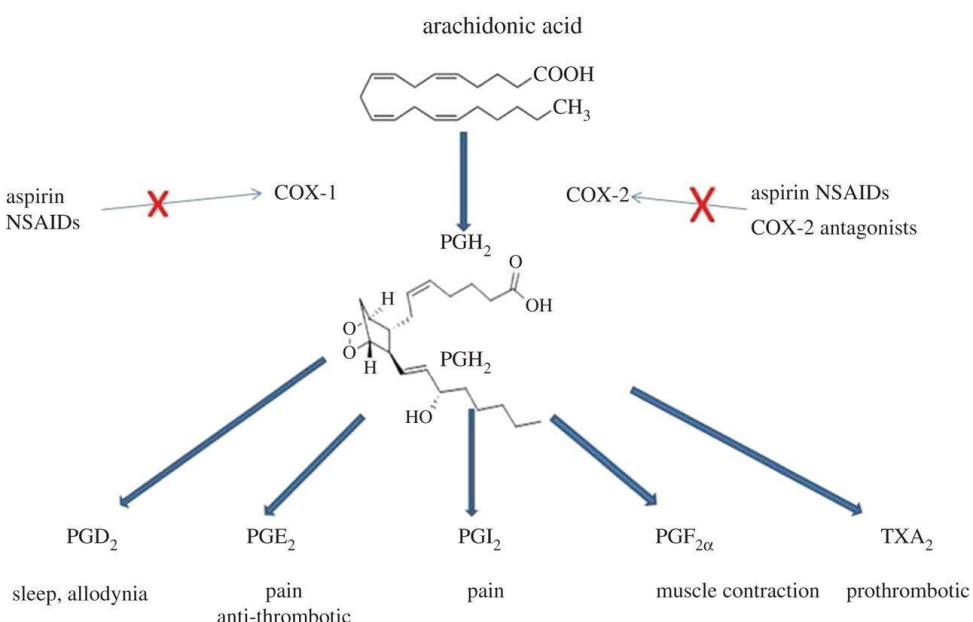
Figure 6: Synthesis of the prostaglandin PGH_2 by the COX-1 and COX-2 enzymes and production of metabolites, such as further prostaglandins (PG) and thromboxane (TX), and their contribution to sleep, allodynia, pain, anti-thrombotic and prothrombotic reactions, and muscle contraction (adopted from Wood (2015)).

However, COX-1 is an important enzyme for the generation of prostaglandins involved in various physiological functions, e.g. vascular homeostasis, gastric function, platelet activity renal function (Kam and See 2000). However, its action may be suppressed together with COX-2 by Aspirin®, leading to various side effects, such as gastrointestinal symptoms, mucosal damages and stomach ulcerations or even gastrointestinal bleeding if used for a longer period of time (Hawkey 2001, Huang et al. 2011, Flower 2003).

Nevertheless, comparative analysis of acetylsalicylic acid (Aspirin®) and *Salix* extracts conducted by Shara and Stohs (2015) showed less side effects of the plant based extract. Therefore, *Salix* as herbal medicinal plant was discussed further in section 1.3.2.

1.3.2 *Salix* L. as medicinal product

Standardized extract of willow bark (24% salicin) has a higher anti-inflammatory effect in comparison to acetylsalicylic acid as shown in an *in vivo* air pouch rat model (Khayyal et al. 2005). Thus, the advantages of *Salix* for medicinal purposes were described further.

In vitro tests by Fiebich and Appel (2003) exhibited the suppressive potential of bark extract against cytokines and prostaglandin E_2. Further, binding affinity studies investigating the docking score, which is used in drug development to analyze the interaction of the drugs with the relevant target, suggested that the anti-inflammatory potential may be triggered by the binding of the hydroxyl groups of salicin (-9.966 docking score) to COX-2, which docking score is higher than that of acetylsalicylic acid (-5.412 docking score) (Mahdi 2014). In particular, previous literature has already described some bioactive compounds (section 1.4), which can influence the bioactivity of *Salix*.

For the phytopharmaceutical production, *Salix* bark extracts are of high interest, making the plant breeding potential purposeful in relation to the bioenergy production, and compound isolation and analysis (Bubner et al. 2018). To obtain high concentrations of phenolic glucosides, such as salicylates, contained in *Salix* bark, it is important to examine various parameters, such as species, clone selection, and harvest time, which can influence the compound concentration in

the bark (Bubner et al. 2018, Förster et al. 2008). Thus, scaling up the extraction of natural plant compounds can have a prospective impact in pharmaceutical companies by producing herbal medicinal drugs (Ahmed et al. 2011, Förster et al. 2008).

Salicylates in willow bark may be administered orally, which follows absorption and hydrolysis of the compounds into salicin and further into saligenin, which is converted into salicylic acid upon oxidation (Figure 4) in the blood and liver (European Medicines Agency 2017b). Even though compounds, such as salicylates, flavonoids, and polyphenols are contained in the willow bark and may show anti-inflammatory effects, *Salix* extract as herbal medicinal product is standardized to salicin (Shara and Stohs 2015). *In vitro* studies using *Salix* against cytokine and PGE$_2$ release level, indicated that salicin and salicylic acid, contained in the plant, are not the only key compounds possessing an anti-inflammatory potential (Fiebich and Appel 2003).

In accordance to that, Knuth et al. (2011) performed additional *in vitro* experiments detecting catechol as the main bioactive metabolite derived from salicortin contained in willow bark extract which could explain the anti-inflammatory potential of salicylates after absorption and metabolization, in contrast to salicylic acid, saligenin, and salicin showing reduced or no bioactivity. Later *in vivo* studies on humans and rats, revealed that catechol sulphate is a main phase-II metabolite (Knuth et al. 2013). Indeed, it has been reviewed that catechol holding anti-inflammatory properties and acting neuroprotective, was stimulated by lipopolysaccharides (LPS) and showed reduction of cytokine and nitric oxide levels (Zheng et al. 2008). Previous reports by Ruuhola, Julkunen-Tiitto, and Vainiotalo (2003) on salicortin degradation revealed that salicylate hydrolysis in presence of alkaline conditions or esterases produces salicin and 2-hydroxy-3-cyclohexenone (2-HCH), which thereafter form saligenin by the action of *β*-glucosidase, and then catechol and *o*-quinone through oxidation, respectively.

Pharmacokinetics of salicin have shown that after oral administration and metabolization, salicylic acid was available in serum in the highest amounts (peak serum level: 1.2 mg/L) besides salicyluric acid and gentisic acid (Schmid, Kötter, and Heide 2001). However, additional human studies performed by Knuth et al.

(2013) could not detect salicyluric acid and gentisic acid in serum samples. In the same human studies, it has been proposed that salicylate metabolites, such as catechol and its conjugates, as well as salicylic acid, may play an important role in the anti-inflammatory potential of *Salix* bark extract (Knuth et al. 2013).

Further, research on the neuroprotective activity of salicylates, which structures were determined by 2D-NMR, was conducted using methanol extract (80%) of *S. glandulosa* twigs (Kim et al. 2015). Activity-guided fractionation showed that cochinchiside A (**4**), comprising a benzoyl group at position C3', had the highest neuroprotective bioactivity in comparison to acetylsalicortin (**5**), salicin (**1**), and tremulacin (**6**) (Figure 7), which consists of a benzoyl group at position C2' (Kim et al. 2015). Comparison between salicortin (**7**, Figure 7) and three acetylated compounds, 2'-*O*-, 3'-*O*-, and 6'-*O*-acetylsalicortin showed that non-acetylated **7** had the highest anti-inflammatory effect against nitric oxide with high neutrophine production (Kim et al. 2015). Similarly, inhibition of LPS-induced nitric oxide was the highest using **7** with an absent acetyl group among all tested compounds (Kim et al. 2015).
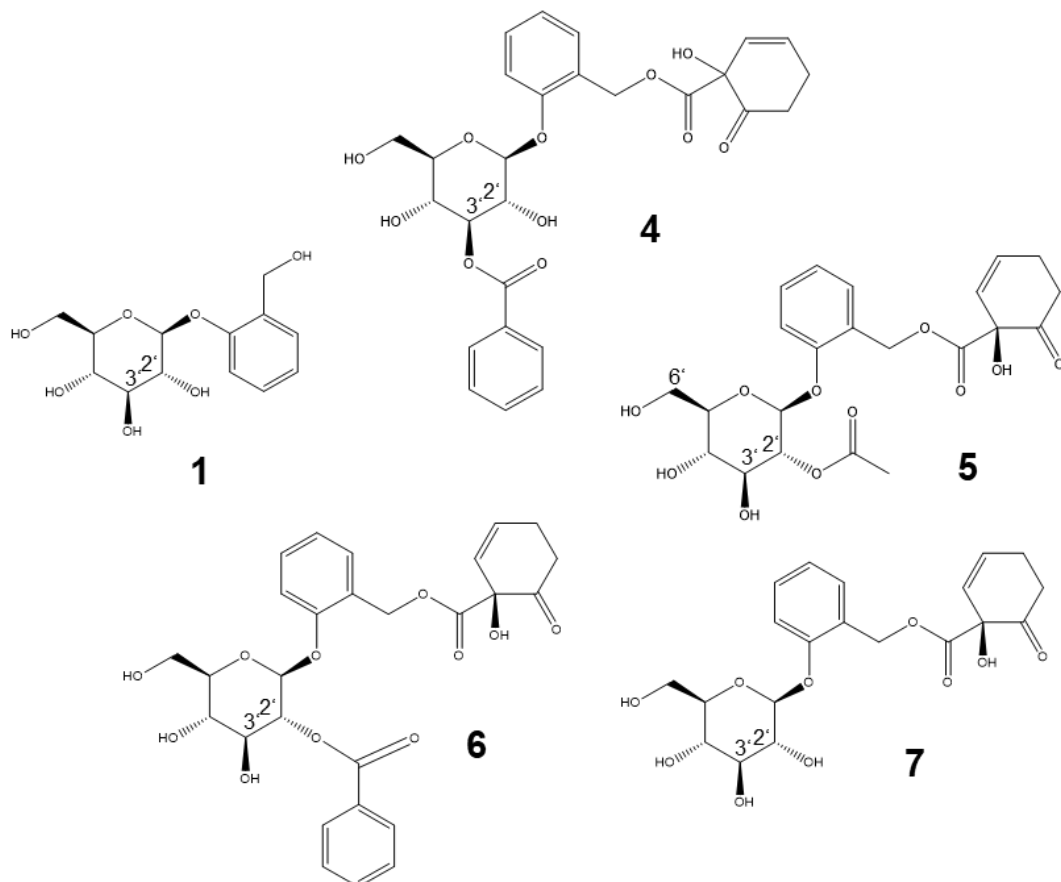
Figure 7: Chemical structures of salicin (**1**), cochinchiside A (**4**), 2'-O-acetylsalicortin (**5**), tremulacin (**6**), and salicortin (**7**).

Additionally, methanol extracts of leaves from *S. mucronate* were also analyzed upon their structure-activity relationship by Dissanayake et al. (2017), showing that **6**, **7**, **5**, and **1** act against lipidperoxidation (LPO; 56-86% at 5 µg/mL) and COX enzymes (22-75% at 25 µg/mL), with **5** being more antioxidative and **6** more anti-inflammatory in contrast to the other examined salicylates. Particularly, **1** showed the lowest activity among the four analyzed compounds (Dissanayake et al. 2017). For another salicylate, salidroside, neuropharmacological effects have been suggested in *in vitro* and *in vivo* experiments, showing bioactive properties against Alzheimer's, Parkinson's, and Huntington's disease, and depression, anxiety, stroke, traumatic brain injury, and epilepsy (Zhong et al. 2018).

Overall, previous studies showed that herbal anti-inflammatory products have a higher efficacy than placebo in treating rheumatic diseases, such as arthritis and back pain (Ernst and Chrubasik 2000). Specifically, 1,360 mg/day *Salix* bark intake in a duration of two weeks, showed relief against osteoarthritis (Schmid et al. 1998). In other studies, *S. alba* bark administration showed cure against low back pain (Chrubasik et al. 2000, Gagnier et al. 2007).

Besides the medicinal properties of willow bark, there are also applications in food supplement development, for instance, for sports performance or weight loss (Matyjaszczyk 2018). On the other side, *Salix* bark extract has been recognized as an active substance, which is an approved fungicide in arboriculture and viticulture (European Community (EC) No. 1107/2009; Deniau et al. (2019)).

Furthermore, pharmaceuticals need to be approved in order to be sold on the market. Approvals of herbal medicine, such as willow bark, is being done by the Committee on Herbal Medicinal Products (HMPC) part of the European Medicines Agency (EMA). The EMA has provided information regarding the use of *Salix* as herbal medicinal drug, and according to the HMPC it is safe and efficient as a medicinal product, having been used and being on the market for many years. Approval of *Salix* bark, belonging to the analgesics and antipyretics, must be submitted to the national authorities in any case of drug production according to the EMA. Particularly, in the herbal monograph of the European Union published by the EMA in 2017, whole or fragmented dried *Salix* bark is described as a "herbal medicinal product" in order to cure temporarily low back

pain, and as "traditional herbal medicinal product" against minor articular pain, fever with cold, and headache for long time use (European Medicines Agency 2017b). An orally administrated dosage of 393-1,572 mg/day of *Salix* bark, taken no longer than four weeks is recommended for analgesic and antipyretic effects, however, the corresponding content of **1** in *Salix* should not exceed 240 mg/day (European Medicines Agency 2017b).

In a risk assessment by the European Food Safety Authority (EFSA), it has been postulated that heavy metals (e.g. cadmium) and salicylate allergies may be taken under consideration when consuming willow bark (Matyjaszczyk 2018). For instance, cadmium can be toxic for kidney and bones if consumed in excess, thus the EFSA suggests a limited allowed concentration of 2.5 µg/kg body weight of weekly intake (Matyjaszczyk 2018). This limit has been published after toxicological studies by the Joint FAO/WHO Expert Committee on Food Additives (JECFA) in 2010 and the Panel on Contaminants in the Food Chain of the European Food Safety Authority (CONTAM Panel), which is valid until today (Matyjaszczyk 2018). However, further toxicological studies upon *Salix* as herbal medical product are needed. Moreover, the accountability of salicylates from *Salix* bark possessing pharmacological properties needs further investigation according to a review by the United states Pharmacopeia (USP) published in 2019 (Oketch-Rabah et al. 2019).

1.4 *Salicaceae* compounds

Salix extracts have an economic impact in the food, nutraceutical, pharmaceutical, and cosmetic industry, besides their use in bioenergy production and other environmental applications (Ramos et al. 2019). A lot of studies over the years have focused on the pharmaceutical potential of *S. alba*, however, there are many more *Salix* species and crosses which need to be analyzed further (Karp 2014). In addition to some objective usages of the woody plant in Stone Age, the medicinal effects were widely known in the past, such as for treating osteoarthritis or dental decay (Reinhard, Hamilton, and Hevly 1991, Kuzovkina and Quigley 2005).

As described in section 1.3.2, willow bark is highly effective for use in herbal drug production. The inner and outer *Salix* bark compartments are different upon their

phytochemical composition, e.g. there is a higher content of ash extracts and polysaccharides in the inner bark, and lignin and phenolic compounds in the outer bark (Dou et al. 2016, Sjöström 1981). Compounds like waxes, fatty acids, terpenes, flavonoids, and lignans are higher concentrated in the willow bark, which also contains condensed tannins and suberin in comparison to heartwood content (Dou et al. 2016, Hon and Shiraishi 2000). Further, it is suggested that flavonoid biosynthesis starts in the cambium of the willow stem (Figure 8) and the cork cambium, from where single natural compounds are transported to the heartwood and outer bark, respectively (Hergert and Goldschmid 1958, Todd and Robinson 1956).
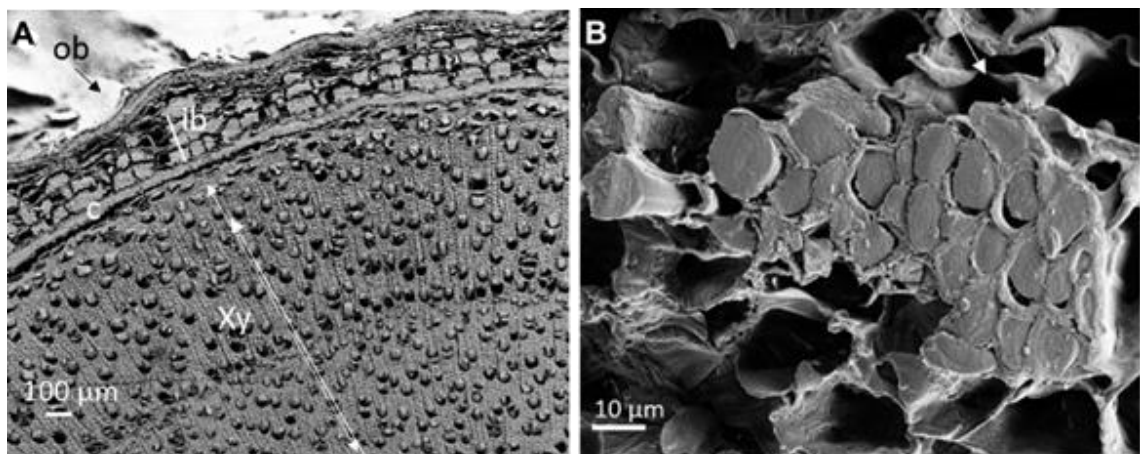
Figure 8: Willow bark morphology depicted in SEM images showing the (A) cross section of a willow stem (Xy: xylem, ib: inner bark, ob: outer bark, c: cambium), and (B) several bast cells forming a single sclerenchyma bundle (modified from Dou et al. (2016)).

After comparison of various *Salix* species and their compound composition, it was assumed that the phytochemicals differ between plant tissues and species (Julkunen-Tiitto 1985a). Thus, plant secondary metabolites could be found in high amounts in the *Salicaceae* family, which act against pathogens and play an important role as effective signal compounds (Pei and McCracken 2005). Moreover, female willow plants are producing seeds and the male pollen, and both expressing different compound composition (Lloyd and Webb 1977, Hou et al. 2017). The different phytochemicals and their content depends also on the plant genetics and soil fertilization, as well as on environmental factors (Bryant, Reichardt, and Clausen 1992, Nichols-Orians, Fritz, and Clausen 1993, Orians et al. 2003).

1.4.1 *Salix* phytochemicals

In the current section, phytochemicals identified in *Salicaceae* plants will be reviewed, which are also the focus of the present work and have been reported to have potential pharmacological properties. In the study of Pearl and Darling (1968) the *P. balsamifera* tree was analyzed, belonging to the *Salicaceae* family and showing a diversity of compounds and higher concentrations of salicin (**1**) in the twig bark (0.33%) than in the trunk bark (0.05%). Further investigation of three salicylates in clones of *S. myrsinifolia* twigs showed high abundance of salicortin (mean 9.98 mg/g DW; **7**, Figure 9), followed by HCH-salicortin (mean 3.81 mg/g DW, **8**) and **1** (mean 1.74 mg/g DW) (Heiska et al. 2007). Previous gas chromatographic analysis of methanol (50%) extracts of leaves of the same species, also detected **1** and **7** (Figure 9; Julkunen-Tiitto (1985b)). In general, phenolic and alcohol groups of compounds belonging to the *Salicaceae* plants are commonly attached to the *O*-glycoside moiety (Julkunen-Tiitto 1985a).

Furthermore, Tahvanainen, Julkunen-Tiitto, and Kettunen (1985) analyzed leaves from eight willow species, showing that among them, *S. nigricans* (51.106 mg/g DW), *S. dasyclados* (12.112 mg/g DW), *S. triandra* (7.845 mg/g DW), and *S.* cv. *aquatica* (7.825 mg/g DW) had the highest phenolic glucoside (**1**, **7**, fragilin (**9**, Figure 9), triandrin, salidroside, picein, and unknowns) concentrations, followed by *S. pentandra* (7.559 mg/g DW), *S. phylicifolia* (1.792 mg/g DW), *S. caprea* (1.221 mg/g DW) and *S. viminalis* (1.527 mg/g DW) with lower amounts. *Salix* leaves from various species were examined also by Binns, Blunden, and Woods (1968) using the two-way thin-layer chromatography (TLC) method. Particularly, *S. pentandra* var. Lumley contained besides cyanidin, also **1**, **7**, salidroside, **9**, tremuloidin, vimalin, and grandidentatin, however, the identification of triandrin and populin was uncertain (Binns, Blunden, and Woods 1968). Later, leaves of the same species were analyzed once again, containing (non-)acetylated salicylates, such as **1**, **7**, diglucoside salicin (**10**), 2'-*O*-acetyl-salicin (**11**), 2'-*O*-acetylsalicortin (**5**), lasiandrin (**13**), 2',6'-*O*-diacetylsalicortin (**12**), tremulacin (**6**) (Figure 9), and a salicortin derivative (named salicortin-2), which were confirmed by HPLC/API-ES (atmospheric pressure ionization-electrospray) mass spectrometer in the positive ionization mode (Ruuhola and Julkunen-Tiitto 2003, Ruuhola, Julkunen-Tiitto, and Vainiotalo 2003).

glucose   hydroxy cyclohexenonoyl   benzoyl group   acetyl group
(HCH)

1: R_1, R_2, R_3, R_4 = H
5: R_1, R_2 = H, R_3 = acetyl group, R_4 = HCH
6: R_1, R_2 = H, R_3 = benzyl group, R_4 = HCH
7: R_1, R_2, R_3 = H, R_4 = HCH
8: R_1 = HCH, R_2, R_3 = H, R_4 = HCH
9: R_1 = acetyl group, R_2, R_3, R_4 = H
10: R_1, R_2, R_3 = H, R_4 = glucose
11: R_1, R_2, R_4 = H, R_3 = acetyl group
12: R_1, R_3 = acetyl group, R_2 = H, R_4 = HCH
13: R_1, R_4 = HCH, R_2 = H, R_3 = acetyl group
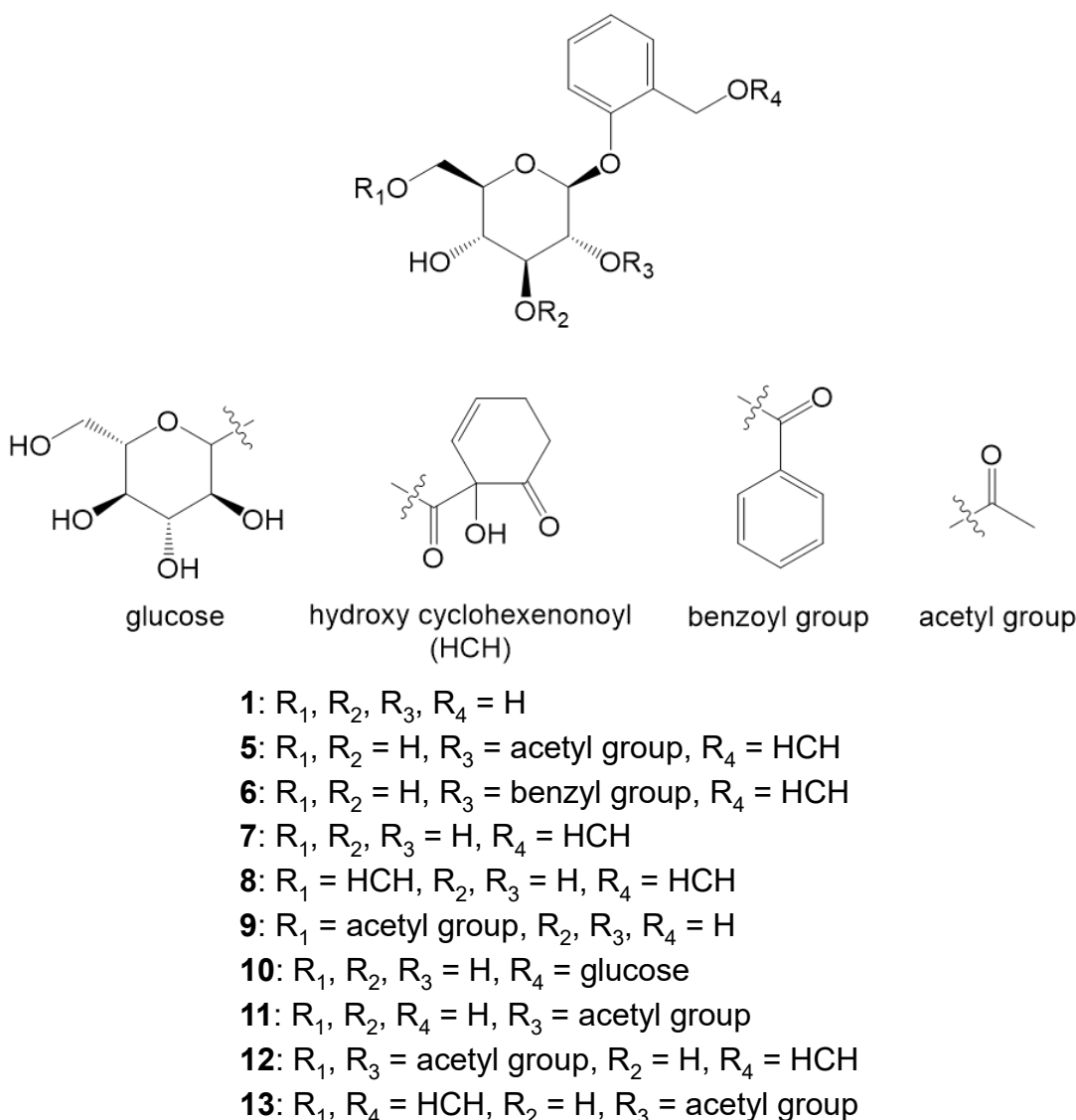
Figure 9: Chemical structures of selected salicylates: salicin (**1**), 2'-*O*-acetylsalicortin (**5**), tremulacin (**6**), salicortin (**7**), HCH-salicortin (**8**), fragilin (6'-*O*-acetylsalicin) (**9**), diglucoside salicin (**10**), 2'-O-acetylsalicin (**11**), 2',6'-*O*-diacetylsalicortin (**12**), and lasiandrin (**13**).

Moreover, with the same technique, salicylates **1**, **6**, **7**, and tremuloidin, as well as flavanones like naringenin-7-glucoside (prunin), and eriodictyol-7-glucoside, flavones such as apigenin-7-glucoside, luteolin, and three luteolin-glucosides were identified in the methanol extract of *S. purpurea* leaves (Julkunen-Tiitto and Sorsa 2001). For the salicylates, like **6**, **7**, and **8** isolated from *P. trichocarpa* × *deltoides* Beaupré leaves there was additional data available confirming their absolute configuration by circular dichroism (CD) spectroscopy and NMR (Feistel et al. 2015). Despite the identification of **8** in *Populus* species, such as in *P. tremula* (Keefover-Ring et al. 2014), there is no NMR data available. In *P. tremula* leaves, compounds like 2'-*O*-cinnamoylsalicortin, **5**, **11**,

acetyltremulacin, and salicyloylsalicin could be detected by means of UHPLC-ToF-MS (ESI⁻) (Abreu et al. 2011, Keefover-Ring, Carlsson, and Albrectsen 2014). Acetyltremulacin extracted with 50% methanol from leaves of *S. pentandra*, was also tentatively detected by means of HPLC/API-ES mass spectrometry (Ruuhola, Julkunen-Tiitto, and Vainiotalo 2003).

Additionally, **5**, **11**, and **13** were found in leaves and twigs of *S. lasiandra*, and structure determination was performed by NMR (Reichardt et al. 1992). Moreover, compound **9** was postulated for the first time in the bark of *S. fragilis* (Thieme 1964). Later, Thieme (1971), Tahvanainen, Julkunen-Tiitto, and Kettunen (1985), and Julkunen-Tiitto (1985a) detected salidroside in the same plant, which is suggested that it provides plant resistance.

Further analysis applying spectroscopic techniques for their detection, e.g. UV, IR, FAB-MS, and NMR showed that bark of *S. pentandra* contains salicylates, like **1**, **7**, **11**, and **5**, and flavonoids, such as grandidentatin, triandrin, and ampelopsin (Shao et al. 1989). Quantitative analysis has been performed on three different *Salix* clones, showing high amounts of **7** in *S. purpurea* and *S. daphnoides*, and of **5** in *S. pentandra* among various other available compounds (Förster et al. 2009). Investigations using mass spectrometry and NMR analysis, showed that the compound purpurein was available in *S. purpurea* bark material (Pearl and Darling 1970b). Additionally, populoside, salireposide, grandidentoside, and grandidentatin were isolated from *P. grandidentata* bark and identified by Erickson, Pearl, and Darling (1970). In the same year Pearl and Darling (1970a) postulated compounds, such as **1**, **7**, salicyloylsalicin, salicyloylsalicin-2-benzoate, salireposide, naringenin, purpurein, (+)-catechin, isoquercitrin, naringenin, naringenin-5-*β-D*-glucoside, and isosalipurposide, which were isolated from ethanolic extract of *S. purpurea* bark through fractionation on a polyamide column and were characterized by TLC.

Kammerer et al. (2005) investigated *S. daphnoides* methanol bark extract, applying triple quadrupole mass spectrometry (ESI negative) and phytochemical identification of saligenin, salicylic acid, **1**, isosalicin, picein, salidroside, triandrin, salicoylsalicin, **7**, isosalipurposide, salipurposide, naringenin-7-*O*-glucoside (prunin), and **6** was performed by comparison to reference compounds. Further, from *S. koriyanagi* stem, salicin-7-sulfate was purified by means of HPLC equipped with a C₁₈ column and was identified by means of LC-MS and NMR

techniques (Noleto-Dias et al. 2018). Moreover, an anti-adipogenic ethyl acetate fraction was isolated from a methanol (80%) extract of *S. pseudo-lasiogyne* twig resulting in the identification of **5**, **12**, 3'-*O*-acetylsalicortin, 6'-*O*-acetylsalicortin, and **7**, and in the detection of also non-adipogenic compounds, like 3'-*O*-acetylsalicin, **11**, **1**, 2'-*O*-(*E*)-coumaroylsalicortin, grandidentatin, and saligenin by means of NMR (Lee et al. 2013, Yang et al. 2013). Other studies were employed on ethanolic (70%) extract of *S. alba* bark, tentatively identifying several compounds, such as salicylic acid, **1**, salidroside, saligenin, tremuloidin, salicoylsalicin, **6**, and **7**, by means of UHPLC-ESI$^-$ mass spectrometry (Maistro et al. 2019).

Further, compound variety and concentration was investigated in respect to the seasonal *Salix* plant growth. General observations done by Förster et al. (2009), showed a total salicylate content increase of 32.5, 72.2, and 72.5% in *S. pentandra*, *S. daphnoides*, and *S. purpurea*, respectively, through the months August to October. However, specifically for *S. pentandra,* **11** and **5** content reduced throughout March to June, whereas the concentration of **5** increased from June to July, and high contents of **1** and **7** were detectable between March and June, but **7** was less available during the months of June and July (Förster et al. 2008).

However, even though many phytochemicals were detected in *Salix* species and clones, there is still need for further structure elucidation by means of 1D/2D-NMR experiments, and identification of unknown and novel compounds in the plants with medicinal properties. Moreover, most compounds in the literature have been identified merely by means of LC-MS analysis and studies have hardly provided any valuable bioactivity results of the phytochemicals. An overview of previously described salicylates in *Salicaceae* plants is shown in Table 1 and some of their representative chemical structures are depicted in Figure 9.

Table 1: Overview of salicylates extracted from *Salix* and *Populus* plants and identified by LC-MS and/or NMR analysis.

salicylates	related literature
salicin (**1**) 3'-*O*-acetylsalicortin 6'-*O*-acetylsalicortin	Kim et al. (2015), Yang et al. (2013)
salicortin (**7**)	Feistel et al. (2015), Kim et al. (2015), Reichardt et al. (1992)
2'-*O*-acetylsalicin (**11**) 2'-*O*-acetylsalicortin (**5**) fragilin (6'-*O*-acetylsalicin, **9**)	Kim et al. (2015), Reichardt et al. (1992), Yang et al. (2013)
lasiandrin (**13**)	Reichardt et al. (1992), Ruuhola and Julkunen-Tiitto (2003)
tremulacin (**6**) HCH-salicortin (**8**)	Feistel et al. (2015)
tremuloidin	Kim et al. (2015)
populin (salicin-6'-benzoate)	Kumari, Upadhyay, and Khosla (2016)
2'-*O*-cinnamoyl-salicortin	Keefover-Ring et al. (2014), Yang et al. (2013)
salicin-7-sulfate	Noleto-Dias et al. (2018)
2',6'-*O*-diacetylsalicortin (**12**)	Yang et al. (2013)

1.4.2 Biosynthesis of salicylates

Salicylates have been previously described as salicylic acid salts and esters by Ekinci, Şentürk, and Küfrevioğlu (2011), which are mainly known as phenolic glucosides. Even though the term salicylates is mentioned as such in some publications, there are also others that use the word 'salicinoids' to describe this group of phenolic glucosides highly abundant in *Salicaceae* plants (Feistel et al. 2018, Häikiö et al. 2009, Keefover-Ring et al. 2014). Further, the term 'salicylates' has been used by Feistel et al. (2018), referring to salicyl alcohol (saligenin) derivatives.

There are various biosynthetic pathways of salicylates discussed in the literature. According to Ruuhola (2001), salicylate metabolization of salicin ester compounds, such as tremuloidin, tremulacin (**6**), salicortin (**7**), 2'-*O*-acetylsalicortin (**5**), 2'-*O*-acetylsalicin (**11**), and diglucoside salicin (**10**) revealed salicin (**1**) as the main precursor and degradation product (Figure 10).
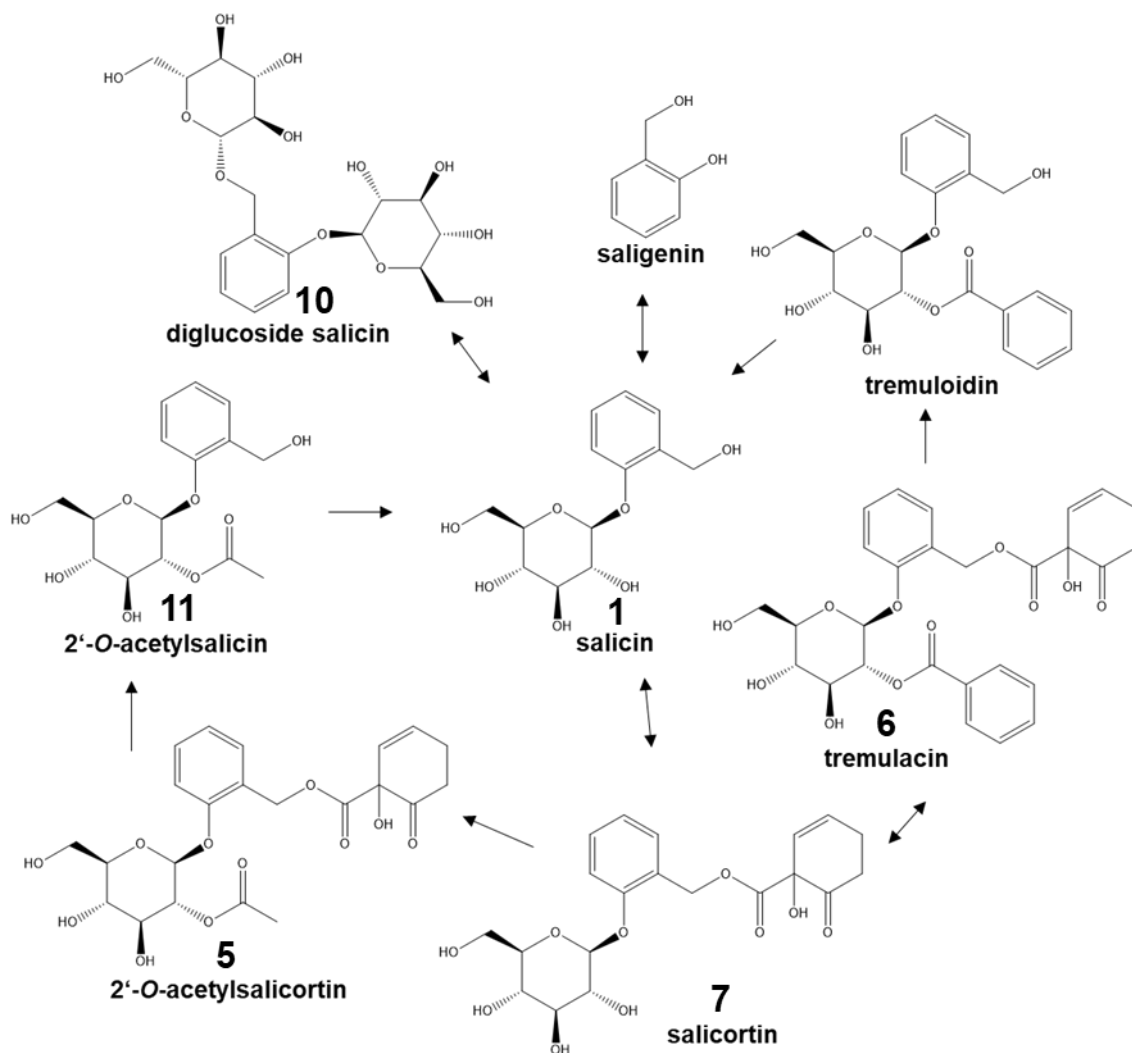
Figure 10: Salicylate metabolic grid (modified from Ruuhola (2001)). Salicin (**1**) is the main precursor or degradation compound of tremuloidin, tremulacin (**6**), salicortin (**7**), 2'-*O*-acetylsalicortin (**5**), 2'-*O*-acetylsalicin (**11**), and diglucoside salicin (**10**).

These salicylates are formed through the shikimate and phenylalanine or isochorismate biosynthetic pathway (Figure 11; Lefevere, Bauters, and Gheysen (2020), Ruuhola and Julkunen-Tiitto (2000)). According to this pathway, **1** is synthesized in *Populus* and *Salix* plants through deamination, *ortho*-hydroxylation, *β*-oxidation, C2 unit elimination and glycosylation (Figure 11; Mahdi (2014)). Salicylates have the potential to be soluble in water and thus allowing their storage in plant cell vacuoles, which provides them with natural protection against esterases and *β*-glucosidases (Ruuhola 2001).
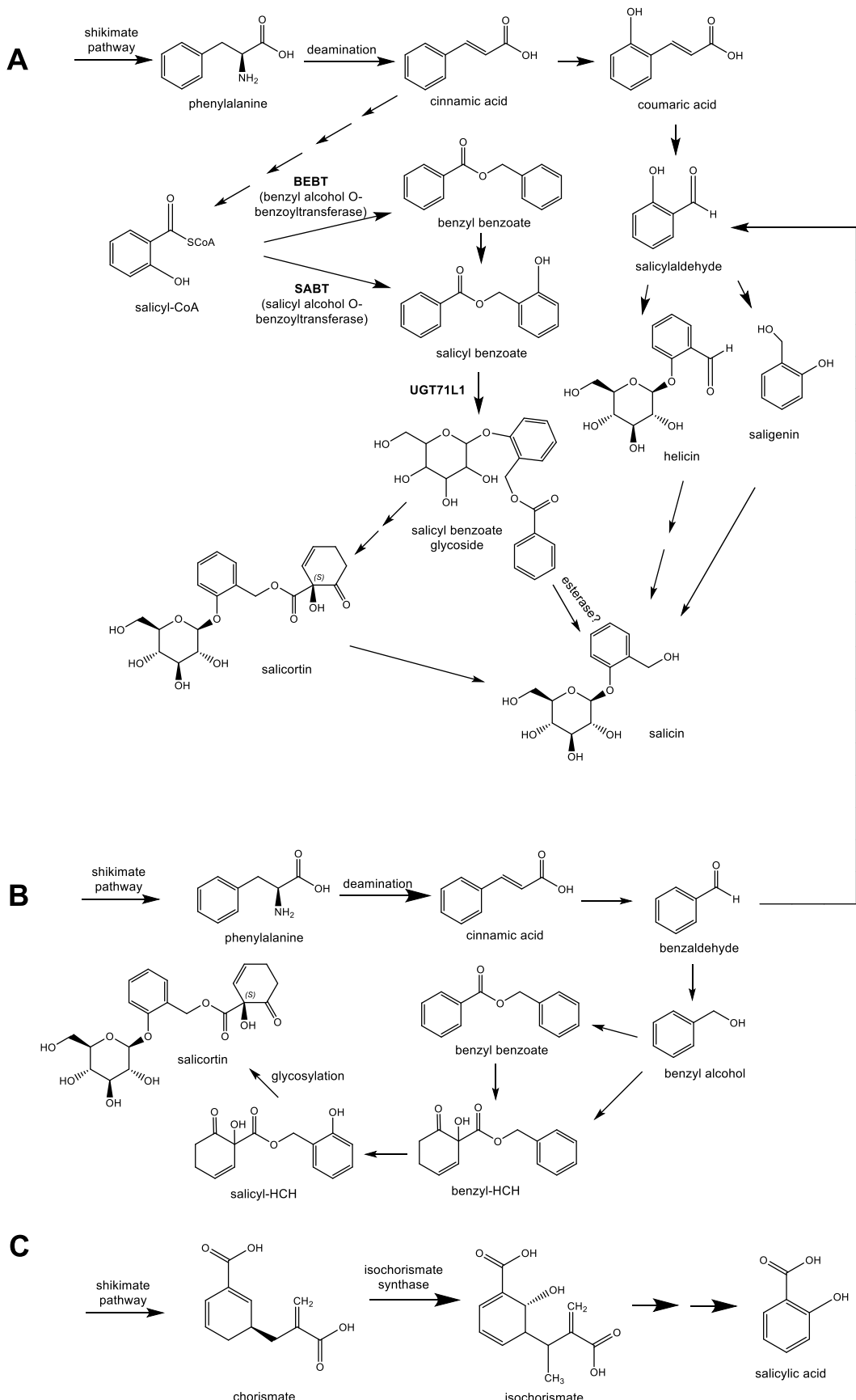
Figure 11: Proposed phenylalanine and isochorismate biosynthetic pathway of salicylates (modified from Babst, Harding, and Tsai (2010), Fellenberg et al. (2020), Lefevere, Bauters, and Gheysen (2020)). Proposed **(A)** salicyl and benzoate pathway, **(B)** benzoate pathway, and **(C)** new direct synthesis of salicylic acid from isochorismate.

Furthermore, **1** is suggested as a possible precursor of some known salicylates (Babst, Harding, and Tsai 2010, Ruuhola, Julkunen-Tiitto, and Vainiotalo 2003). This compound can bind to sugar moieties and organic acids forming further salicylate compounds, such as the acetyl or 1-hydroxy-6-oxo-2-cyclohexene-1-carboxylic acid (HCH; **14**; Figure 12) residues, which is a precursor of *o*-quinone (**16**, Figure 12) (Feistel 2018, Feistel et al. 2018).

In addition, the term 'salicylates' has been also used to describe salicylic acid derivatives, like methyl salicylic acid (Klessig, Tian, and Choi 2016). However, through radiolabeling experiments it has been shown that saligenin (**15**, Figure 12) and **1** have been derived from *o*-coumaric acid and not from salicylic acid, and even though **1** is produced by saligenin glycosylation, its direct precursor is *β*-isosalicin (**17**, Figure 12) (Zenk 1967). This compound (**17**) has been identified by means of HPLC-UV-MS/MS analysis in *S. daphnoides*, however, it was not detectable in any other *Salicaceae* plant (Babst, Harding, and Tsai 2010, Kammerer et al. 2005).
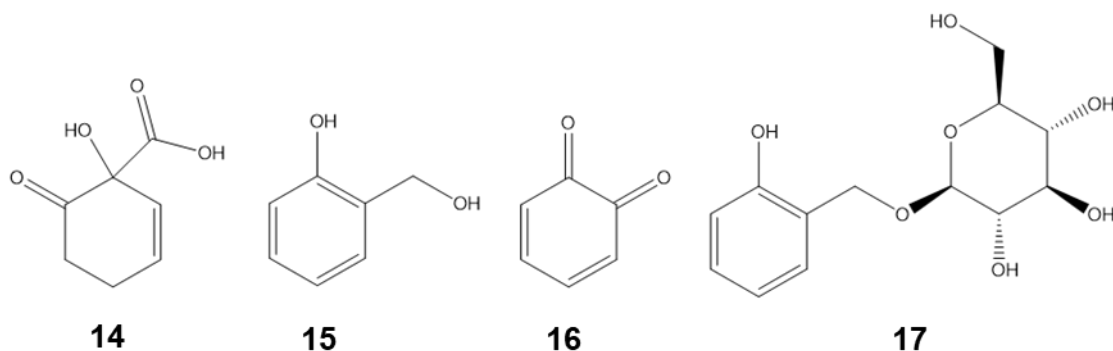
Figure 12: Chemical structures of 1-hydroxy-6-oxo-2-cyclohexene-1-carbocylic acid (HCH; **14**), saligenin (**15**), *o*-quinone (**16**), and *β*-isosalicin (**17**).

However, the exact pathways leading to these compounds are still under investigation (Figure 11; Fellenberg et al. (2020)). In particular, *phenylalanine ammonia-lyase* converts *L*-phenylalanine, which was formed by the shikimate pathway, into *trans*-cinnamic acid through deamination, and subsequent *ortho*-hydroxylation forms *o*-coumaric acid (Figure 11A, Babst, Harding, and Tsai (2010), Julkunen-Tiitto and Meier (1992)). Moreover, salicyloyl-CoA reduction can form the intermediate salicylaldehyde, which is glycosylated and reduced further into helicin (salicylic acid *β-D*-glucoside) and **15**, respectively, resulting in

the production of **1**, and finally **7** through HCH attachment (Babst, Harding, and Tsai 2010, Zenk 1967).

Latest findings using CRISPR/Cas9 knockout experiments on *Populus* roots showed that the UDP-glycosyltransferase UGT71L1 is responsible for the salicylate biosynthesis using salicyl benzoate as an intermediate and forming e.g. **6**, **7** or tremuloidin (Fellenberg et al. 2020). In the same year Kulasekaran et al. (2020) postulated the two isozymes, SpUGT71L2 and SpUGT71L3 glycosyltransferases from *S. purpurea*, glycosylating salicyl-7-benzoate. Salicyl-7-benzoate and the glycoside thereof are supposed to be intermediate compounds resulting in the biosynthesis of **6** and **7** by UGT71L genes (Kulasekaran et al. 2020).

However, another biosynthetic pathway (Figure 11B) suggests that the HCH moiety of **7** could be derived from benzoic acid and benzaldehyde, which are intermediates of cinnamic acid (Babst, Harding, and Tsai 2010, Zenk 1967). Through the benzoate pathway (Figure 11B), the benzyl alcohol might form benzyl-HCH, which undergoes 2-hydroxylation, yields salicyl-HCH, and after glycosylation finally forms **7** (Babst, Harding, and Tsai 2010). The precise pathway is still under investigation and the literature has only proposed pathways, which may form salicylates.

2 AIMS OF THE PROJECT

Willow bark (*Salix* cortex) has been approved by the EMA as herbal medicinal plant due to its anti-inflammatory, anti-pyretic, and analgesic effect, acting against pain, fever, headaches, and inflammation (European Medicines Agency 2017b). These properties are mainly attributed to the secondary metabolite composition of the plant. Interestingly, approved *Salix* bark extracts are standardized to salicin, despite the variety of available phytochemicals in the bark and studies hinting at the presence of further anti-inflammatory compounds besides salicin. *Salix* bark contains waxes, fatty acids, terpenes, flavonoids, tannins, procyanidins, organic acids, phenolics, lignans, sterols, and suberin, some of which may be potential bioactives reducing pain and inflammation. Further, phenolic glucosides like salicylates have been identified in various *Salix* species and crosses, however, there is little evidence about phytochemical bioactivity and comprehensive structure elucidation is partly missing.

Nevertheless, a few studies using *Salix* twigs revealed the neuroprotective properties of salicylates, such as 2'-*O*-, 3'-*O*-, and 6'-*O*-acetylsalicortin, and salicortin (Kim et al. 2015), and anti-adipogenic effect of 2',6'-*O*-diacetylsalicortin, 2'-*O*-, 3'-*O*-, 6'-*O*-acetylsalicortin, and salicortin (Lee et al. 2013, Yang et al. 2013). Moreover, Dissanayake et al. (2017) could show anti-inflammatory activity of tremulacin, salicortin, 2'-*O*-acetylsalicortin, and salicin against COX enzymes. However, previous studies did not analyze a variety of *Salix* extracts and different plants need further investigation upon their chemical composition.

Thus, the current project aimed at investigating the chemoprofile and structure-bioactivity relationship of *Salix* bark for pharmaceutical use. Therefore, different *Salix* species and crosses from nine genotypes *S. alba, S. daphnoides, S. humboldtiana, S. lasiandra, S. nigra, S. pentandra, S. purpurea, S. x rubens, and S. viminalis* were investigated by means of untargeted metabolomics in combination with principal component analysis (PCA). Afterwards, the most interesting species and crosses within different groups should be selected, and the PGE$_2$ release level of these selected *Salix* species should be evaluated to provide evidence about their anti-inflammatory potential.

The *Salix* cortex with highest anti-inflammatory effect should be applied to sequential solvent extraction and bioactivity-guided fractionation using a

combination of *in vitro* bioassays and analytical techniques. The bioactive phytochemicals should be isolated by means of (semi-)preparative HPLC, and their structure should be elucidated by means of LC-MS and 1D/2D-NMR experiments. Afterwards, the bioactivity of these compounds should be evaluated by means of anti-inflammatory activity assays.

Finally, these phytochemicals should be mapped quantitatively to gain further understanding of the distribution of these salicylates in different *Salix* species and crosses for future preparation, breeding, and standardization of a novel pharmacological *Salix* extract. Furthermore, correlation of quantitative data with half-maximal inhibitory concentration (IC_{50}) should identify the key compounds of selected *Salix* extracts contributing to the overall anti-inflammatory potential.

3 RESULTS AND DISCUSSION

3.1 Untargeted chemoprofiling of 92 *Salix* genotypes

First, in order to gain insight into the chemical composition of bark material of 92 various *Salix* species and crosses (Table 2, section 4.1.1) untargeted UHPLC-ToF-MS (ESI-) profiling and grouping was performed. The analysis was crucial for preselection of certain genotypes for further bioactivity-guided fractionation and compound identification of potent extracts.

Thus, the analysis of technical replicates of *Salix* genotypes was executed as described in section 4.2. The generated raw MS data by LC-MS were imported into Progenesis QI software and after processing, the tag filtration of identified abundant ions by means of ANOVA *p*-value and Max-fold change for high significance resulted in 7,819 filtered compounds out of 15,352. The imported in-house database containing structural information of salicylates (.mol files) as well as the automatic detection format of compounds helped identifying possible biomarkers for phytopharmaceutical production and breeding purposes. The autodetect option was chosen due to the unknown origin of the structural information. In total, 810 compounds were detected by untargeted metabolic profiling. In order to group the *Salix* genotypes according to similarity in their chemical composition, a generated principal component analysis (PCA) was generated grouping the 92 different species and crosses into five groups (Figure 13). The coefficients, principal component 1 (PC1) explaining 18.82% of the variance and PC2 10.87% (two principal components), are original variables combined linearly and accumulating in the 'PCA loading matrix' (Lever, Krzywinski, and Altman 2017).

All QC reference samples group close to each other and are located central of the PCA showing reproducible results. After grouping of the genotypes using PC1 and PC2, the five groups were compared with each other. Group 1 contains predominantly *S. daphnoides* species and crosses, which are grouped separately from group 2 containing mainly *S. viminalis* species and crosses, but also *S. humboldiana* and *S. nigra* genotypes. This shows that the chemical composition and probably also the bioactivity of two groups may differ.

S. pentandra species and crosses are assembled in group 3, which also contained *S. alba*, *S. alba* x *S. x rubens*, *S. lasiandra*, and *S. humboldtiana* x *S. purpurea* genotypes. On the other side, group 4 holds mostly species and crosses of *S. purpurea*, whereas VI1xDA1_9 within group 5 is the only *S. viminalis* clone grouping in the center of the PCA under the QC reference far away from the other *Salix* genotypes. Considering that genotypes belonging to the same group have similar chemical profiles, grouping is an important tool to reduce high sample amounts through preselection of genotypes. *S. viminalis*, *S. humboldtiana*, and *S. purpurea* crosses are assembled in different groups, revealing that different crosses of the same species may have different chemical profiles. The species and crosses of each group are depicted in Table 6 (section 4.1.1) and Figure 13.

The resulting groups of the PCA in the current work were compared to a targeted analysis with the same 92 *Salix* genotypes performed by HUB, which is described in the publication of Förster et al. (2021). Almost all species and crosses were grouping exactly the same, except VI1 (group 3, here group 2), VI1xDA1_9 (group 3, here group 5), VI6 (group 3, here group 2), HU1xVI6_1 (group 3, here group 2), HU1xPU1_3 (group 3, here group 4), PE2xAL5_1 (group 3, here group 1), HU1xPU1 (group 4, here group 3), and both crosses of PU3 and VI3 (group 4, here group 3). This may have occurred, due to the bigger variety of compounds found in the in-house salicylate database, as well as in the online database containing all possible compounds scanned by the searching tool (Progenesis QI) and used in the present study. Whereas, in the work by Förster et al. (2021) only a few selected phytochemicals (e.g. salicin, salicortin, 2'-*O*-acetylsalicortin, tremulacin, eriodictyol-7-glycoside, naringenin-5-glycoside, naringenin-7-glycoside, luteolin-7-glycoside, quercetin-hexoside, isosalipurposide, ampelopsin, (epi-)catechin, triandrin, caffeic acid, purpurein, salireposide, and syrengin) were analyzed even though the same *Salix* genotypes were evaluated. In particular, in the described PCA of Figure 13, *m/z* values of plausible lactones, xylosides, terpenes, fatty acids, and furans were detected after compound searching by the software and may have influenced the grouping of the untargeted analysis due to the higher amount and variety of compounds.
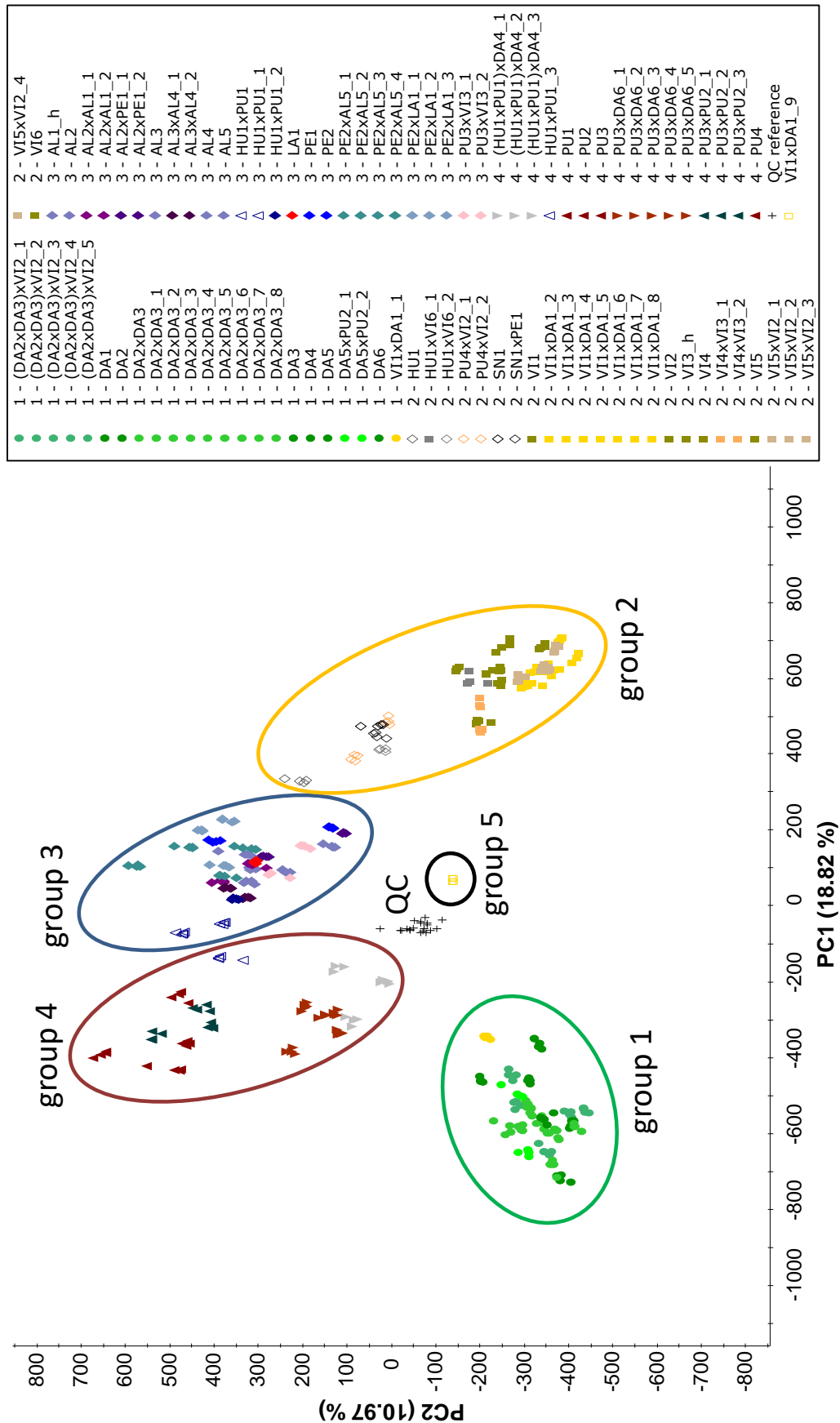
Figure 13: Principal component analysis (PCA) score plot of 92 *Salix* species and crosses grouped into five groups using the Progenesis QI software (adopted from Förster et al. (2021)). Black crosses: quality control (QC) reference.

For comparison of the groups regarding the chemical composition and up- and downregulation of the compounds in different groups, 14,202 processed data out of 15,352 after tag filtration were exported to EZinfo and S-plots were produced. Subsequently, two groups were selected, and OPLS-DA modelling was performed using the values of the parameters shown in Table A1 of the Appendix section. This model provided discriminant and multivariate data analysis, and allowed metabolic differentiation between *Salix* species, crosses or groups (Bylesjö et al. 2006). The overall *in silico* experiment gave only putative identified mass spectrometric data. The main purpose of the grouping in the present study was the preselection of *Salix* genotypes upon their chemical composition, whereas detailed identification was conducted later by activity-guided fractionation. By using the untargeted screening of the 92 *Salix* species and crosses, specific phenolic compounds were identified to be differently up- or downregulated within the resulted five groups of the PCA, which is illustrated further by the S-plots (Figure 14).

The S-plots (Figure 14) of the selected groups exhibited metabolites on both ends, -1 (bottom left) and 1 (top right), representing the mass and retention time of candidate markers. In the center of the S-plot compounds were gathered with no significant variance between the groups. The values over 98% of R2Y and Q2 revealed satisfying separation of the compared groups (Table A1, Appendix section).
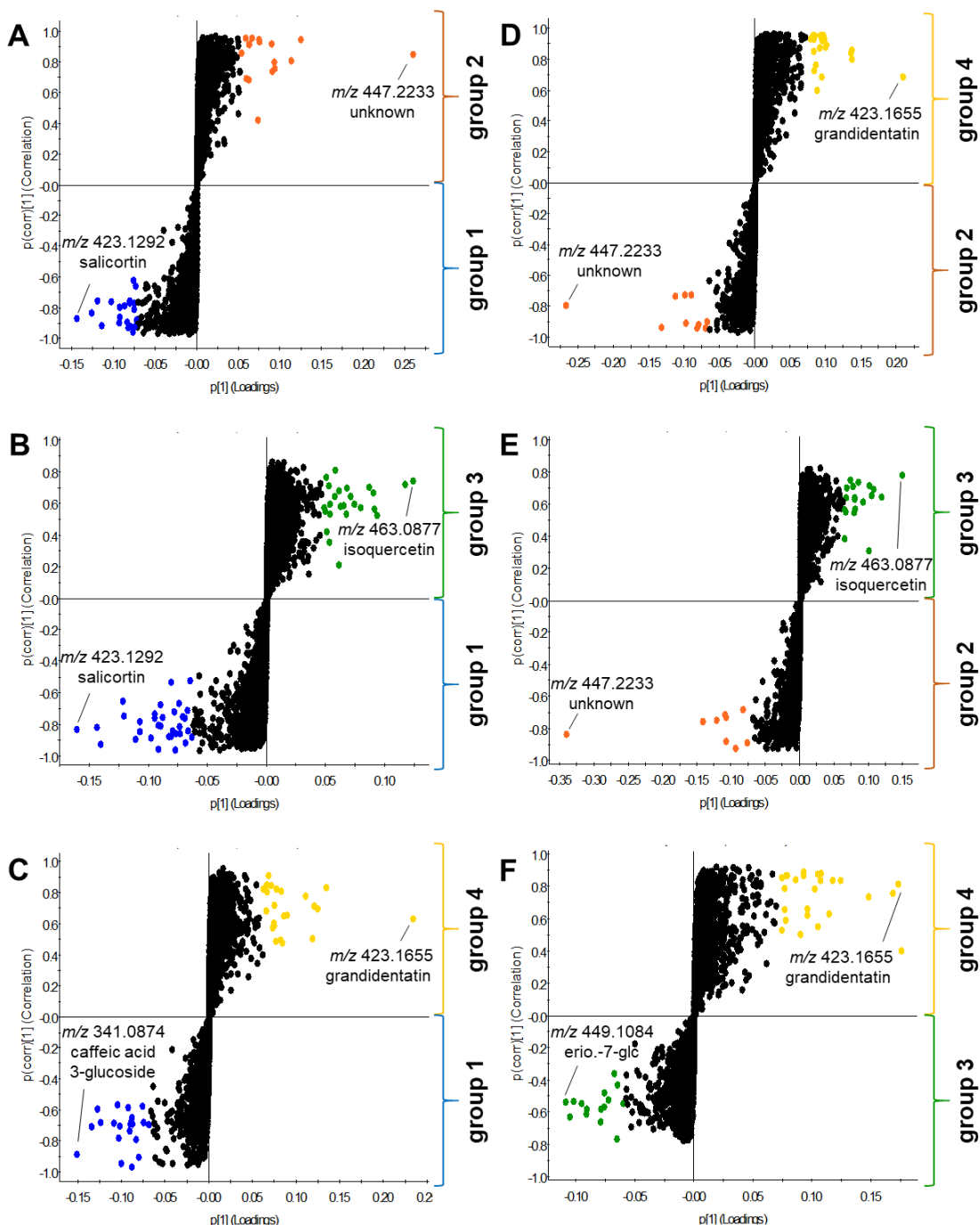
Figure 14 (A-F): Comparison between groups 1 to 4 from the PCA using S-plots based on the OPLS-DA model. Markers on the bottom left and top right are marked blue, orange, green, and yellow for each group 1, 2, 3, and 4, respectively. Exemplary, salicortin and caffeic acid-3-glucoside, unknown compound, isoquercetin and eriodictyol-7-glucoside, grandidentatin were showing the highest variance between the groups. Colored dots represent possible other upregulated compounds.

The colored known and unknown biomarkers of each group in the S-plots gave information about retention time, *m/z* values, adducts or fragments, mass error (data not shown), and about whether the compounds of the *in silico* fragment

database were up- or downregulated in a group. The m/z values were assigned to plausible compounds of the database. For instance, possible compounds being the most upregulated within the S-plots (Figure 14) were following: salicortin (m/z 423.13 [M-H]$^-$) and caffeic acid-3-glucoside (m/z 341.09 [M-H]$^-$), in group 1, in group 2 an unknown compound baring m/z 447.22, in group 4 grandidentatin (m/z 423.17 [M-H]$^-$), and in group 3 isoquercetin (m/z 463.09 [M-H]$^-$) and eriodictyol-7-glucoside (m/z 449.11 [M-H]$^-$). Table 2 shows detected compounds being upregulated in the respective groups, which can mostly be found colored in the S-plots of Figure 14. If compounds were down-regulated or not available in a group it was listed accordingly (Table 2). These findings can also help future work in identifying *Salix* genotypes from which single phytochemicals can be isolated in higher amounts. Group 5 comprising a single Salix genotype and being located in the center of the PCS was not compared with any group, since the comparison was done by groups containing a variety of genotypes.

Table 2: Detected possible compounds in the four groups of the PCA, which were found to be upregulated. x: available in the group, -: not available or down-regulated in the group, bold: salicylates.

possible compounds	group 1	group 2	group 3	group 4
grandidentoside	x	-	-	-
Catechin	x	-	-	x
2',6'-*O*-diacetylsalicortin	x	-	-	-
tremulacin	x	-	-	x
caffeic acid-3-glucoside	x	-	-	-
phloridzin	x	-	-	-
caffeic acid	x	-	-	-
salicortin	x	-	-	x
salipurposide	x	-	-	x
salicin	x	-	-	x
hesperitin	x	-	-	x
HCH-salicortin	x	-	-	x
gambiriin	x	-	-	-
brucein B	x	-	-	-
swertisin	x	-	-	-
lasiandrin	x	-	x	-
acetylsalicyloylsalicin	x	-	-	-
apigetrin	x	-	x	-
prodelphinidin C	-	x	x	-
lamioside	-	x	-	x
khellin	-	x	-	-
atractyloside A	-	x	-	-
procyanidin B2	-	-	x	x
astringin	-	-	x	x
eriodictyol-7-glucoside	-	-	x	-
isoquercetin	-	-	x	x
cynaroside	-	-	x	x
cinnamtannin A3	-	-	x	x

possible compounds	group 1	group 2	group 3	group 4
cinnamtannin A4	-	-	x	x
arecatannin	-	-	x	x
aklaviketone	-	-	x	-
grandidentatin	-	-	x	x
scoparol	-	-	-	x
naringenin	-	-	-	x
furcatin	-	-	-	x
kanokoside A	-	-	-	x
pulmatin	-	-	-	x
gallocatechin	-	-	-	x
ginkgolide C	-	-	-	x
naringenin chalcone	-	-	-	x

Moreover, quantified compounds in the targeted analysis by Förster et al. (2021) were compared to the untargeted profiling of the current work. In particular, of within both studies, salicylates, such as salicin, salicortin and tremulacin, were mainly contained in *S. daphnoides* species and crosses of group 1, but could also be found in species and crosses of group 4, which was also verified by Förster et al. (2008). In addition to these findings, S-plots could show HCH-salicortin, lasiandrin, 2',6'-*O*-diacetylsalicortin, and acetylsalicyloylsalicin as possible markers within group 1, whereas lasiandrin was more upregulated in group 3 within the present work. In addition, flavonoids, flavan-3-ols, and tannins were mainly found in group 3 and 4. However, it is not omitted that various compounds may be also contained in other groups.

Although some *m/z* values could not be assigned to any compound, the produced data could offer valuable information for preselection of *Salix* genotypes and can be used for further activity-guided fractionation (section 3.3). Moreover, for future studies it may be possible to use purified single compounds as references by screening them together with the 92 *Salix* genotypes and getting precise results. In the next sections, compound purification, identification and structure elucidation, as well as quantitative data will shed light into the overall chemical composition of a bioactive *Salix* representative (sections 3.3-3.7). Moreover, it will be possible to evaluate quantitative differences within the 92 *Salix* species and crosses (sections 3.7), which will be helpful for future herbal drug production.

3.2 Preselection of *Salix* genotype candidates and bioactivity

PCA analysis of the UPLC-ToF-MS data of 92 *Salix* genotypes revealed five groups (section 3.1), which was valuable for preselection of *Salix* representatives for breeding and medicinal purposes. Therefore, 28 *Salix* species and crosses were selected for bioactivity determination performed by UKF (Figure 15), in order to discover *Salix* extracts that can inhibit the cyclooxygenase (COX) enzyme reaction and PGE_2 (prostaglandin E_2) formation, leading to an anti-inflammatory activity. Selection of *Salix* candidates was based on phenolic glucoside content, variety of *Salix* species and crosses, and high bark material yield (Förster et al. 2021), which was performed by HUB. The 28 selected plant bark materials of species (VI1, DA1, PE1, AL3, PE2, PU2, HU1, SN1, VI3_h, AL1_h) and crosses (VI1xDA1_1, (DA2xDA3)xVI2_3, DA2xDA3_8, DA5xPU2_1, VI1xDA1_4, VI4xVI3_2, PU4xVI2_1, HU1xVI6_1, SN1xPE1, AL2xAL1_1, PE2xLA1_1, PE2xAL5_2, HU1xPU1_1, (HU1xPU1)xDA4_3, PU3xDA6_2, PU3xPU2_3, HU1xPU1_3, VI1xDA1_9) were standardized by HUB to 10 mg/mL phenolic glucoside content and used for the bioactivity-assay, which is a THP-1/macrophage model performed by UKF (section 4.11.1).

For the experimental procedure lipopolysaccharide (LPS), a molecule contained in the cell wall of gram-negative bacteria, was used to trigger inflammation and which can lead to cytokine production (Eliopoulos et al. 2002). Toll-like receptors (TLRs) of macrophages can recognize the LPS endogenous danger signal, activating the immune system by secreting cytokines and chemokines (Mosser and Edwards 2008, Grassin-Delyle et al. 2020). The inflamed tissues in turn strongly induce COX-2 enzyme activation and consequently increase PGE_2 production (Uematsu et al. 2002, Ricciotti and FitzGerald 2011). Willow bark can, however, act anti-inflammatory against COX-1 and COX-2 (Maroon, Bost, and Maroon 2010, Fiebich and Appel 2003). Therefore, it is of interest to investigate which compounds are bioactive in potent plants and can reduce inflammation.

In order to detect the most potent willow bark extract, released PGE_2 levels were measured using the PGE_2 ELISA kit (section 4.11.4). Released low PGE_2 level revealed a higher anti-inflammatory potential of a *Salix* extract. Extract B was used as control and extracts with lower PGE_2 release level than extract B were possible bioactive candidates, since they showed a higher anti-inflammatory

effect than the previously existing extract B. Moreover, *S. purpurea* mix was tested, but did not show any potency. Commercially obtained Aspirin® demonstrated an anti-inflammatory effect (Figure 15). Aim was the selection of a *Salix* genotype with high anti-inflammatory potential and reduced side effects for further studies on the structure-activity relationship. Moreover, the selected candidate should be more anti-inflammatory than previously existing extract B. The representatives PE1, followed by AL3, PE2, PU4xVI2_1, AL2xAL1_1, PE2xLA1_1, HU1xPU1_1, (HU1xPU1)xDA4_3, PU3xDA6_2, and VI1xDA1_9 showed the highest anti-inflammatory effect which was expressed as reduced PGE$_2$ release level in the assay (Figure 15). The same experiment was performed by UKF, comparing acetylsalicylic acid (Aspirin®), *S. pentandra* (PE1, S6), and extract B, revealing their anti-inflammatory potential against bacterial LPS, but also against SARS-CoV-2 peptide mixture (Le et al. 2021). However, by comparing PE1 and acetylsalicylic acid (Aspirin®) at the same concentration on COX inhibitory activity, the *Salix* extract was inhibiting better than acetylsalicylic acid (Aspirin®), even compared to extract B (Le et al. 2021), which may be due to a highly bioactive compound or a synergistic interplay between several bioactives.
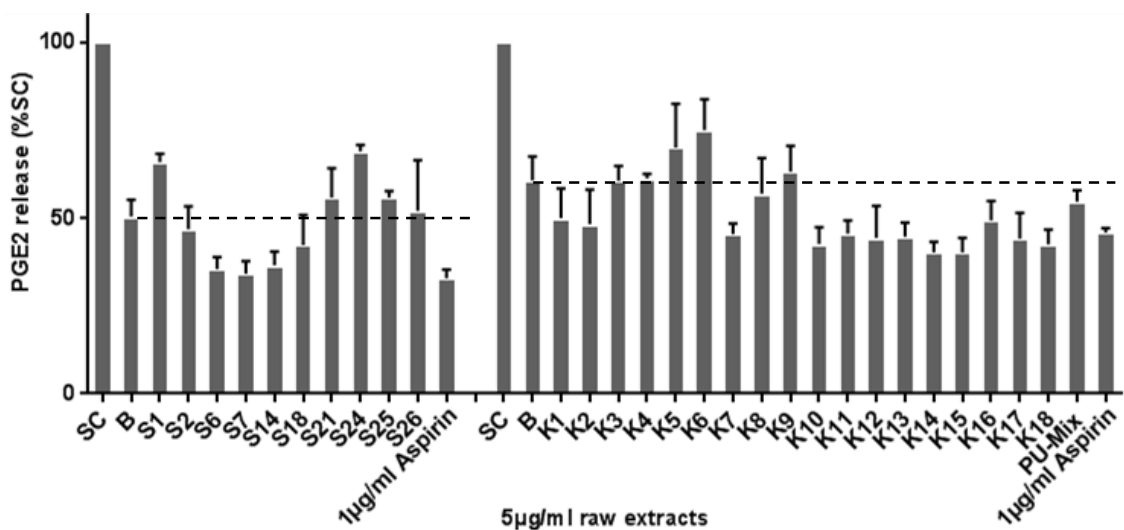
Figure 15: Anti-inflammatory activity of selected *Salix* species (S) and crosses (K) using the THP-1/macrophage model. PGE$_2$ release was quantified in differentiated and stimulated THP-1 cells after exposure to the species and crosses. S1: VI1, S2: DA1, S6: PE1, S7: AL3, S14: PE2, S18: PU2, S21: HU1, S24: SN1, S25: VI3_h, S26: AL1_h, K1: VI1xDA1_1, K2: (DA2xDA3)xVI2_3, K3: DA2xDA3_8, K4: DA5xPU2_1, K5: VI1xDA1_4, K6: VI4xVI3_2, K7: PU4xVI2_1, K8: HU1xVI6_1, K9: SN1xPE1, K10: AL2xAL1_1, K11: PE2xLA1_1, K12: PE2xAL5_2, K13: HU1xPU1_1, K14: (HU1xPU1)xDA4_3, K15: PU3xDA6_2, K16: PU3xPU2_3, K17: HU1xPU1_3, K18: VI1xDA1_9, SC: solvent control (0.1% DMSO), B: extract B (control), PU-Mix: *S. purpurea* mix (data obtained from UKF).

In order to select a single *Salix* candidate for the bioactivity-guided fractionation, additional experiments regarding the antioxidant capacity and cytotoxicity were performed by UKF. The tests revealed that *S. pentandra* (PE1, S6), belonging to group 3 by principal component analysis (Figure 13), had the highest antioxidant potential and a reduced amount of cytotoxicity (Gomes et al. 2021) in comparison to Aspirin® and extract B. Consequently, PE1 was used as the main bioactive representative for activity-guided fractionation and isolation of bioactives. The *S. viminalis* cross, VI4xVI3_2 (K6), belonging to group 2 showed the lowest bioactivity and was therefore used as negative control.

3.3 Activity-guided extraction and fractionation of *S. pentandra* (PE1)

3.3.1 Sequential solvent extraction of *S. pentandra* (PE1)

In order to identify compounds triggering the anti-inflammatory effect of willow bark and to investigate whether the extracts or single compounds are responsible for the bioactivity, powdered bark material of bioactive *S. pentandra* (PE1) was extracted by vacuum filtration using methanol, methanol/water (v/v, 70/30), and water as described in section 4.4.1. The methanol extract had the highest yield with 29.57% grounded willow bark in comparison to the methanol/water (v/v, 70/30; 2.30%) and water (2.23%) extracts (Table 3).

Table 3: Sequential solvent extraction yields of *S. pentandra* (PE1) bark.

extraction solvent	yield [%]
methanol	29.57
methanol/water (v/v, 70/30)	2.30
water	2.23

Furthermore, in order to examine the chemical composition of the most bioactive extract, the methanol, methanol/water and water extracts were tested on their bioactivity by UKF, as described in section 4.11 (Table 16). The methanol extract showed the highest anti-inflammatory potential with the lowest PGE_2 release level being 55% at 50 µg/mL in comparison to the solvent control and the two other extracts (Table 16A). Thus, the methanol/water and water extract could not show

any inhibitory potential against PGE_2 release (Table 16A). Additional studies on the effect of the three extracts on human recombinant COX enzymes could show that methanol and methanol/water extracts were able to inhibit enzyme activity, however, inhibition of COX-2 was much higher when using acetylsalicylic acid (Table 16 B, C). It is also important to note that Ruuhola, Julkunen-Tiitto, and Vainiotalo (2003) reported no salicylate degradation of the extracted leaves using methanol. Therefore, it was suggested that bark extraction using this solvent would not lead to degradation of important salicylates.
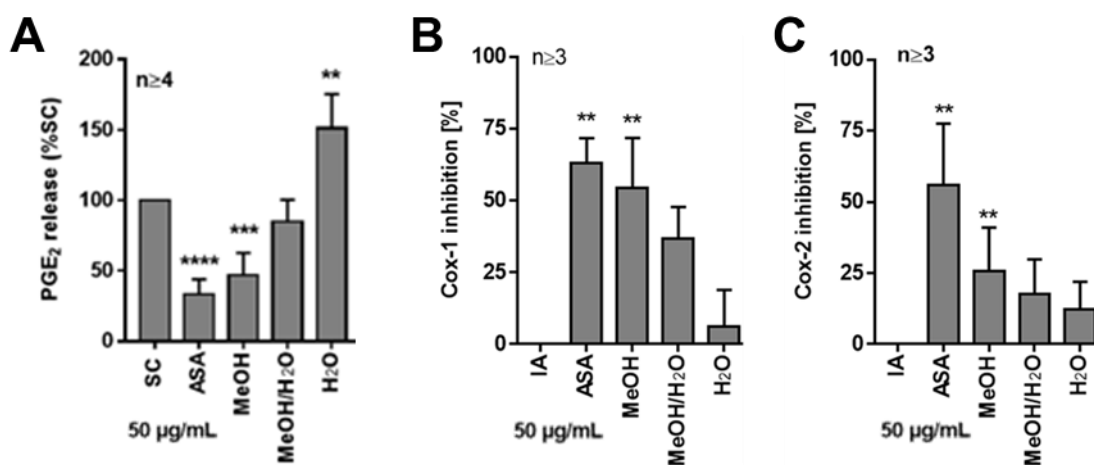
Figure 16: Bioactivity expressed as **(A)** levels of inhibition of PGE_2 release when treated with methanol, methanol/water (v/v, 70/30), and water extracts of *S. pentandra* bark and exposed to human PBMC. Bioactivity was compared to solvent control (SC, 1% distilled water) and 1 µg/mL acetylsalicylic acid (ASA). **(B)** COX-1 and **(C)** COX-2 enzyme activity determination by quantification of PGF2α and determination of COX-1 and COX-2 inhibition comparing initial COX protein activity (IA) to the extracts. Asterisks: significant difference between extracts and SC, such as ** $p < 0.01$, *** $p < 0.001$, and **** $p < 0.0001$ (adopted from Antoniadou et al. (2021)).

In a recent publication by Le et al. (2021), the same *S. pentandra* genotype (PE1, S6) showed a higher inhibitory activity against COX enzyme than the methanol extract (Table 16 B, C) of the current work. By comparing the used PE1 samples, Le et al. (2021) used PE1 extract standardized to 10 mg/mL phenolic glucoside content, which might have led to differences in the bioactivity. The bioactive methanol extract showing anti-inflammatory activity against PGE_2 release was used for further fractionation by means of solid-phase extraction, phytochemical isolation, and structure elucidation in order to understand which chemical compositions and single phytochemicals are responsible for the bioactivity of the extract.

3.3.2 Solid-phase extraction of methanol extract

Bioactive methanol extract of *S. pentandra* bark was analyzed by UPLC-ToF-MS showing complex compound composition (data not shown). Therefore, to isolate phytochemicals for structure characterization, first, pre-fractionation was performed by solid-phase extraction using C_{18} cartridges as stationary phase, and methanol and water as mobile phase (section 4.4.2). By solid-phase extraction, eleven SPE fractions F1 to F11 were obtained (Figure 17). Higher yields were found in hydrophilic fractions containing polar compounds. From SPE fraction F5 26.59% methanol extract were obtained, showing the highest yield in contrast to the other fractions.
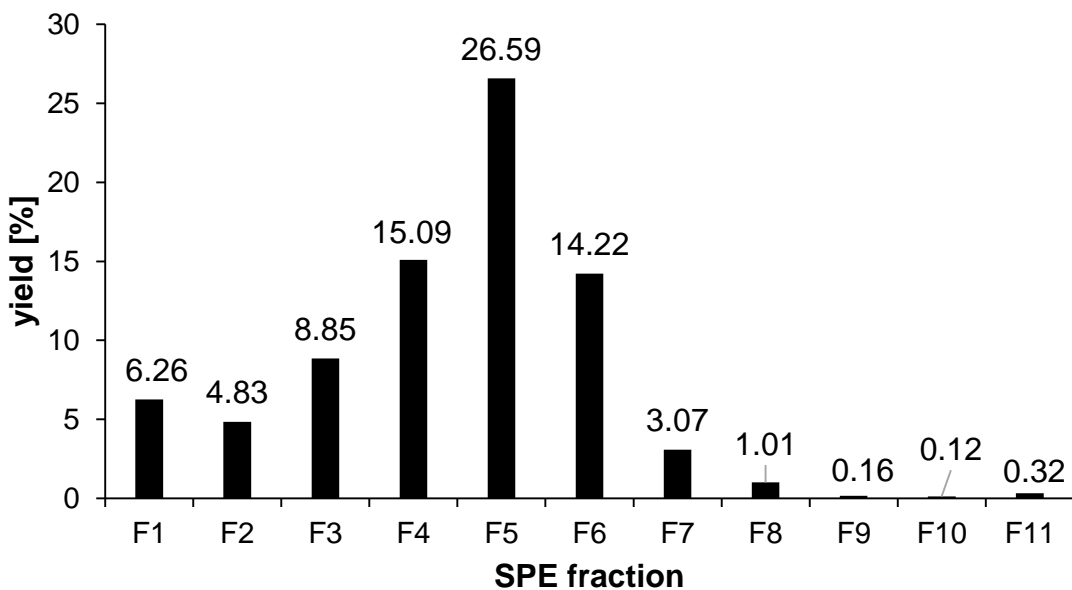
Figure 17: Yield of SPE fractions F1 to F11 collected from the methanol extract of *S. pentandra*.

Furthermore, the eleven SPE fractions were screened by UPLC-ToF-MS and compared with each other from the most hydrophilic SPE fraction F1 to the most hydrophobic SPE fraction F11, giving information about the complexity of each chemical composition by the various chromatographic peaks (Figure 18). It also helps understanding the chemical character of possible compounds in the fractions.
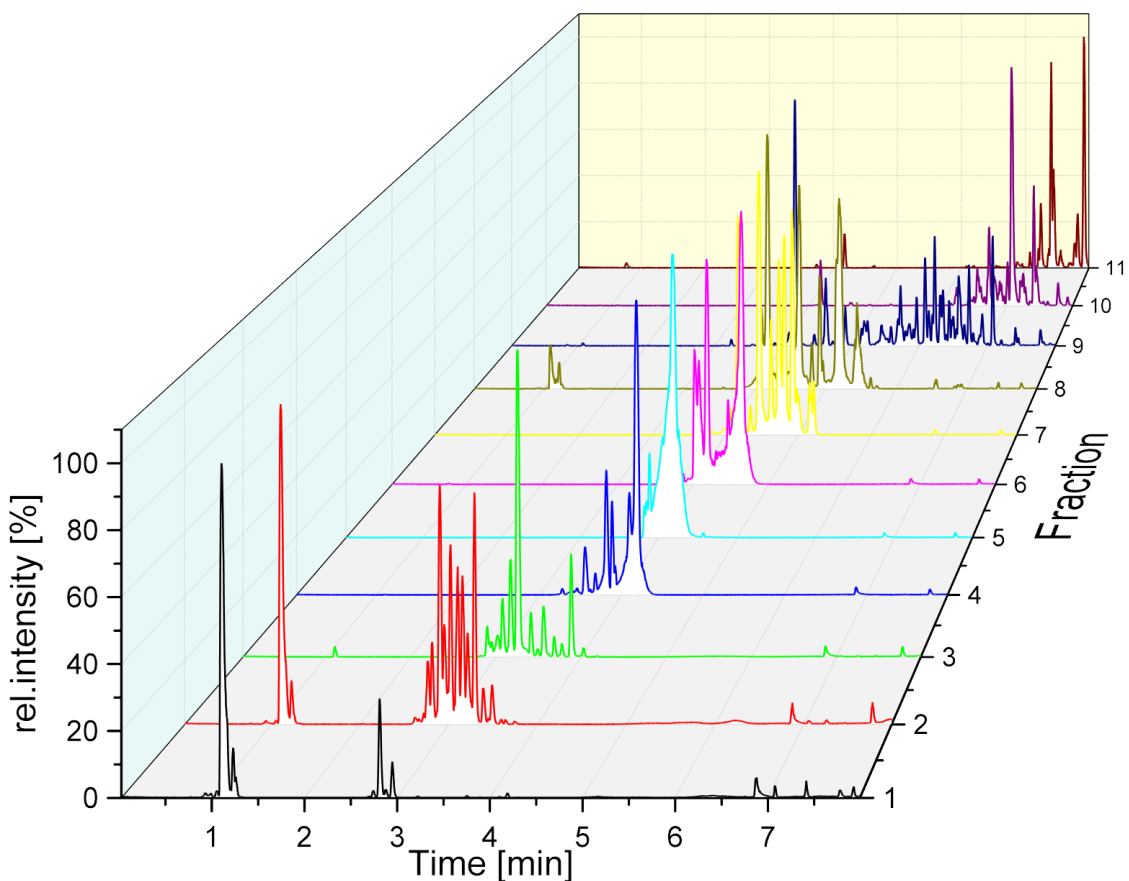
Figure 18: Extracted UPLC-ToF-MS ion chromatograms of eleven SPE fractions (F1-F11) derived from methanol extract of *S. pentandra*.

Additionally, the lyophilized SPE fractions were prepared relating to their natural concentrations as contained in the methanol extract in order to analyze their bioactivity, which was performed by UKF (Figure 19). After quantification of the PGE$_2$ release, as described in section 4.11, it could be shown that fractions F5 and F6 were the most potent among the analyzed fractions. However, F5 had the highest statistical significance of $p < 0.05$ (Figure 19, Antoniadou et al. (2021)).
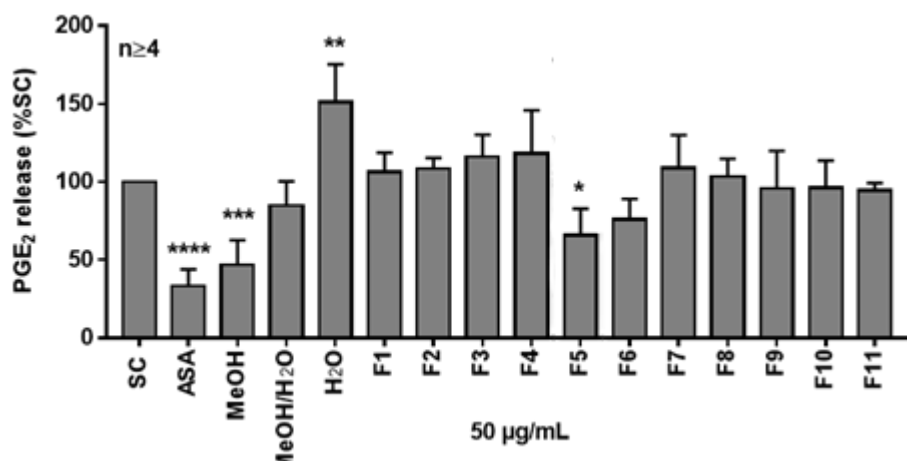
Figure 19: Bioactivity expressed as levels of inhibition of PGE_2 release when treated with methanol, methanol/water (v/v, 70/30), and water extracts of *S. pentandra* bark and SPE fractions F1-F11 derived from the methanol extract, and exposed to human PBMC. Bioactivity was compared to solvent control (SC, 1% distilled water) and 1 μg/mL acetylsalicylic acid (ASA). Asterisks: significant difference between extracts and SC, such as * $p < 0.05$, ** $p < 0.01$, *** $p < 0.001$, and **** $p < 0.0001$ (adopted from Antoniadou et al. (2021)).

Moreover, COX-1 and COX-2 enzyme inhibitory activity was evaluated between fractions F4, F5, and F6 in order to examine any phytochemical carryover (Antoniadou et al. 2021). The analysis showed that fraction F5 inhibited both COX-1 (47%) and COX-2 (17%) enzyme activity similarly as the methanol extract (Antoniadou et al. 2021). On the other side, no inhibitory activity could be shown for F4 and F6, revealing no compound carryover (data not shown). In order to investigate the chemical composition of the bioactive fractions F5 and F6, further purification steps were performed by means of RP-HPLC fractionation, which are described in the next sections.

3.4 Detection of possible salicylates in *S. pentandra* by precursor ion scan and information-dependent acquisition experiments

The term 'salicylates' has been described in a few publications over the years as salicylic acid derivatives (Binder and Zeiller 1993, Ekinci, Sentürk, and Küfrevioğlu 2011, Hedner and Everts 1998). Salicylic acid is a known derivative, as it exists as a natural compound in the plants, which is produced during shikimate biosynthetic pathway, and can form salicin and other salicylate glucosides through the glycosylation reaction (section 1.4.2, Figure 10), but is

also considered as a metabolite and degradation product (Mahdi 2014, Ruuhola and Julkunen-Tiitto 2003). Thus, it is of interest to analyze salicin as well as salicylic acid and saligenin, which are precursors of most of the salicylates, such as salicortin, 2'-*O*-acetylsalicortin, and temulacin (Ruuhola and Julkunen-Tiitto 2003) and have been shown to have anti-inflammatory properties as proposed by Ekinci, Şentürk, and Küfrevioğlu (2011) and mentioned already in section 1.3.2. In the current work, it was important to scan bioactive *S. pentandra* extracts for possible salicylates, which may trigger the anti-inflammatory potential.

3.4.1 Precursor ion (PI) scan of *S. pentandra* extracts

The precursor ion (PI) scan was performed by means of QTrap-LC-MS/MS as described in section 4.8.1. For the experiment, precursor ions were scanned first in Q1 over a mass range of 300 to 1,000 Da. After ion fragmentation in the collision cell Q2, a variety of *m/z* values of compounds (precursors) carrying these fragment ions, like salicylic acid (137.1 Da), saligenin (123.1 Da), and salicin (285.2 Da) ions (Figure 20), were scanned (Q3) and detected (Sciex 2019). The experiment was performed using the potent methanol extract and SPE fraction F5 of *S. pentandra*, providing in the first step information about possible additional compounds.
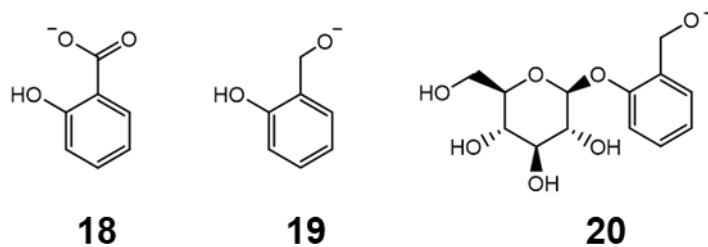
Figure 20: Salicylic acid (**18**), saligenin (**19**), and salicin (**20**) fragment ions, holding 137.1 Da, 123.1 Da, and 285.2 Da, respectively.

Precursor ion scan of saligenin detected the compound salicin, as it is part of the chemical structure. However, in general salicylates were detected by means of precursor ion scan of salicylic acid. The ion mass of 137.1 Da was detected after salicylate fragmentation generating the hydrolyzed form of 1-hydroxy-6-oxo-2-

cyclohexene-1-carboxylic acid (HCH) residue, which was proposed by Kammerer et al. (2005) and has the same mass as salicylic acid (Figure 21). Salicylates, such as salicortin, 2'-O-acetylsalicortin, tremulacin, and lasiandrin have been previously described by e.g. Abreu et al. (2011), Feistel et al. (2015) and Keefover-Ring et al. (2014) and hold the HCH residue (Figure 21).

salicylate substructure

salicortin: R_1, R2, R3 = H
2'-O-acetylsalicortin: R_1, R_2 = H, R_3 = acetyl group
tremulacin: R_1, R_2 = H, R_3 = benzyl group
lasiandrin: R_1 = HCH, R_2 = H, R_3 = acetyl group
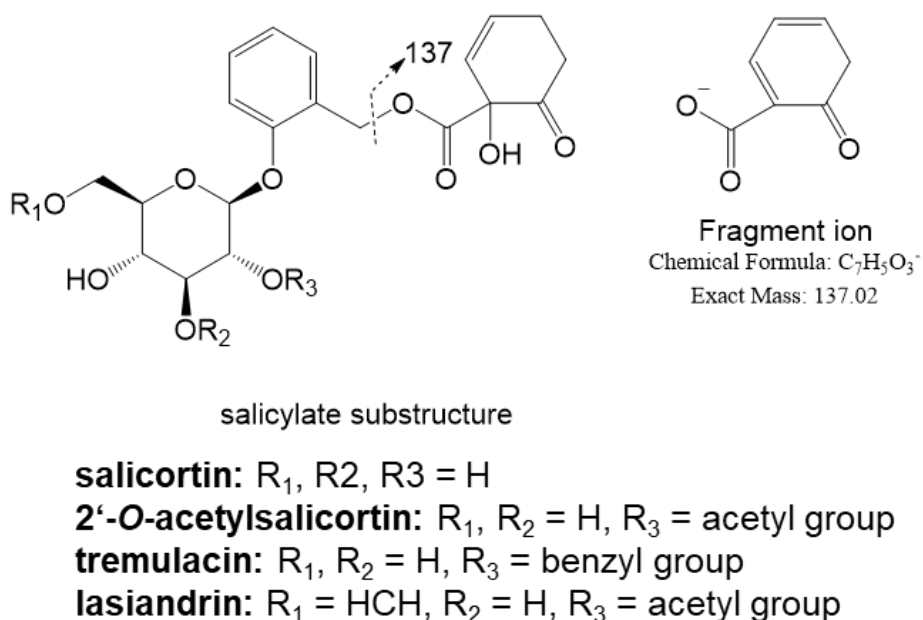
Figure 21: Salicylate structures of salicortin, 2'-O-acetylsalicortin (**III**), tremulacin (**VII**), and lasiandrin (**VI**) producing a fragment ion with a mass of 137 Da, which represents the fragment ion of the hydrolyzed form of the 1-hydroxy-6-oxo-2-cyclohexene-1-carboxylic acid (HCH) group.

The extracted mass spectra of the screened bioactive methanol extract and SPE fraction F5 from the precursor ion scan of salicylic acid are exhibited in Figure 22 A and B, respectively. Exact masses of the detected *m/z* values were compared with available databases and literature (Table 4). The list of all plausible salicylates provided by this untargeted technique gave a valuable overview for further isolation and identification of single compounds from bioactive fractions.
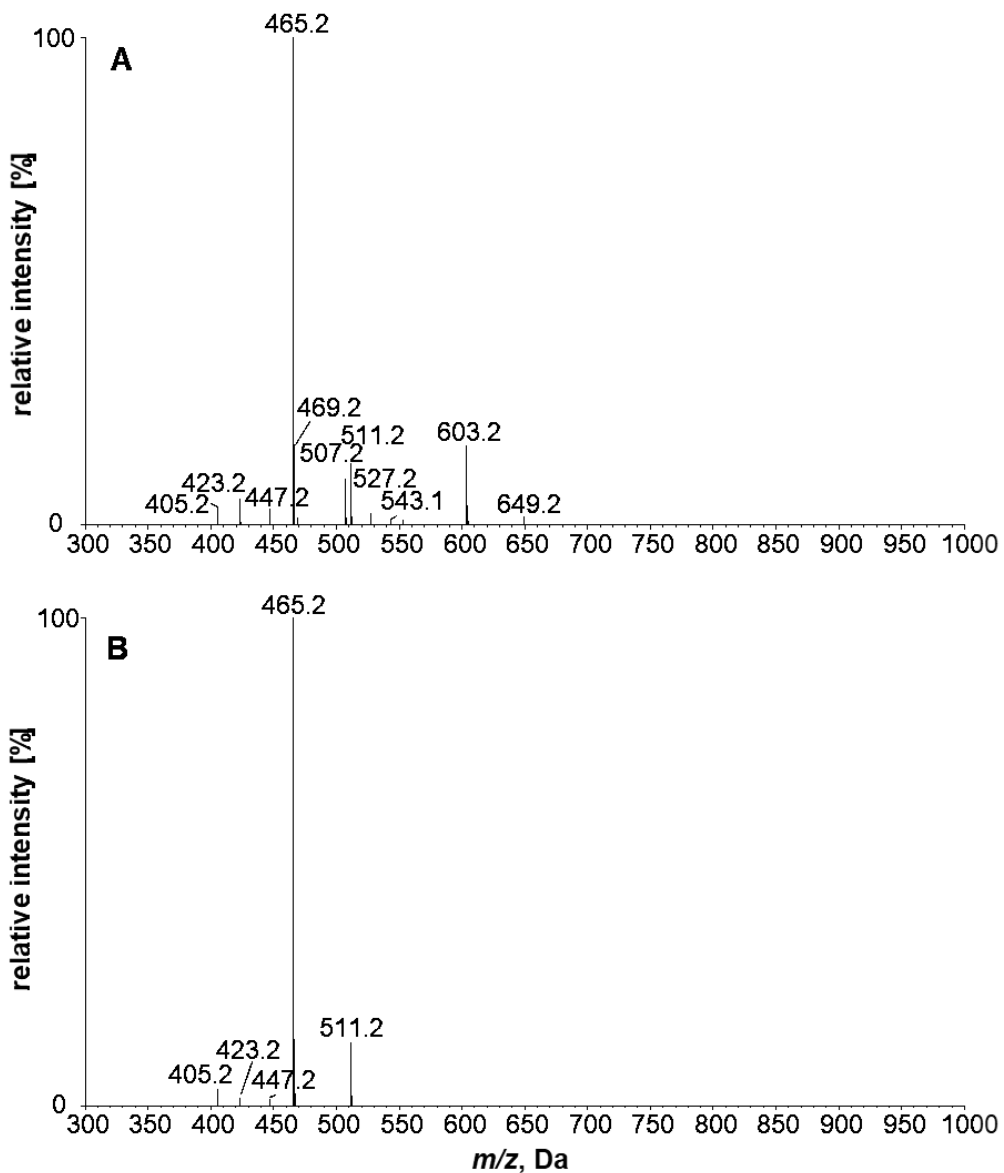
Figure 22: Extracted spectra of **(A)** S6 methanol extract and **(B)** SPE fraction F5 of *S. pentandra* from precursor ion scan of salicylic acid (ESI negative mode).

Consequently, acetylsalicortin (m/z 465.2 [M-H]⁻, m/z 511.2 [M+HCO$_2$H-H]⁻) and lasiandrin (m/z 603.2 [M-H]⁻, m/z 649.2 [M+HCO$_2$H-H]⁻) were plausible salicylates in the methanol extract. Besides others, following precursor ions could be detected in SPE fraction F5: m/z 405.2 for deltoidin, nigracin, salicyloylsalicin, salireposide or trichocarpin, m/z 423.2 for salicortin, m/z 447.2 for an unknown compound, and m/z 465.2 for acetylsalicortin (Figure 22 and Table 4). The screening of the bioactive methanol extract provided initial information about possible compounds, which further need to be structurally elucidated and verified.

Table 4: Detected *m/z* values of product masses of derivatives from precursor ion scan of salicylic acid.

detected *m/z* values	exact mass	possible salicylates
405.2	406.1264	deltoidin
		nigracin
		salicyloylsalicin
		salireposide
		trichocarpin
423.3	424.1369	salicortin
	424.1730	grandidentanin
		Isograndidentatin A
		Isograndidentatin B
447.2	448.1369	populoside A
465.1	466.1475	2'-*O*-acetylsalicortin
465.2		3'-*O*-acetylsalicortin
		6'-*O*-acetylsalicortin
507.3	508.1581	2',6'-*O*-diacetylsalicortin
527.2	528.1632	tremulacin
543.1	544.1581	2-hydroxybenzoylsalicortin
		HCH-deltoidin
		HCH-salicyloylsalicin
		HCH-nigracin (2'-Bz)
		HCH-nigracin (6'-Bz)
603.2	604.1792	lasiandrin

3.4.2 Information-dependent acquisition (IDA) experiment of *S. pentandra* extracts

Furthermore, the information-dependent acquisition (IDA) experiment was performed to discover known and unknown compounds contained in the bioactive *S. pentandra* methanol extract by means of Triple-ToF LC-MS/MS (section 4.8.2). First, precursor ions were scanned over a mass range of *m/z* 50 to 1,000 and then, the 15 most intense precursor ions were scanned using MS to MS/MS switching (Decaestecker et al. 2004). After importing the data into the PeakView® software and data processing, hits of possible compound masses, MS[1] (Figure 23 B), MS[2] (Figure 23 C) spectra, and the respective IDA chromatograms (Figure 23 A) were shown and evaluated. For instance, in the methanol extract, 2'-*O*-acetylsalicortin was detected at 465.14 Da ([M-H]⁻) (Figure 23 B). The respective mass fragments were usual for this compound and 2'-*O*-acetylsalicortin could be validated (Figure 23 C). However, further studies are needed to be performed for isolation and identification of the compounds for complete compound characterization by NMR.
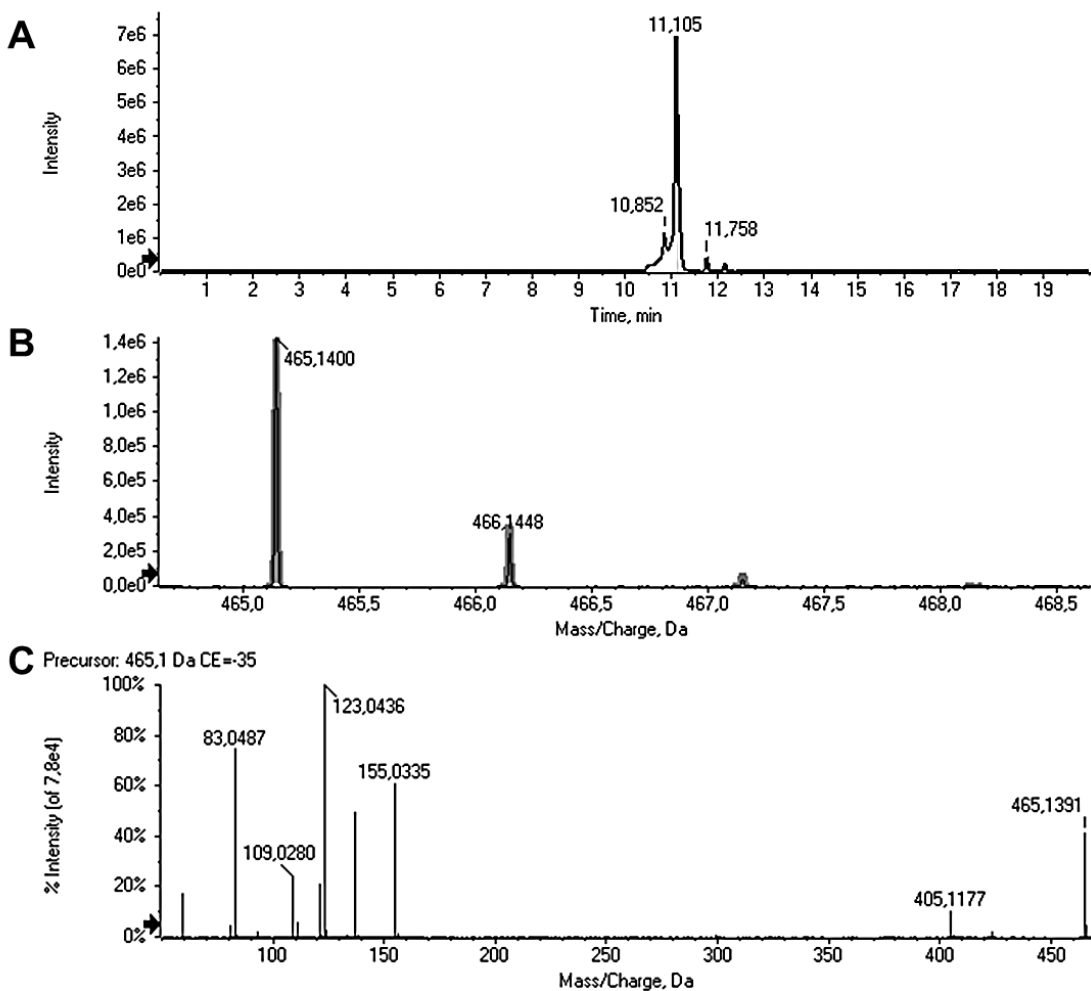
Figure 23: (A) Extracted ion chromatogram as well as **(B)** MS^1 spectrum with detected isotopes and **(C)** MS^2 spectrum with fragment ions of the most intense precursor ion 465.1400 Da of the tentatively detected 2'-*O*-acetylsalicortin in the *S. pentandra* methanol extract.

Besides 2'-*O*-acetylsalicortin, the experiment allowed further investigation of following tentatively identified compounds (Table 5) in the methanol extract: salicin, 2'-*O*-acetylsalicin or fragilin, deltoidin, salicortin, grandidentoside, cinnamrutinose A, diglucoside salicin, 2',6'-*O*-diacetylsalicortin, tremulacin, 2'-(*Z*)-cinnamoylsalicortin or 2'-(*E*)-cinnamoylsalicortin, HCH-salicortin, 6'-acetyl-tremulacin, HCH-acetylsalicyloylsalicin, and lasiandrin. As in the PI scan, the IDA experiment provided similar results detecting mainly salicylates, which will be also examined by further activity-guided fractionation in section 3.5.

Table 5: Hits of tentatively identified compounds in the bioactive methanol extract obtained from the PeakView® software (compound list and imported database obtained from Keefover-Ring et al. (2014)). -: not detected, x: detected.

possible compounds	molecular formula	exact mass [M]	detected in the methanol extract
salicin	$C_{13}H_{18}O_7$	286.1052	x
picein	$C_{14}H_{18}O_7$	298.1050	-
salidroside	$C_{14}H_{20}O_7$	300.1210	-
triandrin/sachaliside	$C_{15}H_{20}O_7$	312.1210	-
vimalin	$C_{16}H_{22}O_7$	326.1370	-
2'-*O*-acetylsalicin fragilin	$C_{15}H_{20}O_8$	328.1158	x
diacetylsalicin	$C_{17}H_{22}O_9$	370.1264	-
tremuloidin chaenomeloidin populin	$C_{20}H_{22}O_8$	390.1315	-
deltoidin nigracin salicyloylsalicin salireposide trichocarpin	$C_{20}H_{22}O_9$	406.1264	x
cinnamoylsalicin	$C_{22}H_{24}O_8$	416.1471	-
salicortin	$C_{20}H_{24}O_{10}$	424.1369	x
grandidentanin isograndidentatin A isograndidentatin B	$C_{21}H_{28}O_9$	424.1730	-
populoside B trichocarposide	$C_{22}H_{24}O_9$	432.1420	-
grandidentoside	$C_{21}H_{28}O_{10}$	440.1683	x
cinnamrutinose A	$C_{21}H_{30}O_{10}$	442.1840	x
populoside populoside A acetylsalicyloylsalicin	$C_{22}H_{24}O_{10}$	448.1369	-
diglucoside salicin	$C_{19}H_{28}O_{12}$	448.1581	x
acetylcinnamoylsalicin	$C_{24}H_{26}O_9$	458.1577	-
populoside C	$C_{23}H_{26}O_{10}$	462.1526	-
2'-*O*-acetylsalicortin	$C_{22}H_{26}O_{11}$	466.1475	x
diacetylsalicyloylsalicin	$C_{24}H_{26}O_{11}$	490.1475	-
6'-benzoyltremuloidin	$C_{27}H_{26}O_9$	494.1577	-
2',6'-*O*-diacetylsalicortin	$C_{24}H_{28}O_{12}$	508.1581	x
salicyloyltremuloidin	$C_{27}H_{26}O_{10}$	510.1526	-
6'-benzoylcinnamoylsalicin 6'-cinnamoyltremuloidin	$C_{29}H_{28}O_9$	520.1733	-
tremulacin	$C_{27}H_{28}O_{11}$	528.1632	x
cinnamoylsalicyloylsalicin	$C_{29}H_{28}O_{10}$	536.1683	-
2-hydroxybenzoylsalicortin	$C_{27}H_{28}O_{12}$	544.1581	-
HCH-deltoidin HCH-salicyloylsalicin HCH-nigracin (2'-Bz) HCH-nigracin (6'-Bz)	$C_{27}H_{28}O_{12}$	544.1581	-
dicinnamoylsalicin	$C_{31}H_{30}O_9$	546.1890	-

possible compounds	molecular formula	exact mass [M]	detected in the methanol extract
acetylsalicyloyltremuloidin	$C_{29}H_{28}O_{11}$	552.1632	-
2'-(Z)-cinnamoylsalicortin 2'-(E)-cinnamoylsalicortin	$C_{29}H_{30}O_{11}$	554.1788	x
HCH-salicortin	$C_{27}H_{30}O_{13}$	562.1686	x
6'-acetyltremulacin	$C_{29}H_{30}O_{12}$	570.1737	x
HCH-acetylsalicyloylsalicin	$C_{29}H_{30}O_{13}$	586.1686	x
acetylcinnamoylsalicortin	$C_{31}H_{32}O_{12}$	596.1894	-
lasiandrin	$C_{29}H_{32}O_{14}$	604.1792	x
6'-benzoyltremulacin	$C_{34}H_{32}O_{12}$	632.1894	-
HCH-salicyloyltremuloidin	$C_{34}H_{32}O_{13}$	648.1843	-
6'-cinnamoyltremulacin	$C_{36}H_{34}O_{12}$	658.2050	-
HCH-tremulacin	$C_{34}H_{34}O_{14}$	666.1949	-
dicinnamoylsalicyloylsalicin	$C_{38}H_{34}O_{11}$	666.2101	-
dicinnamoylsalicortin	$C_{38}H_{36}O_{12}$	684.2207	-
HCH-cinnamoylsalicortin	$C_{36}H_{36}O_{14}$	692.2105	-
tremulacinol	$C_{27}H_{30}O_{11}$	530.1788	-
6'-O-benzoylsalicortinol	$C_{27}H_{30}O_{11}$	530.1700	-

3.5 Isolation and identification of *S. pentandra* phytochemicals

3.5.1 SPE fraction F5: subfractionation and compound identification

Isolation and characterization of phytochemicals will shed light into whether single compounds or the overall chemical composition of *S. pentandra* are responsible for the anti-inflammatory potential of the willow bark of the plant. This was achieved by activity-guided fractionation. The most bioactive SPE fraction F5 was further subfractionated using preparative HPLC-UV as described in section 4.4.4. After development of a suitable HPLC method, fraction F5 was further separated on a preparative phenyl-hexyl column, since aromatic *Salix* phytochemicals can be isolated through strong π-π interactions. Fractionation was performed using the diode-array detector at a wavelength of 200 nm, at which the highest absorption was obtained, enabling the collection of the subfractions F5-1 to F5-6 (Figure 24).
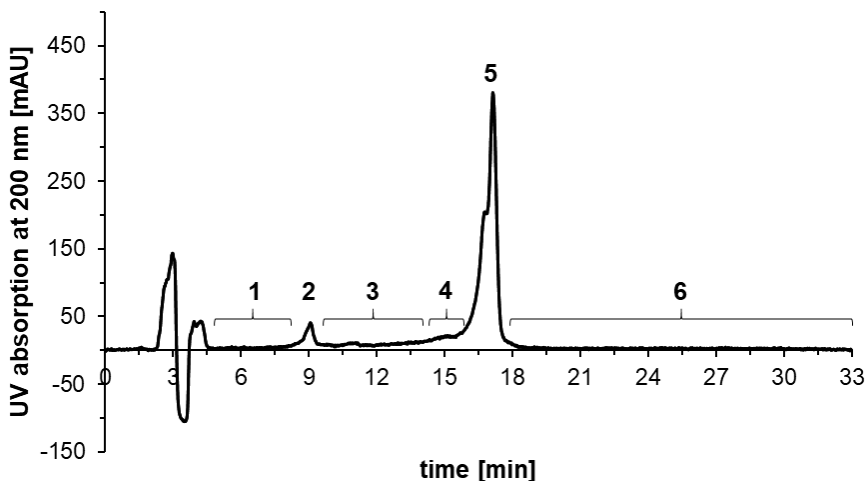
Figure 24: Preparative HPLC-UV chromatogram of SPE fraction F5 at 200 nm subfractionated into six subfractions F5-1 to F5-6 (acquired from Antoniadou et al. (2021)).

Afterwards, bioactivity of each subfraction F5-1 to F5-6 was investigated (Figure 25) as described in section 4.11. Subsequently, subfraction F5-5 had the highest anti-inflammatory potential, which was explained by the inhibiting potential of this fraction on PGE_2 release similarly to that of SPE fraction F5 (Figure 19, section 3.3.2). In contrast, the other five subfractions showed no efficacy. Thus, the chemical composition of fraction F5-5 was analyzed further in order to discover possible bioactive phytochemicals.
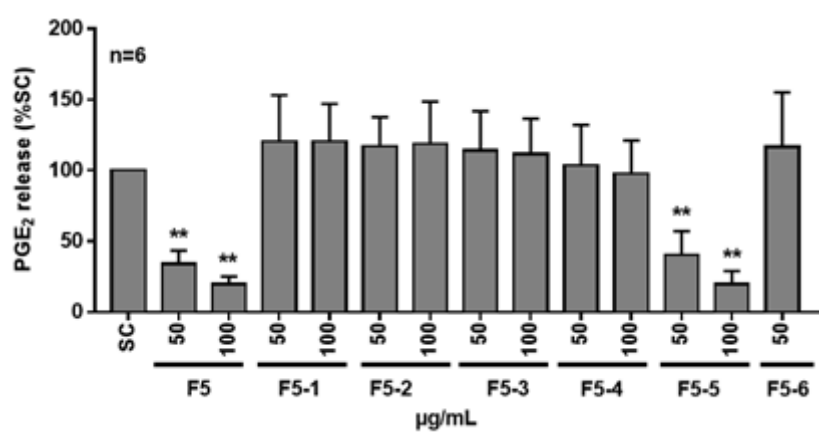
Figure 25: Bioactivity expressed as levels of inhibition of PGE_2 release when treated with subfractions F5-1 to F5-6 diluted in DMSO and exposed to human PBMC. Bioactivity was compared to solvent control (SC, 0.1% DMSO). Asterisks: significant difference between extracts and SC, such as ** $p < 0.01$ (adopted from Antoniadou et al. (2021)).

Subfractionation of fraction F5-5 was performed by means of semi-preparative HPLC-UV as described in section 4.4.4 using the pentafluorophenyl column, which was able to separate aromatic compounds. According to the UV signal at 200 nm, eight subfractions, F5-5-1 to F5-5-8, were collected (Figure 26).
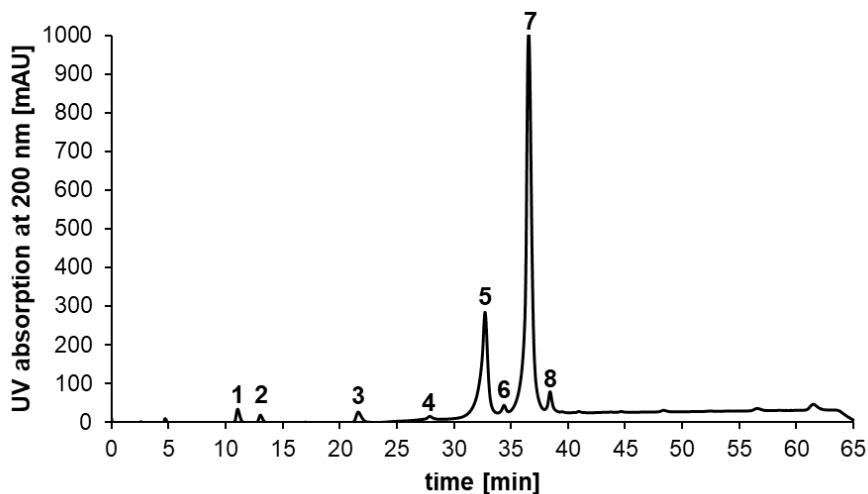
Figure 26: Semi-preparative HPLC-UV chromatogram of fraction F5-5 at 200 nm subfractionated into eight subfractions F5-5-1 to F5-5-8 (acquired from Antoniadou et al. (2021)).

As a result, it was possible to isolate three salicylates 2'-*O*-acetylsalicin (**I**), 3'-*O*-acetylsalicortin (**II**), and 2'-*O*-acetylsalicortin (**III**) and identify them by LC-MS and 1D/2D-NMR spectroscopy. The purity was confirmed by qHNMR and UPLC-ToF-MS. Screening of the compounds by means of UPLC-ToF-MS allowed also determination of their exact masses and molecular formula, through pseudo-molecular ion (parent ions) detection (section 4.4.3.2). Moreover, structure determination was performed by fragmentation of each compound acquiring MS/MS data using QTrap-LC-MS flow injection analysis (FIA) (section 4.7.2.1). In addition, 1D/2D-NMR analysis (section 4.9.4), CD-spectroscopy (section 4.9.3), and monosaccharide determination (section 4.6) were used for the elucidation of the absolute configuration. All NMR data of the identified compounds are displayed in the Appendix section.

3.5.1.1 Structure determination of 2'-*O*-acetylsalicin (I)

Screening of subfraction F5-5-3 by means of UPLC-ESI⁻-ToF-MS gave the parent ion of *m/z* 373.1130 corresponding to [M+HCO₂H-H]⁻ forming a formic acid adduct in the negative ionization mode for 2'-*O*-acetylsalicin (**I**). The MS² spectrum showed the fragments of the compound, such as *m/z* 123 for saligenin and *m/z* 175 for the sugar moiety (Figure 27).
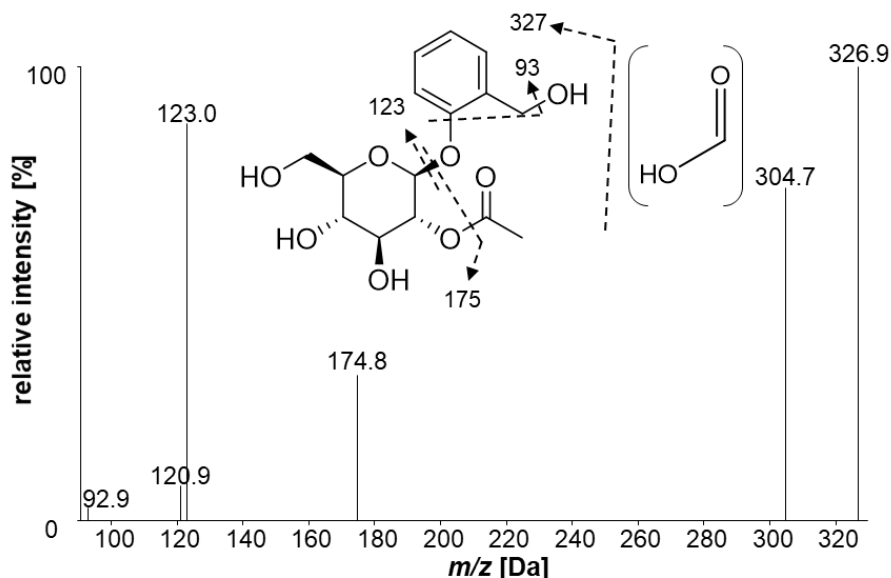
Figure 27: Centroided MS² spectrum of the precursor ion of 2'-*O*-acetylsalicin (**I**) with a formic acid adduct, 373.0 Da, depicting the fragmentation pattern (adopted from Antoniadou et al. (2021)).

Further, for the salicylate structure determination of **I**, 2D-NMR was applied. First, by means of ¹H-NMR (Figure 28 A), signals at δ_H = 7.38 [H-C(3)], 7.21 [H-C(5)], 7.13 [H-C(6)], and 7.03 [H-C(4)] ppm were downshifted, indicating the aromatic ring. According to the ¹³C-NMR (Figure 28 B), the two quaternary carbons C(1) and C(2) were resonating at δ_C = 155.85 and 131.92 ppm, respectively. Further, HO-CH₂ [H-C(7)] moiety holding two overlapped proton signals was detected at δ_H = 4.55 ppm and by HMBC experiment (data not shown) it could be revealed that H-C(7) was attached to the phenol ring at position C(2) (δ_C = 131.92 ppm). The protons revealed a quartet with coupling constants of $^2J_{H,H}$ = 15.46 and 13.60 Hz. The two methylene units, C(6') and C(7), of **I** were shifted closely at δ_C = 62.4 and 59.97 ppm, respectively. However, there were two protons

resonating at δ_H = 3.71 and 3.91 ppm indicative for the methylene protons H$_\alpha$-C(6') and H$_\beta$-C(6') of the sugar, respectively.
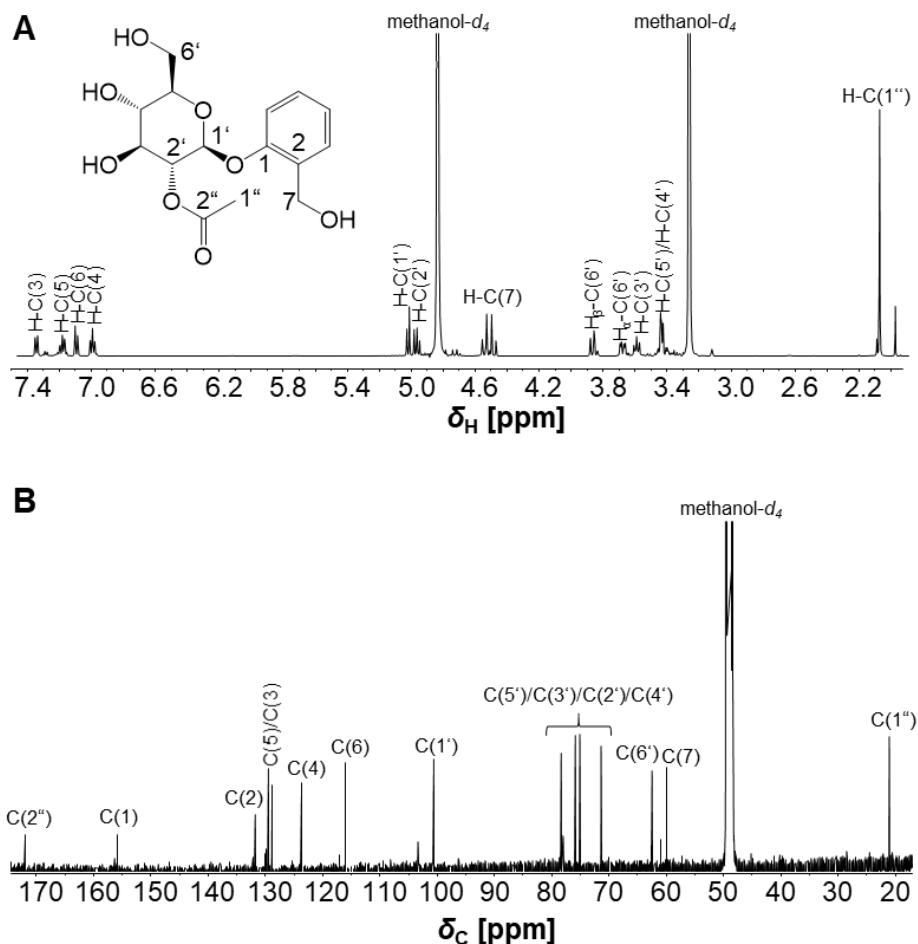
Figure 28: (A) ^{1}H-NMR and **(B)** ^{13}C-NMR of 2'-*O*-acetylsalicin (**I**) with the assigned proton and carbon signals (500.13/125.77 MHz, methanol-d_4).

Furthermore, by means of the HMBC-spectrum the coupling between the doublet of the aliphatic hydrocarbon at δ_H = 5.05 ppm [H-C(1')] was verified, baring a coupling constant of 8.05 Hz, and the aglycone saligenin at position C(1) (155.85 ppm). Moreover, in the HMBC-spectrum it could be revealed the acetylation of salicin at position 2', through coupling of the carbon C(2") (170.55 ppm) of the carboxyl group with the carbonyl proton H-C(1") (2.14 ppm) and H-C(2') of the sugar at δ_H = 5.03 ppm. The spectroscopic data was comparable to that of Reichardt et al. (1992). However, the compound had just a very low purity (40%), which was confirmed by qHNMR analysis, and a second compound structure in the mixture could not be elucidated, due to overlapping or

not visible signals because of very low concentrations. Compound **I** was used together with the impurity for bioactivity determination in section 3.6.

I has been identified previously by NMR analysis in twigs and leaves of *S. lasiandra* and in *S. pseudo-lasiogyne* and *S. glandulosa* twigs (Kim et al. 2015, Reichardt et al. 1992, Yang et al. 2013). Even though the compound was detected in *S. pentandra* leaves performing HPLC/API-ES mass spectrometry, there was no NMR data available in the publications (Ruuhola 2001, Ruuhola and Julkunen-Tiitto 2003, Ruuhola, Julkunen-Tiitto, and Vainiotalo 2003).

3.5.1.2 Structure determination of 3'-*O*-acetylsalicortin (II)

For structure determination of 3'-*O*-acetylsalicortin (**II**) by NMR, first a UPLC-ESI⁻-ToF-MS screening of subfraction F5-5-5 was performed. The chromatogram showed one peak and the extracted spectrum gave the pseudo-molecular ion *m/z* 465.1421 ([M-H]⁻). The mass and the structure of the salicylate **II** was compared with the literature (Kim et al. 2015), and was determined by means of 2D-NMR. The MS^2 spectrum of the precursor ion of the salicylate is depicted in Figure 29 and shows the fragment ion *m/z* 155 corresponding to the 1-hydroxy-6-oxo-2-cyclohexene-1-carboxylic acid (HCH) residue and its hydrolyzed form at *m/z* 137, which were not formed for 2'-*O*-acetylsalicin (**I**) and both fragment ions are characteristic for salicortin derivatives. The ions at *m/z* 405 for salicortin with an absent alcohol group, and *m/z* 83 for the decarboxylated HCH group are also unique for these derivatives. Furthermore, the fragment *m/z* 123 corresponds to saligenin.
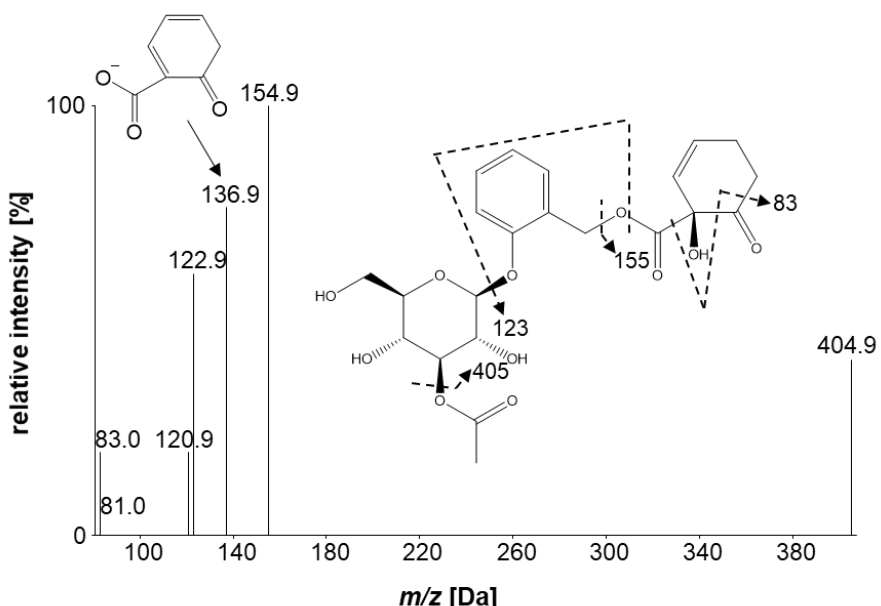
Figure 29: Centroided MS^2 spectrum of the precursor ion of 3'-*O*-acetylsalicortin (**II**), 465.0 Da, depicting the fragmentation pattern (acquired from Antoniadou et al. (2021)).

The identification of **II** by 2D-NMR spectroscopy could shed light into the position of the acetyl group, which was compared to the 2'-*O*-acetylated salicortin (**III**) as described in section 3.5.1.3. In order to keep the two similar acetylsalicortin compounds apart, the HMBC spectra were considered. The acetylation of **II** at position 3' could be distinguished due to the coupling of the proton H-C(3') at 5.08 ppm with the carbon C(2") of the acetyl-moiety at 120.79 ppm (Figure 30). In order to annotate the exact positions, the 2'-*O*-acetylation of compound **III** (see section 3.5.1.3) was taken as reference, since the chemical shift of 5.02 ppm revealed the acetylation at position C-2', in contrast for **II**, the chemical shift of the proton H-C(2') was 3.64 ppm. This indicated that the acetylation was not at position C-2', but at position C-3'. Moreover, this was also confirmed by the coupling of the proton H-C(2') at 3.64 ppm with the anomeric carbon C(1') resonating at 102.03 ppm of **II**, which was not the case for the proton H-C(3') (Figure 30). The NMR signals of the other positions of the phytochemical were confirmed by comparison to **III** (section 3.5.1.3), since they were structurally similar. The purity of 98% was revealed by qHNMR analysis.
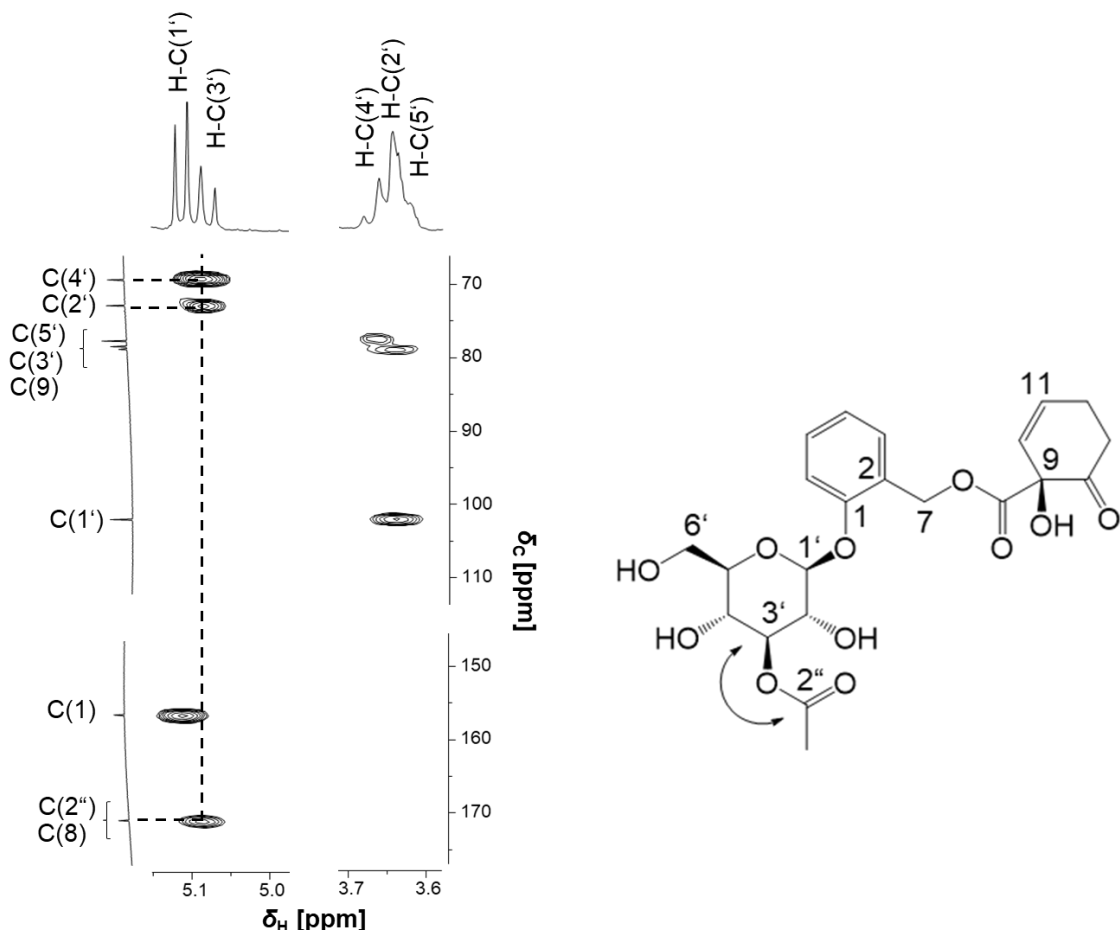
Figure 30: Excerpt (δ_H = 5.2-5.0 ppm and 3.7-3.6 ppm, δ_C = 70-110 ppm and 150-170 ppm) of the HMBC spectrum (500.13/125.77 MHz, acetone-d_6) of **II** to indicate the correlation of the sugar unit at position 3' with the acetyl group at 2".

The compound 3'-*O*-acetylated salicortin (**II**) has been identified previously in *S. pseudo-lasiogyne* and *S. glandulosa* by Kim et al. (2015) and Yang et al. (2013), however, it has never been detected in *S. pentandra* before.

3.5.1.3 Structure determination of 2'-*O*-acetylsalicortin (III)

Further, the salicylate 2'-*O*-acetylsalicortin (**III**) was isolated from subfraction F5-5-7 and identified similarly to **II**. The fragmentation pattern as well as the molecular weight were similar for both, revealing the pseudo-molecular ion of *m/z* 465.1434 ([M-H]⁻) for **III**. The MS/MS spectrum showed the same signals as described for **II** (Figure 29) with the exception that the signal of *m/z* 404.9 was missing. For structure elucidation, first, the chemical shifts obtained from the qHNMR spectrum were observed (Figure 31). Protons of the aromatic ring

(δ_H = 7.0-7.4 ppm) and double bond (δ_H = 6.15 and 5.75 ppm) were resonating at high frequencies. Protons of the ester (ROO-CH$_2$), ether (β-anomeric proton), and alcohol (R-HC-OH) were shifted between 4.90 and 5.10 ppm. At lower frequencies, protons of the sugar residue could be annotated at δ_H = 3.40-3.80 ppm, the methylene protons at δ_H = 2.30-2.90 ppm, and the methyl group at δ_H = 2.07 ppm. The proton signals H-C(5'), H-C(4'), H-C(3), and H-C(5) were overlapping and it was not possible to assign the coupling constants. The methyl group comprising three protons was confirmed by the integral of 3.
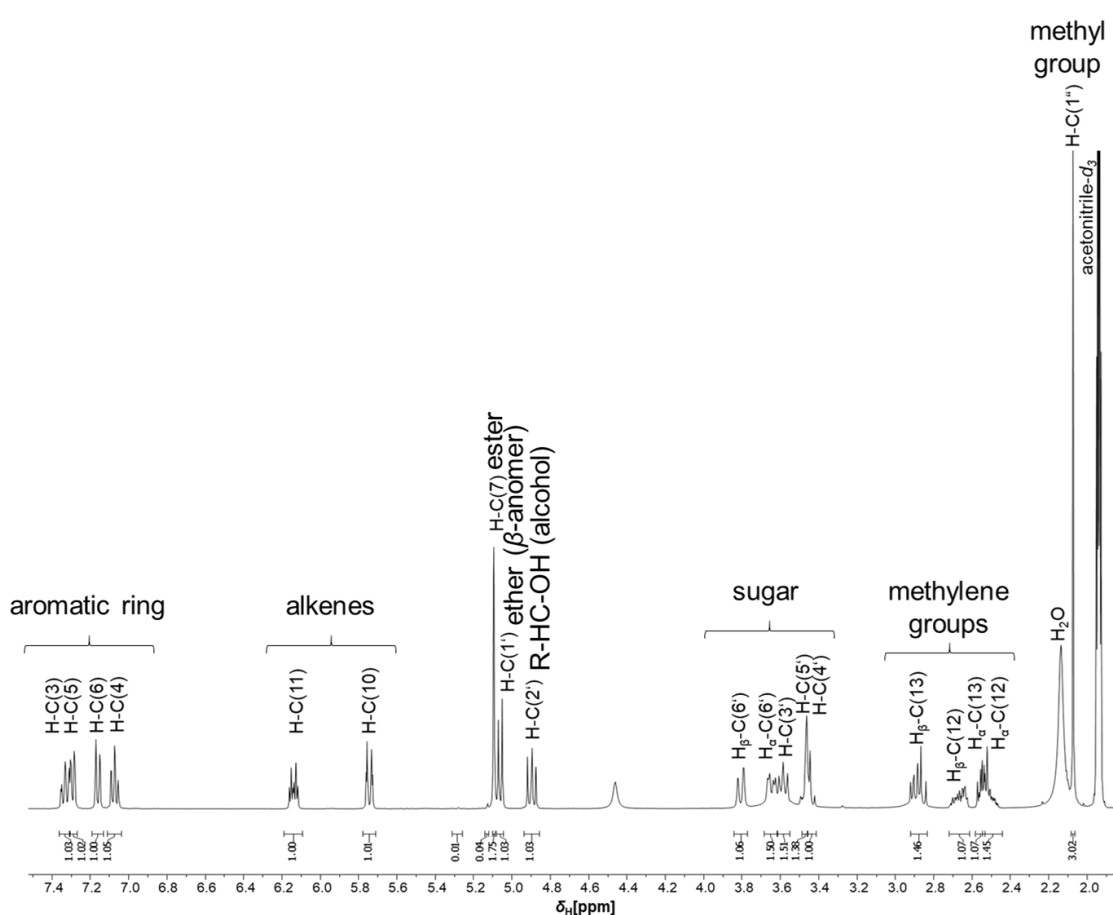
Figure 31: qHNMR spectrum (400.13 MHz, acetonitrile-d_3) of **III** and the respective integrals of the proton signals.

The position of the acetylation of the salicylate was confirmed by the HMBC experiment (Figure 32). Accordingly, the proton H-C(1") observed at 2.07 ppm and the carbon C(2") at 170.20 ppm of the acetyl unit showed homo- and heteronuclear couplings with the proton H-C(2') of the glucose at 5.02 ppm. The anomeric proton H-C(1') of the glucose holding a coupling constant of

$^3J_{C,H} = 7.16$ Hz was resonating at 5.13 ppm and was coupling with the carbon C(1) of the phenol ring at 155.88 ppm. This could also be distinguished using NMR analysis. ^{1}H-NMR signals of the phenol ring were resonating at 7.31 ppm [H-C(3)], 7.05 ppm [H-C(4)], 7.28 ppm [H-C(5)], and 7.21 ppm [H-C(6)]. According to Zanger (1972) it is known that the substitution of an aromatic compound can be determined through the coupling constants, as for example an *ortho* position has coupling constants between 7 and 9 Hz. Thus, it was possible to assign the *ortho*-substitution of the phenol ring of **III** through the coupling constants $^4J_{H,H} = 7.50$ and 8.0 Hz for H-C(4) and H-C(6), respectively. Further, the coupling of the determined phenol ring with the HCH unit could be revealed by the HMBC signals of the protons H-C(7) of the methylene group resonating at 5.18 ppm which were correlating with the quaternary carbon C(2) and the carbonyl carbon C(8) at δ_H = 125.94 and 170.79 ppm, respectively (Figure 32).
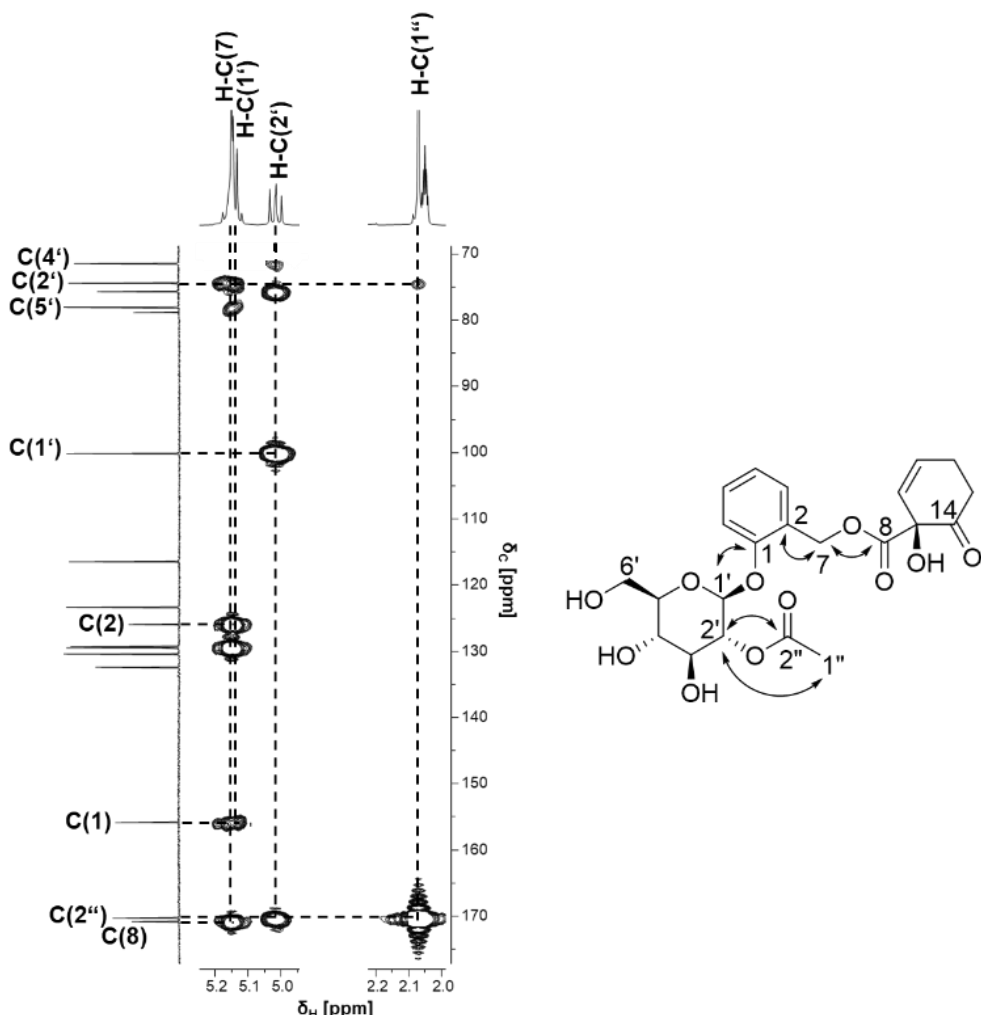
Figure 32: Excerpt (δ_H = 5.2-5.0 ppm and 2.2-2.0 ppm, δ_C = 70-175 ppm) of the HMBC spectrum (500.13/125.77 MHz, acetone-d_6) of **III** indicating the correlation of the sugar unit with the acetyl group and phenol ring, and the correlation between the methylene proton H-C(7) with the phenol ring and the carbonyl carbon C(8) (acquired from Antoniadou et al. (2021)).

The protons of the HCH residue could be assigned through proton, proton-correlations using the COSY experiment. Thereby, the protons H-C(10) and H-C(11) of the double bond, resonating at 5.80 and 6.14 ppm, respectively, were correlating with the methylene protons of H-C(12) and H-C(13) (Figure 33 A). The double bond revealed *cis*-coupling constants of $^3J_{H,H} = 9.82$ and 9.78 Hz for H-C(11) and H-C(10), respectively (Figure 33 B). Both coupling patterns showed doublets of triplets. Moreover, by means of the HMBC spectrum it was possible to assign positions 9 and 14 of the HCH moiety. The chiral carbon C(9) resonating at 78.81 ppm was correlating with H-C(11) of the double bond, and the carbon of the carbonyl group C(14) at 206.20 ppm with the protons H-C(10), H-C(12), and H-C(13). Thus, salicylate 2'-*O*-acetylsalicortin (**III**) from the bioactive fraction F5-5 was fully characterized. The 99% purity of **III** was confirmed by qHNMR (Figure 31).
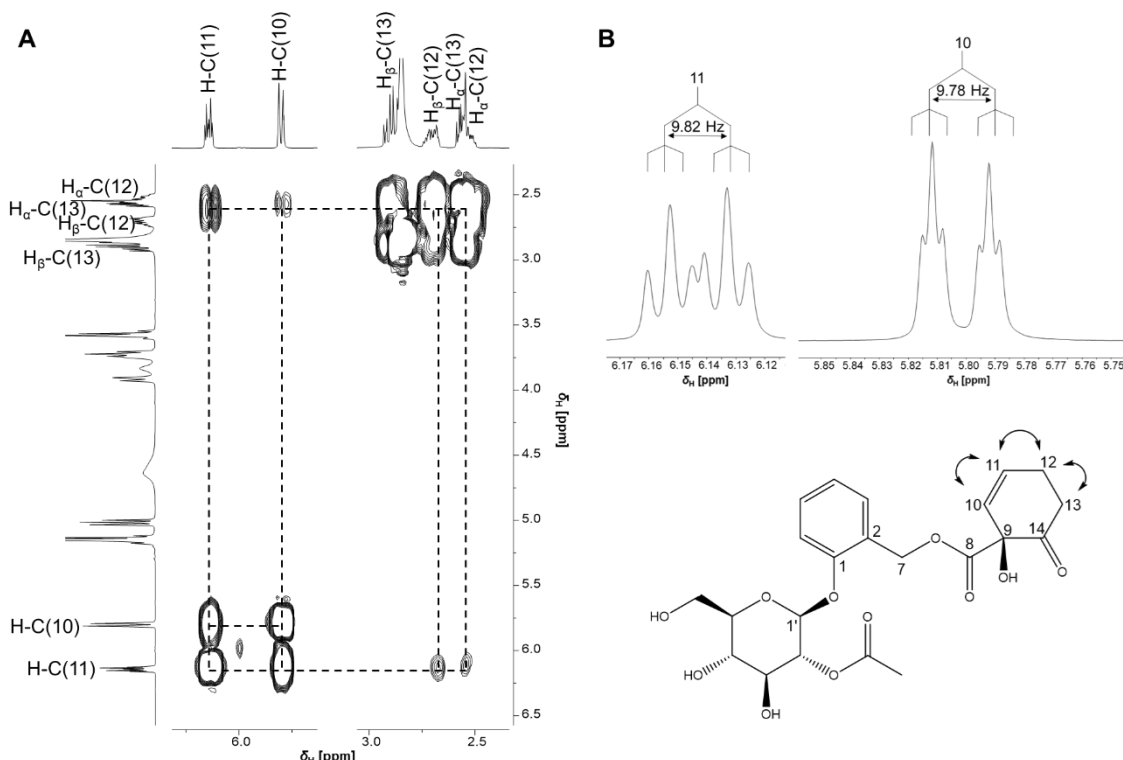
Figure 33: Excerpt ($\delta_H = 6.5$-2.5 ppm) of the COSY spectrum (500.13 MHz, acetone-d_6) of **III** showing **(A)** the correlations between the double bond [H-C(10), H-C(11)] and the two methylene groups [H-C(12), H-C(13)], and **(B)** the *cis*-coupling constants of 9.82 and 9.78 Hz for H-C(11) and H-C(10), respectively, and their doublet of triplets coupling pattern.

In previous studies, **III** has been detected in leaves of *S. pentandra* using HPLC/API-ES mass spectrometry (Ruuhola 2001, Ruuhola and Julkunen-Tiitto

2003, Ruuhola, Julkunen-Tiitto, and Vainiotalo 2003). In the bark and leaves of the same plant, **III** was revealed also by HPLC-UV (Meier et al. 1992). This salicylate was also identified by NMR in *S. lasiandra* (Reichardt et al. 1992), however, the positions C-1 to C-6 of the aromatic ring and the positions C-10 and C-11 of the double bond were incorrectly annotated. Moreover, structure elucidation of **III** from *S. glandulosa* and *S. pseudo-lasogyne* twigs was also performed by NMR (Kim et al. 2015, Yang et al. 2013).

3.5.1.4 Structure determination of cinnamrutinose A (IV) from fraction F5-2

Furthermore, non-bioactive fraction F5-2 was fractionated (Figure 34) in order to identify compounds for comparison with other phytochemicals based on their bioactivity. Moreover, it was important to investigate whether single compounds or the fractions are potent. Therefore, three subfractions F5-2-1 to F5-2-3 were collected and cinnamrutinose A (**IV**) was identified in subfraction F5-2-2 (section 4.4.4). After UPLC-ToF-MS analysis the pseudo-molecular ion of **IV** with a formic acid adduct could be detected at *m/z* 487.1824 ([M+HCO$_2$H-H]$^-$).
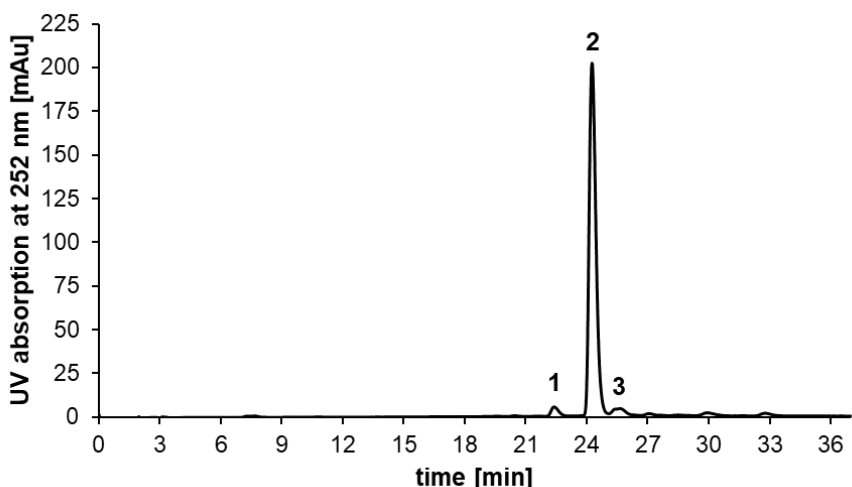
Figure 34: Semi-preparative HPLC-UV chromatogram of fraction F5-2 at 252 nm subfractionated into three subfractions F5-2-1 to F5-2-3 (obtained from Antoniadou et al. (2021)).

Further, the MS/MS spectrum revealed the fragmentation pattern of **IV** (Figure 35). Two sugars were possibly part of the structure, due to the fragment

ions of *m/z* 161 and 163. The masses of sugars were similar, thus it was not possible at this stage to distinguish them. The fragment ion of *m/z* 103 was corresponding to the cinnamoyl residue.
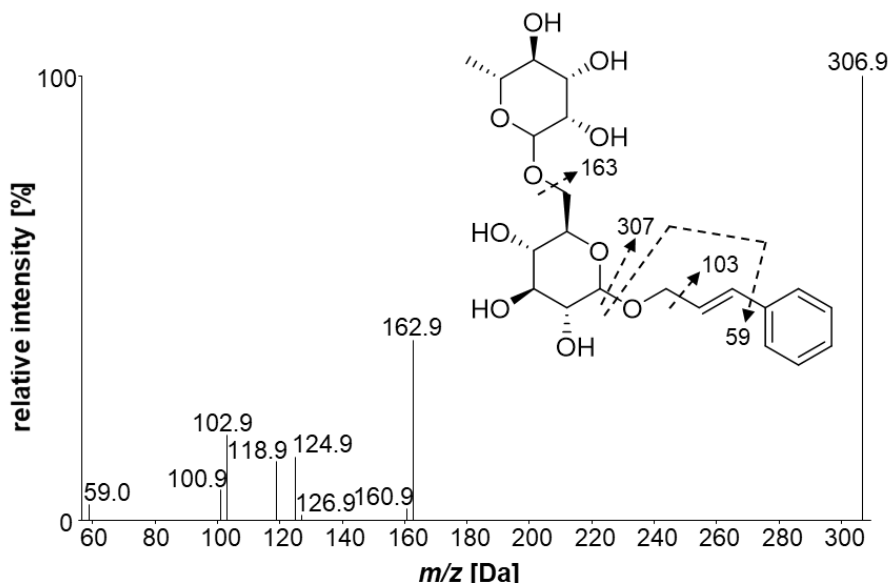
Figure 35: Centroided MS^2 spectrum of the precursor ion of cinnamrutinose A (**IV**), 441.1 Da, depicting the fragmentation pattern (acquired from Antoniadou et al. (2021)).

Two-dimensional NMR analysis confirmed the structure of the non-salicylate **IV**, which data were compared with the literature (Jossang, Jossang, and Bodo 1994). Proton signals of *L*-rhamnose and *D*-glucose were resonating at δ_H 3.14-4.31 ppm. The coupling of the two sugars was determined by the HMBC experiment. Particularly, the proton at position 6' (3.88 ppm) of *D*-glucose was coupling with the carbon at position C(1") (101.66 ppm) of *L*-rhamnose. The carbon C(1') of *D*-glucose, resonating at 102.85 ppm, was coupling with the protons H$_\alpha$-C(1) and H$_\beta$-C(1) at 4.24 and 4.43 ppm, showing that the sugar residue was attached to the cinnamoyl group (Figure 36). The carbon C(1), resonating at 70.11 ppm, was also coupling with the protons of the double bond, H-C(2) at 6.35 ppm and H-C(3) at 6.69 ppm. Coupling constants of $^3J_{\text{H-H}}$ = 16.14 and 15.89 Hz of the alkenes H-C(2) and H-C(3), respectively, revealed the *trans* configuration of the compound. Moreover, the proton positions H-C(5) and H-C(9) as well as H-C(6) and H-C(8) annotated for the phenol ring were mirrored. The precise configuration of the sugars was determined by a derivatization experiment described in section 3.5.4 and 4.5.
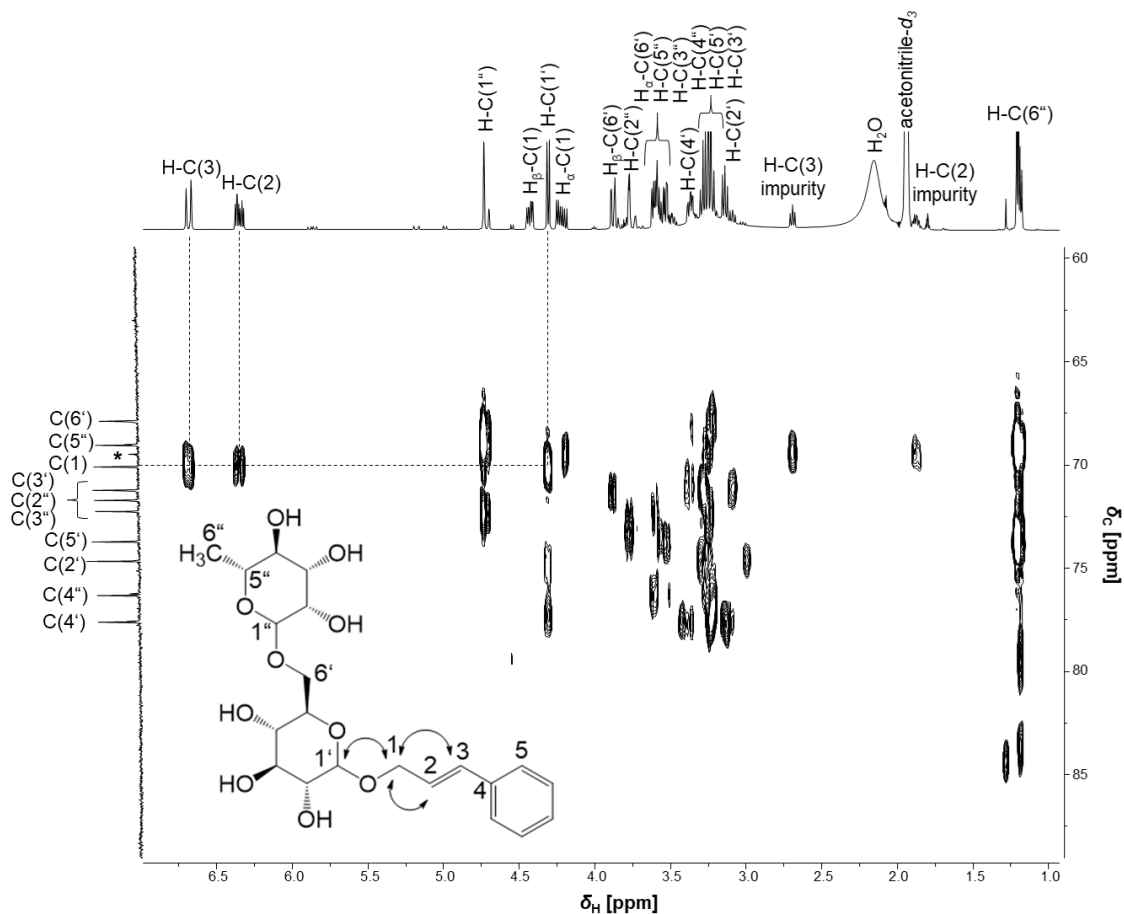
Figure 36: Excerpt (δ_H = 6.5-1.0 ppm and δ_C = 60-85 ppm) of the HMBC spectrum (500.13/125.77 MHz, acetonitrile-d_3) of **IV** showing the correlations between the carbon C(1) of the cinnamoyl group with the protons H-C(2) and H-C(3) of the double bond and the proton H-C(1') of *D*-glucose. Asterisk: carbon coupling to H-C(2) and H-C(3) of the compound of the impurity.

qHNMR analysis revealed a purity of 74% for compound **IV** and a pseudo-molecular ion of *m/z* 489.20 ([M+HCO$_2$H-H]$^-$) could be determined for this impurity by UPLC-ToF-MS analysis. The structure of this second compound in fraction F5-2-2 could be identified only partially due to the low intensity and concentration by means of NMR analysis. The compounds differed by *m/z* 2 and positions C-2 and C-3 of the structures. The HSQC experiment showed that δ_H = 1.89 and 2.71 ppm and δ_C 31.37 and 31.74 ppm for positions C-2 and C-3, respectively, were not part of **IV** and thus indicate that the compound of the impurity holds two methylene groups (Figure 37).
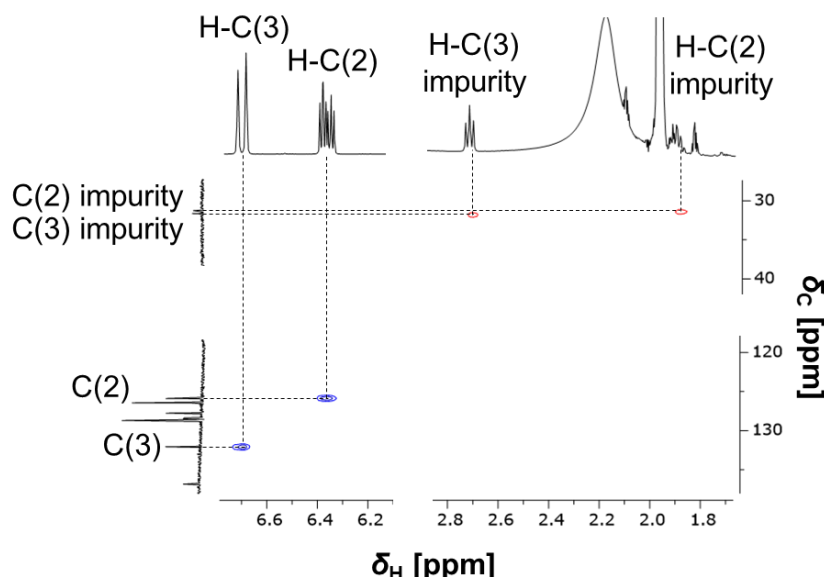
Figure 37: Excerpt of the HSQC spectrum (500.13/125.77 MHz, acetonitrile-d_3) of **IV** showing the carbon-proton correlations of the double bond of **IV** and the two methylene groups of the impurity.

By HMBC, couplings of the assigned positions of the impurity with positions of the phenol ring and sugar could be detected, however, signal overlapping and low sensitivity made the structure elucidation of the compound of the impurity impossible. Taking into account the mass-to-charge ratio obtained from the UPLC-ToF-MS analysis and the detected methylene groups as mentioned above, it was possible to propose the similarity and difference only at positions C-2 and C-3 of the structure to **IV**.

Overall, compound **IV** does not belong to the salicylates and has never been found in *S. pentandra* before. However, it was detected in other species of the *Salicaceae* family, such as in stems of *S. triandra* x *dasyclados* and *P. tremula*, and leaves of *P. euphratica* (Jossang, Jossang, and Bodo 1994, Noleto-Dias et al. 2019, Wei, Rena, and Yang 2015).

3.5.2 SPE fraction F6: subfractionation and compound identification

Next to SPE fraction F5, SPE fraction F6 was purified and single compounds were examined upon their anti-inflammatory potential. By using the preparative phenyl-hexyl column, chromatographic separation by means of HPLC-UV at

200 nm was possible (section 4.4.5). In this way, fractions F6-1 to F6-14 (Figure 38) were collected and lyophilized.
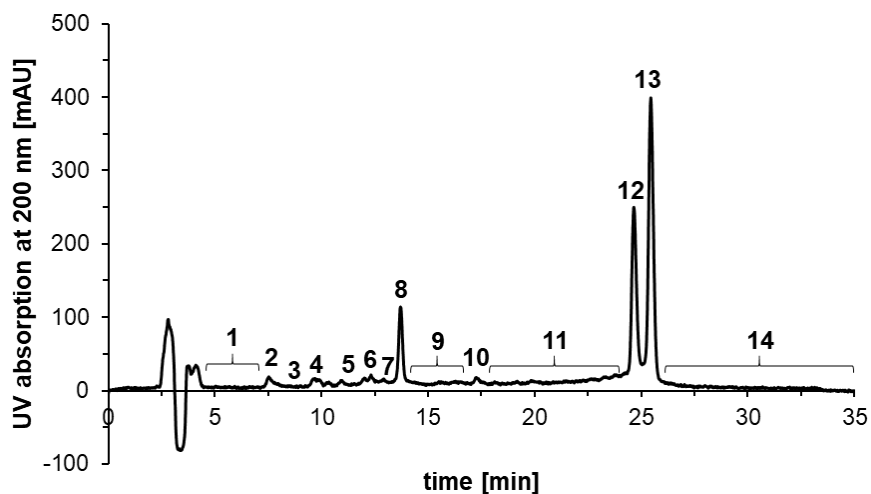
Figure 38: Preparative HPLC-UV chromatogram of SPE fraction F6 at 200 nm subfractionated into fourteen subfractions F6-1 to F6-14 (obtained from Antoniadou et al. (2021)).

Then, the bioactivity of each fraction was determined, showing no inhibitory activity on PGE_2 for any of the fractions (data not shown). However, in order to explain whether single phytochemicals or the total chemical composition of the fractions were potent, fraction F6 was further subfractionated. Thereby, 2',6'-*O*-diacetylsalicortin (**V**) from subfraction F6-12-2 and lasiandrin (**VI**) from F6-13-2 were identified by LC-MS and 2D-NMR analysis, and were used for further investigation of the anti-inflammatory potential.

3.5.2.1 Structure determination of 2',6'-*O*-diacetylsalicortin (V)

Fraction F6-12 was separated chromatographically by means of HPLC-UV on a semi-preparative pentafluorophenyl column, and subfractions F6-12-1 to F6-12-3 were collected (Figure 39). The salicylate 2',6'-*O*-diacetylsalicortin (**V**) was isolated from subfraction F6-12-2 and was analyzed by means of UPLC-ToF-MS revealing a pseudo-molecular ion of *m/z* 507.1551 ([M-H]⁻).
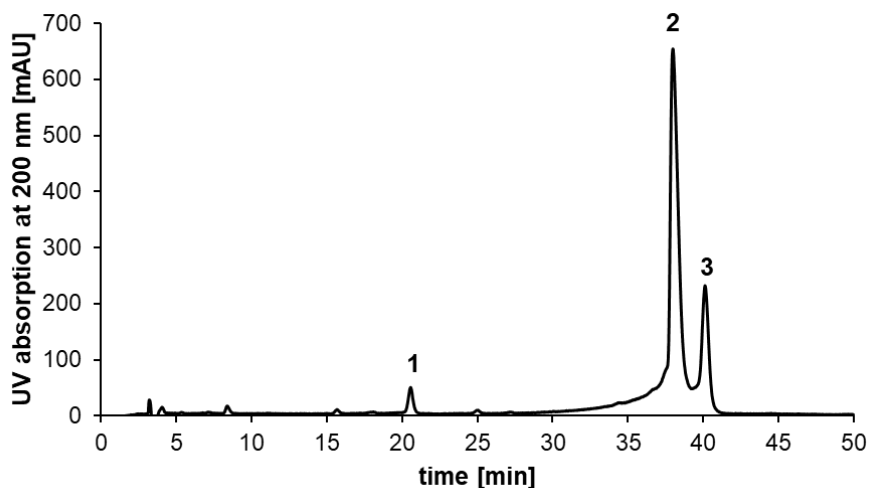
Figure 39: Semi-preparative HPLC-UV chromatogram of fraction F6-12 at 200 nm separated into three subfractions F6-12-1 to F6-12-3 (adopted from Antoniadou et al. (2021)).

The fragmentation pattern showed the same ions as for **III**, however, for **V** the signal intensity of 137 Da, corresponding to the HCH group, was higher. The two compounds differed in the amount of attached acetyl groups. Therefore, **V** contains two acetyl groups instead of one, which are attached to the glucose moiety at positions C-2' and C-6'. This difference, however, could not be distinguished, because of the identical fragmentation patterns. Therefore, the structure of **V** was confirmed by means of 1D/2D-NMR.

Comparison of the ^{1}H-NMR spectra of **V** and **III** showed high spectral similarity (Figure 40). Differences could be detected in the chemical shifts of the glucose at positions H-C(3'), H-C(4'), H-C(5'), and H-C(6'). Slight shifts to higher frequencies were visible for the protons H-C(3') and H-C(5') and at much higher frequencies for the protons H_α-C(6') and H_β-C(6') of the methylene group of **V** in comparison to the chemical shifts of **III**. This effect occurred most likely due to the second acetyl group attached to the sugar at position C-6'. The NMR data for both can be found in the Appendix section.
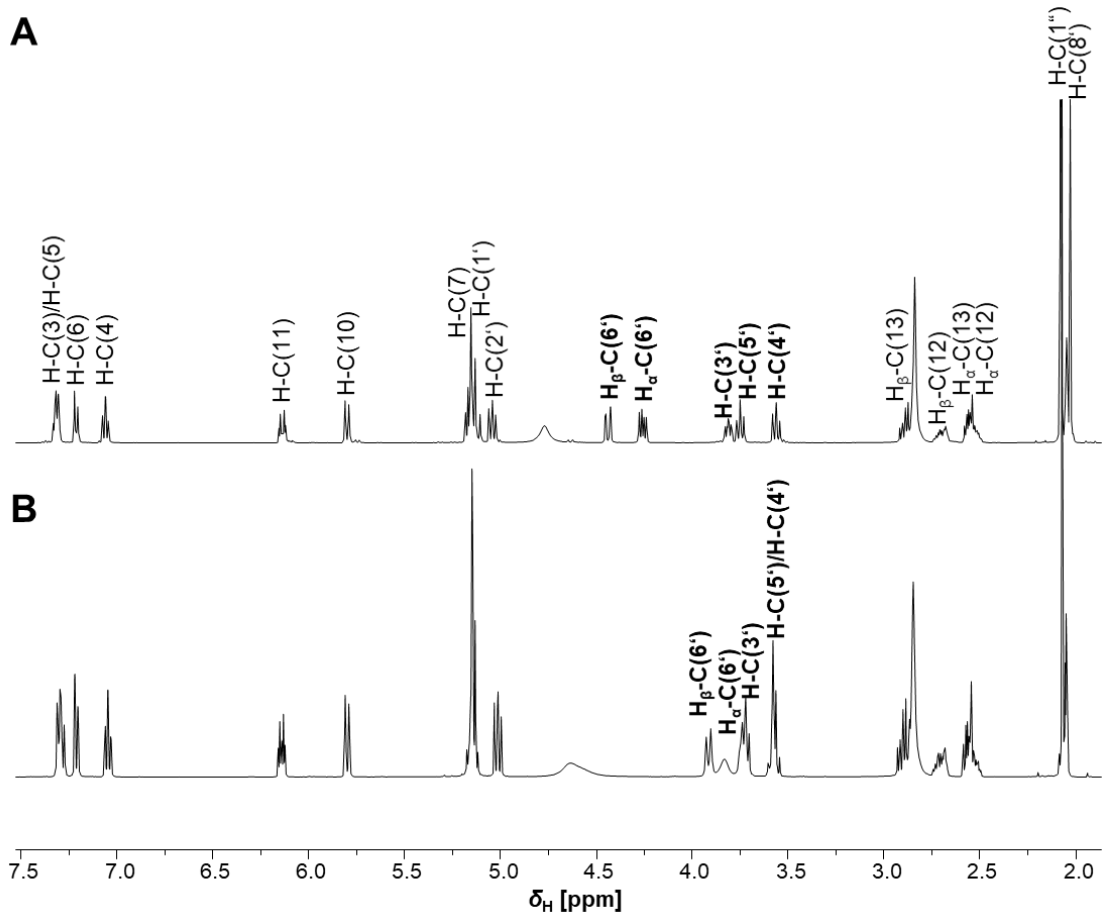
Figure 40: ^{1}H-NMR spectra (500.13 MHz, acetone-d_6) of **(A) V** and **(B) III**. Chemical shift differences of the glucose moiety of both compounds are highlighted in bold.

Observations of the HMBC spectrum revealed heteronuclear couplings of the protons H-C(1") at 2.10 ppm of the methyl group and H-C(8') at 2.03 ppm with the carbons C(2') at 74.26 ppm and C(6') at 64.01 ppm, respectively, which showed that positions C-2' and C-6' of the glucose unit were acetylated (Figure 41). Moreover, by means of the same experiment, it was possible to assign the two carbon signals, C(2") and C(7'), of both carboxyl moieties, resonating at 170.27 ppm and 170.92 ppm. Further, the β-anomeric carbon C(1') annotated at 100.06 ppm and the quaternary carbon C(1) of the phenol ring at 155.78 ppm could be confirmed by mans of the chemical shift (Figure 41).
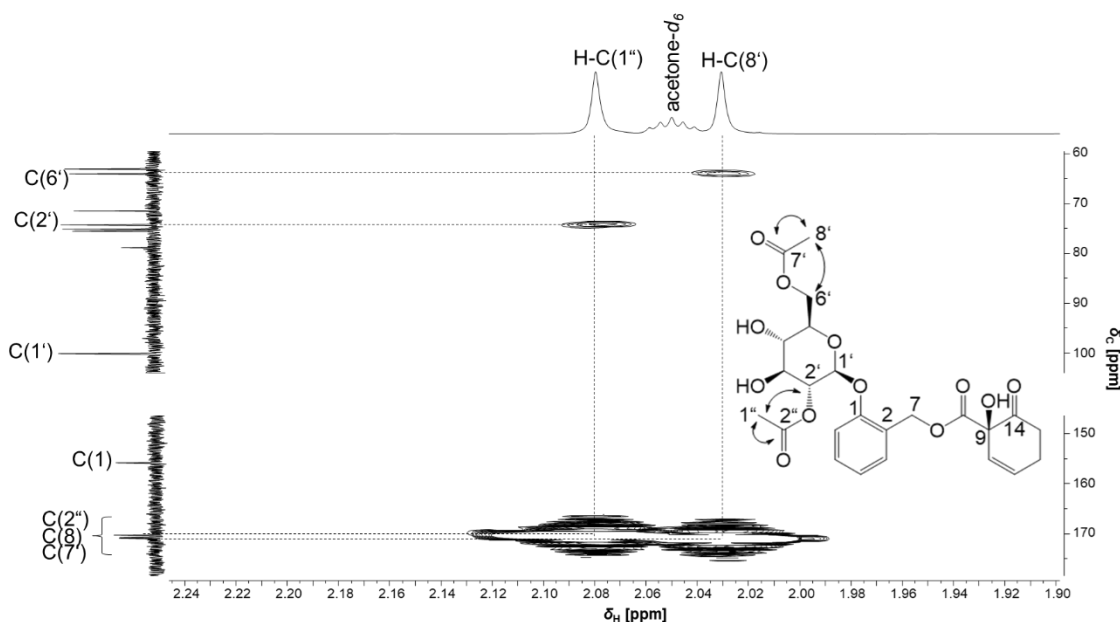
Figure 41: Excerpt (δ_H = 2.24-1.90 ppm, and δ_C = 60-100 ppm and 150-175 ppm) of the HMBC spectrum (500.13/125.77 MHz, acetone-d_6) of **V** showing the correlations of the proton H-C(1") with the carbons C(2') and C(2"), and the proton H-C(8') with the carbons C(6') and C(7').

The salicylate **V** has been previously identified in *S. pseudo-lasiogyne* and *S. glandulosa* twigs by NMR, to which data of the spectra of the current work were comparable (Kim et al. 2015, Yang et al. 2013). Even though it has been found also in leaves of *S. pentandra*, the authors detected the compound tentatively by HPLC/API-ES mass spectrometry and did not describe any structure elucidation by NMR spectroscopy (Ruuhola and Julkunen-Tiitto 2003, Ruuhola, Julkunen-Tiitto, and Vainiotalo 2003). The current study verified that bark of *S. pentandra* contains **V**, which purity was 96% by means of qHNMR analysis.

3.5.2.2 Structure determination of lasiandrin (VI)

Furthermore, lasiandrin (**VI**) was isolated from subfraction F6-13-2. Therefore, fraction F6-13 was purified by means of HPLC-UV and semi-preparative pentafluorophenyl column (Figure 42). Following the UV signal at 200 nm, fractions F6-13-1 and F6-13-2 were collected and freeze-dried. The pseudo-molecular ion of compound **VI** detected in fraction F6-13-2 revealed *m/z* 603.1762 ([M-H]⁻), which was analyzed by UPLC-ToF-MS.
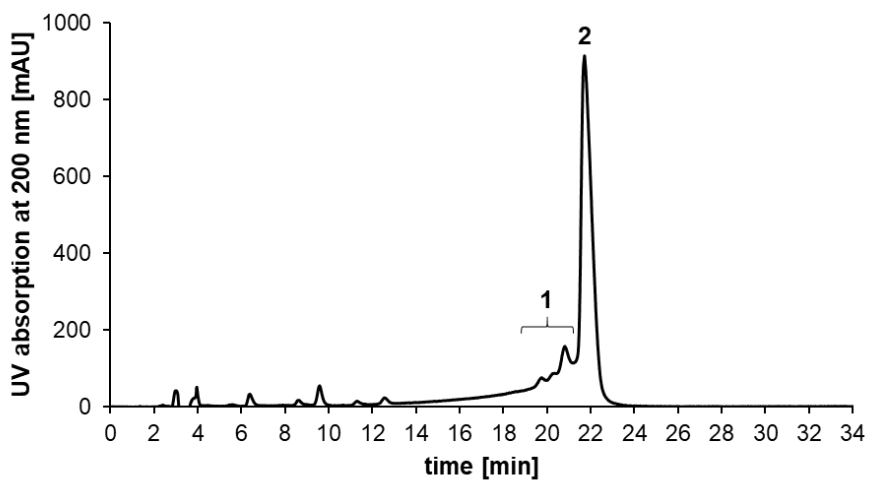
Figure 42: Semi-preparative HPLC-UV chromatogram of fraction F6-13 at 200 nm subfractionated into two subfractions F6-13-1 and F6-13-2 (adopted from Antoniadou et al. (2021)).

For structure elucidation first the MS/MS spectrum was analyzed (Figure 43). The fragment ion *m/z* 465 corresponds to the compound without one HCH group. The fragment ions of *m/z* 155 and 137 were assigned to the HCH groups and their hydrolyzed form, respectively, whereas the ion of *m/z* 111 corresponded to the HCH moiety without the carboxyl group.
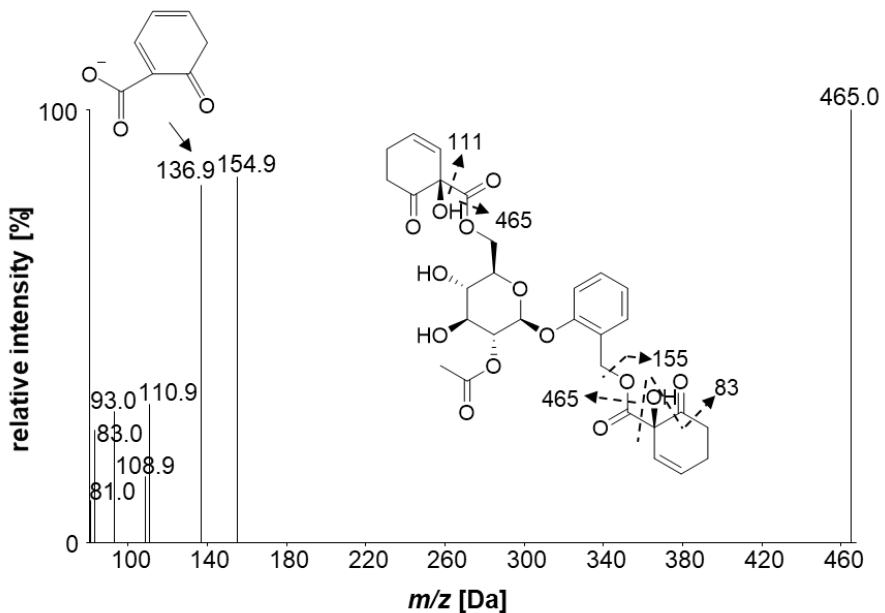
Figure 43: Centroided MS^2 spectrum of the precursor ion of lasiandrin (**VI**), 603.2 Da, depicting the fragmentation pattern (acquired from Antoniadou et al. (2021)).

Furthermore, through ^{1}H-NMR and ^{13}C-NMR spectroscopy similar chemical shifts of **V** and **VI** could be revealed. However, instead of an acetyl group at position 6' of the sugar moiety as it is the case for **V**, a second HCH group was attached to the compound **VI**. According to the COSY spectrum, two HCH groups were detected showing correlations between the protons H-C(10), H-C(11), and H-C(12) resonating at 5.80, 6.14, and 2.46 - 2.54/2.62 - 2.73 ppm, respectively, and correlations among the protons H-C(10'), H-C(11'), and H-C(12') at 5.75, 6.08, and 2.46 - 2.54/2.62 - 2.73 ppm, respectively (Figure 44). The double bonds were *cis* configured and were confirmed by the coupling constants of approximately $^3J_{\text{H-H}}$ = 9.80 Hz for both (section 3.5.1.3). Moreover, protons of H$_\alpha$-C(12/12')/H$_\beta$-C(12/12') (2.46 - 2.54/2.62 - 2.73 ppm) and H$_\alpha$-C(13/13')/H$_\beta$-C(13/13') (2.53 - 2.59/ 2.84 - 2.92 ppm) were overlapping, hampering the assignment of the chemical shifts of each HCH position. On the other side, positions C-10/C-10' and C-11/C-11', as well as the chiral carbons C(9) and C(9') could be assigned as described further.
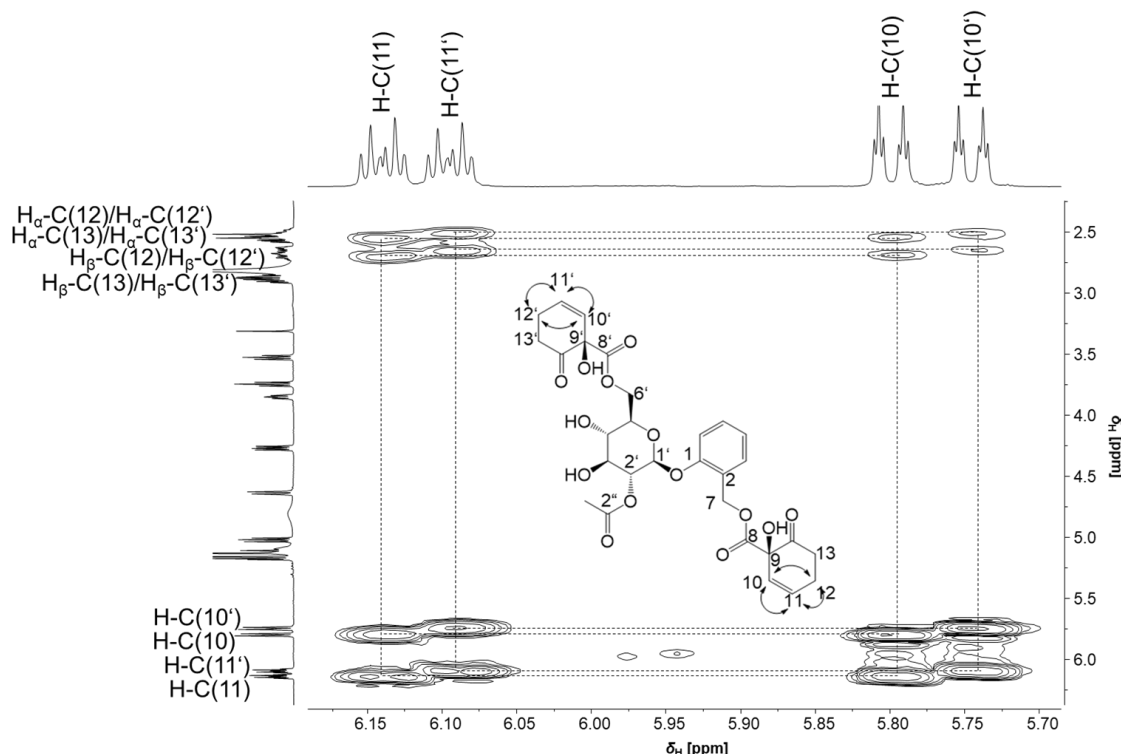
Figure 44: Excerpt (δ_H = 6.50-2.50 ppm) of the COSY spectrum (600.13 MHz, acetone-d_6) of **VI** showing the correlations between the double bonds [H-C(10)/H-C(11), and H-C(10')/H-C(11')] and the methylene groups [H-C(12)/H-C(12')].

Carbons C(8) and C(8') resonating at 170.78 ppm, and C(14) and C(14') at 206.18 ppm were also overlapping (Figure 45 A and B). Carbons C(9)/C(9') were showing two peaks (Figure 45 A), which is also revealing overlapping of carbon signals. Moreover, carbon-proton correlations were revealed for the HCH groups by means of the HMBC experiment. Hereby, the carbon C(9') resonating at 78.82 ppm was correlating with the proton H-C(11') and H-C(12') at 6.08 and 2.46-2.54 ppm, respectively. Moreover, couplings between the carbon C(8') (170.78 ppm) of the carboxyl group and the protons H_α-C(6') (4.27 ppm) and H_β-C(6') (4.64 ppm) of the glucose indicated the binding of one of the two HCH groups to position C-6' (Figure 45 B). In contrast, correlations of C(8) (170.78 ppm) with H-C(7) and H-C(7) showed the attachment of a second HCH unit at position C-7. Further, the carbons C(14') and C(14) of the carbonyl groups, overlapping with the carbons of the solvent acetone-d_6, were resonating at 206.18 ppm and were correlating with the protons H-C(12')/H-C(13') and H-C(12)/H-C(13), respectively. It was also possible to confirm the acetylation at position C-2' of the glucose of **VI** by the coupling of the carbon C(2") (170.27 ppm) with the protons H-C(2') (74.26 ppm) and H-C(1") (21.01 ppm) (Figure 45 B).
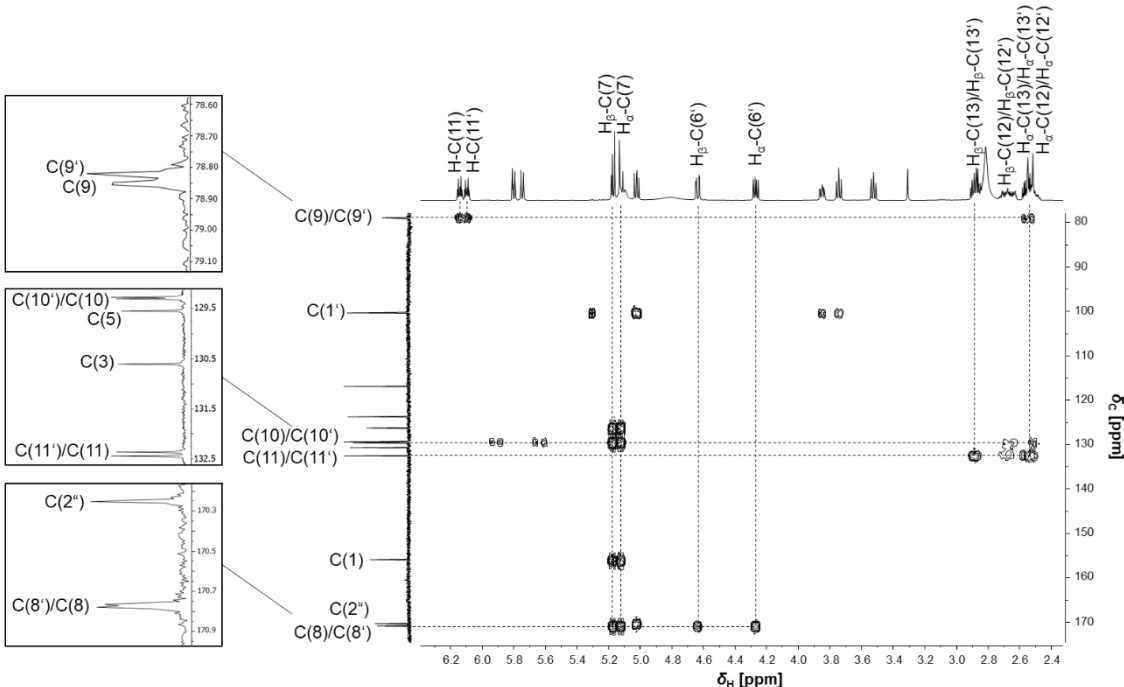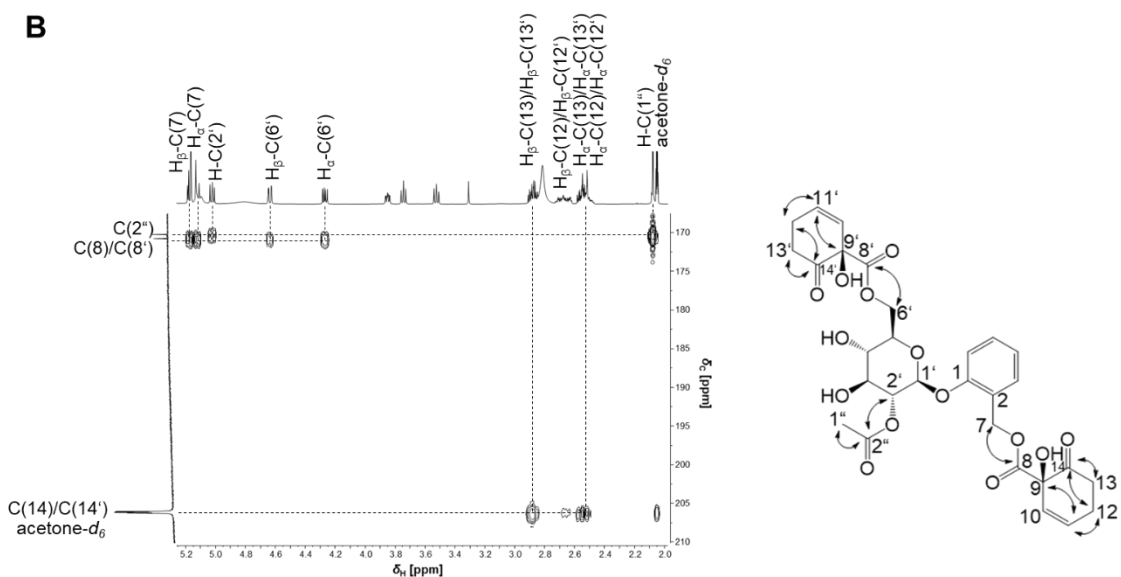
Figure 45: Excerpts, **(A)** δ_H = 6.2-2.4 ppm and δ_C = 80-175 ppm, **(B)** δ_H = 5.2-2.0 ppm and δ_C = 170-210 ppm, of the HMBC spectrum (600.13/150.90 MHz, acetone-d_6) of **VI**, showing couplings of the HCH groups with the glucose and the phenol ring, and couplings between the glucose and the acetyl group.

Consequently, protons H-C(6') of the methylene groups of **V** ($^3J_{H-H}$ = 11.75/2.30 Hz, 11.95/6.24 Hz) and **VI** ($^3J_{H-H}$ = 11.80/2.06 Hz, 11.82/6.79 Hz; Figure 46) hold an acetyl or HCH residue attached at position C-6' by a carboxyl unit and showed similar coupling constants in comparison to **II** ($^3J_{H-H}$ = 11.35/2.99 Hz, 11.39/3.69 Hz), which contains an alcohol at the same

position of the glucose. All have coupling patterns of doublet of doublets (dd) showing coupling of the proton H_C-C(6') with two non-equivalent hydrogens H_α-C(6') and H_β-C(6') with different coupling constants (Figure 46).
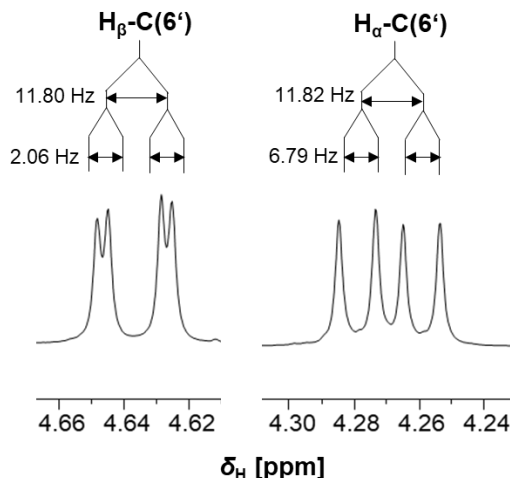
Figure 46: Coupling pattern of proton signals, H_α-C(6') and H_β-C(6'), into doublet of doublets (dd) and of their assigned coupling constants (J [Hz]) extracted from the ^{1}H-NMR (600.13 MHz, acetone-d_6) of compound **VI**.

The purity of 98% of the isolated salicylate **VI** was determined by qHNMR analysis. In previous studies the phytochemical was tentatively identified in leaves of *S. pentandra* using HPLC/API-ES mass spectrometry without any NMR data available (Ruuhola and Julkunen-Tiitto 2003). Moreover, Keefover-Ring et al. (2014) also detected the compound tentatively in *P. tremula* by UHPLC-ESI-ToF comparing the *m/z* values and MS/MS fragments using the MassLynx software with other species containing this compound. Structure elucidation of **VI** from *S. lasiandra* using NMR spectroscopy was postulated by Reichardt et al. (1992). However, the assignment of the chemical positions of the phenol ring and double bonds were not correlating with this previous publication. Therefore, the current study provided complete structure elucidation by LC-MS/MS and NMR analysis for the first time. Moreover, it was possible to confirm that *S. pentandra* bark material consists of **VI**, besides other identified compounds, which has not been described in literature before.

3.5.3 SPE fraction F7: subfractionation and compound isolation

Furthermore, besides SPE fractions F5 and F6, SPE fraction F7 was purified by preparative HPLC-UV and single compounds were investigated upon their bioactivity, which will be compared to compounds from SPE fractions F5 and F6. Therefore, a phenyl-hexyl column was used for chromatographic separation and monitoring the effluent at 200 nm enabled collecting fourteen fractions, F7-1 to F7-14 (Figure 47) as described in section 4.4.6.
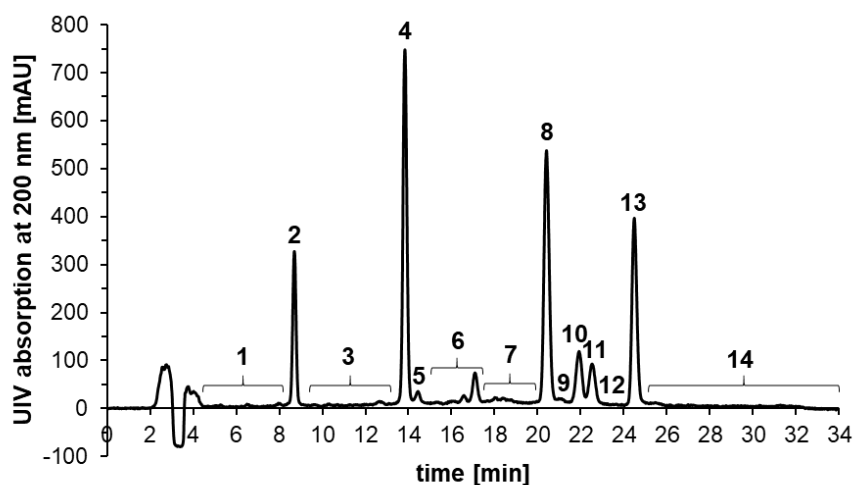
Figure 47: Preparative HPLC-UV chromatogram of fraction F7 at 200 nm subfractionated into fourteen subfractions F7-1 to F7-14 (adopted from Antoniadou et al. (2021)).

For each fraction, the activity against PGE_2 release was determined, showing no anti-inflammatory effect (data not shown). Nevertheless, fractions F7-8 and F7-4 were purified by semi-preparative HPLC-UV to check if single phytochemicals in the fractions may be bioactive and concentration dependent. The compound quantity, as well as the chemical composition in a fraction are factors which can influence bioactivity. Thus, it was possible to identify tremulacin (**VII**) from subfraction F7-8-4 and a mixture of three compounds from subfraction F7-4-6 containing 2'-*O*-acetylsalicortin (**III**) and two diastereomeric compounds of *β*-D-glucopyranoside, 2-[[[(1-hydroxy-6,6-dihydroxy-2-cyclohexen-1-yl)-dihydroxy]-oxy]methyl]phenyl, 2-acetate (**VIII**). The diastereomers were novel and were only possible to be detected by an acetalization reaction, but single compounds could not be purified from this mixture in the current work due to the lability of the

phytochemicals. The structures of the compounds **VII** and **VIII** were elucidated by LC-MS/MS and NMR analysis.

3.5.3.1 Structure determination of tremulacin (VII)

For the purification and structure elucidation of tremulacin (**VII**), fraction F7-8 was separated chromatographically by semi-preparative HPLC-UV equipped with a pentafluorophenyl column into five subfractions F7-8-1 to F7-8-5 (Figure 48). Salicylate **VII** with pseudo-molecular ion of m/z 527.1586 ([M-H]$^-$) was detected in subfraction F7-8-4, which was determined by UPLC-ToF-MS.
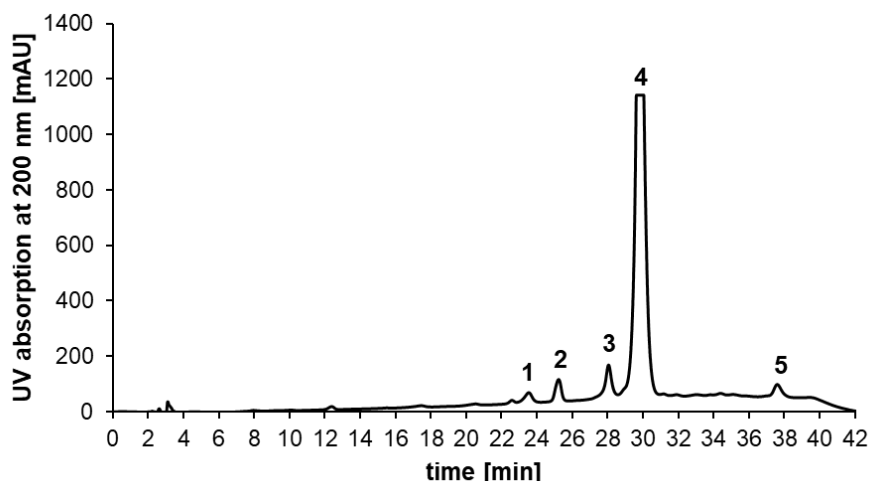
Figure 48: Semi-preparative HPLC-UV chromatogram of fraction F7-8 at 200 nm subfractionated into five subfractions F7-8-1 to F7-8-5 (obtained from Antoniadou et al. (2021)).

Moreover, the fragmentation pattern of the compound was investigated by LC-MS/MS, showing the signal of the fragment ion m/z 121 and 123 corresponding to the benzoic acid and saligenin of **VII**, respectively (Figure 49). Unique for **VII** is also the fragment ion m/z 77, indicating the benzene ring, which signal was not detected in any other MS/MS spectrum of the identified salicylates of the current work.
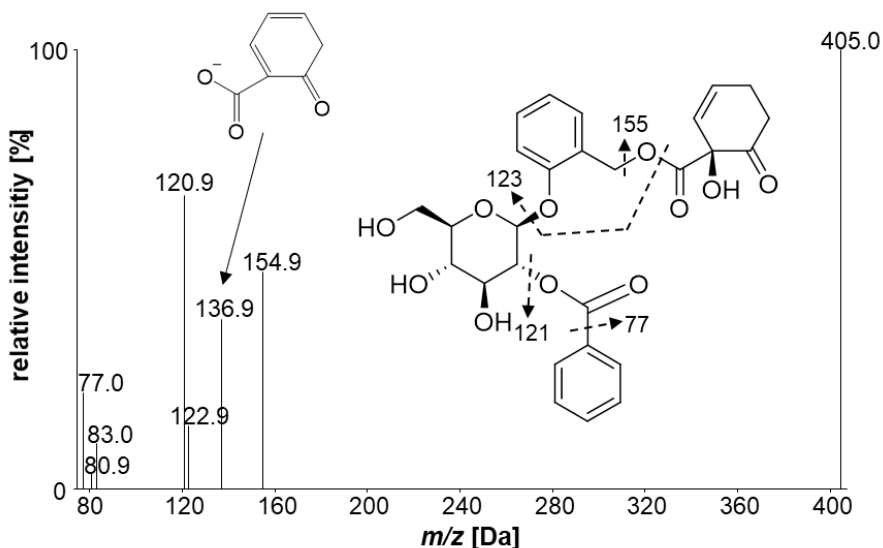
Figure 49: Centroided MS^2 spectrum of the precursor ion of tremulacin (**VII**), 527.0 Da, depicting the fragmentation pattern (adopted from Antoniadou et al. (2021)).

1D/2D-NMR spectroscopy elucidated the attachment of the benzoic acid moiety at the glucose at position C-2'. Observations of the ^{1}H-NMR and HSQC spectra revealed chemical shifts ($δ_H$) at higher frequencies for the benzoic acid unit in comparison to the phenol ring, which was bound to position C-1' of the glucose (Figure 50). The symmetrical aromatic ring led to the detection of similar chemical shifts of $δ_H$ = 7.98 ppm and $δ_C$ = 129.34 ppm for positions C-3" and C-7". Mirroring due to the symmetry occurred also for positions C-4" and C-6" resonating at $δ_H$ = 7.52 ppm and $δ_C$ = 128.68 ppm. In the same benzene ring, position C-5" could be annotated at $δ_H$ = 7.65 ppm and $δ_C$ = 133.38 ppm.
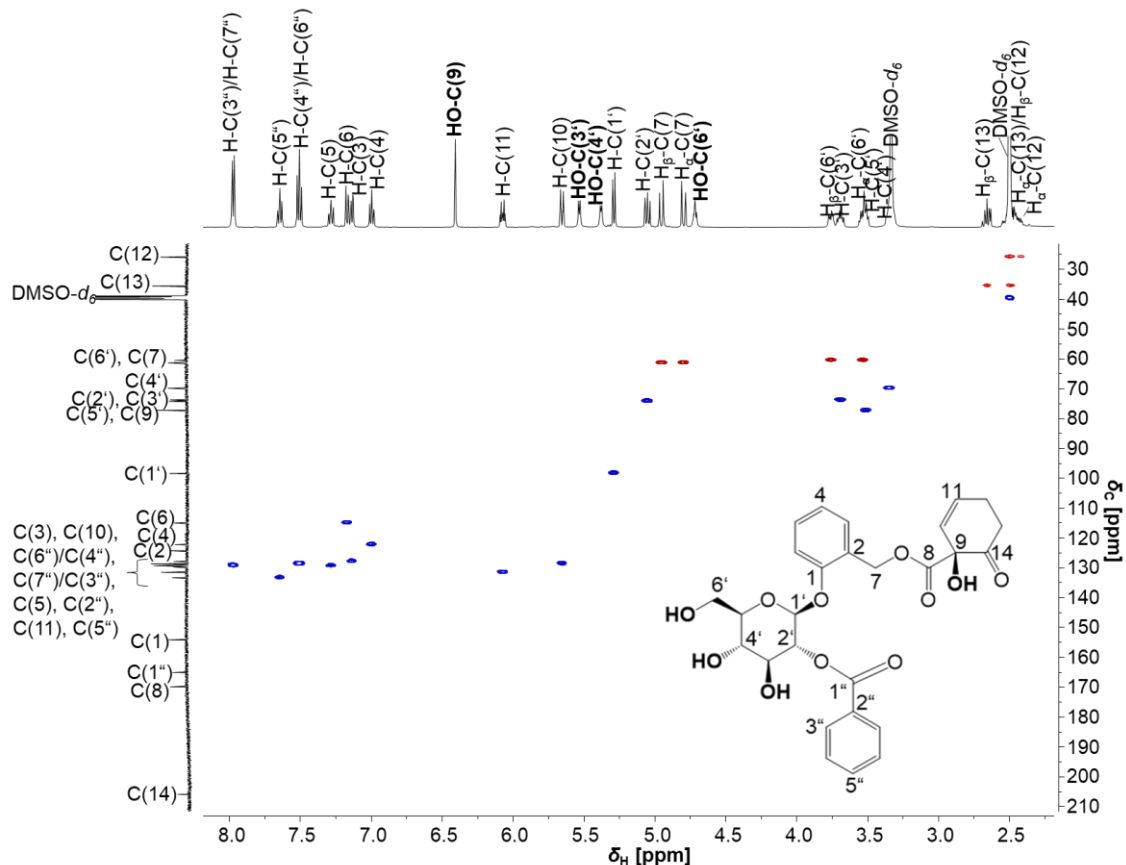
Figure 50: HSQC spectrum [500.13/125.77 MHz, dimethyl sulfoxide-d_6 (DMSO-d_6)] of **VII** depicting the carbons and their corresponding protons, as well as the alcohol groups (bold) of HO-C(3'), HO-C(4'), HO-C(6'), and HO-C(9), resonating at δ_H = 5.53, 5.38, 4.72, and 6.41 ppm, respectively.

Due to the use of dimethyl sulfoxide-d_6 as solvent, it was possible to distinguish the alcohol groups at positions C-3', C-4', C-6', and C-9 of the ^{1}H-NMR, resonating at 5.53 [HO-C(3')], 5.38 [HO-C(4')], 4.72 [HO-C(6')], and 6.41 ppm [HO-C(9)]. In particular, the chemical shifts of the alcohols could be detected through heteronuclear and homonuclear correlations observed in the HMBC experiment (Figure 51). The alcohol group HO-C(9) (6.41 ppm) was correlating with the carbons C(14) (205.92 ppm), C(8) (169.86 ppm), C(10) (128.66 ppm), and C(9) (77.35 ppm). Even though the carbon-proton correlations of HO-C(3') and HO-C(4') were weaker, it was possible to interpret both chemical shifts within the sugar moiety. Both alcohols were coupling with C(4') (69.89 ppm), C(2') (73.79 ppm), and C(3') (74.29 ppm), however, unique was the correlation between OH-C(4') and C(5') (77.28 ppm). Hereby, HO-C(3') and HO-C(4') were resonating at δ_H = 5.53 and 5.38 ppm, respectively. The alcohol at position C-6' [HO-C(6')] was detected at 4.72 ppm through the coupling with the carbons C(5')

(77.28 ppm) and C(6') (60.54 ppm). Chemical shifts of the alcohol positions and correlation analysis allowed correct assignment of carbons and protons of the sugar moiety and further structure elucidation.
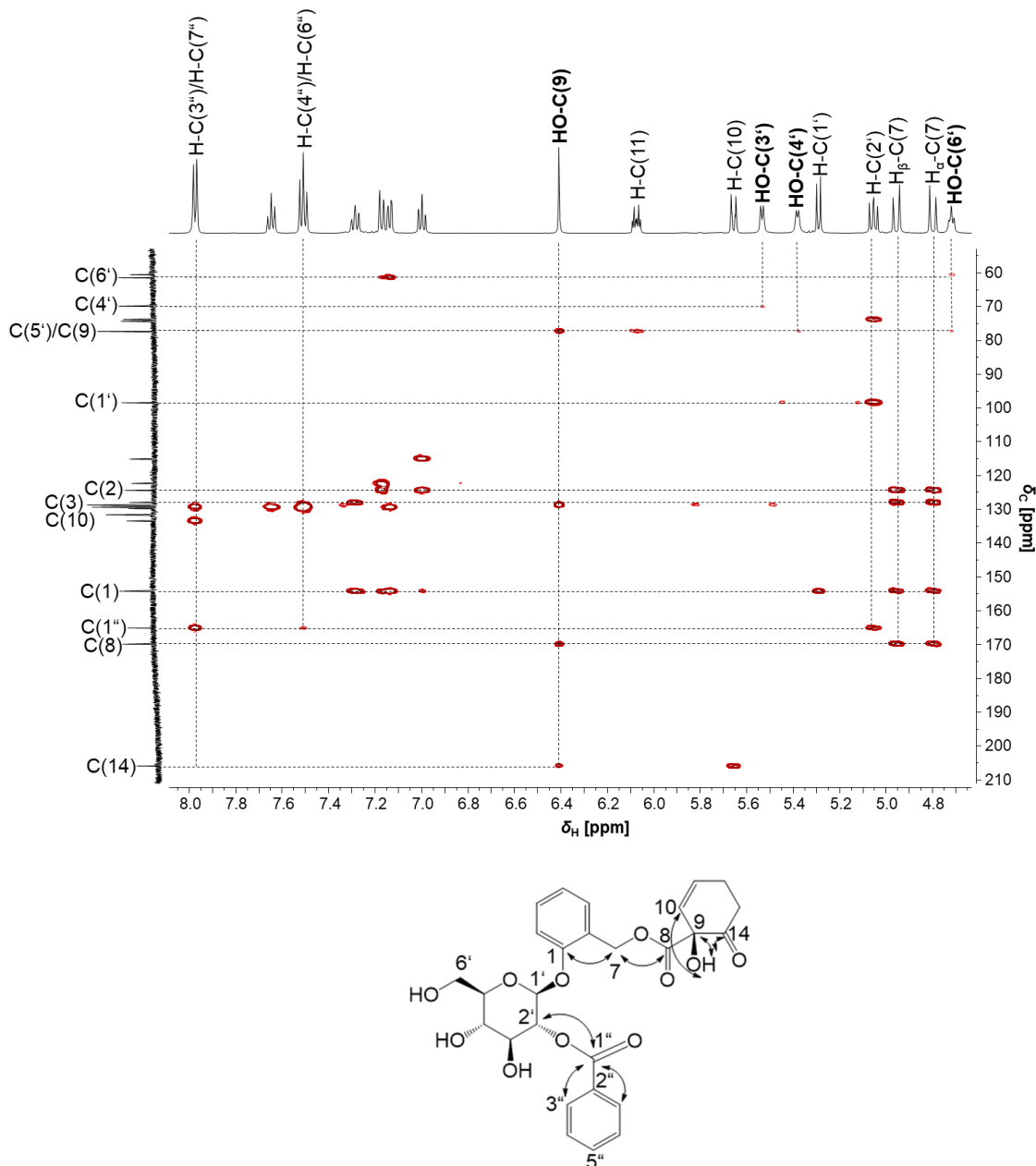
Figure 51: Excerpt (δ_H = 8.0-4.7 ppm and δ_C = 60-210 ppm) of the HMBC spectrum (500.13/125.77 MHz, dimethyl sulfoxide-d_6) of **VII** showing correlations between the glucose and the benzoic acid, and the phenol ring with the HCH group.

Furthermore, the binding of the benzoic acid to the glucose at position C-2' was elucidated by means of the HMBC experiment (Figure 51). In particular, proton

H-C(2') of the glucose residue at δ_H = 5.05 ppm was correlating with the carbon C(1") (165.10 ppm) of the carboxyl group of the benzoic acid. Protons H-C(3")/H-C(7") of the benzene ring were coupling with the carbons C(5") and C(1"), resonating at δ_C = 133.38 ppm and 165.10 ppm, respectively. Whereas, the protons H-C(4")/H-C(6") were coupling with C(2") (129.74 ppm). In this way, assignment of the benzoic acid positions and the coupling with the glucose could be interpreted.

After structure elucidation of **VII**, qHNMR analysis revealed purity of 99%. The compound has been tentatively identified in the methanol extract of *S. repens and S. pentandra* leaves (Ruuhola, Julkunen-Tiitto, and Vainiotalo 2003). In 1971, **VII** was isolated and crystallized from *P. tremuloides* bark (Pearl and Darling 1971). Later, the compound could be identified by NMR spectroscopy after isolation from *S. chaenomeloides* leaves (Mizuno et al. 1991), *S. glandulosa* twigs (Kim et al. 2015), *S. tetrasperma Roxb* leaves (El-Shazly, El-Sayed, and Fikrey 2012), *S. acutifolia* bark (Zapesochnaya et al. 2002), and from a *Salix* cortex ethanol (70%) drug extract (Knuth et al. 2013). In the current work, however, identification of the compound was performed using a combination of various analytical methods for the activity-guided fractionation, such as LC-MS/MS, 2D-NMR, and further other explained in the next sections. Moreover, it was possible to yield the compound in high purity, which was not annotated in the previous publications and is significant for the bioactivity determination.

3.5.3.2 Structure determination of compounds from fraction F7-4

Next to fraction F7-8, fraction F7-4 was subfractionated into six subfractions, F7-4-1 to F7-4-6, by means of semi-preparative HPLC-UV at 200 nm on a pentafluorophenyl column (Figure 52) as described in section 4.4.6. After collection and lyophilization of subfraction F7-4-6 (at 33.5 min) and re-injection into the device, compound in the fraction eluted at the same time, however, this time the peak intensity at 16.5 min (fraction F7-4-1) was higher than that at 33.5 min (data not shown). This led to the hypothesis that phytochemicals within fraction F7-4 are instable and are most probably undergoing a chemical reaction or isomerizing over time, since F7-4-1 and F7-4-6 showed similar pseudo-molecular ions of *m/z* 465.14 by means of UPLC-ToF-MS.
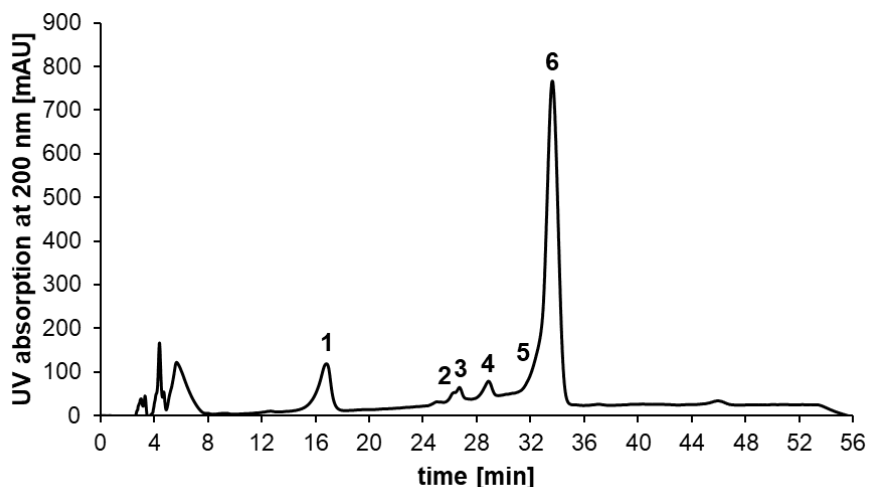
Figure 52: Semi-preparative HPLC-UV chromatogram of fraction F7-4 at 200 nm subfractionated into six subfractions F7-4-1 to F7-4-6 (obtained from Antoniadou et al. (2021)).

In order to investigate the stability of the fraction during incubation, two samples were prepared using F7-4 diluted in methanol and in water. Right after dilution without incubation, samples were analyzed by means of analytical HPLC-UV using a pentafluorophenyl column. Further, they were incubated for 24 h at room temperature and analyzed again. Thereafter, the samples were left on the bench over three days, and investigated another time. All runs were compared to previously purified 2'-*O*-acetylsalicortin (**III**) (Figure 53 C), which had the same parent ion of *m/z* 465.14 ([M-H]⁻) similarly to fractions F7-4-1 and F7-4-6. The chromatograms before and after incubation in comparison to **III** are depicted in Figure 53. As described for the semi-preparative runs, peak signals of F7-4-1 in methanol (Figure 53 A) or water (Figure 53 B) were higher after 24 h than before incubation, which is indicative for instability of contained compounds in the fraction. The same peak pattern and intensities could be observed after three days, showing that a possible chemical reaction had stopped after some time. The fraction in water showed an additional peak of fraction F7-4-7, but the peak of fraction F7-4-6 disappeared in comparison to the fractions of the sample diluted in methanol. The higher peak intensity of subfraction F7-4-1 in the incubation experiment (Figure 53 A and B) as well as in the semi-preparative run (Figure 52) clearly indicated that it contained the salicylate **III**.
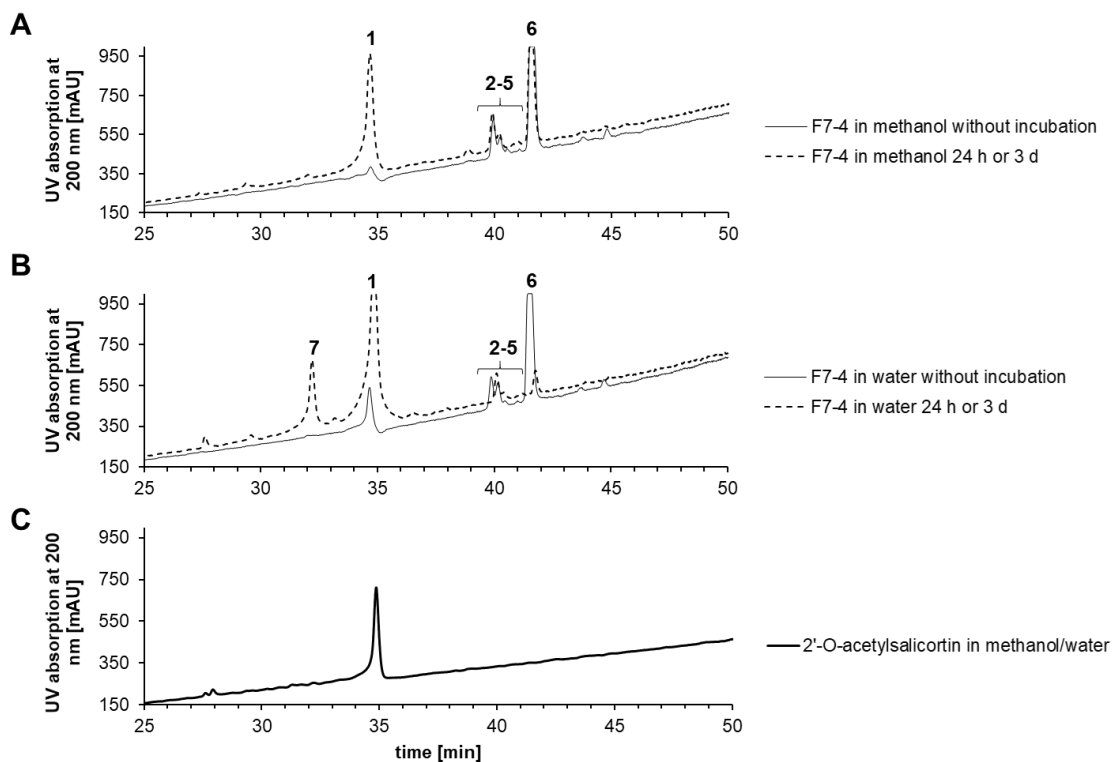
Figure 53: Excerpts of the analytical HPLC-UV chromatograms (25-50 min of the 75 min run) of the incubation experiment of fraction F7-4. F7-4 diluted in **(A)** methanol and **(B)** water before and after incubation for 24 h or 3 days at room temperature in comparison to **(C)** 2'-*O*-acetylsalicortin (**III**) in methanol/water (v/v, 1/1) (modified from Antoniadou et al. (2021)).

First NMR spectroscopic analysis of F7-4-6 in methanol-d_6 showed for each proton and carbon three signals corresponding to three different compounds (A, B, and C). For instance, in the COSY experiment protons H-C(10 A) (5.78 ppm), H-C(10 B) (5.59 ppm), H-C(10 C) (5.53 ppm) were correlating with H-C(11 A) (6.17 ppm), H-C(11 B) (6.02 ppm), H-C(11 C) (5.98 ppm), respectively (Figure 54). Weak signals in the ^{1}H-NMR and ^{13}C-NMR spectra of compound A revealed that they are matching the signals of **III**. Therefore, compound A was confirmed to be **III** (F7-4-1). Furthermore, proton-proton correlations were similar for compounds B and C with just slight δ_H shifting to higher frequencies for C. It was also possible to show correlations between H-C(11 C), H-C(12 C) and H-C(13 C). However, proton chemical shifts of positions C-12 and C-13 were not possible to keep apart, due to overlapping of the signals. Correlation were possible though and the patterns were assigned as multiplets (m).

Overall comparison between the chemical shifts of the compounds by HSQC experiment showed that compounds B and C had a high similarity with compound

A, and signals were mostly shifting to similar frequencies (data not shown). It was, however, not possible to detect just one compound in fraction F7-4-6, because of the labile character of the compound over time in the NMR reaction tube.
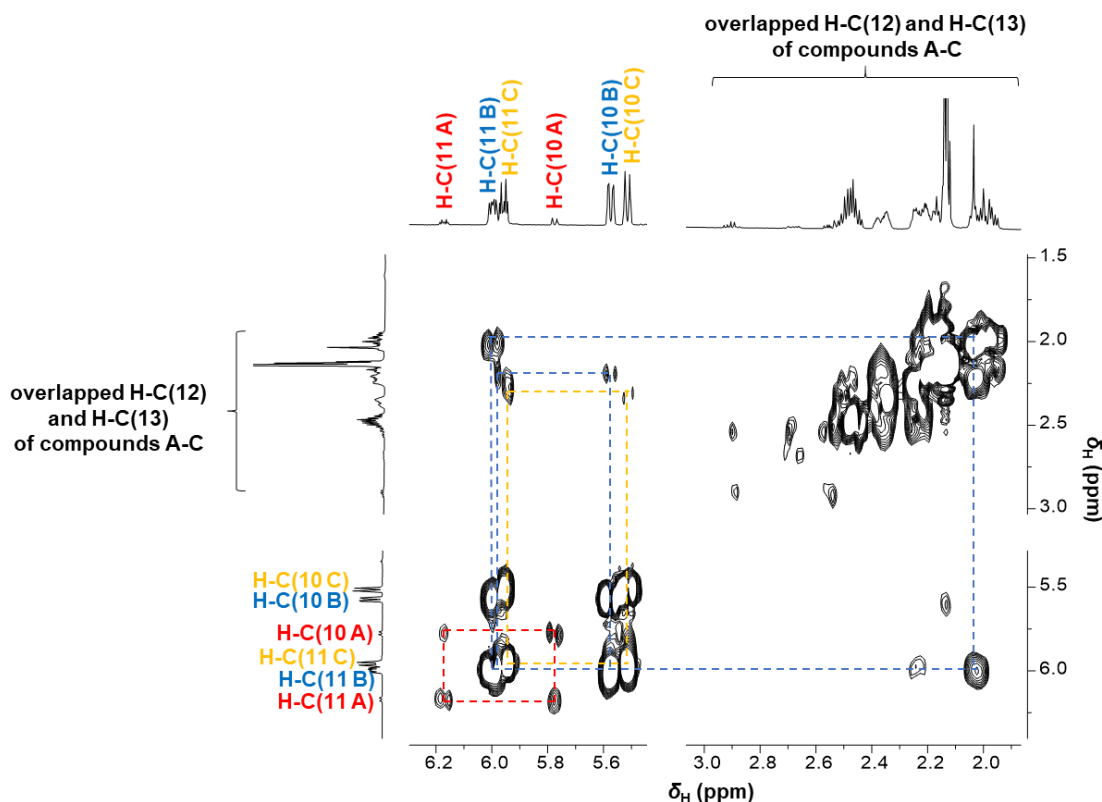
Figure 54: Excerpt (δ_H = 1.5-6.2 ppm) of the COSY spectrum (500.13 MHz, methanol-d_4) of fraction F7-4-6 containing 2'-O-acetylsalicortin (**III**, compound A, red) and compounds B (blue) and C (yellow). The spectrum shows correlations of the protons H-C(10) with H-C(11), and H-C(11) with H-C(12) and H-C(13) (modified from Antoniadou et al. (2021)).

Unique signals for the salicylates appeared at 104.47 and 111.81 ppm showing no correlations with any proton in the HSQC spectrum (data not shown). This led to the hypothesis that position C-14 was quaternary, due to no correlation with a proton. The carbon C(14) signal of the carbonyl group belonging to the HCH moiety was resonating at approximately 206 ppm for all the previously identified salicylates (**II**, **III**, **V-VII**). However, in the case of compounds B and C, the signals of position C-14 could not be assigned at this same chemical shift, but at δ_C = 104.47 and 111.81 ppm, respectively. In the HMBC spectrum, couplings between these unique carbon signals with the protons H-C(10 B), H-C(10 C), H-C(12), and H-C(13) could be revealed, confirming that C(14 B) and C(14 C)

were resonating at 104.47 and 111.81 ppm, respectively (Figure 55). Further, the chemical shifts of the carbons suggested that two alcohol groups were attached to this position. Even though the overall chemical shifts were quite similar to that of **III**, differences could be observed mostly in the shifts of positions of the carbon signals within the HCH moiety. Thus, C(9 B) was resonating at 86.75 ppm and C(9 C) at higher frequencies of 77.33 ppm (Figure 55). All other positions of compounds B and C were similar to A.
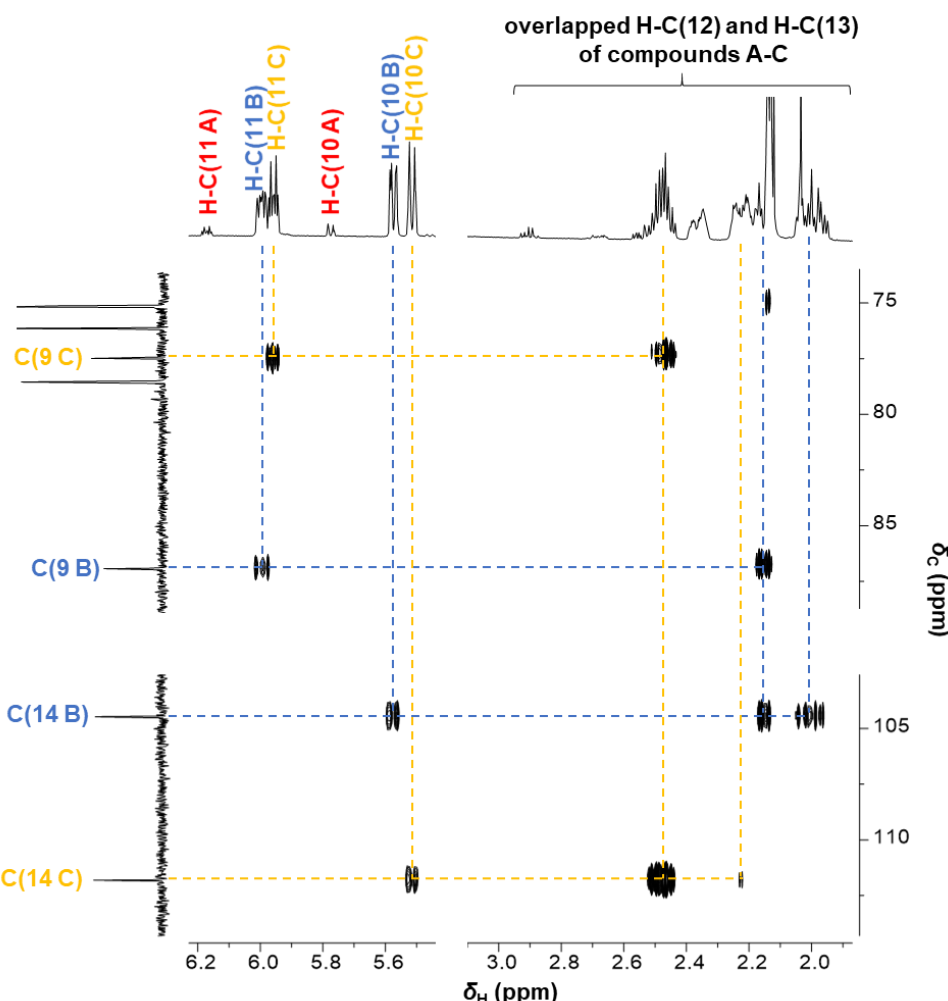
Figure 55: Excerpt (δ_H = 2.0-6.2 ppm, δ_C = 75-110 ppm) of the HMBC spectrum (500.13/125.77 MHz, methanol-d_4) of fraction F7-4-6 containing 2'-*O*-acetylsalicortin (**III**, compound A, red) and compounds B (blue) and C (yellow). The spectrum shows correlations of the carbons C(9 B,C) and C(14 B,C) with the protons H-C(11 B,C) and H-C(10 B,C), respectively, as well as with H-C(12 B,C) and H-C(13 B,C) (adopted from Antoniadou et al. (2021)).

Further, it was investigated whether two alcohol groups were indeed bound to the quaternary carbon C(14). Due to the previously detected similar mass-to-charge ratios by means of UPLC-ToF-MS, it was supposed that in-source fragmentation led to water (18.01 Da) fragment ion cleavage and thus to misannotation of the compounds showing similar parent ions for all three compounds. Therefore, confirmation of the phytochemical structures of compounds B and C was performed by an acetalization reaction to protect the geminal diol group at position C-14. Particularly, fraction F7-4 was incubated in anhydrous acetone using the catalyst p-toluenesulfonic acid, which can lead to acetalization of the alcohol groups of the compounds. Consequently, for the verification of the experiment, the samples were analyzed by means of UPLC-ToF-MS (ESI$^-$) (Figure 56 A-C).

The chromatogram showed three peaks with the same mass-to-charge ratios of m/z 465.14 in fraction F7-4 (Figure 56 A). One of the peaks represent the parent ion of compound A (**III**). The peak at 4.88 min correspond to the parent ion (m/z 563.21) of the acetalized compounds B and C comprising two acetal groups and a geminal diol group at position C-14 (Figure 56 B and C). By means of fragmentation, the chemical structure of novel β-D-glucopyranoside, 2-[[[(1-hydroxy-6,6-dihydroxy-2-cyclo-hexen-1-yl)dihydroxy]oxy]methyl]phenyl, 2-acetate (**VIII**) could be confirmed with a mass of 484.16 Da ([M], not visible in the mass spectra) (Figure 56 D). Acetal groups were bound to alcohols at positions C-3' and C-4' of the sugar moiety, as well as at position C-14 or both positions C-9 and C-14, forming ethers (Figure 56 D). Particularly, in the extracted MS^2 spectrum, the characteristic signal at m/z 316.95 (Figure 56 C) was assigned to the phenol ring attached to the HCH moiety containing one acetal group bound to the alcohols of positions C-9 and/or C-14. The MS^1 fragmentation pattern revealed the acetalized compound **VIII** with a formic acid adduct at m/z 609.22 (Figure 56 B). **VIII** with water cleavage could be assigned holding a pseudo-molecular ion of m/z 465.14 ([M-H$_2$O-H]$^-$), which formed also a formic acid adduct at m/z 511.15 ([M+HCO$_2$H-H$_2$O-H]$^-$).
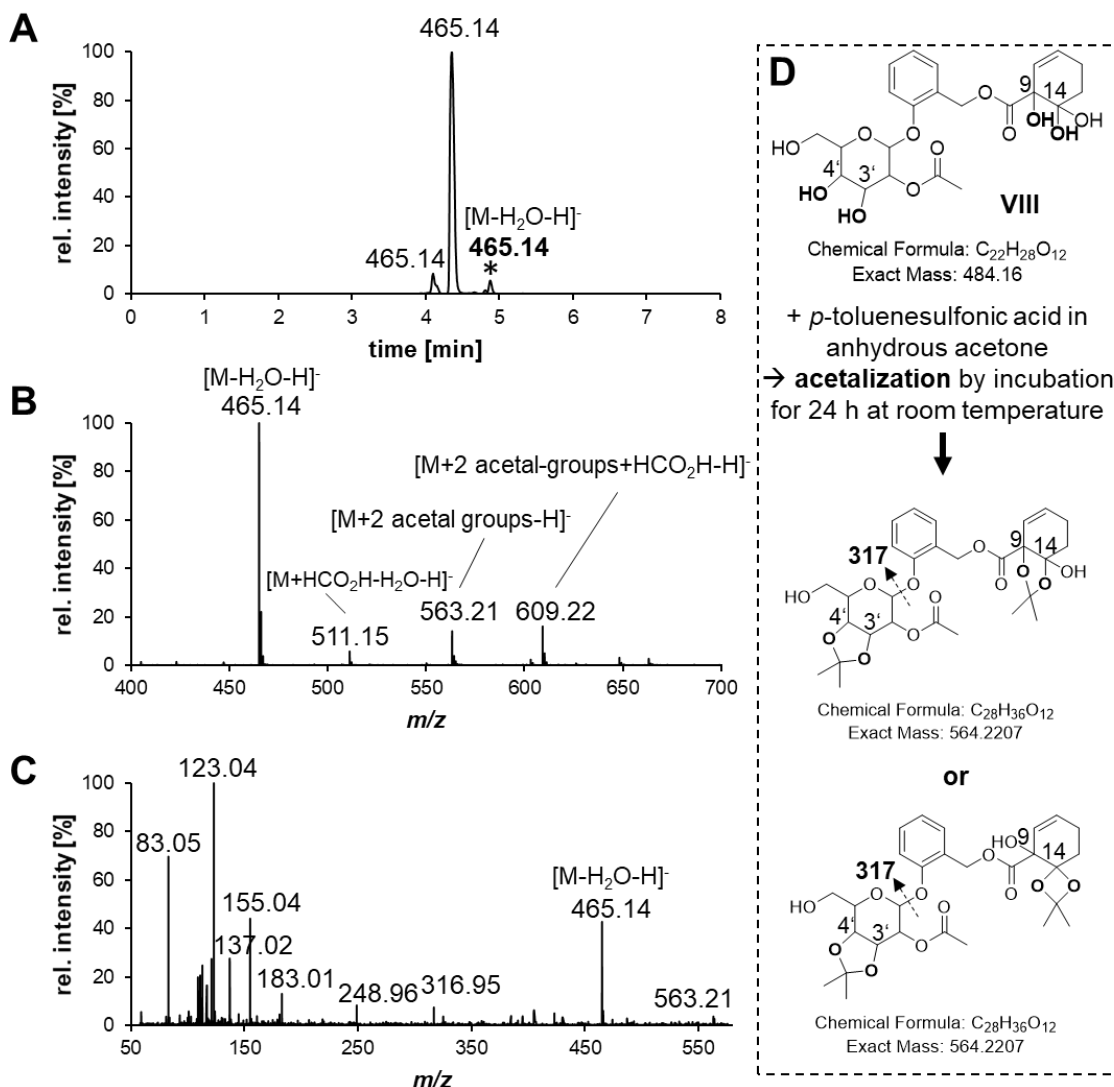
Figure 56: (A) LC-MS chromatogram, extracted **(B)** MS[1]- and **(C)** MS[2] spectra after the **(D)** acetalization reaction of fraction F7-4 detecting compound **VIII** (M = 484.16 Da). Alcohol groups at positions C-3', C-4', C-9, and C-14 were acetalized (M = 564.22 Da). Asterisk: peak at 4.88 min was used for the extraction of the mass spectra.

However, it was not possible to differentiate the chemical structures of compounds B and C due to signal overlapping. Thus, annotations of the chemical shifts in the Appendix section showed similar shifts for some positions of both compounds. The similar chemical shifts observed in the NMR spectrum hinted at diastereomers of phytochemical **VIII**, which indeed holds a geminal diol group at position C-14. Overall, these diastereomers degrade over time and produce **III** (Figure 53). The plausible assigned compound **VIII** is novel and has not been identified before. For future studies, the acetalized compounds need to be extracted in higher yields for purification and identification purposes by HPLC, LC-MS, and NMR.

3.5.4 Determination of monosaccharide configuration in target metabolites

The structures of the isolated compounds 2'-O-acetylsalicin (**I**), 3'-*O*-acetyl-salicortin (**II**), 2'-*O*-acetylsalicortin (**III**), cinnamrutinose A (**IV**), 2',6'-*O*-di-acetylsalicortin (**V**), lasiandrin (**VI**), and tremulacin (**VII**) contain monosaccharide moieties. Even though it is possible to characterize sugars by NMR, some of the proton signals of the sugars were overlapping. Therefore, the determination of the sugars was performed as described in section 4.6, adopting the protocols by Schmid et al. (2018) and Tanaka et al. (2007). After acidic hydrolysis of previously purified compounds (**I-VII**), monosaccharides were extracted using ethyl acetate followed by derivatization with *L*-cysteine methyl ester hydrochloride in anhydrous pyridine and phenethyl isothiocyanate. Subsequently, the derivatized compounds were screened by LC-MS in positive ionization mode, and retention times as well as MS/MS data of the sugar moieties derived from the phytochemicals were compared to the reference sugars (Figure 57).

D-Glucose and *L*-glucose revealed the same mass transition traces *m/z* 461.02/298.10, however, it was possible to differentiate them due to the different retention times of the signals. The retention times of each reference monosaccharide were compared to the monosaccharides released upon acidic hydrolysis of the compounds, which were as followed: *L*-glucose at 13.05 min, *D*-glucose at 13.80 min, *D*-galactose at 12.74 min, *L*-rhamnose at 12.82 min, *D*-xylose at 9.56 min, *D*-glucuronic acid at 9.04 min, and *D*-galacturonic acid at 9.34 min. In general, compounds **I-III** and **V-VII** contained one *D*-glucose (Figure 57), except cinnamrutinose A (**IV**) containing two sugars, *D*-glucose and *L*-rhamnose. Therefore, it was possible to determine the sugar moieties of all isolated compounds of *S. pentandra*. All sugar moieties of the compounds **I**, **III** and **VI** (Reichardt et al. 1992), **II** (Kim et al. 2015), **IV** (Jossang, Jossang, and Bodo 1994, Noleto-Dias et al. 2019), **V** (Yang et al. 2013), and **VII** (Feistel et al. 2015) were determined only by NMR. Such derivatization reaction of salicylates was performed for the first time in the present work. Since compound **VIII** was not purely isolated, sugar determination was not performed for this.
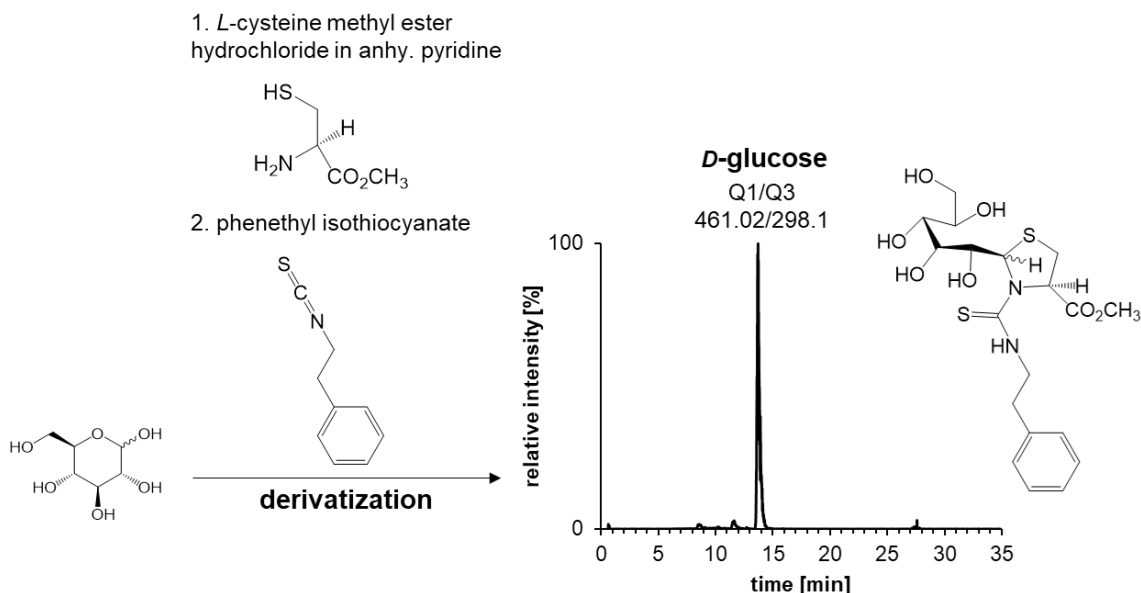
Figure 57: Derivatization reaction (modified from Tanaka et al. (2007)) of extracted *D*-glucose of hydrolyzed compound **III** and the corresponding ion chromatogram and MRM transitions.

3.5.5 Determination of *S/R* absolute configuration of target metabolites

Furthermore, the absolute *S/R* configuration was investigated, since the isolated compounds 3'-*O*-acetylsalicortin (**II**), 2-*O*-acetylsalicortin (**III**), 2',6'-*O*-di-acetylsalicortin (**V**), lasiandrin (**VI**), and tremulacin (**VII**) comprise of a HCH residue, which has a chiral center C(9). Thus, the characterization of the compounds will give insight to the biosynthetic pathway and compound groups that derive from a certain compound of the pathway. Therefore, circular dichroism (CD) spectroscopy was performed as described in section 4.9.3. Following molar ellipticity ($\Delta\varepsilon$) values were obtained for each of the five compounds: $\Delta\varepsilon$ = -11.7 mdeg (0.43 mM in methanol, λ_{max} = 221 nm) for **II**, $\Delta\varepsilon$ = -15.5 mdeg (0.43 mM in methanol, λ_{max} = 220 nm) for **III**, $\Delta\varepsilon$ = -14.4 mdeg (0.39 mM in methanol, λ_{max} = 220 nm) for **V**, $\Delta\varepsilon$ = -17.2 mdeg (0.33 mM in methanol, λ_{max} = 216 nm) for **VI**, and $\Delta\varepsilon$ = -19.6 and -8.8 mdeg (0.38 mM in methanol, λ_{max} = 228, 209 nm) for **VII**. All CD spectra of the analyzed compounds clearly describe a negative molar ellipticity (Figure 58), which were compared to already existing literature and showed that all isolated salicylates comprised of an *S* configuration (Feistel et al. 2015, Yang et al. 2013).
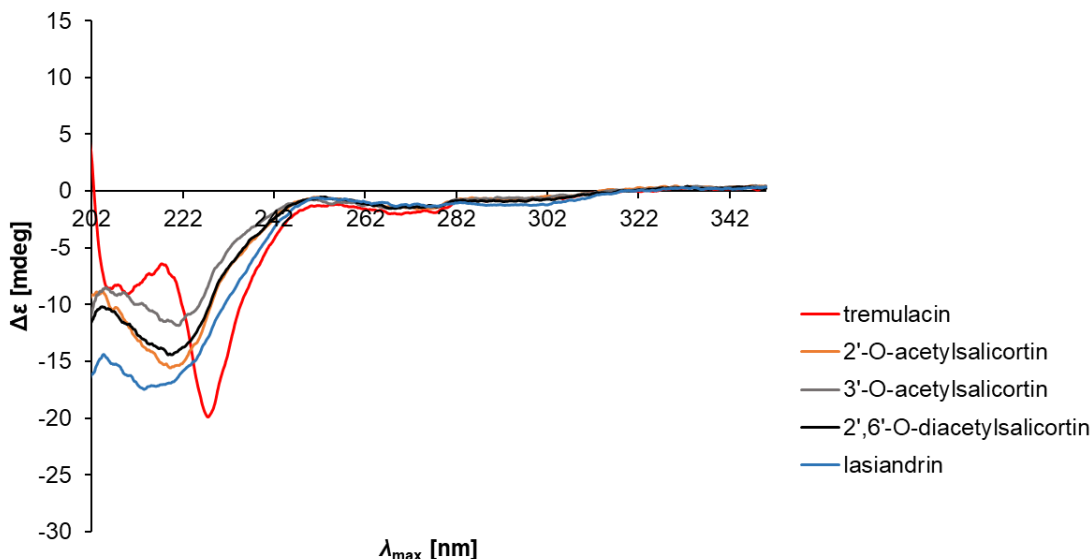
Figure 58: Circular dichroism spectra of analyzed salicylates, tremulacin (**VII**), 2-*O*-acetylsalicortin (**III**), 3'-*O*-acetylsalicortin (**II**), 2',6'-*O*-diacetylsalicortin (**V**), and lasiandrin (**VI**) containing a hydroxyl cyclohexenonoyl group with a chiral center at C(9). The molar ellipticity ($\Delta\varepsilon$) is plotted against the maximum wavelength (λ_{max}) (acquired from Antoniadou et al. (2021)).

Two negative molar ellipticity values were characteristic for **VII**, as postulated by Feistel et al. (2015). Nevertheless, comparison of **VII** with the literature showed that one of the maximum molar ellipticity values ($\Delta\varepsilon$ = -19.6 mdeg) was lower at an also lower maximum wavelength (228 nm), being -10.5 mdeg at 239 nm (at 25°C) (Feistel et al. 2015). This difference of the maximum ellipticity values occurred probably due to the different measurement temperature being 20°C in the current work. In particular, according to Kelly, Jess, and Price (2005), the temperature can influence CD spectroscopy. However, at 239 nm, **VII** had indeed a similar molar ellipticity of -6.3 mdeg.

Moreover, Feistel et al. (2015) postulated in general that for salicylates the *S* configuration is common. This may be explained by similar biosynthetic pathways, the shikimate pathways of salicylates, which are derived from *trans*-cinnamic acid forming salicyl-CoA and salicyl benzoate (Fellenberg et al. 2020). After glucosylation by glucosyltransferases, salicylates containing the characteristic HCH moiety can be derived from the pathway described in Figure 10 of the introduction section (Fellenberg et al. 2020).

3.5.6 Discussion

Until now, *Salix* cortex preparations for medicinal purposes are usually being standardized to 240 mg salicin (European Medicines Agency 2017b, Fiebich and Appel 2003). As described in the introduction section of the present work, many compounds have been identified in *Salix* before, however, no systemic evidence was obtained about key phytochemicals with anti-inflammatory properties by activity-guided fractionation. In the present work, the isolated phytochemicals from potent methanol extract of a *S. pentandra* clone (PE1) were salicylates.

Phytochemical composition of bioactive bark material of *S. pentandra* belonging to group 3 of the PCA plot (Figure 13, section 3.1) was investigated in order to isolate and identify phytochemicals by means of HPLC-UV, LC-MS, and NMR. Through activity-guided fractionation of anti-inflammatory methanol extract, eleven SPE fractions F1-F11 were obtained. After determination of the anti-inflammatory potential, fraction F5 showed the highest potency among all fractions (Figure 19, section 3.3.2).

Compounds could then be isolated and structurally elucidated from SPE fractions F5 (v/v, 40/60 methanol/water fraction), F6 (v/v, 1/1 methanol/water fraction), and F7 (v/v, 60/40 methanol/water fraction) (Figure 59). Therefore, preparative and semi-preparative fractionation by means of HPLC-UV was performed. Subfraction F5-5 revealed the highest bioactivity, in comparison to the other subfractions of F5 and subfractions of F6 and F7 (Figure 25, section 3.5.1). For the elucidation of the single compounds, LC-MS and 2D-NMR techniques were used identifying 2'-*O*-acetylsalicin (**I**), 3'-*O*-acetylsalicortin (**II**), 2'-*O*-acetyl-salicortin (**III**), cinnamrutinose A (**IV**), 2',6'-*O*-diacetylsalicortin (**V**), lasiandrin (**VI**), and tremulacin (**VII**) (Figure 59, Table 6, and Appendix section).
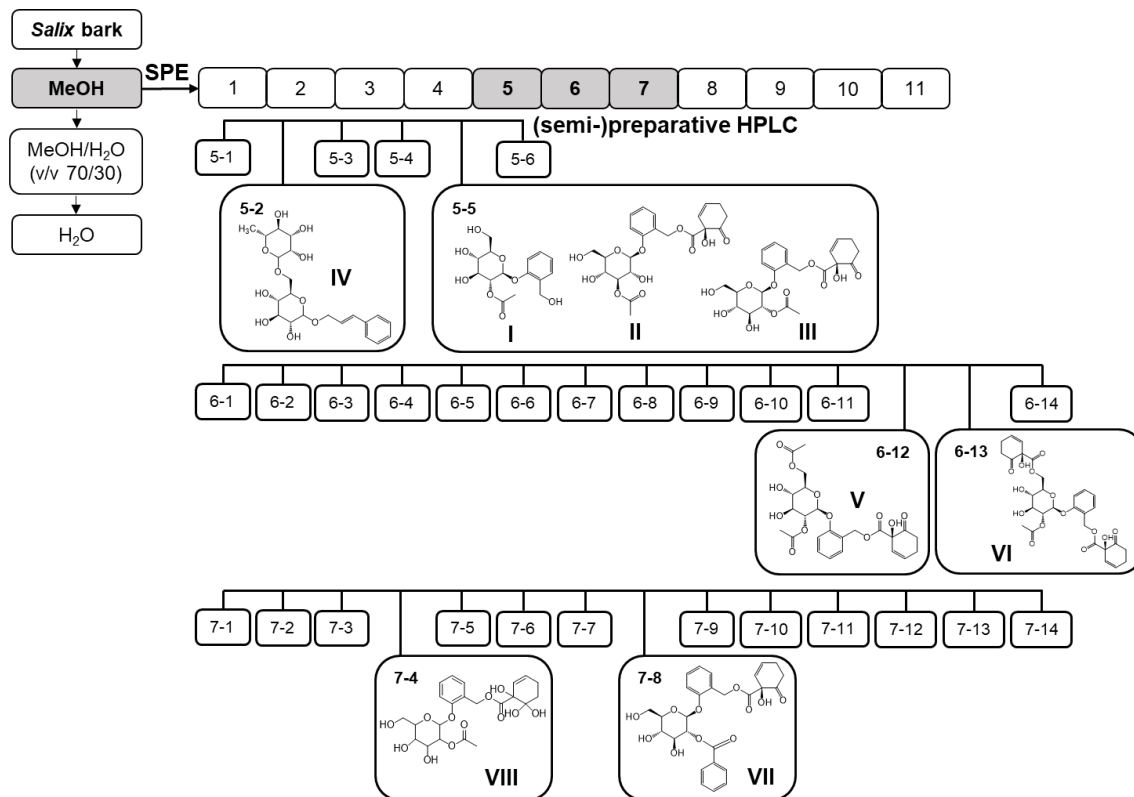
Figure 59: Activity-guided fractionation of anti-inflammatory methanol extract of *S. pentandra* bark material (grey). SPE fractions F5, F6, and F7 (grey) were subfractionated by (semi-)preparative HPLC-UV, and structure elucidation identified cinnamrutinose A (**IV**, F5-2-6), 2'-*O*-acetylsalicin (**I**, F5-5-3), 3'-*O*-acetyl-salicortin (**II**, F5-5-5), 2'-*O*-acetylsalicortin (**III**, F5-5-7), 2',6'-*O*-diacetylsalicortin (**V**, F6-12-2), lasiandrin (**VI**, F6-13-2), tremulacin (**VII**, F7-8-4), and *β*-D-glucopyranoside, 2-[[[(1-hydroxy-6,6-dihydroxy-2-cyclohexen-1-yl)dihydroxy]oxy]-methyl]phenyl, 2-acetate (**VIII**, F7-4-6) as potentially active compounds (modified from Antoniadou et al. (2021)).

Precursor ion (PI) scan (section 3.4.1) and information-dependent acquisition (IDA) experiments (section 3.4.2) enabled the detection also of these salicylic acid derivatives or salicylates **I-III** and **V-VII**. Moreover, two novel diastereomers of *β*-D-glucopyranoside, 2-[[[(1-hydroxy-6,6-dihydroxy-2-cyclohexen-1-yl)dihydroxy]-oxy]-methyl]phenyl, 2-acetate (**VIII**) were identified for the first time in the present work and could only be distinguished by LC-MS after an acetalization experiment. **IV** was identified as a non-salicylate. All compounds **I**, **III** and **VI** (Reichardt et al. 1992), **II** (Kim et al. 2015), **IV** (Jossang, Jossang, and Bodo 1994, Noleto-Dias et al. 2019), **V** (Yang et al. 2013), and **VII** (Feistel et al. 2015) isolated from *S. pentandra* in the present work (section 3.5) were previously isolated and identified from various other *Salix* species and thus current NMR data was compared with the literature (Table 6).

Table 6: Overview of the isolated *Salix* phytochemicals **I-VIII** from SPE fractions F5, F6, and F7, and the corresponding literature of identified compounds in *Salix* and *Populus* species. Asterisks: *compounds found in *S. pentandra* by tentative identification using HPLC/API-ES mass spectrometry (absent NMR data), **compounds not detected in *S. pentandra* previously.

No.	isolated *Salix* phytochemicals	isolated from fraction	identified in literature
I	2'-*O*-acetylsalicin*	SPE F5, F5-5-3 (HPLC-UV)	Kim et al. (2015), Reichardt et al. (1992), Yang et al. (2013); Ruuhola (2001), Ruuhola and Julkunen-Tiitto (2003), Ruuhola, Julkunen-Tiitto, and Vainiotalo (2003)*
II	3'-*O*-acetylsalicortin**	SPE F5, F5-5-5 (HPLC-UV)	Kim et al. (2015) and Yang et al. (2013)
III	2'-*O*-acetylsalicortin*	SPE F5, F5-5-7 (HPLC-UV)	Ruuhola (2001), Ruuhola and Julkunen-Tiitto (2003), Ruuhola, Julkunen-Tiitto, and Vainiotalo (2003)*; Meier et al. (1992)*; Reichardt et al. (1992); Kim et al. (2015), Yang et al. (2013)
IV	cinnamrutinose A**	SPE F5, F5-2-2 (HPLC-UV)	Jossang, Jossang, and Bodo (1994), Noleto-Dias et al. (2019), Wei, Rena, and Yang (2015)
V	2',6'-*O*-diacetylsalicortin*	SPE F6, F6-12-2 (HPLC-UV)	Kim et al. (2015), Yang et al. (2013); Ruuhola and Julkunen-Tiitto (2003), Ruuhola, Julkunen-Tiitto, and Vainiotalo (2003)*
VI	lasiandrin*	SPE F6, F6-13-2 (HPLC-UV)	Ruuhola and Julkunen-Tiitto (2003)*; Keefover-Ring et al. (2014); Reichardt et al. (1992)
VII	tremulacin*	SPE F7, F7-8-4 (HPLC-UV)	Ruuhola, Julkunen-Tiitto, and Vainiotalo (2003)*; Pearl and Darling (1971); Mizuno et al. (1991), Kim et al. (2015); El-Shazly, El-Sayed, and Fikrey (2012); Zapesochnaya et al. (2002); Knuth et al. (2013)
VIII	*β*-D-glucopyranoside, 2-[[[(1-hydroxy-6,6-dihydroxy-2-cyclohexen-1-yl)-dihydroxy] oxy]methyl]-phenyl, 2-acetate**	SPE F7, F7-4-6 (HPLC-UV)	Not described

Even though Ruuhola, Julkunen-Tiitto, and Vainiotalo (2003) and the IDA experiment of the present work (section 3.4.2) detected 6'-acetyltremulacin and a diglucoside salicin in methanolic extracts of *S. pentandra*, the compounds were

not identified by activity-guided fractionation. Most probably, these compounds were not identified in potent fractions or were not available at all in the specific *Salix* clone PE1 of the present work, since the genotypes were different.

Compounds **I-III** and **V-VIII** were *cis* configured and contained a *D*-glucose (sections 3.5.4 and 3.5.5). Exception was the non-salicylate **IV** being *trans*-configured and containing *D*-glucose attached to *L*-rhamnose. Certainly, it was possible to confirm the compound structures of the previously tentatively identified compounds in *S. pentandra* (sections 3.4.1 and 3.4.2), which were mostly salicylates. However, PCA analysis and S-plots (section 3.1) exhibited that among the isolated compounds, only lasiandrin (**VI**) was upregulated in group 3.

The bioactive methanol extract of *S. pentandra* was compared to other *Salix* extracts of published literature. Lee et al. (2013) and Yang et al. (2013) fractionated a methanolic extract (80%) of *S. pseudo-lasiogyne* twigs into *n*-hexane, ethyl acetate, water, and *n*-butanol fractions. The authors could state, that the ethyl acetate fraction had the highest adipogenic (Lee et al. 2013) and neuroprotective (Yang et al. 2013) activity, which contained **I-III,** and **V**, but also other compounds not detected in *S. pentandra*. These compounds were identified by NMR spectroscopy and comparison with reference compounds after isolation by means of HPLC-UV using a C_{18}-column as stationary phase, and solvents methanol and water as mobile phase (Yang et al. 2013). Compounds **I** (ethyl acetate fraction), **II-III** (chloroform fractions), and **VII** (ethyl acetate fraction) from a methanolic extract (80%) of *S. glandulosa* twigs could be isolated using a C_{18}-column and examined on neuroprotective activity against nitric oxide in LPS triggered murine microglial cells from the cell line BV2 (Kim et al. 2015).

Furthermore, fractionation of acetone extracts (using a Soxhlet apparatus) of *S. lasiandra* leaves and twigs revealed **I**, **III**, and **VI** by reversed-phase flash chromatography and subsequent NMR spectroscopy (Reichardt et al. 1992). Chemical shifts of the phenol ring as well as of the double bond were falsely annotated by the authors and were reviewed in the present work, assigning the carbons and protons correctly (section 3.5.2.2, Appendix section). Salicylate **VII** could be also isolated from methanol (70%) extract of *P. trichocarpa* x *deltoides* Beaupré leaves, which was fractionated by solid-phase extraction and subsequent HPLC separation (mobile phase: methanol and water in 0.1% formic

acid, solid phase: C_{18}-column) (Feistel et al. 2015). Furthermore, Knuth et al. (2013) elucidated the structure of **VII** after isolation from a commercially obtained ethanolic (70%) willow bark extract (Hermes Arzneimittel GmbH) performing flash chromatography (reversed-phase C_{18} and normal phase Si 60). Non-salicylate compound **IV** was previously isolated from *Populus* species, *P. euphratica* (Wei, Rena, and Yang 2015) and *P. tremula* (Jossang, Jossang, and Bodo 1994), but also from aqueous ethanol extract of *S. triandra* x *dasyclados* stems by means of semi-preparative HPLC-UV holding a reversed-phase C_{18}-column (Noleto-Dias et al. 2019). All of the above publications were oriented only in the identification of phytochemicals in *Salix* and did not investigate their bioactive potential.

To sum up, previous studies used in general C_{18} columns as stationary phase for the chromatographic fractionation in order to isolate and identify the compounds from willow bark. In the current work, the HPLC-UV device was equipped with phenyl-hexyl and pentafluorophenyl columns for (semi-)preparative chromatographic separation and isolation of the phytochemicals **I-VIII** by fractionation (Figure 59, Table 6). These columns were mainly used, since the compounds are phenolic glucosides, which can undergo π-π interactions for chromatographic separation. Since the purity was mainly not described in the publications, no statement can be made upon improvement in purity by using different columns. According to the literature, compounds from bark material were usually extracted using organic solvents as it was the case in the current work. However, the percentage of 80 or 70% solvent extract showed in this present study no bioactivity in comparison to previous work. Here, the highest anti-inflammatory potential was revealed only for the methanol (100%) extract. This could be due to the different used *Salix* genotype with potentially different anti-inflammatory properties. Moreover, previous studies found the compounds **I**, **III**, and **V-VII** in leaves of *S. pentandra* by means of HPLC/API-ES mass spectrometry (Ruuhola and Julkunen-Tiitto 2003, Ruuhola, Julkunen-Tiitto, and Vainiotalo 2003). However, these compounds as well as **II**, **IV**, and **VIII** have never been identified in bark material of *S. pentandra* before.

Previous studies suggested that the water extract of STW 33-I (Proaktiv®, herbal drug of *Salix* bark extract) consisting of polyphenols and flavonoids, and the derived aqueous fraction consisting of proanthocyanidins were both more potent, inhibiting COX-2 enzyme activity and thus, LPS-stimulated monocytes, in

comparison to an ethanol fraction containing mainly salicin (Nahrstedt et al. 2007). The authors assumed that since the whole water extract and aqueous fraction are potent, salicylic acid derivatives do not contribute to the overall effect (Nahrstedt et al. 2007). However, studies did not investigate various *Salix* genotypes and were only focused on a standardized aqueous willow bark extract. Indeed, these findings could be disproved, due to the outcomes of the present work revealing that the water extract of *S. pentandra* was not bioactive at all. Moreover, it was not possible to distinguish which *Salix* genotype was used for the preparation of the herbal drug Proaktiv® (STEIGERWALD Arzneimittelwerk GmbH). Furthermore, studies on this specific drug did not elucidate any compound structure by LC-MS and NMR (Nahrstedt et al. 2007, Bonaterra et al. 2010).

To continue, Bonaterra et al. (2010) postulated that salicin alone was not leading to the overall anti-inflammatory effect in clinical studies. Therefore, in the current study, a rapid screening was performed using an already established targeted LC-MS/MS method (section 4.8.3) with tuned polyphenols (method obtained from Tina Schmittnägel; Chair of Food Chemistry and Molecular Sensory Science), salicylates **I-III**, **V-VII** and non-salicylate **IV** of the current work. The screening was performed using two *Salix* genotypes, a positive control *S. pentandra* (PE1), exhibiting the highest anti-inflammatory potential, and a negative control *S. viminalis* x *S. viminalis* (*schwerinii* x *viminalis*) (VI4xVI3_2) which was a non-bioactive genotype (section 3.2). The extracted ion chromatograms depicted in Figure 60 A and B were compared, indicating that salicylates are indeed mainly contained in the bioactive *S. pentandra*, whereas *S. viminalis* x *S. viminalis* (*schwerinii* x *viminalis*) mostly consists of polyphenols, for instance, catechin, gallocatechin, procyanidin, quercetin-3-glucoside, myricetin-3-glucoside, taxifolin, and acetylsalicortin with a lower peak intensity. Additionally, there were also a few other compounds in both spectra detected, however, with much lower peak intensity (data not shown). A list of the analyzed polyphenols is shown in Table A13 of the Appendix section.
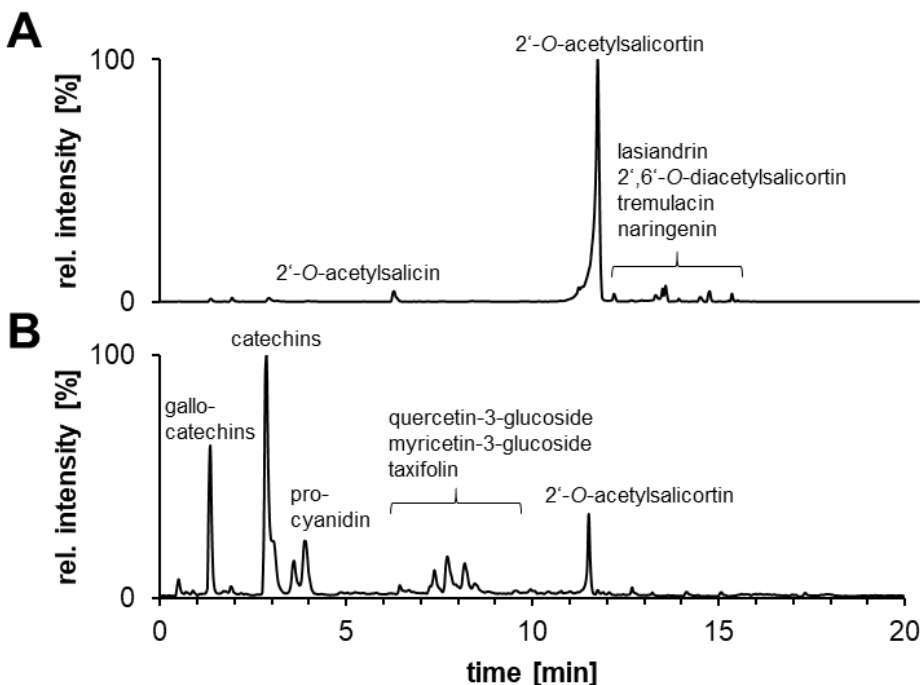
Figure 60: Extracted ion chromatograms of **(A)** positive control (bioactive) *S. pentandra* (PE1) extract and **(B)** negative control (non-bioactive) *S. viminalis* x *S. viminalis* (*schwerinii* x *viminalis*) (VI4xVI3_2) extract.

Therefore, the suggestion of Nahrstedt et al. (2007), that polyphenols are responsible for the anti-inflammatory effect was doubtful. The findings of the current work showed that salicylates may be the potential phytochemicals holding pharmacological properties. For this reason, further bioactivity tests on single compounds of section 3.6 will shed light into the anti-inflammatory potential since only little information about the potency is available in the publications as described in this section. Further, it is of significance to investigate whether the extracts, fractions or single phytochemicals trigger the anti-inflammatory potential against PGE$_2$ release. Finally, quantitative analysis has to reveal whether high concentrations of salicin or other isolated compounds were responsible for the high bioactivity of *S. pentandra*.

3.6 Bioactivity of *Salix* phytochemicals

The hypothesis that single phytochemicals may have a different anti-inflammatory effect than the whole extracts or fractions was investigated further. Moreover, high bioactivity of single compounds may help targeted breeding performance for the production of *Salix* genotypes with high content of a specific

compound, and thus help drug production. Further, it has been described by European Medicines Agency (2017b) and Ruuhola, Julkunen-Tiitto, and Vainiotalo (2003) that salicylic acid, salicin, catechol, and salicortin are degradation and/or metabolization products of salicylates. In particular, Ruuhola, Julkunen-Tiitto, and Vainiotalo (2003) found that an acetylsalicin isomer, salicin, and catechol were main degradation products of salicylates contained in an analyzed *S. pentandra* species. Another study by Knuth et al. (2011) revealed, that salicortin is bioactive, because it metabolizes to catechol, whereas salicin, saligenin, and salicylic acid had a lower activity or were not active at all. Thus, in order to examine whether the isolated compounds **I**-**VII** and fraction F7-4-6 (containing **III** and two diastereomers of **VIII**), the degradation or their metabolization compounds (salicylic acid, saligenin, salicin, salicortin, and catechol) induced the anti-inflammatory activity, a bioactivity assay was performed. For the investigation, first, the PBMC cells were treated with 5 and 25 µg/mL of each compound and stimulated with lipopolysaccharides. Then, the PGE_2 release was quantified and the anti-inflammatory effect of the compounds was determined (Figure 61).

Isolated 2'-*O*-acetylsalicin (**I**) with contaminations (only 40% purity), and commercially obtained salicylic acid, saligenin, and salicin had no anti-inflammatory potential showing no PGE_2 inhibition. The same was observed also for cinnamrutinose A (**IV**), which is a non-salicylate. Both **I** and **IV** were isolated from *S. pentandra* with low purity. Thus, the impurity may contain compounds that can inhibit the bioactivity. On the other side, the anti-inflammatory effect depends on the concentration of an individual compound. In particular, tremulacin (**VII**) was potent at 25 µg/mL, however, could not block PGE_2 release at a lower concentration of 5 µg/mL. In contrast, fraction F7-4-6 containing a mixture of **III** and two diastereomeric compounds **VIII,** and the salicylates 3'-*O*-acetylsalicortin (**II**), 2'-*O*-acetylsalicortin (**III**), 2',6'-*O*-diacetylsalicortin (**V**), lasiandrin (**VI**), salicortin, and the degradation and metabolization product catechol revealed an anti-inflammatory potential at both concentrations 5 and 25 µg/mL (Figure 61).
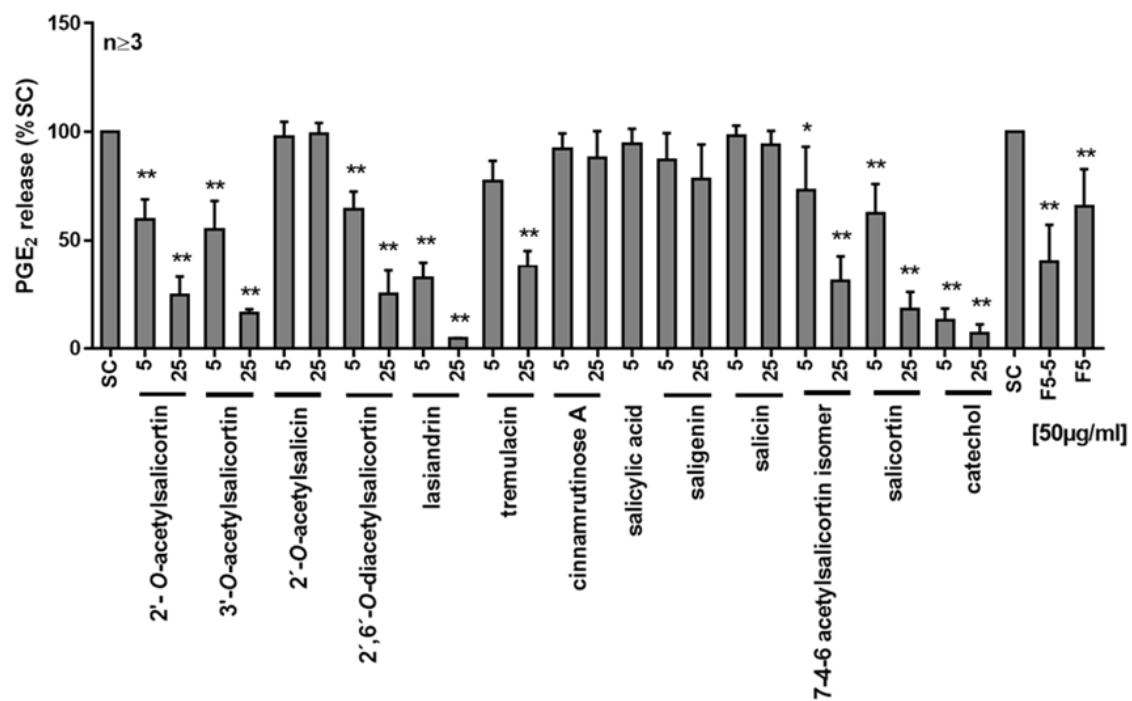
Figure 61: Bioactivity of compounds (5 and 25 µg/mL) **I-VII** and fraction F7-4-6 containing two novel diastereomeric compounds (**VIII**) isolated from methanol extract of *S. pentandra*, and degradation and/or metabolization compounds, like salicylic acid, saligenin, salicin, salicortin, and catechol, compared to fraction F5-5 and F5. Bioactivity was compared to solvent control (SC, 1% distilled water). Asterisks: significant difference between compounds or fractions and SC, such as * $p < 0.05$ and ** $p < 0.01$ (adopted from Antoniadou et al. (2021)).

It was observed that the compounds 2'-*O*-acetylsalicin (**I**), cinnamrutinose A (**IV**), salicin, saligenin, and salicylic acid, with an absent HCH moiety in their chemical structure could not inhibit inflammation. Indeed, it can be assumed that the presence of HCH in the phytochemicals plays a role in their overall anti-inflammatory potential. For example, bioactive salicortin, which is also the substructure of most salicylates, contains an HCH group. This can be explained by the decarboxylation of the 1-hydroxy-6-oxo-2-cyclohexene carboxylic acid anion generates 2-hydroxy-3-cyclohexenone (2-HCH) in absence of enzymes, forming enol and keto (6-hydroxy-2-cyclohexenone) tautomers, which after oxidation and under cell culture conditions produce bioactive catechol (Figure 62) (Julkunen-Tiitto and Meier 1992, Knuth et al. 2013, Knuth et al. 2011, Ruuhola, Julkunen-Tiitto, and Vainiotalo 2003).
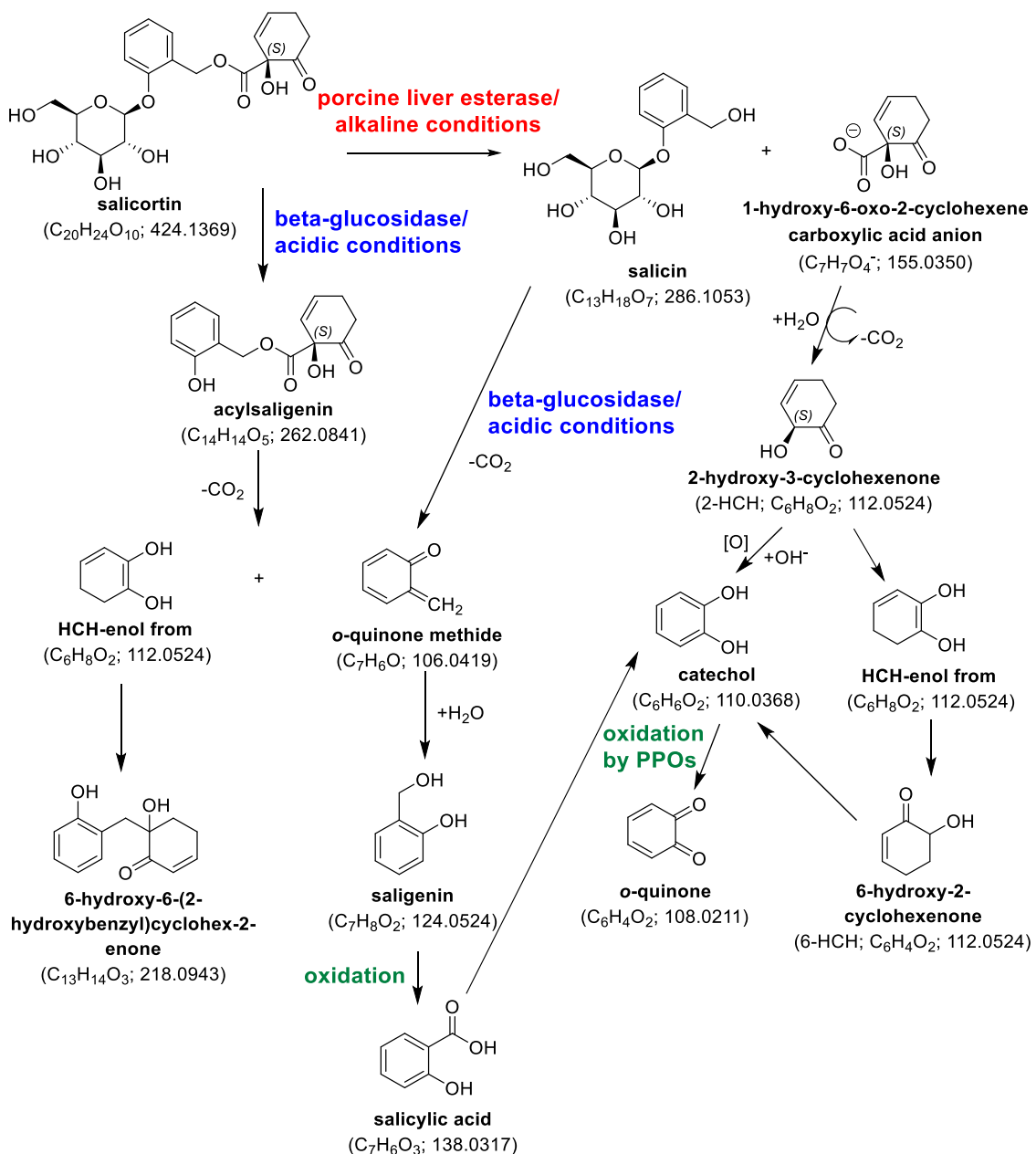
Figure 62: Degradation and metabolization scheme of salicortin to HCH, saligenin, salicylic acid, and catechol (modified from Clausen, Koller, and Reichardt (1990), Feistel et al. (2018), Julkunen-Tiitto and Meier (1992), Ruuhola, Julkunen-Tiitto, and Vainiotalo (2003), Zhu et al. (1998)). PPO: polyphenol oxidase.

Among all investigated compounds (Figure 61), catechol showed the highest bioactivity at 5 µg/mL (5 µg/mL: 14%+/-5%; 25 µg/mL: 8%+/-4%), which was similar to the bioactive **VI** at 25 µg/mL (5 µg/mL: 33%+/-7%; 25 µg/mL: 5%+/-0%). **VI** consists of two HCH groups, which most probably is the reason why this compound had the highest anti-inflammatory potential among all isolated salicylates. The HCH groups can degrade to catechol (Ruuhola, Julkunen-Tiitto,

and Vainiotalo 2003) (Figure 62), which has been also postulated as highly potent and is in turn a degradation product of salicortin (Knuth et al. 2011).

Previous work revealed that the bioactivity of salicortin and **VII** (isolated from an ethanol extract of commercially obtained *Salix* cortex) had been already tested using endothelial cell cultures stimulated with TNF-α by performing the ICAM-1 assay (Knuth 2013, Knuth et al. 2011). ICAM-1 expression shows the overall inflammatory response (Almenar-Queralt et al. 1995) and in the study of Knuth et al., 50 µM **VII** could reduce ICAM-1 expression to 75.0% in contrast to salicortin reducing to 52.4% and thus being more anti-inflammatory (Knuth 2013, Knuth et al. 2011). In the current work at comparable concentrations similar results were obtained, revealing that 25 µg/mL salicortin (58.82 µM) inhibited PGE$_2$ release to 28% and was more anti-inflammatory than **VII** (47.30 µM; 37%). The benzoic acid at position C(2') of the glucose of **VII** may reduce the bioactivity. Similarly, it has been shown in the literature that COX-1 enzyme inhibition using **III** (75%) and salicortin (71%) was higher in contrast to the application of salicin (58%) or **VII** (22%) (Dissanayake et al. 2017). Particularly, the anti-inflammatory effect of salicortin was attributed to its degradation to catechol as described in previous studies (Knuth 2013, Knuth et al. 2011).

Moreover, Dissanayake et al. (2017) investigated the four *S. mucronata* compounds (**III**, **VII**, salicortin, salicin) further, showing for **III** the highest inhibitory potential on COX-2 enzyme with 46% at 25 µg/mL in comparison to salicortin (38%), salicin (30%), and **VII** (8%). In another study, acetylsalicortin compounds from *S. pseudo-lasiogyne* twigs were examined on nitric oxide inhibitory effect in murine microglia BV2 cells that were stimulated with LPS, showing a higher bioactivity of **II** than of **III** (Kim et al. 2015). However, in the current work the anti-inflammatory effect of **II** (5 µg/mL 59%+/-9%; 25 µg/mL 25%+/-8%) and **III** (5 µg/mL 55%+/-13%; 25 µg/mL 16%+/-2%) on PGE$_2$ release did not differ greatly, and a similar inhibitory effect could be observed even for **V** (5 µg/mL 64%+/-8%; 25 µg/mL 25%+/-11%).

In general, in the present work it has been observed that salicylates containing HCH moieties have a higher anti-inflammatory potential than compounds without. According to previous analyses on salicortin, this can happen due to the degradation of the compound to catechol in cell culture conditions (Knuth 2013, Knuth et al. 2011), which most probably is also the case in the isolated

compounds of this work. However, the salicylate **VI** containing two HCH groups had the highest bioactivity, even though it was isolated from a less bioactive fraction F6-13. The most potent fraction F5-5 consisted of compounds **I-III** with a lower anti-inflammatory effect than **VI** or no effect at all.

Moreover, standardization of willow bark extract is currently based on salicin content (European Medicines Agency 2017b). However, this is interrogative, since salicin did not show any anti-inflammatory effect in the present study. According to Schmid, Kötter, and Heide (2001), salicin metabolization leads to the formation of mainly salicylic acid, which can be found in serum. As mentioned by the authors and as it was revealed in the current bioassay, salicylic acid was not responsible for the anti-inflammatory effect of the willow bark. Thus, based on these findings, that neither salicin nor salicylic acid can explain the bioactivity, other studies suggested that polyphenols might play a role in the overall effect (Khayyal et al. 2005, Nahrstedt et al. 2007). However, in section 3.5.6 two *Salix* genotypes, positive and negative control, were compared in a targeted screening analysis. Thereby, bioactive *S. pentandra* contained a higher variety of salicylates with high intensities in comparison to the non-bioactive *S. viminalis* x *S. viminalis* (*schwerinii* x *viminalis*) containing a higher variety of polyphenols.

In sum, these outcomes indicate that the overall anti-inflammatory potential of *Salix* cortex is attributed to salicylates and in particular to salicylates with an HCH group. Therefore, the isolated compounds **I-VII** as well as degradation and metabolization compounds were quantified in the 92 *Salix* bark extracts, which is described in the following section 3.7.

3.7 Quantitative analysis of *Salix* phytochemicals

3.7.1 Method development and validation

In order to quantify the identified phytochemicals in the 92 *Salix* species and crosses and reveal if their concentrations play a role in the overall bioactivity, a fast and sensitive quantitative method by means of LC-MS/MS has never been developed in combination with half-maximal inhibitory concentration (IC_{50}) determination.

Previous studies used HPLC methods to quantify salicin, salicortin, 2'-*O*-acetylsalicin (**I**), 2'-*O*-acetylsalicortin (**III**), 2',6'-*O*-diacetylsalicortin (**V**), and tremulacin (**VII**) (Julkunen-Tiitto and Sorsa 2001, Pobłocka-Olech et al. 2007, Rubert-Nason et al. 2014, Ruuhola, Julkunen-Tiitto, and Vainiotalo 2003, Shivatare et al. 2014), and LC-MS/MS methods to determine the concentration of salicin, salicylic acid, salicortin, **I**, **III**, and **VII** (Förster et al. 2021, Kammerer et al. 2005). However, compounds such as saligenin, 3'-*O*-acetylsalicortin (**II**), cinnamrutinose A (**IV**), and lasiandrin (**VI**) were not quantified in any *Salix* genotype in past studies. Moreover, validation of the LC-MS/MS quantitation methods were in past studies only partially performed or not at all (Förster et al. 2021, Julkunen-Tiitto and Sorsa 2001, Kammerer et al. 2005).

For the quantitation, purified compounds **I-VII** from methanol extract of *S. pentandra* (PE1) and degradation/metabolization compounds salicin, saligenin, salicylic acid, and salicortin were analyzed in the 92 *Salix* extracts. In this way, it was possible to map the compounds in order to distinguish how the concentration differs between *Salix* species and crosses. The novel compound **VIII** was not purified and could not be quantified in the current work due to fast degradation to **III**.

In all of the described methods a C_{18} column was used, except in the method by Förster et al. (2021) using HPLC-DAD-ESI-MS[3] and a C_{16} column. In the present work, a C_{18} column, acetonitrile/water in 0.1% formic acid, and a run time of 10 min were effective conditions for the chromatographic separation and quantitation of the (non-)salicylates by means of LC-MS/MS (section 4.7.2.5). After co-chromatography of the compounds, mass transitions (precursor ion/product ion, Q1/Q3) and retention times were obtained for each. For example, even though for **II** and **III** the mass transitions of *m/z* 464.986 → 137.100 and *m/z* 464.946 → 136.800 were very similar, it was possible to keep them apart due to their different retention times of 3.17 and 3.57 min, respectively (Figure 63, Table 8). Furthermore, for the quantitative analysis and in order to distinguish any sample loss, the internal standard (IS) salicylic acid-d_4 was used.
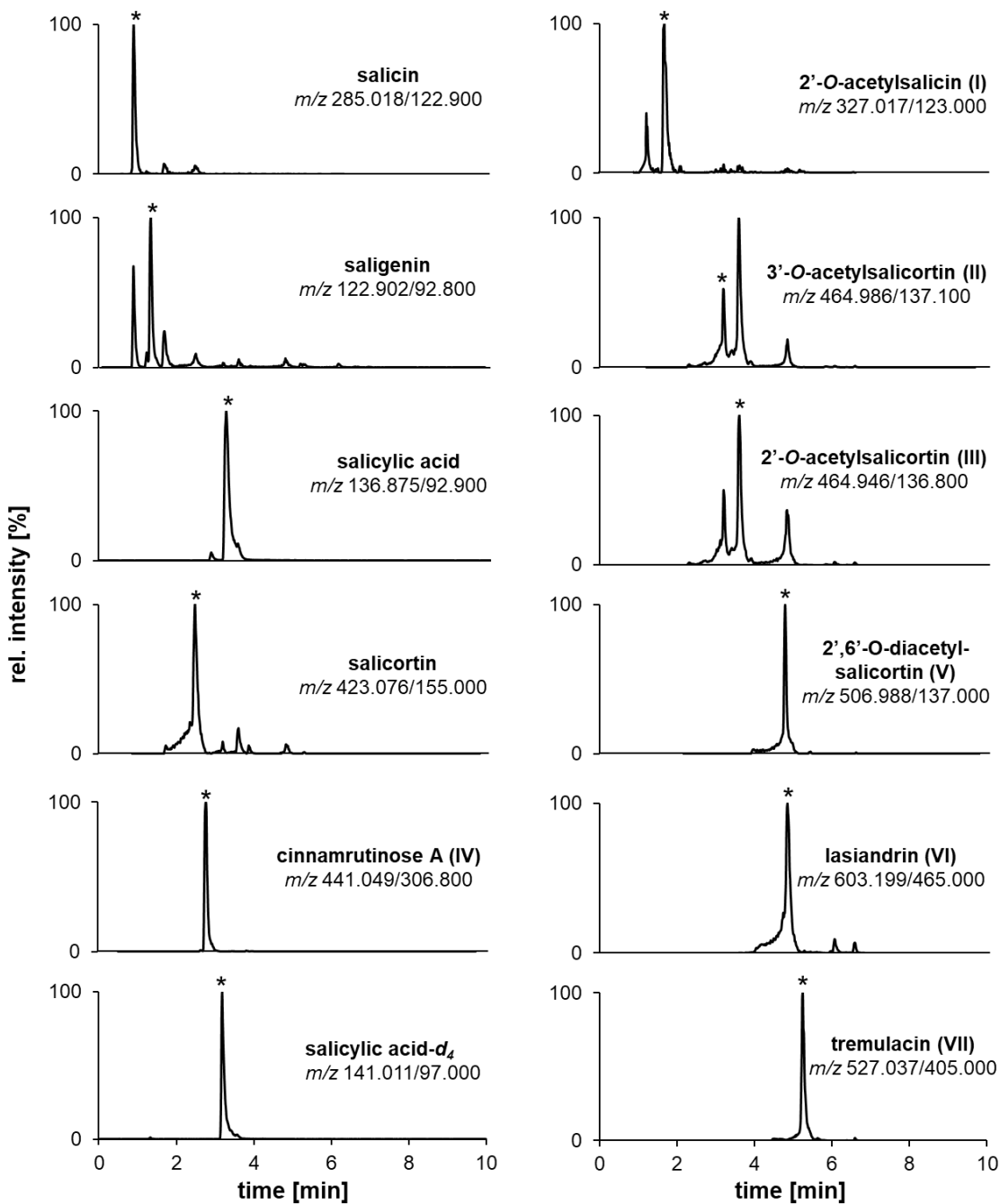
Figure 63: Extracted ion chromatograms (XIC) and MRM transitions of analytes (asterisks) salicin, saligenin, salicylic acid, salicortin, and **I-VII**, as well as of the internal standard salicylic acid-d_4.

The 92 *Salix* genotypes were extracted using methanol and spiked with IS before quantification. Further, for validation of the method, linearity, reproducibility, and recovery rates were determined. Low LoQ and LoD values confirmed the satisfying sensitivity of the method, which were ranging from 4.38 to 875.00 nmol/L and from 4.38 to 250 nmol/L, respectively, being within the analyte limits of quantification and detection for all analyzed compounds (Table 7). The

correlation coefficient calculating if the data points are within the regression revealed $R^2 \geq 0.993$, which shows acceptable linearity of the calibration curve (area against concentration) of each analyte.

Table 7: Linear regression, coefficients of determination (R^2), inter- and intraday precision, recovery rates, LoQ and LoD for the analysis of salicin, saligenin, salicylic acid, salicortin, and compounds **I-VII**.

analyte	retention time [min]	linear regression (y)	R^2	interday precision [%]	intraday precision [%]	recovery [%]	LoQ [nmol/L]	LoD [nmol/L]
salicin	0.88	$6.86453e^{-4}x + 6.27676e^{-4}$	0.993	10.4	7.2	106	43.80	4.38
saligenin	1.32	$0.00139x - 5.91251e^{-4}$	0.999	4.4	1.4	90	43.80	4.38
salicylic acid	3.25	$0.05808x + 0.01610$	0.998	21.1	5.9	441	25.00	10.00
salicortin	2.46	$0.00462x + 0.00106$	0.998	1.7	2.7	108	250.00	100.00
I	3.57	$2.26701e^{-4}x - 3.91643e^{-5}$	0.999	5.1	7.7	95	875.00	219.00
II	3.17	$0.00611x + 0.00199$	0.998	2.5	1.6	112	87.50	250.00
III	3.57	$0.00262x + 9.13923e^{-4}$	0.996	1.7	1.5	80	100.00	8.75
IV	2.77	$0.00300x + 0.00385$	0.999	8.1	1.0	108	43.80	4.38
V	4.75	$0.00311x + 0.00245$	0.993	2.0	5.0	85	500.00	25.00
VI	4.80	$0.00483x + 5.18313e^{-4}$	0.998	5.1	3.6	81	87.50	43.80
VII	5.24	$0.01454x + 4.79262e^{-4}$	0.999	8.6	8.5	94	4.38	50.00

Further, the recovery rates of spiked analytes into the matrix (non analyte-free) were 80-112%, which was within the accepted range. Comparable were the results of previous extraction methods of salicylates (salicin, salicortin, **VII**, tremuloidin) from *S. purpurea* leaves using methanol and showing a recovery rate over 98% after HPLC-DAD without any further validation experiments (Julkunen-Tiitto and Sorsa 2001). The intraday precision using spiked triplicates of *S. pentandra* bark extract and interday precision without spiking were expressed as RSD showing good accuracy, repeatability, and reproducibility, being 1.0-8.5% (intraday) and 1.7-10.4% (interday), respectively.

In contrast, salicylic acid showed a recovery rate of 441% being too high, and the interday precision was 21.1%. The high percentages may have derived, because the method is not sensitive enough for salicylic acid quantification and the concentrations in the extract were also very low. Previous studies showed that

by using blood plasma extraction methods, the linearity, reproducibility, and recovery results were poor in comparison to the experiments without performed extraction (Coudray et al. 1996). In the publication of Kammerer et al. (2005), the validation of the LC-MS/MS quantitation method was only verified by LoD values for salicylic acid in *Salix* species. In feed samples using methanol in 0.1% hydrochloric acid as extraction solvent, salicylic acid showed acceptable recovery rates of 98.3-101%, R^2, LoD/LoQ, and inter-/intraday precision values (Protasiuk and Olejnik 2018). In contrast, Deng et al. (2003) used a GC-MS method after derivatizing salicylic acid. Anyhow, without matrix or extract, for salicylic acid it was possible to successfully quantify the compound in previous studies. Even though for all compounds the validation experiments were acceptable, for salicylic acid a more sensitive method during extraction procedures needs to be developed in the future. Since salicylic acid was not showing any anti-inflammatory effect and was very low concentrated, as shown in the next section 3.7.2, no further method development was performed in the current study.

After successful method development and validation of the isolated salicylates **I**-**VII**, as well as of metabolization compounds, salicortin, saligenin, and salicin, quantification was performed next in various 92 *Salix* genotypes.

3.7.2 Quantitation of salicylates in *Salix* bark

In order to understand quantitative difference, as well as the correlation between the compound concentration in *Salix* and the inhibitory activity against PGE_2 release, 92 *Salix* species and crosses were prepared and quantified in biological triplicates. LC-MS screening confirmed the presence of the phytochemicals salicin (**1**), saligenin (**2**), salicortin (**3**), and 2'-*O*-acetylsalicin (**I**), 3'-*O*-acetylsalicortin (**II**), 2'-*O*-acetylsalicortin (**III**), cinnamrutinose A (**IV**), 2',6'-*O*-diacetylsalicortin (**V**), lasiandrin (**VI**), and tremulacin (**VII**) in bioactive *S. pentandra* (PE1) extract in various concentrations, but salicylic acid (**4**) was not detected at all (Table A12, Appendix).

The overview of the compound concentrations and RSD values in the 92 *Salix* genotypes are depicted in Table A12 (Appendix) and the abbreviations of the Salix species and crosses are summarized in Table 9 (section 4.1.1). For a better visualization of the quantitative data, a clustered heatmap (Euclidean distance,

average linkage) was generated by using the website heatmapper.ca (Babicki et al. 2016) demonstrating differences in the phytochemical accumulation among the 92 *Salix* species and crosses (Figure 64). Ten groups (A-J) were formed from this clustering method in comparison to the untargeted PCA clustering, which resulted into five groups (1-5). Remarkable were **I-III** and **VI**, trending in high amounts within *S. pentandra* genotypes and AL2xPE1_2 and AL2xPE1_1 clones (group D and I). In contrast, *S. lasiandra*, *S. purpurea*, *S. daphnoides*, *S. humboldtiana*, *S. nigra*, *S. viminalis* (mainly group H), and some *S. alba* clones (e.g. AL1_h, AL2, AL3, AL4, AL5 of group G and F) were low in compound variety and quantity.

Accordingly, non-bioactive compounds **2** and **4** were very low concentrated in all genotypes being below 0.72 µmol/g. **1** and **3** are mostly accumulating in group A, *S. daphnoides* genotypes of group C, as well as in (DA2xDA3)xVI2_2 and (DA2xDA3)xVI2_3 of group J (Figure 64). The highest concentration of **1** was detected in DA2xDA3 with 27.08 µmol/g and of **3** in (DA2xDA3)xVI2_2 with 267.40 µmol/g. In bioactive PE1 (group I), **1** and **3** had just a concentration of 2.13 and 7.82 µmol/g, respectively. *Salix* bark extract is currently standardized to **1** (European Medicines Agency 2017b), which does not have the highest concentration among the analyzed salicylates and does not inhibit PGE_2 release as shown in the last sections. Thus, the current results of PE1 showed once again that **1** is indeed not the compound that triggers the bioactivity of the genotype.
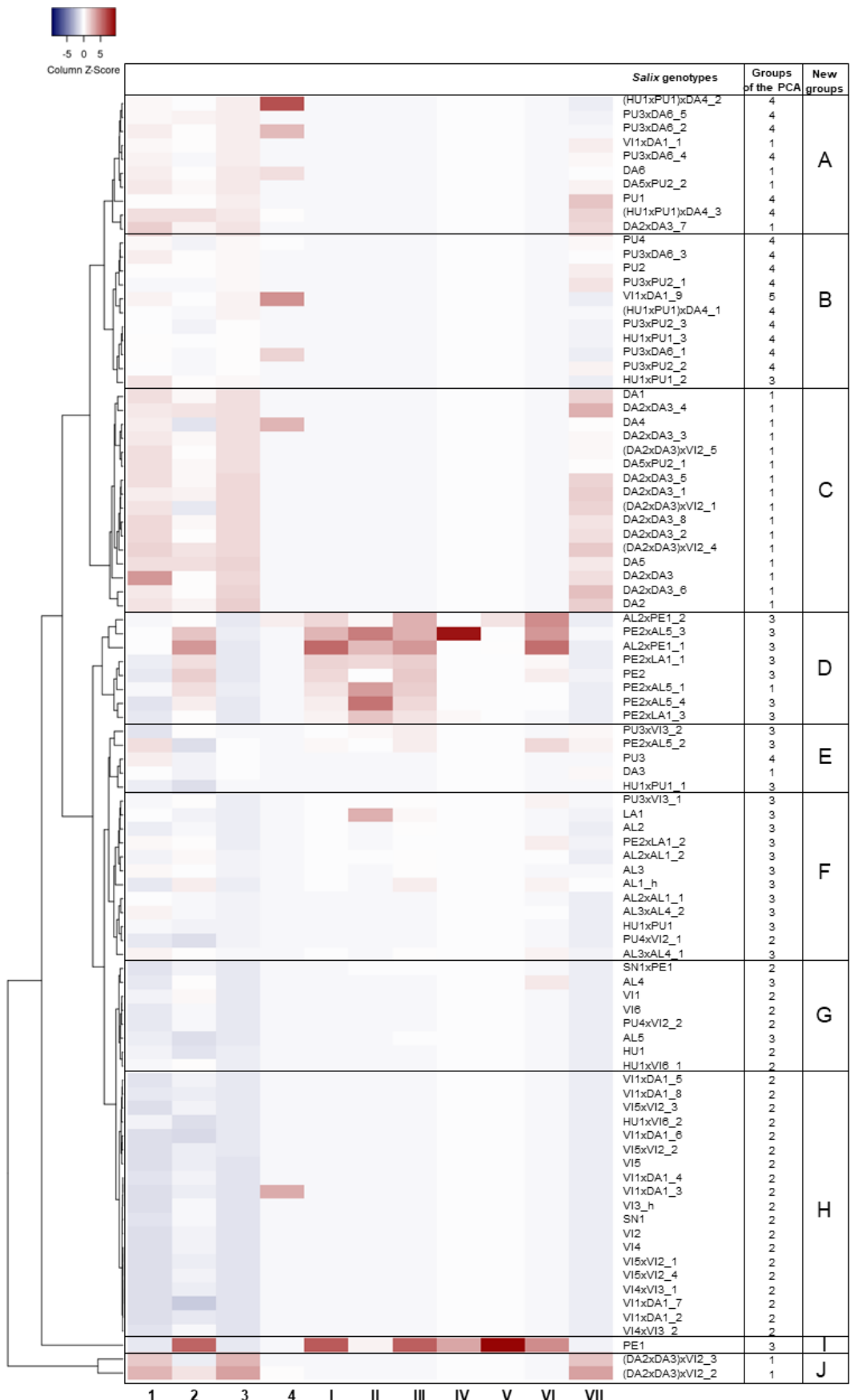
Figure 64: Column scaled heatmap of salicin (**1**), saligenin (**2**), salicortin (**3**), salicylic acid (**4**), 2'-*O*-acetylsalicin (**I**), 3'-*O*-acetylsalicortin (**II**), 2'-*O*-acetylsalicortin (**III**), cinnamrutinose A (**IV**), 2',6'-*O*-diacetylsalicortin (**V**), lasiandrin (**VI**), and tremulacin (**VII**) in 92 *Salix* species and crosses forming ten groups A-J.

Compounds, **1**, **2**, **3**, as well as **VII** were trending mainly in *S. daphnoides* genotypes of groups A-C. **VII** was found highly abundant not only in *S. daphnoides* clones, but also in *S. purpurea* clones, whereas it was detected lower concentrated in *S. pentandra* (e.g. PE1 contained 2.04 µmol/g of **VII**), *S. viminalis*, and *S. alba* clones. The highest concentrations could be detected in (DA2xDA3)xVI2_2 (25.30 µmol/g), DA2xDA3_4 (21.77 µmol/g), and DA2xDA3_6 (18.40 µmol/g). In contrast, the variety of isolated and identified compounds **I-VI** were trending in *S. pentandra* and *S. alba* (e.g. AL2xPE1_2 and AL2xPE1_1) clones belonging in their vast majority to group 3. Particularly, non-salicylate and non-bioactive **IV** was predominantly detected in PE2xAL5_3 (3.08 µmol/g), PE1 (1.19 µmol/g), PE2xLA1_3 (0.15 µmol/g), PU3 (0.06 µmol/g), and PE2xAL5_1 (0.01 µmol/g) in very low concentrations.

Phytochemical **I**, not inhibiting PGE_2 activity, was highly abundant in PE1 (25.06 µmol/g) and AL2xPE1_1 (22.58 µmol/g). On the other side, **II** was very low concentrated in all 92 *Salix* genotypes, being below the concentration of 0.55 µmol/g. However, **I**, **III** and **V** were detected with the highest concentrations of 25.06, 118.27, and 18.04 µmol/g, respectively, in bioactive PE1 in contrast to the other analyzed extracts. Among the investigated phytochemicals, the most anti-inflammatory **VI** was upregulated in *Salix* bark extracts of group 3, such as in AL2xPE1_1 (18.06 µmol/g), PE1 (14.56 µmol/g), AL2xPE1_2 (14.17 µmol/g), and PE2xAL5_3 (13.09 µmol/g).

The heatmap (Figure 64) as well as the graphic in Figure 65 pointed out high similarity between *S. pentandra* PE1 (group I) and the *S. alba* x *S. pentandra* cross AL2xPE1_1 (group D). Both candidates belonging to group 3 exhibited also similar phenolic glucoside content of 38.79 mg/g DW (PE1) and 34.47 mg/g DW (AL2xPE1_1) (Förster et al. 2021). The non-bioactive compounds, such as **2**, **4**, and **IV** were lower concentrated, and potent **VI** was slightly more upregulated in AL2xPE1_1 than in PE1. Since the cross was not previously examined on its potential to inhibit PGE_2 release as it can be observed in Figure 15 (section 3.2), further research needs to be performed to ensure its future use as a phytopharmaceutical extract.

Additionally, PE2, belonging to the same species *S. pentandra* but different genotype, showed very low concentration of potent **VI** and neither contain **IV** nor **V** in comparison to PE1 (Figure 65). However, similar concentrations of **3** and no

content of **4** could be detected for all three extracts, PE1 (7.82 µmol/g), AL2xPE1_1 (9.22 µmol/g) and PE2 (12.21 µmol/g). This shows, however, phytochemical composition differences between same species, which indicates genetic variations among willow plants. Therefore, biomarkers to trace anti-inflammatory potential of willow bark extract in order to develop herbal medical products are of high importance and were discussed in this work, recommending bark extracts of various *Salix* species and crosses (Figure 64) containing upregulated bioactive phytochemicals (Figure 61, section 3.6).
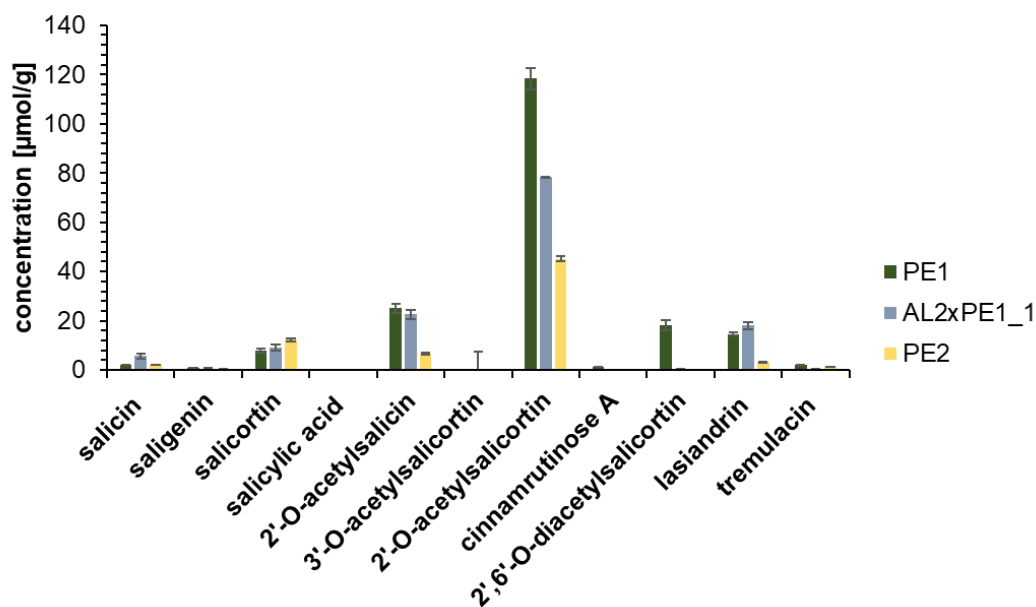
Figure 65: Concentrations (µmol/g) of analyzed phytochemicals in selected *Salix* genotypes PE1, PE2, and AL2xPE1_1.

Furthermore, the half-maximal inhibitory concentration (IC_{50}) was investigated for all anti-inflammatory compounds (**3**, **II**, **III**, **V**, **VI**, **VII**) in the 92 *Salix* genotypes (Table 8). **II** was very low concentrated in all *Salix* extracts and showed a too high IC_{50} value of 12.41 µM. Thus, the compound was not responsible for the bioactivity of any of the willow bark extracts. In contrast, the concentrations of salicortin, **III**, **V**, and **VI** in potent PE1 bark extract were higher than the half-maximal concentrations IC_{50} = 17.18, 16.33, 17.24, and 3.77 µM, respectively, indicating that these phytochemicals are more likely responsible for the PGE_2 inhibitory activity of the extract (Table 8). However, for potential candidate AL2xPE1_1, the low concentration of **V** and **VII** made both compounds not able

to block PGE_2 release at half-maximal concentration in the extract, whereas, **3**, **III**, and **VI** were trending at higher concentrations than the determined IC_{50} values of each compound. As **VI** was the most potent compound, AL2xPE1_1 could be indeed another potential phytopharmaceutical candidate.

Table 8: Concentrations of the analytes salicin (**1**), saligenin (**2**), salicortin (**3**), salicylic acid (**4**), and **I-VII** in *S. pentandra* (PE1) extract, PGE_2 release concentrations of each compound and standard deviations (%) and the corresponding IC_{50} values (PGE_2 release levels and IC_{50} data were obtained from UKF).

analyte	mean concentration [µmol/g]	mean concentration [µM]	PGE_2 release at 5 µg/mL [%]	PGE_2 release at 25 µg/mL [%]	IC_{50} [µg/mL]	IC_{50} [µM]
1	2.13	5.60	97+/-5	84+/-7	-	-
2	0.72	1.89	87+/-12	78+/-16	-	-
3	7.82	20.56	62+/-14	18+/-8	7.29	17.18
4	0.00	0.00	94+/-7	-	-	-
I	25.06	66.02	98+/-7	99+/-5	-	-
II	0.07	0.56	55+/-13	16+/-2	5.79	12.41
III	118.27	311.63	59+/-9	25+/-8	7.61	16.33
IV	1.19	5.27	92+/-7	88+/-14	-	-
V	18.04	47.56	64+/-8	25+/-11	8.76	17.24
VI	14.56	38.35	33+/-7	5+/-0	2.28	3.77
VII	2.04	5.37	77+/-9	38+/-7	16.13	30.48

3.7.3 Discussion

After isolation and structure determination of the compounds **I-VII** in *S. pentandra* species PE1 by means of activity-guided fractionation, the question emerged if the concentrations of these phytochemicals are responsible for the bioactivity of willow bark. Analysis of the bioactivity of the single compounds showed that **VI** was the most anti-inflammatory compound followed by **II**, **III**, **V** and **VII**, whereas **I** and **IV** were not inhibiting PGE_2 release (section 3.6). These compounds (**I-VII**) were quantitatively analyzed in 92 *Salix* species and crosses by developing also a LC-MS/MS method, which was validated successfully.

Moreover, the present work revealed SPE fraction F5 as the most potent among the eleven examined fractions, even though bioactive **VI** was isolated from fraction F6. Further, the concentrations of the phytochemicals in willow bark extract may play a role in blocking PGE_2 release and thus acting anti-inflammatory. In addition, degradation/metabolization compounds salicin (**1**),

saligenin (**2**), salicortin (**3**), and salicylic acid (**4**) were analyzed to examine whether their concentration play a role in the bioactivity and if the available compounds were degrading in the extracts. Saligenin and salicylic acid were very low concentrated and gave the evidence of no degradation of the salicylates. In general, salicylates tend to degrade and metabolize to saligenin and salicylic acid (Knuth et al. 2011, Ruuhola, Julkunen-Tiitto, and Vainiotalo 2003). In bioactive PE1, salicin was downregulated, a compound to which willow bark extracts are currently standardized to. For instance, Shara and Stohs (2015) have analyzed the potential of a standardized *S. alba* extract as an anti-inflammatory extract, drawing attention on the possibility that besides salicin further salicylates and phytochemicals may trigger the bioactivity. These previous publications, however, did not analyze the chemical composition.

The developed LC-MS/MS method and quantitative analysis, led to the assumption that high concentration of **III** (494.10 µmol/g) in fraction F5 was responsible for the bioactivity of the fraction. Moreover, the chemical composition of fraction F6 may have contained compounds inhibiting the anti-inflammatory effect of the fraction, but pure **VI** was more potent. On the other side, the chemical composition and concentrations of the phytochemicals **3**, **III**, **V**, and **VI** in PE1 being above the IC_{50} value showed the high potency and importance of these compounds to inhibit PGE_2 release. In contrast, the content of non-bioactive **IV** and **I** in PE1 was low.

Furthermore, the purified and identified compounds **I-VI** were trending in *S. pentandra* and *S. alba* genotypes of group 3, whereas salicortin and **VII** was upregulated mainly in *S. daphnoides* genotypes of group 1 followed by *S. purpurea* and a few *S. humboldtiana* genotypes of group 4 (Figure 13, section 3.1). The high abundance of salicortin in group 1 was previously shown in the S-plots (Figure 14, section 3.1) and could be confirmed by means of quantitative analysis. In contrast, group 2 of the PCA consisted of *S. viminalis*, *S. nigra*, and few *S. humboldtiana* species and crosses with very low salicylate content. Previous quantitative analysis of the same 92 *Salix* genotypes by means of HPLC-DAD-ESI-MS[3] focused on the determination of the salicylates **1**, **3**, **I**, **III**, and **VII** as well as of a few other phytochemicals such as flavonoids (eriodictyol-7-glucoside, naringenin-5-glucoside isomers, naringenin-7-glucoside, luteolin-7-glucoside, quercetin-hexoside, isosalipurposide, ampelopsin), flavan-3-ols

(catechin, epicatechin), and other phenolic compounds (caffeic acid derivatives, purpurein, salireposide, syrengin). That study could also show that salicylates were trending in cluster 3 comprising *S. pentandra* and *S. alba* species and crosses (Förster et al. 2021).

However, the present work was of higher sensitivity, since **1**, **3**, **I**, and **III** were not detected at all in a few *Salix* bark extracts examined by Förster et al. (2021) in comparison to the present study. For instance, VI2 did contain **1** (0.02 µmol/g) and **3** (2.53 µmol/g) in very low concentrations, in contrast to the studies of Förster et al. (2021), whereas similarly in both studies **I** and **III** were not found at all in this extract. Moreover, PE1 containing **1**, **2**, **3**, **I**-**VII** was analyzed also by Förster et al. (2021), but could not detect the low content of **3** (7.82 µmol/g), and **2**, **4**, **II**, **V**, **IV**, and **V** had not been quantified at all.

Previous research by Reichardt et al. (1992) identified salicortin, **I**, **III**, and **VI** in *S. lasiandra*, but did not quantify them. These compounds were also found in the present work in *S. lasiandra* genotypes LA1, PE2xLA1_1, PE2xLA1_2, and PE2xLA1_3, belonging to group 3, however, **I**, **III**, and **VI** were more upregulated in PE1 than in *S. lasiandra* clones. Förster et al. (2021) postulated also a reduced salicylate content in the same *S. lasiandra* species and crosses. **I** and **III** were high concentrated in PE1 and AL2xPE1_1 which did support the findings of Förster et al. (2021) performing HPLC-DAD-ESI-MS[3]. The high sensitivity of the quantitative method might have played a role in these differences.

Group 5 consisting of one *S. viminalis* x *S. daphnoides* extract, VI1xDA1_9, and grouping apart from the other groups in the middle of the PCA near the QC references (Figure 13, section 3.1), showed higher concentration of **1** and **3**, however, **I**-**VI** were not present in this extract in contrast to PE1. Whereas, non-bioactive *S. viminalis* x *S. viminalis* (*schwerinii* x *viminalis*) extract, VI4xVI3_2, revealed concentrations below 0.52 µmol/g for almost all salicylates and did not contain **4**, **II**, **IV**, and **V**. In Figure 66, exemplary, bioactive PE1, non-bioactive VI4xVI3_2, and VI1xDA1_9 were compared upon their phytochemical concentrations. The total phenolic concentration of 10.64 mg/g DW was much lower compared to PE1 (38.79 mg/g DW) (Förster et al. 2021), which may also have triggered the reduced bioactivity of VI4xVI3_2. This confirmed the statement of the screening analysis of section 3.5.6 (Figure 60), showing that VI4xVI3_2

contained predominantly polyphenols and led to the result that salicylates are responsible for the bioactivity.
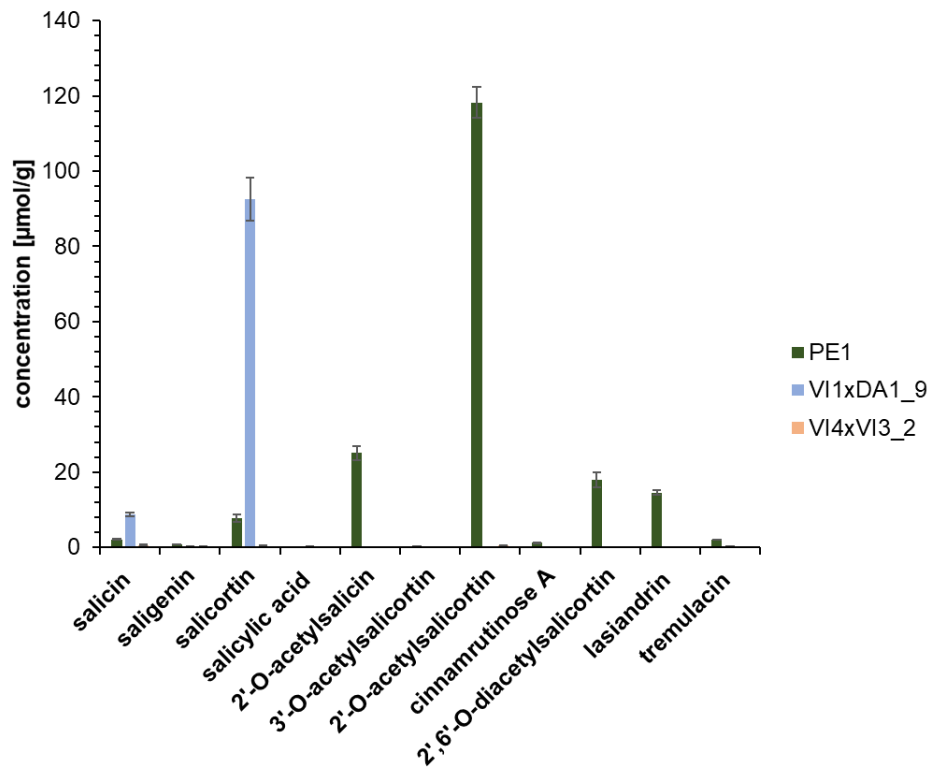
Figure 66: Quantitative comparison of analyzed phytochemicals in bioactive PE1 of group 3, VI1xDA1_9 of group 5, and non-bioactive VI4xVI3_2 of group 2.

Furthermore, comparing known literature data with the present study regarding *S. pentandra*, even though **I** was not anti-inflammatory against PGE$_2$ release, it was analyzed in past studies exhibiting inhibitory activity against nitric oxide at high IC$_{50}$ value of 123.36 µM (Kim et al. 2015). This shows that **I** may be effective reducing nitric oxide, but not PGE$_2$ levels. In contrast, high content of **III** in *S. pentandra* has been already revealed (Förster et al. 2021, Förster et al. 2009, Ruuhola, Julkunen-Tiitto, and Vainiotalo 2003). Particularly, in methanol extract of micropropagated *S. pentandra* leaves, **1** (~3 mg/g FW), **3** (~2 mg/g FW), **I** (~1 mg/g FW), **V** (~4 mg/g FW), and **VII** (~0.90 mg/g FW) besides high abundant **III** compound (~10 mg/g FW) could be quantified performing HPLC-DAD analysis (Julkunen-Tiitto and Sorsa 2001, Ruuhola, Julkunen-Tiitto, and Vainiotalo 2003). On the other side, non-micropropagated leaf extracts (50% methanol) showed slightly higher concentrations of the same compounds (Ruuhola, Julkunen-Tiitto, and Vainiotalo 2003). In the present study, however, higher sensitivity and

precision could be achieved with a validated LC-MS/MS method observing data for a huge amount of different *Salix* genotypes.

Additionally, inhibition potential of **3**, **II**, **III**, and **VII** besides **I** from *S. glandulosa* and *S. pseudo-lasiogyne* against nitric oxide in LPS-stimulated BV2 cells have been determined by Kim et al. (2015) and Yang et al. (2013), showing similar IC_{50} values in both studies. The concentrations of **III** in AL2xPE1_1 and PE1 may be able to inhibit nitric oxide activity at half-maximal concentrations described for *S. glandulosa* in the study of Kim et al. (2015). Nevertheless, the determination of the IC_{50} values regarding PGE_2 inhibitory of **II**, **III**, **V**, **VI**, and **VII** was novel in the present work and was not described previously in the literature. These compounds could successfully act against PGE_2 release at half-maximal concentration. Moreover, for the first time in this study, **2**, salicylates **II** and **VI**, and non-salicylate **IV** could be quantified in *Salix* extracts by means of a developed sensitive LC-MS/MS method.

Finally, the importance of salicylates from *Salix* bark for the phytopharmaceutical production was confirmed. However, further studies on *in vivo* bioavailability, cytotoxicity, and anti-oxidative activity of *Salix* bark extracts and especially of anti-inflammatory PE1, inhibiting PGE_2 release, needs further research in order to produce a highly valuable herbal medicinal product.

Identifying *Salix* species or crosses with high amounts of potent compounds as specified in this study would help future breeding programs. Additionally, standardization procedure of phytopharmaceutical willow bark needs further investigation. For instance, instead of standardizing to **1**, compounds comprising a HCH moiety could be used for this purpose, which may increase the anti-inflammatory potential. The present work could also confirm the correlation between bioactivity and salicylate composition.

4 EXPERIMENTAL SECTION

4.1 Materials and reagents

4.1.1 *Salix* genotype collection

Salix genotypes were provided by HUB and have been annotated in Förster et al. (2021). The plant collection originated from Germany, Poland, Austria, Rumania, and USA and was obtained in the period 2006-2009. Further, *Salix* parental forms were cultivated in 2012, and crosses were generated in 2015 by HUB from the species *Salix alba*, *Salix daphnoides*, *Salix humboldtiana*, *Salix lasiandra*, *Salix nigra*, *Salix pentandra*, *Salix purpurea*, *Salix* x *rubens*, and *Salix viminalis*. After obtaining the bark of the woody plant with a vegetable peeler (section 4.3), it was frozen at -80°C, and freeze-dried for further analysis. An overview of the provided *Salix* extracts and their assigned group (extracted from the PCA analysis) is depicted in Table 9.

Table 9: Origin and area of cultivation of the 92 *Salix* species and crosses (adapted from Förster et al. (2021)). S: species, K: clones, h: hybrid, G: cultivated in Germany, ZP: cultivated in Zepernick/Germany, DA: cultivated in Berlin-Dahlem/Germany.

species	abbreviation	key name	cultivation	origin	group
S. viminalis	VI1	S1	ZP	chance seedling Waldsieversdorf 2011, G	2
S. daphnoides	DA1	S2	DA	Mecklenburg-Vorpommern, Pampow, G	1
S. viminalis x *S. daphnoides*	VI1xDA1_1	K1	DA	new cross HU Berlin 2014, G	1
S. viminalis x *S. daphnoides*	VI1xDA1_2	K19	DA	new cross HU Berlin 2014, G	2
S. viminalis x *S. daphnoides*	VI1xDA1_3	K20	DA	new cross HU Berlin 2014, G	2
S. viminalis x *S. daphnoides*	VI1xDA1_4	K5	DA	new cross HU Berlin 2014, G	2
S. viminalis x *S. daphnoides*	VI1xDA1_5	K21	DA	new cross HU Berlin 2014, G	2
S. viminalis x *S. daphnoides*	VI1xDA1_6	K22	DA	new cross HU Berlin 2014, G	2
S. viminalis x *S. daphnoides*	VI1xDA1_7	K23	DA	new cross HU Berlin 2014, G	2
S. viminalis x *S. daphnoides*	VI1xDA1_8	K24	DA	new cross HU Berlin 2014, G	2
S. viminalis x *S. daphnoides*	VI1xDA1_9	K18	DA	new cross HU Berlin 2014, G	5

species	abbreviation	key name	cultivation	origin	group
S. viminalis	VI2	S20	Wriezen	Swedish clone, 'Jorr', sold by Lantmännen Agroenergie AB	2
S. daphnoides	DA2xDA3	S27	ZP	new cross HU Berlin 2011, G	1
S. daphnoides x *S. viminalis*	(DA2xDA3)xVI2_1	K25	DA	new cross HU Berlin 2014, G	1
S. daphnoides x *S. viminalis*	(DA2xDA3)xVI2_2	K26	DA	new cross HU Berlin 2014, G	1
S. daphnoides x *S. viminalis*	(DA2xDA3)xVI2_3	K2	DA	new cross HU Berlin 2014, G	1
S. daphnoides x *S. viminalis*	(DA2xDA3)xVI2_4	K27	DA	new cross HU Berlin 2014, G	1
S. daphnoides x *S. viminalis*	(DA2xDA3)xVI2_5	K28	DA	new cross HU Berlin 2014, G	1
S. humboldtiana x *S. purpurea*	HU1xPU1	K29	ZP	new cross Waldsieversdorf 2011, G	3
S. daphnoides	DA4	S3	DA	Mecklenburg-Vorpommern, Zarrendorf, G	1
(S. humboldtiana x *S. purpurea)* x *S. daphnoides*	(HU1xPU1)xDA4_1	K30	DA	new cross HU Berlin 2014, G	4
(S. humboldtiana x *S. purpurea)* x *S. daphnoides*	(HU1xPU1)xDA4_2	K31	DA	new cross HU Berlin 2014, G	4
(S. humboldtiana x *S. purpurea)* x *S. daphnoides*	(HU1xPU1)xDA4_3	K14	DA	new cross HU Berlin 2014, G	4
S. viminalis (schwerinii x *viminalis)*	VI3_h	S25	WS	Swedish clone 'Olof', sold by Lantmännen Agroenergie AB	2
S. viminalis	VI4	S4	DA	Swedish clone '79036' breeding company Svalöf-Weibull AB	2
S. viminalis x *S. viminalis (schwerinii* x *viminalis)*	VI4xVI3_1	K32	ZP	new cross Waldsieversdorf 2012, G	2
S. viminalis x *S. viminalis (schwerinii* x *viminalis)*	VI4xVI3_2	K6	ZP	new cross Waldsieversdorf 2012, G	2
S. alba x *S.* x *rubens*	AL1_h	S26	ZP	Baja, 'B38', University of Sopron, Hungary	3
S. alba	AL2	S5	ZP	Thüringen, Erfurt, Höngeda, G	3
S. alba x *S. alba* x *S.* x *rubens*	AL2xAL1_1	K10	DA	new cross Waldsieversdorf 2014, G	3

species	abbreviation	key name	cultivation	origin	group
S. alba x *S. alba* x *S. x rubens*	AL2xAL1_2	K33	DA	new cross Waldsieversdorf 2014, G	3
S. pentandra	PE1	S6	DA	Brandenburg, Eggersdorf, G	3
S. alba x *S. pentandra*	AL2xPE1_1	K34	DA	new cross Waldsieversdorf 2014, G	3
S. alba x *S. pentandra*	AL2xPE1_2	K35	DA	new cross Waldsieversdorf 2014, G	3
S. alba	AL3	S7	ZP	Brandenburg, Waldsieversdorf , G	3
S. alba	AL4	S8	ZP	Bukarest, Institutul de Cercetări Forestiere, Romania	3
S. alba x *S. alba*	AL3xAL4_1	K36	DA	new cross Waldsieversdorf 2014, G	3
S. alba x *S. alba*	AL3xAL4_2	K37	DA	new cross Waldsieversdorf 2014, G	3
S. viminalis	VI5	S9	DA	English clone, 'Bowles', UK National Willows Collection	2
S. viminalis x *S. viminalis*	VI5xVI2_1	K38	DA	new cross Waldsieversdorf 2011, G	2
S. viminalis x *S. viminalis*	VI5xVI2_2	K39	DA	new cross Waldsieversdorf 2011, G	2
S. viminalis x *S. viminalis*	VI5xVI2_3	K40	DA	new cross Waldsieversdorf 2011, G	2
S. viminalis x *S. viminalis*	VI5xVI2_4	K41	DA	new cross Waldsieversdorf 2011, G	2
S. daphnoides	DA3	S10	DA	Baden-Württemberg, Laimnau Argen, G	1
S. daphnoides	DA2	S11	DA	Westpommern, Miedzyzdroje, Poland	1
S. daphnoides	DA2xDA3_1	K42	DA	new cross HU Berlin 2011, G	1
S. daphnoides	DA2xDA3_2	K43	DA	new cross HU Berlin 2011, G	1
S. daphnoides	DA2xDA3_3	K44	DA	new cross HU Berlin 2011, G	1
S. daphnoides	DA2xDA3_4	K45	DA	new cross HU Berlin 2011, G	1
S. daphnoides	DA2xDA3_5	K46	DA	new cross HU Berlin 2011, G	1

species	abbreviation	key name	cultivation	origin	group
S. daphnoides	DA2xDA3_6	K47	DA	new cross HU Berlin 2011, G	1
S. daphnoides	DA2xDA3_7	K48	DA	new cross HU Berlin 2011, G	1
S. daphnoides	DA2xDA3_8	K3	DA	new cross HU Berlin 2011, G	1
S. daphnoides	DA5	S12	DA	Westpommern, Dziwnow, Poland	1
S. purpurea	PU2	S18	DA	Baden-Württemberg, Birkenried Pfohren, G	4
S. daphnoides x *S. purpurea*	DA5xPU2_1	K4	ZP	new cross HU Berlin 2012, G	1
S. daphnoides x *S. purpurea*	DA5xPU2_2	K49	ZP	new cross HU Berlin 2012, G	1
S. lasiandra	LA1	S13	ZP	Maryland, National Plant Materials Center Beltsville, Soil Conservation Service, USA	3
S. pentandra	PE2	S14	DA	Salzburg, Zell am See, Zeller Moos, Austria	3
S. pentandra x *S. lasiandra*	PE2xLA1_1	K11	DA	new cross HU Berlin 2014, G	3
S. pentandra x *S. lasiandra*	PE2xLA1_2	K50	DA	new cross HU Berlin 2014, G	3
S. pentandra x *S. lasiandra*	PE2xLA1_3	K51	DA	new cross HU Berlin 2014, G	3
S. alba	AL5	S15	ZP	Mecklenburg-Vorpommern, Schloen, G	3
S. pentandra x *S. alba*	PE2xAL5_1	K52	DA	new cross HU Berlin 2013, G	1
S. pentandra x *S. alba*	PE2xAL5_2	K12	DA	new cross HU Berlin 2013, G	3
S. pentandra x *S. alba*	PE2xAL5_3	K53	DA	new cross HU Berlin 2013, G	3
S. pentandra x *S. alba*	PE2xAL5_4	K54	DA	new cross HU Berlin 2013, G	3
S. daphnoides	DA6	S16	DA	Mecklenburg-Vorpommern, Zarrendorf, G	1
S. purpurea	PU3	S17	ZP	Bayern, Miesbach, Aschenbach, G	4
S. purpurea x *S. daphnoides*	PU3xDA6_1	K55	DA	new cross Waldsieversdorf 2014, G	4
S. purpurea x *S. daphnoides*	PU3xDA6_2	K15	DA	new cross Waldsieversdorf 2014, G	4
S. purpurea x *S. daphnoides*	PU3xDA6_3	K56	DA	new cross Waldsieversdorf 2014, G	4

species	abbreviation	key name	cultivation	origin	group
S. purpurea x *S. daphnoides*	PU3xDA6_4	K57	DA	new cross Waldsieversdorf 2014, G	4
S. purpurea x *S. daphnoides*	PU3xDA6_5	K58	DA	new cross Waldsieversdorf 2014, G	4
S. purpurea x *S. viminalis (schwerinii x viminalis)*	PU3xVI3_1	K59	ZP	new cross Waldsieversdorf 2012, G	3
S. purpurea x *S. viminalis (schwerinii x viminalis)*	PU3xVI3_2	K60	ZP	new cross Waldsieversdorf 2012, G	3
S. purpurea x *S. purpurea*	PU3xPU2_1	K61	ZP	new cross Waldsieversdorf 2012, G	4
S. purpurea x *S. purpurea*	PU3xPU2_2	K62	ZP	new cross Waldsieversdorf 2012, G	4
S. purpurea x *S. purpurea*	PU3xPU2_3	K16	ZP	new cross Waldsieversdorf 2012, G	4
S. purpurea	PU4	S19	DA	Bayern, Weilheim-Schongau, Ammer, G	4
S. purpurea x *S. viminalis*	PU4xVI2_1	K7	DA	new cross Waldsieversdorf 2011, G	2
S. purpurea x *S. viminalis*	PU4xVI2_2	K63	DA	new cross Waldsieversdorf 2011, G	2
S. humboldtiana	HU1	S21	WS	Swedish clone, 'SH2' breeding company Svalöf-Weibull AB	2
S. viminalis	VI6	S22	WS	Swedish clone, '78195' breeding company Svalöf-Weibull AB	2
S. humboldtiana x *S. viminalis*	HU1xVI6_1	K8	ZP	new cross Waldsieversdorf 2012, G	2
S. humboldtiana x *S. viminalis*	HU1xVI6_2	K65	ZP	new cross Waldsieversdorf 2012, G	2
S. purpurea	PU1	S23	DA	Bayern, Garmisch-Partenkirchen, Oberau, G	4
S. humboldtiana x *S. purpurea*	HU1xPU1_1	K13	DA	new cross Waldsieversdorf 2011, G	3
S. humboldtiana x *S. purpurea*	HU1xPU1_2	K66	DA	new cross Waldsieversdorf 2011, G	3

species	abbreviation	key name	cultivation	origin	group
S. humboldtiana x *S. purpurea*	HU1xPU1_3	K17	DA	new cross Waldsieversdorf 2011, G	4
S. nigra	SN1	S24	Garzau	unknown	2
S. nigra x *S. pentandra*	SN1xPE1	K9	ZP	new cross Waldsieversdorf 2012, G	2
extract B	-	B	-	*Salix*-mix from a pharmaceutical company	-

4.1.2 Chemicals and reagents

The following reagents and chemicals with p.a.-quality were used for extraction, fractionation, analysis, and screening. Ultrapure water was provided from the Milli-Q® Advantage A10 (Millipore, Schwalbach, Germany) and Elix® water purification system (Merck S.A.S., Molsheim, France). For the analytical and preparative HPLC, as well as for the screening and quantitative analysis by mass spectrometry, solvents of HPLC and LC-MS-grade were used, respectively.

acetone (LiChrosolv), Merck KGaA, Darmstadt, Germany

acetonitrile (HPLC gradient grade), J.T. Baker®, Deventer, Netherlands

acetonitrile (HPLC gradient grade), Fischer scientific GmbH, Schwerte, Germany

acetonitrile (LC-MS reagent), J.T. Baker®, Deventer, Netherlands

anhydrous pyridine (purity 99.8%), Sigma-Aldrich, Darmstadt, Germany

catechol (purity ≥95.0% (GC)), Sigma-Aldrich, Darmstadt, Germany

deuterated acetone (acetone-d_6, CD_3COCD_3), Sigma-Aldrich, Darmstadt, Germany

D-glucose, Sigma-Aldrich, Darmstadt, Germany

D-glucuronic acid (97% purity), Fluka Chemika, Buchs, Switzerland

D-salicin, Carbosynth, Bertshire, UK

D-xylose, Sigma-Aldrich, Darmstadt, Germany

ethanol (absolute, purity ≥ 99.8%, AnalaR NORMAPUR®, ACS, Reag.Ph.Eur. analytical reagent), VWR, Darmstadt, Germany

ethyl acetate, BDH, Prolabo, Briare, France

formic acid, Merck KGaA, Darmstadt, Germany

hexadeuterodimethyl sulfoxide (Dimethyl sulfoxide-d_6, DMSO-d_6, $((CD_3)_2SO)$, Sigma-Aldrich, Darmstadt, Germany

hydrochloric acid (fuming, 37%), Merck KGaA, Darmstadt, Germany

hydrochloric acid (0.1 M), Merck KGaA, Darmstadt, Germany

L-cysteine methyl ester hydrochloride (purity 98%), Sigma-Aldrich, Darmstadt, Germany

L-galacturonic acid, Serva Feinbiochemie, Heidelberg, Germany

L-glucose, Sigma-Aldrich, Darmstadt, Germany

L-rhamnose, Sigma-Aldrich, Darmstadt, Germany

MajorMix solution, Waters, Milford, MA, USA

methanol (HPLC gradient grade), J.T. Baker®, Deventer, Netherlands

methanol (LC-MS reagent), J.T. Baker®, Deventer, Netherlands

pentapeptide leucine enkephalin (Tyr-Gly-Gly-Phe-Leu, *m/z* 554.2615 $[M-H]^-$), Merck KGaA, Darmstadt, Germany

phenylethyl isothiocyanate, Sigma-Aldrich, Steinheim, Germany

salicortin (purity 95%, isolated from *Populus* sp.) Biosynth Carbosynth., United Kingdom

salicylic acid (purity ≥ 99%), Carl Roth GmbH & Co. KG, Karlsruhe, Germany

salicylic acid-d_4 (100 µg/mL in acetonitrile), Supelco®, Munich, Germany

salicylic acid-d_4 (powder purity ≥ 97%), Toronto Research Chemicals, Toronto, Canada

saligenin, Sigma-Aldrich, Darmstadt, Germany

sodium hydroxide solution (0.1 M), Sigma-Aldrich, Darmstadt, Germany

tetradeuteromethanol (methanol-d_4, CD_3OD), Sigma-Aldrich, Darmstadt, Germany

trideuteroacetonitrile (acetonitrile-d_3, CD_3CN), Sigma-Aldrich, Darmstadt, Germany

4.1.3 Consumables

bead beater tube (CK28_2 mL), Bertin Technologies, Montigny-le-Bretonneux, France

filter papers (Ø 125 mm), Macherey-Nagel GmbH & Co. KG, Düren, Germany

membrane filters (Minisart® RC 15, pore size 0.45 µm, Ø 15 mm), Sartorius AG, Göttingen, Germany

NMR tubes and caps (177.8 x 4.97 mm, wall thickness 0.38 mm, round bottom), Bruker, Billerica, MA, USA

pipet tips (universal, 2-200 µL, 50-1,000 µL), VWR International GmbH

pipet tips (standard, 0.5-5 mL, 1-10 mL), Brand GmbH & Co. KG, Wertheim, Germany

solid-phase extraction cartridges (C_{18} ec polypropylene, octadecyl modified silica phase, 60 Å, 10 g/70 mL), CHROMABOND®, Macherey-Nagel GmbH & Co. KG, Düren, Germany

syringes (single-use, 1, 3, 5 mL), B. Braun, Melsungen, Germany

vials N9 (flat, screw neck, 1.5 mL, 11.6 x 32 mm, amber or clear), Greiner Bio-one GmbH, Kremsmünster, Austria

vial inserts (15 mm, 0.2 mL, 6 x 31 mm, clear), Macherey-Nagel GmbH & Co. KG, Düren, Germany

vial screw caps (transparent, center hole, PTFE blue, slit, 1 mm), Macherey-Nagel GmbH & Co. KG, Düren, Germany

4.1.4 Materials and devices

balance (AUW-D series), Shimadzu GmbH, Duisburg, Germany

bead beater homogenizer (Precellys Evolution Homogenizer), Bertin Technologies, Montigny-le-Bretonneux, France

büchner funnel (795 mL, Ø 125 mm), VWR International GmbH, Darmstadt, Germany

freeze dryer (Christ Gamma 1-20), Martin Christ Gefriertrocknungsanlagen GmbH, Osterode, Germany conntected to Chemvac Kombipumpstandstand (type 109013-04), Ilmvac GmbG, Ilmenau, Germany

freeze dryer (Christ Delta 1-24 LSC), Martin Christ Gefriertrocknungsanlagen GmbH, Osterode, Germany connected to Chemvac Kombipumpstandstand (type 109015-05), Ilmvac GmbG, Ilmenau, Germany

pipets (variable, 20 µL, 200 µL, 100-1,000 µL, 0.5-5 mL, 1-10 mL), Eppendorf Research, Hamburg, Germany

rotary evaporator (vacuum pump V-700, rotavapor R-210, vac controller V-850, heating bath B-491, recirculating chiller B-740), Büchi Labortechnik AG, Flawil, Switzerland

speedVac vacuum concentrator plus with integrated membrane vacuum pump (without rotor, 230 V/50-60 Hz), Eppendorf, AG, Hamburg, Germany

thermomixer (HLC Heating-ThermoMixer MHL 23), DITABIS AG, Pforzheim, Germany

ultrasonic bath (RK 510 H, 230 V~ (±10%), 50/60 Hz, 2.5 A, 180/640 W, 3.4 kHz) Bandelin Sonorex, Bandelin electronic GmbH & Co. KG, Berlin, Germany

4.1.5 Software and internet resources

Analyst® (version 1.6.2 and 1.6.3), Sciex, Darmstadt, Germany

ChemDraw (version 17.0.0.206), PerkinElmer Informatics Inc., Waltham, MA, USA

ChemSpider, Royal Society of Chemistry, Cambridge, UK

ChromPass (version 1.9), Jasco, Groß-Umstadt, Germany

EZinfo (version 3.0), Umetrics, Sartorius Stedim Biotech, Umeå, Sweden

Galaxie (version 1.10), Agilent Technologies, Oberhaching, Germany

MassLynx™ (version 4.1), Waters, Manchester, UK

MestReNova (version 12.0.3), Mestrelab Research S.L., Santiago de Compostela, Spain

MultiQuant™ (version 3.0.3), Sciex, Darmstadt, Germany

PeakView® (version 2.2), Sciex, Darmstadt, Germany

Progenesis QI (version 2.1), Waters, Manchester, UK

Progenesis SDF (structure data file) Studio, Waters, Manchester, UK

SciFinder, a CAS solution, American Chemical Society (ACS), Chemistry for life©, Washington, DC, USA

Spectra Manager™ Suite, Jasco, Tokyo, Japan

TopSpin™ (version 4.0.6), Bruker, Rheinstetten, Germany

UNIFI (version 1.8), Waters, Milford, MA, USA

4.2 Untargeted chemoprofiling

In order to observe the chemoprofile of the 92 *Salix* species and crosses (Table 9, section 4.1.1), and group them upon their chemical composition, a principal component analysis (PCA) was performed by means of UPLC-ToF-MS screening (LC-MS system 1). First, according to the extraction protocol by Förster et al. (2021), 10 mg of woody plant material was harvested using a vegetable peeler and the obtained bark was lyophilized, and extracted using 500 µL of 0.1% formic acid in methanol/water (v/v, 70/30) and exposing the solutions in ultrasonic bath for 15 min in an ice water, which was centrifuged then for 5 min at 10,000 rpm and 20°C. After obtaining the supernatant, the extraction procedure of the pellet was repeated another two times by adding 200 µL of 0.1% formic acid in methanol/water (v/v, 70/30), and the combined supernatant was subsequently topped with 100 µL ultrapure water to 1 mL, and filtered by 0.22 µm SpinX tubes.

Then, the 92 *Salix* bark extracts were analyzed by means of UPLC-ESI⁻-IMS-ToF-MS (LC-MS system 1) method described in the publication of Förster et al. (2021) (Table 10). Each extract was injected four times (technical replicates) into the UPLC-ToF-MS system A pooled sample, containing a mixture of all *Salix* extracts, was used as a quality control (QC) used for the automatic normalization processing by means of the Progenesis QI v2.1 software (Waters, Manchester, UK) and MS signal error correction. The QC was injected after every ten injections of the *Salix* extract samples (in total 20 times) to keep MS analysis consistency.

Table 10: LC-MS system 1 conditions for the untargeted chemoprofiling.

parameter	description
stationary phase	Acquity UPLC BEH C_{18} column, 1.7 µm, 130 Å, 2.1 x 50 mm, 3/pkg (Waters, Manchester, UK)
column temperature	45°C
mobile phase	A: 0.1% formic acid in water, B: 0.1% formic acid in acetonitrile
ionization	electrospray ionization (ESI)
polarity	negative
injection volume	1 µL
run time	8 min
flow rate	0.4 mL/min
ion source	HDMS^e sensitivity mode
HDMS^e scan time	0.3 s
capillary voltage	2.5 kV
cone gas flow	50 L/h
source temperature	150°C
desolvation temperature	450°C
desolvation gas flow	900 L/h
collision energy	20-40 eV
mass calibration range	m/z 50 – 1,000, calibration using MajorMix solution
lock mass correction solution	50 pg/100 µL of pentapeptide leucine enkephalin in 0.1% formic acid in acetonitrile (v/v, 1/1)
gradient program	1% B, isocratic for 1 min, in 3.5 min to 60% B, in 1 min to 80% B, in 1.5 min to 100% B, isocratic for 1 min, in 0.5 min to 1% B, isocratic for 1.5 min

Subsequently, the fragmentation patterns of the analytes detected in the samples was compared using the MetaScope identification method, which is an *in silico* database in which the analytes are listed. The data of the 92 *Salix* extracts were imported into the Progenesis QI software and 396 profiled MS^e raw data were automatically processed.

Further analysis was performed by the software using a lineup of processes, such as chromatographic peak alignment, experimental design setup, peak picking, deconvolution, compound identification, and compound statistics, and by setting parameters as displayed in Table 11.

Table 11: Progenesis QI settings and parameters used for data analysis.

settings	parameters
peak picking	all runs, automatic limits, default sensitivity, retention time limits of 0.05 - 7.50 min, fragment sensitivity with base peak 1%
ion deconvolution	adducts: $[M-2H]^-$, $[M-H_2O-H]^-$, $[M-H]^-$, $[M+HCO_2H-H]^-$, $[2M-H]^-$, $[2M+HCO_2H-H]^-$, $[2M+CH_2COH-H]^-$, $[3M-H]^-$
tag filtration	ANOVA p-value ≤ 0.05, Max-fold change value ≥ 2
MetaScope method for *in silico* fragment database	auto-detect data format, precursor tolerance 5 ppm, theoretical fragment tolerance 5 ppm.

For principal component analysis, a normalization reference - the quality control sample 7 - was selected by the software. The PCA score plot was created using the tool EZinfo v3.0 (Umetrics, Sweden), which applies Pareto scaling for statistical analysis and is connected to the Progenesis QI software.

In order to compare the created groups, S-plots were performed by orthogonal projection to latent structure discriminant analysis (OPLS-DA), which can detect up- or downregulated compounds.

4.3 *Salix* bark powder preparation

Cortex of 92 *Salix* species and crosses was harvested by HUB using a commercial vegetable peeler (Figure 67). After freeze-drying and grinding, the powdered bark material was provided to the chair of Food Chemistry and Molecular Sensory Science for further extraction, fractionation, and compound identification experiments. For bioactivity assays of the selected 28 *Salix* extracts performed by UKF, *Salix* bark was extracted using 0.1% formic acid in

methanol/water (v/v, 70/30). The freeze-dried extracts were standardized with water to 10 mg/mL phenolic glucoside content and used further to perform bioactivity assays.

Figure 67: *Salix* bark harvesting using a vegetable peeler (adopted from HUB).

4.4 Isolation of *Salix* phytochemicals

4.4.1 Sequential solvent extraction

Powdered *S. pentandra* (PE1) cortex was provided by HUB as described in section 4.3. For the sequential solvent extraction of phytochemicals from bioactive *S. pentandra*, 120 g of powdered bark was mixed first with 680 mL pure methanol, stirred for 30 min at room temperature, and then filtered through a glass funnel with a max. pore size of 100-160 µm under vacuum. The extraction with methanol was repeated another four times. Subsequently, the residue was used further for the extraction with 680 mL of methanol/water (v/v, 70/30) three times. Finally, the residue was extracted three times with 680 mL distilled water. The water extract was filtered through a glass funnel and filter paper. The corresponding extracts were combined, and the organic solvent was removed by means of a rotary evaporator and vacuum at 39°C. Finally, the three liquid phases were lyophilized individually to obtain three *Salix* bark extracts (methanol, methanol/water, and water extracts) with different chemical compositions. The extracts were stored at -20°C until further use.

4.4.2 Pre-fractionation of phytochemicals from *Salix* methanol extract by solid-phase extraction

Solid-phase extraction of bioactive *S. pentandra* methanol extract was performed using C_{18} end-capped 60 Å cartridges. First, the cartridges were preconditioned using 70 mL of methanol without applying vacuum. Then, for the conditioning of the column, 70 mL of v/v, 70/30 of methanol/water, and finally 70 mL of water were added sequentially using vacuum.

For the separation of the bioactive methanol extract of *S. pentandra*, approximately 10 g extract were dissolved in 70 mL water, and added onto the cartridge. The elution of the eleven fractions was achieved in 10%-steps using vacuum as described in Table 12. The organic solvent of each fraction, F1 to F11, was evaporated under reduced pressure and lyophilized separately. For verification of the chemical composition of SPE fractions and the three *Salix* extracts, analytical HPLC (system 1; Table 13) and LC-MS (system 2; Table 14) analysis was performed.

Table 12: Solid-phase extraction using sequential elution of the methanol extract of *S. pentandra* into eleven fractions.

SPE fraction	F1	F2	F3	F4	F5	F6	F7	F8	F9	F10	F11
methanol/water v/v [%]	0/ 100	10/ 90	20/ 80	30/ 70	40/ 60	50/ 50	60/ 40	70/ 30	80/ 20	90/ 10	100/ 0

4.4.3 Verification of chemical composition of *Salix* extracts and SPE fractions

4.4.3.1 Analytical HPLC analysis

The most bioactive SPE fractions F5, F6, and F7 of the potent methanol extract were analyzed by analytical high-performance liquid chromatography (HPLC, system 1). The chromatographic separation using a gradient method from 5 to 100% organic solvent by HPLC can help further to develop a method for the preparative fractionation of bioactive SPE fractions, and further isolation of phytochemicals.

Analytical HPLC was performed using a diode-array (DAD) and an evaporative light-scattering detector (ELSD) in order to separate all possible UV (non-)visible

compounds. Therefore, SPE fractions were diluted in acetonitrile/water (v/v, 70/30) and membrane-filtered (pore size 0.45 µm, Ø 15 mm) to a final concentration of 1 mg/mL. The peak separation was performed by means of HPLC system 1 using the analytical 250 x 4.6 mm Luna® 5 µm phenyl-hexyl column (Table 13).

Table 13: Chromatographic conditions of the HPLC system 1 used for fraction verification and gradient development.

Parameter	Description
stationary phase	Luna® phenyl-hexyl column, 100 Å, 250 x 4.6 mm, 5 µm particle size (Phenomenex Ltd., Aschaffenburg, Deutschland)
mobile phase	A: 0.1% formic acid in water, B: 0.1% formic acid in acetonitrile
detection	DAD and ELSD
wavelength	200 nm
injection volume	30 µL
run time	75 min
flow rate	1 mL/min
gradient program	5% B, isocratic for 5 min, in 55 min to 100% B, isocratic for 5 min, in 4 min to 5% B, isocratic for 6 min

4.4.3.2 LC-MS screening

For the identification and analysis of the mass-to-charge ratios (*m/z*) of the compounds either isolated in pure form or contained in the fractions and extracts, screening was performed by means of UPLC-ToF-MS (LC-MS system 2). The methanol, methanol/water, and water extracts of *S. pentandra* bark, as well as the eleven SPE fractions, fractions of the (semi-)preparative HPLC, and single compounds were screened using the parameters described below (Table 14).

Table 14: LC-MS system 2 conditions used for screening.

Parameter	Description
stationary phase	Acquity UPLC BEH C_{18} column, 150 x 2.1 mm, 1.7 µm (Waters, Mangester, UK)
column temperature	45°C
mobile phase	A: 0.1% formic acid in water, B: 0.1% formic acid in acetonitrile
ionization	electrospray ionization (ESI)
polarity	negative
injection volume	1 µL
run time	8 min
flow rate	0.4 mL/min
ion source	HDMS^e sensitivity mode
HDMS^e scan time	0.1 s
capillary voltage	1.8 kV
cone gas flow	5 L/h
source temperature	120°C
desolvation temperature	450°C
desolvation gas flow	850 L/h
collision energy	20-30 eV
gradient program	1% B, isocratic for 1 min, in 3.5 min to 60% B, in 1 min to 80% B, in 0.5 min to 100% B, isocratic for 1 min, in 0.5 min to 1% B, isocratic for 0.5 min

4.4.4 Subfractionation of SPE fraction F5

The bioactivity assays showed a high potency of SPE fraction F5 (section 3.3.2). Therefore, it was fractionated further by means of HPLC system 1 (Table 15) using 10 mg/mL of the extract, which was diluted in methanol, membrane filtered (0.45 µm), and 500 µL were injected into the HPLC for each run. For chromatographic separation a phenyl-hexyl column and 0.1% formic acid in acetonitrile and water were used.

Table 15: Chromatographic conditions of the HPLC system 1 used for preparative fractionation of SPE fraction F5.

Parameter	Description
stationary phase	Luna® phenyl-hexyl column, 100 Å, 250 x 21.2 mm, 5 µm particle size (Phenomenex Ltd., Aschaffenburg, Deutschland)
mobile phase	A: 0.1% formic acid in water, B: 0.1% formic acid in acetonitrile
detection	DAD
wavelength	200 nm
sample concentration	10 mg/mL in 100% methanol
injection volume	500 µL
run time	33 min
flow rate	20 mL/min
gradient program	22% B, isocratic for 3 min, in 10 min to 23.5% B, isocratic for 15 min, in 2 min to 22% B, isocratic for 3 min

The column effluent was separated into six fractions, F5-1 to F5-6, the organic solvent was evaporated, and finally each fraction was lyophilized. All dried fractions were stored at -20°C until further use.

Then, the anti-inflammatory potential of each subfraction was investigated by UKF (section 3.5.1). The most bioactive fraction F5-5 was purified further by semi-preparative fractionation (Table 16). Subsequently, this fraction was further subfractionated to isolate possible bioactive compounds contained in F5-5 by means of HPLC system 2 (Table 16).

Table 16: Chromatographic conditions of the HPLC system 2 used for semi-preparative fractionation of fraction F5-5.

Parameter	Description
stationary phase	Luna® PFP column, 250 x 10 mm, 5 µm particle size (Phenomenex Ltd., Aschaffenburg, Deutschland)
mobile phase	A: 0.1% formic acid in water, B: 0.1% formic acid in methanol
detection	UV
wavelength	200 nm
sample concentration	5 mg/mL in water
injection volume	300 µL
run time	65 min
flow rate	4.7 mL/min
gradient program	22% B, isocratic for 3 min, in 15 min to 27.7% B, isocratic for 2 min, in 10 min to 52% B, isocratic for 3 min, in 20 min to 57% B, isocratic for 2 min, in 3 min to 22% B, isocratic for 2 min

Phenolic glucosides are UV visible (Aleixandre-Tudo and Du Toit 2018) and were therefore detected and isolated by their maxima using HPLC-UV techniques. Thus, fractions F5-5-1 to F5-5-8 were collected, the solvent was evaporated and freeze-dried. The obtained compounds 2'-*O*-acetylsalicin (**I**), 3'-*O*-acetylsalicortin (**II**), and 2'-*O*-acetylsalicortin (**III**) in F5-5-3, F5-5-5, and F5-5-7, respectively, were identified by means of ultra-high-performance liquid chromatography coupled to mass spectrometry (UHPLC-MS/MS), nuclear magnetic resonance spectroscopy (NMR), and circular dichroism (CD) spectroscopy.

Due to the reduced yield of **I** in fraction F5-5-3, the compound was isolated in higher amounts from SPE fraction F4, more specifically from fraction F4-1. The used parameters are summarized in Table 17.

Table 17: Chromatographic conditions of the HPLC system 1 used for preparative fractionation of SPE fraction F4.

Parameter	Description
stationary phase	Luna® phenyl-hexyl column, 100 Å, 250 x 21.2 mm, 5 µm particle size (Phenomenex Ltd., Aschaffenburg, Deutschland)
mobile phase	A: 0.1% formic acid in water, B: 0.1% formic acid in acetonitrile
detection	DAD
wavelength	200 nm
sample concentration	5 mg/mL in water
injection volume	1 mL
run time	28 min
flow rate	20 mL/min
gradient program	15% B, isocratic for 5 min, in 10 min to 23.5% B, isocratic for 5 min, in 3 min to 15% B, isocratic for 5 min

2'-*O*-acetylsalicin (I)

$C_{15}H_{20}O_8$; UV (water): λ_{max} = 204, 220, 268 nm; LC-ToF-MS (ESI): *m/z* 373.1130 [M+HCO$_2$H-H]$^-$, 327.1070 [M-H]$^-$; LC-MS/MS (DP = -5 V, CE = -76 V): *m/z* (%) 326.92 (100), 304.73 (73), 174.82 (32), 122.95 (87), 120.93 (8), 92.92 (3). ^{1}H-NMR and ^{13}C-NMR data are listed in the Appendix section.

3'-*O*-acetylsalicortin (II)

$C_{22}H_{26}O_{11}$; UV (methanol/water, v/v, 1/1): λ_{max} = 200, 220, 272 nm; LC-ToF-MS (ESI$^-$): *m/z* 511.1458 [M+HCO$_2$H-H]$^-$, 465.1421 [M-H]$^-$; LC-MS/MS (DP = -80 V, CE = -66 V): *m/z* (%) 404.92 (41), 154.92 (100), 136.94 (76), 122.91 (61), 120.94 (19), 83.02 (19), 80.97 (5). ^{1}H-NMR and ^{13}C-NMR data are listed in the Appendix section.

2'-*O*-acetylsalicortin (III)

$C_{22}H_{26}O_{11}$; UV (methanol/water, v/v, 1/1): λ_{max} = 204, 220, 272 nm; LC-ToF-MS (ESI⁻): *m/z* 511.1455 [M+HCO₂H-H]⁻, 465.1434 [M-H]⁻; LC-MS/MS (DP = -160 V, CE = -80 V): *m/z* (%) 154.88 (100), 136.86 (78), 122.86 (57), 120.90 (22), 92.95 (22), 82.99 (19), 80.99 (10). ¹H-NMR and ¹³C-NMR data are listed in the Appendix section.

Further, a non-salicylate compound, cinnamrutinose A (**IV**), was isolated from fraction F5-2-2 by purification of 1 mg/mL subfraction F5-2 diluted in methanol/water (v/v, 1/1). Therefore, the chromatographic conditions shown in Table 18 were used. Subfractions F5-2-1 to F5-2-3 were collected, the organic solvent was removed, freeze-dried, and stored at -20°C until further use.

Table 18: Chromatographic conditions of the HPLC system 2 used for semi-preparative fractionation of fraction F5-2.

Parameter	Description
stationary phase	Luna® PFP column, 250 x 10 mm, 5 µm particle size (Phenomenex Ltd., Aschaffenburg, Deutschland)
mobile phase	A: 0.1% formic acid in water, B: 0.1% formic acid in methanol
detection	UV
wavelength	252 nm
sample concentration	1 mg/mL in methanol/water (v/v, 1/1)
injection volume	300 µL
run time	37 min
flow rate	4.7 mL/min
gradient program	22% B, isocratic for 3 min, in 17 min to 45% B, isocratic for 2 min, in 8 min to 50% B, isocratic for 3 min, in 2 min to 22% B, isocratic for 2 min

cinnamrutinose A (IV)

$C_{21}H_{30}O_{10}$; UV (methanol/water, v/v, 1/1): λ_{max} = 204, 252 nm; LC-ToF-MS (ESI$^-$): m/z 487.1824 [M+HCO$_2$H-H]$^-$, 441.1768 [M-H]$^-$; LC-MS/MS (DP = -55 V, CE = -56 V): m/z (%) 306.92 (100), 162.92 (41), 160.89 (3), 126.91 (1), 124.91 (14), 118.90 (13), 102.92 (19), 100.87 (7), 58.97 (4). ^{1}H-NMR and ^{13}C-NMR data are listed in the Appendix section.

4.4.5 Subfractionation of SPE fraction F6

For the activity-guided fractionation of SPE fraction F6, the gradient depicted in Table 19 was used. Therefore, 5 mg/mL of the extract were diluted in methanol and 600 µL were injected into the HPLC system. The subfractions F6-1 to F6-14 were collected, the solvent was evaporated, freeze-dried, and stored at -20°C until further use.

Table 19: Chromatographic conditions of the HPLC system 1 used for preparative fractionation of SPE fraction F6.

Parameter	Description
stationary phase	Luna® phenyl-hexyl column, 100 Å, 250 x 21.2 mm, 5 µm particle size (Phenomenex Ltd., Aschaffenburg, Germany)
mobile phase	A: 0.1% formic acid in water, B: 0.1% formic acid in acetonitrile
detection	DAD
wavelength	200 nm
injection volume	600 µL
run time	35 min
flow rate	20 mL/min
gradient program	23% B, isocratic for 3 min, in 21 min to 33% B, isocratic for 6 min, in 3 min to 23% B, isocratic for 2 min

Further, fractions F6-12 and F6-13 were subfractionated to allow isolation and structure determination of 2',6'-*O*-diacetylsalicortin (**V**) in F6-12-2 and lasiandrin (**VI**) in F6-13-2, respectively. Purification was performed by means of semi-preparative HPLC applying the parameters as described in Table 20 and Table 21, respectively. Subsequently, the organic solvent of the collected subfractions F6-12-1 to F6-12-3 and F6-13-1 to F6-13-3 was removed and lyophilized. The dried powders were stored at -20°C until further use.

Table 20: Chromatographic conditions of the HPLC system 1 used for semi-preparative fractionation of fraction F6-12.

Parameter	Description
stationary phase	Luna® phenyl-hexyl column, 250 x 10 mm, 5 μm particle size (Phenomenex Ltd., Aschaffenburg, Germany)
mobile phase	A: 0.1% formic acid in water, B: 0.1% formic acid in acetonitrile
detection	UV
sample concentration	10 mg/mL in methanol/water (v/v, 1/1)
wavelength	200 nm
injection volume	150 μL
run time	50 min
flow rate	4.7 mL/min
gradient program	20% B, isocratic for 3 min, in 43.5 min to 32% B, in 1.5 min to 20% B, isocratic for 2 min

Table 21: Chromatographic conditions of the HPLC system 1 used for semi-preparative fractionation of fraction F6-13.

Parameter	Description
stationary phase	Luna® phenyl-hexyl column, 250 x 10 mm, 5 µm particle size (Phenomenex Ltd., Aschaffenburg, Germany)
mobile phase	A: 0.1% formic acid in water, B: 0.1% formic acid in acetonitrile
detection	DAD
wavelength	200 nm
sample concentration	10 mg/mL in methanol/water (v/v, 1/1)
injection volume	200 µL
run time	34 min
flow rate	4.7 mL/min
gradient program	27% B, isocratic for 3 min, in 27 min to 32% B, in 4 min to 27% B

2',6'-*O*-diacetylsalicortin (V)

$C_{24}H_{28}O_{12}$; UV (methanol/water, v/v, 1/1): λ_{max} = 200, 272, 300 nm; LC-ToF-MS (ESI⁻): m/z 553.1569 [M+HCO₂H-H]⁻, 507.1551 [M-H]⁻; LC-MS/MS (DP = -160 V, CE = -62 V): m/z (%) 155.00 (81), 136.90 (100), 122.89 (58), 120.91 (22), 92.94 (23), 82.94 (17), 80.98 (4). ^{1}H-NMR and ^{13}C-NMR data are listed in the Appendix section.

lasiandrin (VI)

$C_{29}H_{32}O_{14}$; UV (methanol/water, v/v, 1/1): λ_{max} = 200, 272, 300 nm; LC-ToF-MS (ESI⁻): m/z 649.1791 [M+HCO₂H-H]⁻, 603.1762 [M-H]⁻; LC-MS/MS (DP = -135 V, CE = -84 V): m/z (%) 464.99 (100), 154.90 (85), 136.91 (83), 110.95 (32), 108.93 (15), 92.95 (30), 82.98 (26), 80.96 (10). ^{1}H-NMR and ^{13}C-NMR data are listed in the Appendix section.

4.4.6 Subfractionation of SPE fraction F7

Subfractionation of 10 mg/mL SPE fraction F7 by means of HPLC was performed using the gradient shown in Table 22. Fractions F7-1 to F7-14 were collected, the solvent was evaporated and freeze-dried. The pulverized extracts were stored at -20°C until further use.

Table 22: Chromatographic conditions of the HPLC system 1 used for preparative fractionation of SPE fraction F7.

Parameter	Description
stationary phase	Luna® phenyl-hexyl column, 100 Å, 250 x 21.2 mm, 5 µm particle size (Phenomenex Ltd., Aschaffenburg, Germany)
mobile phase	A: 0.1% formic acid in water, B: 0.1% formic acid in acetonitrile
detection	DAD
wavelength	200 nm
sample concentration	10 mg/mL in 100% methanol
injection volume	700 µL
run time	34 min
flow rate	20 mL/min
gradient program	28% B, isocratic for 3 min, in 7 min to 32% B, isocratic for 2 min, in 14 min to 37% B, isocratic for 2 min, in 3 min to 28% B, isocratic for 3 min

Furthermore, fraction F7 was subfractionated to purify single compounds. The salicylate tremulacin (**VII**) was isolated from fraction F7-8-4 by semi-preparative HPLC using the parameters shown in Table 23. The subfractions F7-8-1 to F7-8-5 were collected, the organic solvent was evaporated, lyophilized, and the dried extracts were stored at -20°C until further use.

Table 23: Chromatographic conditions of the HPLC system 2 used for semi-preparative fractionation of fraction F7-8.

Parameter	Description
stationary phase	Luna® PFP column, 250 x 10 mm, 5 µm particle size (Phenomenex Ltd., Aschaffenburg, Deutschland)
mobile phase	A: 0.1% formic acid in water, B: 0.1% formic acid in methanol
detection	UV
wavelength	200 nm
sample concentration	10 mg/mL in methanol/water (v/v, 1/1)
injection volume	200 µL
run time	42 min
flow rate	4.7 mL/min
gradient program	26% B, isocratic for 3 min, in 23 min to 62% B, isocratic for 10 min, in 4 min to 26% B, isocratic for 2 min

tremulacin (VII)

$C_{27}H_{28}O_{11}$; UV (methanol/water, v/v, 1/1): λ_{max} = 204, 236, 272 nm; LC-ToF-MS (ESI$^-$): m/z 573.1617 [M+HCO$_2$H-H]$^-$, 527.1586 [M-H]$^-$; LC-MS/MS (DP = -20 V, CE = -86 V): m/z (%) 404.95 (100), 154.90 (49), 136.90 (39), 122.92 (14), 120.94 (67), 82.97 (10), 80.97 (10), 76.97 (22); ^{1}H-NMR and ^{13}C-NMR data are listed in the Appendix section.

Additionally, fraction F7-4 was purified by means of semi-preparative HPLC using the parameters described in Table 24. After subfractionation and solvent evaporation of subfractions F7-4-1 to F7-4-6, **VIII**, containing two diastereomeric compounds of *β*-D-glucopyranoside, 2-[[[(1-hydroxy-6,6-dihydroxy-2-cyclohexen-1-yl) dihydroxy]oxy]methyl]phenyl, 2-acetate, was structurally elucidated in F7-4-6.

Table 24: Chromatographic conditions of the HPLC system 2 used for semi-preparative fractionation of fraction F7-4.

Parameter	Description
stationary phase	Luna® PFP column, 250 x 10 mm, 5 µm particle size (Phenomenex Ltd., Aschaffenburg, Deutschland)
mobile phase	A: 0.1% formic acid in water, B: 0.1% formic acid in methanol
detection	UV
wavelength	200 nm
sample concentration	15 mg/mL in 100% methanol
injection volume	100 µL
run time	56 min
flow rate	4.7 mL/min
gradient program	40% B, isocratic for 3 min, in 17 min to 53% B, isocratic for 2 min, in 26 min to 57% B, isocratic for 2 min, in 3 min to 40% B, isocratic for 3 min

β-D-glucopyranoside, 2-[[[(1-hydroxy-6,6-dihydroxy-2-cyclohexen-1-yl) dihydroxy]oxy]methyl]phenyl, 2-acetate (VIII)

$C_{22}H_{28}O_{12}$; UV (methanol): $\lambda_{max} = 200$ nm; LC-ToF-MS (ESI⁻): m/z 465.140 [M-H_2O-H]⁻; after acetalization: $C_{28}H_{36}O_{12}$; LC-ToF-MS (ESI⁻): m/z 563.2126 [M+C_6H_{12}-H]⁻, where C_6H_{12} represent two acetal groups; LC-MS/MS data not available; ^{1}H-NMR and ^{13}C-NMR data are listed in the Appendix section.

4.5 High-performance liquid chromatography (HPLC) system

The HPLC system 1 was used for analytical and (semi-)preparative fractionation (Table 25). In addition, the HPLC system 2 was applied as an alternative for the semi-preparative fractionation (Table 26). For the analytical chromatography a conic flow cell, and for the (semi-)preparative chromatography a preparative flow cell was used.

Table 25: HPLC system 1.

system	description
pumps	PU-2087 Plus (Jasco, Groß-Umstadt, Germany)
autosampler	AS-2055 (Jasco, Groß-Umstadt, Germany)
DA-detector	MD-2010 Plus (Jasco, Groß-Umstadt, Germany)
ELS-detector	Sedex LT-ELSD Model 90 (Sedere, Alfortville, France)
sample loop	2 mL
software	Galaxie (version 1.10; Agilent Technologies, Oberhaching, Germany)

Table 26: HPLC system 2.

system	description
pumps	PU-2087 Plus (Jasco, Groß-Umstadt, Germany)
degasser	DG-2080-53; 3-line (Jasco, Groß-Umstadt, Germany)
UV/VIS detector	UV-2075 (Jasco, Groß-Umstadt, Germany)
sample loop	2 mL
software	ChromPass (version 1.9; Jasco, Groß-Umstadt, Germany)

4.6 Sugar moiety determination

To determine the absolute configuration of sugar moieties, a literature protocol described in Schmid et al. (2018) and Tanaka et al. (2007) was used with minor modifications. First, compounds **I** to **VII** were dissolved in 50 µL deuterated NMR solvent after spectroscopic analysis, and dried under nitrogen gas stream. Subsequently, to obtain the sugar from the compound, acidic hydrolysis was performed by adding 500 µL of 2 M HCl and subsequent shaking for 1 h at 1,400 rpm and 100°C. Then, the dried samples were dissolved in 750 µL water, and extracted twice by adding 750 µL ethyl acetate. The water layer was centrifuged under vacuum by means of speedVac vacuum concentrator until dryness. Then, the obtained sugar residues and 1 mg of each reference sugar were derivatized by dilution in 1 mL of 2 mg/mL *L*-cysteine methyl ester hydrochloride in anhydrous pyridine and shaking for 1 h at 1,400 rpm and 60°C. Consequently, 5 µL of phenylethyl isothiocyanate was added and shaken using the same conditions. Finally, the samples were evaporated until dryness and

diluted in 500 µL acetonitrile/water (v/v, 1/1), and the obtained derivatized monosaccharides were screened by means of LC-MS system 3.

The gradient and parameters used for the screening to examine the sugar moiety by means of LC-MS system 3 are shown in Table 27. The derivatized sugars obtained from the compounds **I-VII** and reference sugars were compared by their retention time and mass transitions to determine the absolute configuration of the monosaccharides of each analyte.

Table 27: LC-MS system 3 conditions used for the sugar moiety determination of the isolated compounds.

parameter	description
stationary phase	Kinetex F5 column, 100 Å, 1.7 µm, 2.1 x 100 mm (Phenomenex, Aschaffenburg, Germany)
column temperature	40°C
mobile phase	A: 1% formic acid in water, B: 1% formic acid in acetonitrile
ionization	electrospray ionization (ESI)
polarity	positive
injection volume	1 µL
run time	35 min
flow rate	0.4 mL/min
scan type	MRM
ion source voltage	5,500 V
source temperature	500°C
curtain gas	35 psi (N_2)
nebulizer gas	55 psi (N_2)
heater gas	65 psi (N_2)
gradient program	5% B, isocratic for 1.99 min, in 3 min to 20% B, in 21 min to 25% B, in 1 min to 100% B, isocratic for 3 min, in 1 min to 5% B, isocratic for 4 min

The MRM transitions, as well as DP, CE, and CXP values of the sugars *D*-glucose (*m/z* 461.0/298.1, DP = 75 V, CE = 17 V, CXP = 6 V), *L*-glucose (*m/z* 461.0/298.1, DP = 71 V, CE = 17 V, CXP = 6 V), *D*-galactose (*m/z* 461.1/298.2, DP = 71 V, CE = 17 V, CXP = 6 V), *D*-galacturonic acid (*m/z* 475.0/312.1, DP = 91 V, CE = 19 V, CXP = 6 V), *D*-glucuronic acid (*m/z* 475.0/312.1, DP = 61 V, CE = 19 V, CXP = 8 V), and *L*-rhamnose (*m/z* 445.0/282.1, DP = 61 V, CE = 19 V, CXP = 8 V) were obtained from Schmid et al. (2018).

4.7 Quantitation of phytochemicals in *Salix* by LC-MS/MS

4.7.1 Sample preparation

For the quantitation of the isolated compounds and commercially obtained compounds, extracts of 92 *Salix* genotypes (Table 9) were analyzed. Therefore, freeze-dried *Salix* bark extracts were obtained from HUB and extraction was performed according to the protocol of Förster et al. (2021) by modifying it slightly. First, 1 mL of methanol was added to 5 mg powdered bark and 10 µL of 5,025 µM internal standard salicylic acid-*d₄* (IS) was spiked into each *Salix* sample. Subsequent equilibration by shaking for 1 h at room temperature was followed by extraction using 2 mL bead beater tubes and a bead beater homogenizer applying 3 x 25 s with 25 s breaks and 6,500 rpm. Then, the samples were centrifuged for 5 min at 13,400 rpm, and the residue was re-extracted by adding 1 mL methanol. Finally, the supernatants of the same extracts were combined and biological triplicates were prepared, filtered by a 0.45 µm membrane filter, and analyzed by LC-MS system 3.

4.7.2 LC-MS/MS analysis

4.7.2.1 Tuning

For the quantitation, the mass transitions Q1/Q3 were monitored after manual injection (10 µL/min) of the single compounds using the injection pump of the mass spectrometer. Thus, the compounds were diluted in methanol/water

(v/v, 1/1) and tuned in the same LC-MS system 3 in the negative ionization mode. In addition to the isolated *Salix* ingredients, tuning was performed also for the compounds such as salicin, salicylic acid, saligenin, and salicortin, which were commercially obtained.

For method development, a pooled sample containing all compounds was screened using the gradient displayed in Table 29 to ensure a sufficient peak separation. The MRM mass transitions and retention times of each compound obtained from the calibration sample are exhibited in Table 28. The entrance potential (EP) of all tuned compounds in the mass spectrometer was -10 V.

Table 28: Quantifier mass transitions (*m/z*, Da). DP: declustering potential, CE: collision energy, and CXP: collision cell exit potential.

compound	Q1 mass [Da]	Q3 mass [Da]	retention time [min]	DP [V]	CE [V]	CXP [V]
2'-*O*-acetylsalicin (**I**)	373.040	123.000	1.66	-5	-16	-13
3'-*O*-acetylsalicortin (**II**)	464.986	137.100	3.17	-80	-24	-15
2'-*O*-acetylsalicortin (**III**)	464.946	136.800	3.57	-160	-26	-21
cinnamrutinose A (**IV**)	441.049	306.800	2.77	-55	-12	-39
2',6'-*O*-diacetylsalicortin (**V**)	506.988	137.000	4.75	-160	-26	-17
lasiandrin (**VI**)	603.199	465.000	4.80	-135	-18	-21
tremulacin (**VII**)	527.037	405.000	5.24	-20	-26	-39
salicin (**1**)	285.018	122.900	0.88	-60	-12	-13
saligenin (**2**)	122.902	92.800	1.32	-35	-22	-13
salicortin (**3**)	423.076	155.000	2.46	-145	-26	-17
salicylic acid (**4**)	136.875	92.900	3.25	-40	-20	-11
salicylic acid-*d₄* (IS)	141.011	97.000	3.18	-30	-22	-13

4.7.2.2 Calibration

For the generation of the calibration curve, the purified compounds **I** to **VII** and commercially obtained salicin, salicylic acid, saligenin, and salicortin were dissolved in methanol-d_4 or acetonitrile-d_3 and analyzed by qHNMR. In this way, concentrations were calculated accurately and purity could be determined. First, a stock solution of 500 µmol/L containing all analytes was prepared and diluted further in several steps until 0.005 µmol/L. Calibration samples of each dilution factor were supplemented with the IS with a constant concentration of 25 µmol/L

(C$_{final}$). The analytes in each calibration sample had following concentrations: 218.75, 87.5, 43.75, 21.875, 8.75, 4.375, 2.1875, 0.875, 0.4375, 0.219, 0.4375, 0.219, 0.0875, 0.0438, 0.0219, 0.00875, 0.00438 µmol/L. To acquire the calibration curve, the samples were analyzed by LC-MS/MS system 3 (Table 24) and the ratios (analyte/IS) of the peak area were plotted against the ratios (analyte/IS) of the concentration using linear regression and the MultiQuant software. For quantitation of the phytochemicals in *Salix* extracts, linear curves were produced for each analyte using a mathematical calibration function.

4.7.2.3 Recovery rate

For the recovery rate, spiking experiments using of 30%, 70%, and 100% of the expected concentration of each analyte were performed in triplicates. Therefore, three samples containing all analytes, each having different concentration levels, were prepared in 0.1% formic acid in methanol/water (v/v, 70/30). The extraction protocol was obtained from Förster et al. (2021). 1 mg of freeze-dried powdered willow bark of *S. pentandra* was dissolved in 500 µL of spiked sample as described above. The samples were prepared in triplicates and subsequently vortexed and exposed to ultrasonic bath with ice water for 15 min. Then, the samples were centrifuged for 5 min at 10,000 rpm and 20°C. The supernatants were collected, and the residues were re-extracted twice by addition of 200 µL of methanol/water (v/v, 70/30). The supernatants were combined and filled up to 1 mL with water. After vortexing, 1 mg/mL of the samples were substituted with the IS and filtered through a 0.45 µm filter for LC-MS/MS analysis. The final concentration of internal standard in 0.875 mg/mL of each extract was 25 µM.

4.7.2.4 Intraday and interday precision

For the intraday precision analysis, triplicates of spiked *S. pentandra* bark, which were extracted and prepared as described in section 4.7.2.3, were used for the quantitation of the compounds within one day (intraday). The precision was stated as the relative standard deviation (RSD %).

For the interday precision analysis, triplicates were measured on three consecutive days to ensure repeatability of the analysis. The interday precision

was also expressed as the RSD value. Therefore, compounds were quantified and the RSD values over three days were calculated.

4.7.2.5 LC-MS/MS analysis conditions

Quantitation of the isolated phytochemicals **I**-**VII** and the commercially obtained compounds, salicin, salicylic acid, saligenin, and salicortin, was performed by means of LC-MS system 3 (Table 29).

Table 29: LC-MS system 3 conditions used for the quantitation of 92 *Salix* genotypes.

parameter	description
stationary phase	Kinetex C_{18} column, 100 Å, 1.7 µm, 100 x 2.1 mm (Phenomenex, Aschaffenburg, Germany)
column temperature	40°C
mobile phase	A: 0.1% formic acid in water, B: 0.1% formic acid in acetonitrile
ionization	electrospray ionization (ESI)
polarity	negative
injection volume	1 µL
run time	10 min
flow rate	0.4 mL/min
scan type	MRM
ion source voltage	-4,500 V
source temperature	500°C
curtain gas	35 psi (N_2)
nebulizer gas	55 psi (N_2)
heater gas	65 psi (N_2)
gradient program	15% B, isocratic for 0.24 min, in 1.25 min to 20% B, in 3.5 min to 40% B, in 0.5 min to 50% B, in 0.5 min to 70% B, in 0.5 min to 100% B, isocratic for 0.5 min, in 1 min to 15% B, isocratic for 1 min

4.8 Detection of potential additional salicylates in *Salix*

4.8.1 Precursor ion scan

Furthermore, a precursor ion (PI) experiment for the detection of potential additional salicylates by means of LC-MS system 3 (Table 30) was performed over the mass range of *m/z* 300 to 1,000. Thus, it was of interest to scan the precursor ions of salicin, salicylic acid, and saligenin.

For the PI scan, the SPE fraction F5, F6, and F7 were diluted in methanol/water (v/v, 70/30). During the scan a group of salicylate compounds of the subfractions gave the same salicylic acid fragment ion of 137.10 Da, salicin fragment ion of 285.20 Da, or saligenin fragment ion of 123.1 Da in the negative ionization mode.

Table 30: LC-MS system 3 conditions for precursor ion scan. DP: declustering potential, CXP: collision cell exit potential.

parameter	description
stationary phase	Kinetex C_{18} column, 100 Å, 1.7 µm, 2.1 x 100 mm (Phenomenex, Aschaffenburg, Germany)
column temperature	40°C
mobile phase	A: 0.1% formic acid in water, B: 0.1% formic acid in acetonitrile
ionization	electrospray ionization (ESI)
polarity	negative
injection volume	1 µL
run time	6 min
flow rate	0.4 mL/min
scan type	precursor ion scan
ion source voltage	-4,500 V
source temperature	500°C
curtain gas	35 psi (N_2)
nebulizer gas	55 psi (N_2)
heater gas	65 psi (N_2)
DP	-50 V
CXP	-11 V
gradient program	15% B, isocratic for 0.24 min, in 1.25 min to 20% B, in 3.5 min to 40% B, in 0.5 min to 50% B, in 0.5 min to 70% B, in 0.5 min to 100% B, isocratic for 0.5 min, in 1 min to 15% B, isocratic for 1 min

4.8.2 Information dependent acquisition (IDA)

The IDA experiment (ToF-MS/MS) provides information about unknown precursor ions and automatically produces MS/MS spectra (DeWitt et al. 1990). The LC-MS system 4 conditions are exhibited in Table 31.

For the IDA experiment, the samples were scanned through the mass range of m/z 50-1,000 during an accumulation time of 250 ms, collision energy of -10 V, and declustering potential of -80 V. 15 most intense peaks were acquired for the

product ion scan during an accumulation time of 80 ms at declustering potential of -80 V, collision energy of -35 V, and collision energy spread of 15 V. Precursor ions were selected by the ion intensity of over 100 counts/s and the absence of the dynamic exclusion list. Peaks within 6 Da were ignored, the exclude isotopes window was 4 Da, and the mass tolerance was set to 20 ppm.

For data evaluation using the PeakView® software the screened subfractions of F5 and the methanol extract were imported. No reference compounds were analyzed, but a tentatively identified salicylate list obtained from Keefover-Ring et al. (2014) was used and the XIC list was created by adding compound name, chemical formula, and possible adducts. The exact mass in Da was automatically generated.

Table 31: LC-MS system 4 conditions used for information dependent acquisition.

parameter	description
stationary phase	Kinetex C_{18} column, 100 Å, 1.7 µm, 2.1 x 100 mm (Phenomenex, Aschaffenburg, Germany)
column temperature	40°C
mobile phase	A: 0.1% formic acid in water, B: 0.1% formic acid in acetonitrile
ionization	electrospray ionization (ESI)
polarity	negative
injection volume	10 µL for the fraction and 1 µL for the methanol extract
run time	20 min
flow rate	0.3 mL/min
scan type	ToF-MS survey scan
ion source voltage	4,500 V
source temperature	550°C
curtain gas	35 psi (N_2)
nebulizer gas	55 psi (N_2)
heater gas	65 psi (N_2)
gradient program	1% B, isocratic for 2.99 min, in 4.0 min to 10% B, in 3.0 min to 30% B, in 4.0 min to 100% B, isocratic for 2.5 min, in 0.5 min to 1% B, in 3 min to stop

4.8.3 Rapid screening for polyphenols and salicylates

Selected *Salix* genotypes and the bioactive methanol extract of *S. pentandra* were screened for a variety of polyphenols, isolated salicylates from *S. pentandra* **I-VII**, as well as for commercially obtained compounds, such as salicin, salicylic acid, saligenin, and salicortin using a previously developed LC-MS method by Tina Schmittnägel, Chair of Food Chemistry and Molecular Sensory Science (Table 32).

Table 32: LC-MS system 5 conditions used for information dependent acquisition (IDA). This method was developed by Tina Schmittnägel, Chair of Food Chemistry and Molecular Sensory Science.

parameter	description
stationary phase	Kinetex C_{18} column, 100 Å, 1.7 µm, 2.1 x 100 mm (Phenomenex, Aschaffenburg, Germany)
column temperature	50°C
mobile phase	A: 0.1% formic acid in water, B: 0.1% formic acid in acetonitrile
ionization	electrospray ionization (ESI)
polarity	negative
injection volume	1 µL
run time	20 min
flow rate	0.4 mL/min
scan type	MRM
ion source voltage	-4,500 V
source temperature	450°C
curtain gas	40 psi (N_2)
nebulizer gas	55 psi (N_2)
heater gas	65 psi (N_2)
gradient program	5% B, isocratic for 2.5 min, in 3.5 min to 12% B, isocratic for 2.0 min, in 6.0 min to 40% B, in 1.0 min to 100% B, isocratic for 1.0 min, in 1.0 min to 5% B, isocratic for 3 min

The MRM transitions as well as the DP, CE, and CXP values of a few selected polyphenols were obtained from the developed method of Tina Schmittnägel, Chair of Food Chemistry and Molecular Sensory Science (Appendix section, Table A13).

4.9 Spectroscopic methods and devices

4.9.1 Ultraviolet-visible spectroscopy (UV-VIS)

Since the injected samples into the liquid chromatography could absorb light at different wavelengths, a UV detector was employed. In this way, analytes of the extracts, fractions and isolated compounds were detected by diode array, which records UV-VIS spectra.

4.9.2 Liquid chromatography-mass spectrometry (LC-MS)

The untargeted screening of the 92 *Salix* genotypes was performed by means of the UPLC-IMS-ESI$^-$-QToF-MS (LC-MS system 1, Table 33).

Table 33: LC-MS system 1 (UPLC-IMS-ESI$^-$-QToF-MS).

system	description
UPLC system	Acquity i-class UPLC system (Waters, Milford, MA, USA)
pump	Binary Solvent Manager (Waters, Milford, MA, USA)
autosampler	sample manager (Waters, Milford, MA, USA)
ionization	ESI
software	UNIFI (version 1.8; Waters, Milford, MA, USA)
MS system	Vion IMS QToF Ion Mobility Quadrupole Time-of-flight MS (Waters, Manchester, UK)

For the screening of the extracts, SPE fractions, and isolated compounds Synapt G2-S HDMS (LC-MS system 2, Table 34) was used in order to determine the exact masses. The time-of-flight system was calibrated with a 0.5 mM sodium

formate solution in 2-propanol/water (v/v, 9/1) over the mass range of *m/z* 50 to 1,200.

Table 34: LC-MS system 2 (Synapt G2-S HDMS UPLC-ESI⁻-ToF-MS).

system	description
UPLC system	Acquity UPLC core system (Waters, Manchester, UK)
pump	Binary Solvent Manager (Waters, Manchester, UK)
autosampler	Sample Manager (Waters, Manchester, UK)
ionization	ESI
software	MassLynx™ (version 4.1, SCN 851; Waters, Manchester, UK)
MS system	Synapt G2-S HDMS Time-of-flight MS (Waters, Manchester, UK)

For the precursor ion scan, compound tuning, screening, and quantitation experiments the QTrap® 6500 LC-MS system 3 was used with the parameters as described in Table 35. Calibration of the mass spectrometer was performed by a standard solution LC-MS tuning mix for ESI (Agilent, Waldbronn, Germany).

Table 35: LC-MS system 3 (QTrap® 6500 LC-MS/MS).

system	description
UHPLC system	Shimadzu Nexera X2 UHPLC System (Shimadzu, Duisburg, Germany)
pump	LC30AD
autosampler	SIL30AC
column oven	CTO30A
ionization	ESI
software	Analyst 1.6.3 (Sciex, Darmstadt, Germany)
MS system	QTRAP® 6500 LC-MS/MS spectrometer (Sciex, Darmstadt, Germany)

TripleToF® 6600 LC-MS system 4 (Table 36) was used for the detection of potential additional salicylates in *S. pentandra* extracts and fractions, and the

information dependent acquisition (IDA). The software Analyst® was used as the operating software, and PeakView® with the accompanied MasterView® setting for data analysis. The screening was performed over the mass range of *m/z* 50-1,000.

Table 36: LC-MS system 4 (TripleToF® 6600 LC-MS/MS).

system	description
UHPLC system	Shimadzu Nexera X2 UHPLC System (Shimadzu, Duisburg, Germany)
pump	LC30AD
autosampler	SIL30AC
column oven	CTO30A
ionization	ESI
software	Analyst® 1.7.1 (Sciex, Darmstadt, Germany)
MS system	TripleToF® 6600 LC-MS/MS spectrometer (Sciex, Darmstadt, Germany)

For screening of salicylates and polyphenols using the LC-MS parameters of Tina Schmittnägel (Chair of Food Chemistry and Molecular Sensory Science), the QTrap® 6500+ LC-MS/MS system 5 was used (Table 37).

Table 37: LC-MS system 5 (QTrap® 6500+ LC-MS/MS).

system	description
UPLC system	ExionLC System (Sciex, Darmstadt, Germany)
pump	ExionLC Binary Gradient AD Pump
autosampler	ExionLC Autosampler AD Autosampler
column oven	ExionLC Column Oven AC Column Oven
ionization	ESI
software	Analyst 1.6.3 (Sciex, Darmstadt, Germany)
MS system	QTRAP® 6500+ LC-MS/MS spectrometer (Sciex, Darmstadt, Germany)

4.9.3 Determination of the absolute *S*/*R* configuration by CD-spectroscopy

To investigate the absolute configuration of the salicylates, circular dichroism (CD) spectroscopy was performed using the J-810 spectropolarimeter (Fern-UV CD Spektrum; Jasco, Pfungstadt, Germany) equipped with a PT-423S Pelier element. The device was offered by the chair of Biological Chemistry (TU Munich, Prof. Dr. Arne Skerra). The experiment was executed using nitrogen gas and a constant temperature of 20°C, which was controlled manually. Then, 0.2 mg/mL of each single compound was diluted in LC-grade methanol and transferred into a 1 mm quartz cuvette (with a cap), and scanned within the range of 185 and 350 nm. Scanning was performed eight times and chirality was obtained by the molar ellipticity as a function of the wavelength operated by the Spectra Manager™ software (version 1.17.00; Jasco, Tokyo, Japan).

4.9.4 Nuclear magnetic resonance spectroscopy (NMR)

To determine the chemical structure of isolated compounds, NMR was used. Therefore, the 500 MHz UltraShield™ Plus AVANCE III and 600 MHz 9.4 T magnet AVANCE Neo spectrometers holding a 300 K Triple Resonance Cryo-TCI probe (^{1}H/^{13}C/^{15}N; Bruker, Rheinstetten, Germany) were used. The samples were diluted in 600 µL of acetone-d_6, dimethyl sulfoxide-d_6, acetonitrile-d_3, or methanol-d_4, and transferred into an NMR tube for spectroscopic analysis. The internal standard tetramethylsilane (TMS, 0.0 ppm) and deuterated solvents were used as references.

Further, the 400 MHz AVANCE III spectrometer equipped with the Z-gradient 5 mm multinuclear observe probe (Broadband Observe, BBFO$_{PLUS}$, Bruker, Rheinstetten, Germany) was applied for quantitative NMR (qHNMR). For this analysis, calibration was needed using caffeine and *L*-tyrosine, which were dissolved in deuterated water with one drop of deuterium chloride and placed both into an ultrasonic bath for 10 min.

The operating TopSpin™ software (version 4.0.6; Bruker, Rheinstetten, Germany) allowed data processing. Data evaluation and export of spectra used in this work was performed using the MestReNova software (version 12.0.3; Mestrelab Research S.L., Santiago de Compostela, Spain).

4.9.4.1 ^{1}H-NMR

Proton nuclear magnetic resonance (^{1}H-NMR) spectroscopy was performed for the determination of the chemical environment, and proton number of a chemical structure. The chemical shift δ in ppm can help the observation of the functional group positions and the shielding variation (Harris et al. 2002). The multiplicity, such as singlet (s), duplet (d), triplet (t), doublet of doublets (Todd and Robinson 1956), doublet of triplets (dt), pseudo triplet (pt), pseudo quartet (pq), and multiplet (m) can give information about how many hydrogen(s) are nearby the hydrogen(s) of the produced ^{1}H-NMR signal (Bruch 1996, Hesse, Meier, and Zeeh 2005, Friebolin 1991). Additionally, the coupling constant (J, spin-spin coupling) is an important parameter to determine the spin-spin coupling between atoms, being geminal (^2J), vicinal (^3J), and W-type (^4J) as the most characteristic once (McClure 1999).

4.9.4.2 Quantitative ^{1}H-NMR (qHNMR)

Quantitative proton nuclear magnetic resonance (qHNMR) spectroscopy was applied to determine the precise concentration of all isolated compounds, **I-VII**, and commercially obtained reference compounds, salicin, salicylic acid, saligenin, and salicortin, for further quantitative experiments by LC-MS/MS. To determine the concentrations in mmol/L, each of the analyte was diluted in 600 µL of methanol-d_4 or acetonitrile-d_3, and analyzed by qHNMR (400 MHz). Concentration determination, calibration, and signal integration was performed using the ERETIC 2 tool and PULCON (pulse length based concentration determination) method as described by Frank et al. (2014). Proton signals part of the compound were then integrated (Table 38) and used for quantification. Moreover, it was possible to obtain the percentage (%) of purity of each analyte through the peak integral data and the determined concentrations.

Table 38: Integrated qHNMR signals of each analyzed compound for quantification.

compound	δ, proton, no. of protons
I	7.39 ppm, H-C(3), 1H 7.14 ppm, H-C(6), 1H
II	7.16 ppm, H-C(6), 1H 5.74 ppm, H-C(10), 1H
III	7.17 ppm, H-C(6), 1H 7.07 ppm, H-C(4), 1H
IV	6.35 ppm, H-C(2), 1H 6.69 ppm, H-C(3), 1H
V	7.32 ppm, H-C(3) and H-C(5), 2H 7.11 ppm, H-C(4) and H-C(6), 2H
VI	5.73 ppm, H-C(10) and H-C(10'), 2H 6.14 ppm, H-C(11) and H-C(11'), 2H
VII	7.64 ppm, H-C(5"), 1H 7.04 ppm, H-C(4), 1H
salicin	7.35 ppm, H-C(5), 1H 7.05 ppm, H-C(4), 1H
salicylic acid	7.11-7.18 ppm, H-C(3) and H-C(5), 2H 6.80-6.86 ppm, H-C(4) and H-C(6), 2H
saligenin	7.85 ppm, H-C(3), 1H 7.52 ppm, H-C(5), 1H
salicortin	7.22 ppm, H-C(6), 1H 7.04 ppm, H-C(4), 1H

4.9.4.3 ^{13}C-NMR

The application of the carbon nuclear magnetic resonance (^{13}C-NMR) spectroscopy is a useful technique for the analysis of the number of carbons in a compound. The chemical shift δ is measured in ppm. The abundance of ^{13}C in nature is 1.1% and only one signal for each carbon is produced in the ^{13}C-NMR spectra (Solomons, Fryhle, and Snyder 2016). Additionally, the gyromagnetic ratio γ is four times lower than that of ^{1}H, leading to longer echo times (Golman et al. 2003). Optimized and increased signal-to-noise ratio was achieved by decoupling the ^{1}H-broadband resulting in visible non-split spectra (de Graaf 2005, Vollhardt and Schore 1989).

4.9.4.4 Correlation spectroscopy (COSY)

The ^{1}H,^{1}H correlations were obtained by means of two-dimensional nuclear magnetic resonance spectroscopy (2D NMR). Therefore, homonuclear correlation spectroscopy (COSY) was performed using the diagonally plotted

one-dimensional ^{1}H-NMR spectrum (Gonnella 2020). Additionally, two (geminal, $^2J_{H,H}$) or three (vicinal, $^3J_{H,H}$) through-bond proton couplings lead to cross-peaks or correlation-peaks, which occur out of the diagonal spectrum (Gonnella 2020, Hesse et al. 2014). Generally, the mutual *J*-coupling of two spins appears as cross-peak, otherwise the multiplet disappears (Levitt 2013).

4.9.4.5 Heteronuclear single quantum coherence spectroscopy (HSQC)

To determine the chemical shift correlation of protons to the corresponding carbons, the two-dimensional heteronuclear single quantum coherence spectroscopy (HSQC) was performed. From the initially recorded ^{1}H-NMR and ^{1}C-NMR spectra, a correlation of the pair frequencies is formed (Danten 2006). In the case of quaternary carbons there is no proton correlation. If a structure contains a carbon with two protons (CH$_2$), two signals with a defined chemical shift will be visible, but for CH$_3$ there is only a single one (Reynolds 2017). In this two-dimensional NMR experiment, the top horizontal spectrum represents the ^{1}H-NMR and the left vertical spectrum the ^{13}C-NMR.

4.9.4.6 Heteronuclear multiple bond correlation spectroscopy (HMBC)

Similar to the HSQC, the heteronuclear multiple bond correlation spectroscopy (HMBC) is also a two-dimensional experiment and describes the ^{13}C,^{1}H correlation, but in a manner of $^2J_{C,H}$ to $^4J_{C,H}$ long-range couplings and not $^1J_{C,H}$ direct bindings as it is the case in HSQC (Reynolds 2017).

4.10 Acetalization reaction of fraction F7-4

Acetalization of fraction F7-4 was performed to determine the chemical structure of the suggested compounds. First, 3.6 mg of freeze-dried fraction F7-4 and 0.05 mg of the catalyst *p*-toluenesulfonic acid were dissolved all together in 300 µL of anhydrous acetone. Subsequently, acetalization was achieved by incubation for 24 h at room temperature. Then, the sample was neutralized using sodium bicarbonate. After drying under nitrogen, dilution in 300 µL

methanol/water (v/v, 70/30) and centrifugation, the supernatant of the sample was analyzed by means of UPLC-ToF-MS using LC-MS system 2.

4.11 Bioactivity studies

4.11.1 Determination of the anti-inflammatory potential by THP-1/macrophage model

For the determination of the anti-inflammatory potential of selected *Salix* species and crosses, PGE_2 release levels were determined by the THP-1/macrophage model (performed by UKF). First, the RPMI 1640 medium was supplemented with 10% heat-inactivated fetal calf serum (FCS), 2 mM *L*-glutamine, 100 U/mL penicillin, and 100 µg/mL streptomycin (Gibco™ Life Technologies GmbH, Darmstadt, Germany). The cell culture was incubated at 37°C in a humidified incubator at 5% CO_2 and 95% air atmosphere. Then, the THP-1 cells (3×10^5 cells/mL in a 48-well cell culture plate) were differentiated to macrophages in the presence of 2.5 ng/mL phorbol 12-myristate 13-acetate (PMA) for 72 h, and the cells were washed with pre-warmed PBS. After a resting time of 24 h in fresh RPMI 1640 medium with supplements mentioned above, the cells were pretreated with *Salix* extracts and subsequently stimulated with 100 ng/mL lipopolysaccharides (LPS obtained from *Escherichia coli* O11:B4; Sigma-Aldrich, Taufkirchen, Germany) for 24 h. As solvent control 1% distilled sterile water and as positive control 1 µg/mL Aspirin® were used. Finally, PGE_2 release was quantified in the supernatant by means of the PGE_2 ELISA kit (Cayman Chemical, Hamburg, Germany).

4.11.2 Isolation of human peripheral blood mononuclear cells (PBMC)

All bioactivity assays of the current work were performed by UKF applying the methods described in Antoniadou et al. (2021). For *in vitro* analysis a protocol obtained from Tran et al. (2016) was used. Therefore, buffy coats from healthy adult donors (blood transfusion center at UKF) were received to extract human peripheral blood mononuclear cells (PBMC), which were dissolved in 10% heat-

inactivated FCS, 2 mM L-glutamine, 100 U/mL penicillin, and 100 µg/mL streptomycin in RPMI 1640 medium.

4.11.3 Sample preparation and exposure to PBMC

Before pre-treatment of PBMC, stock solutions were prepared. Therefore, 10 mg/mL of the three extracts (methanol, methanol/water, water), and 5 mg/mL of the SPE fractions (F1-F11) were diluted in distilled water. The fractions were prepared to have the same concentration as in their natural conditions in the methanol extract of the plant (Table A2, Appendix section). Additionally, compounds **I-VII**, salicin, salicylic acid, saligenin, and salicortin, and fraction F7-4-6 containing **III** and two diastereomeres of **VIII,** were dissolved in distilled water. In contrast, fractions F5-1 to F5-6 were dissolved in DMSO. Stock solutions were stored at -80°C until further use. Solvent was used as control.

The samples were exposed to PBMC for 30 min. Then, stimulation was performed by adding 100 ng/mL LPS and incubating the samples at 37°C for 24 h in a humidified incubator with 5% CO_2/95% air atmosphere.

4.11.4 Determination of COX-1/-2 activity inhibition: quantification of PGE_2 release and IC_{50}-values

After stimulation, the cell-free supernatants were collected and PGE_2 release levels were measured by PGE_2 ELISA kit. The lower the PGE_2 level the higher the anti-inflammatory effect of the extracts or compounds. Moreover, COX-1 and COX-2 enzyme activity inhibition was investigated using the human Cayman COX Inhibitor Screening Assay kits. This assay quantifies the prostaglandin PGF2α that is produced after reduction of $SnCl_2$ of the prostaglandin H_2 (PGH_2), which is expressed by the COX enzyme. As positive control, acetylsalicylic acid was used.

The protocols of the kits for the quantification were obtained from the manufacturer Cayman Chemical (Hamburg, Germany), and the obtained data from the ELISA assays were processed by the GraphPad Prism 6.0 software (La Jolla, California, USA). For all assays, the evaluated data showed the mean +SD. The ordinary one-way ANOVA test and Dunnett's multiple comparison test were

applied for the determination of the statistical significance [statistically significant: $p < 0.05$ (*), highly statistically significant: $p < 0.01$ (**)].

For the determination of the IC_{50}-values of the salicylates acting anti-inflammatory, the GraphPad Prism software as well as the log(inhibitor) vs. normalized response equation were used, and the concentration-response curves were plotted. This experiment was performed at concentrations of 0.25, 1.00, 5.00, and 25.00 µg/mL for **II**, **III**, and **VII**, and 5.00 and 25.00 µg/mL for salicortin, **V**, and **VI**.

5 SUMMARY

Willow (*Salix* L.) bark is a widely known medicinal plant material containing analgesic and antipyretic phytochemical ingredients, revealing *Salix* as an important source for plant-based drug production in the pharmaceutical industry. Even the European Medicines Agency has approved *Salix* cortex as herbal medicinal product with therapeutic effects (European Medicines Agency 2017a).

In the current work, 92 willow bark extracts derived from *S. alba*, *S. daphnoides*, *S. humboldtiana*, *S. lasiandra*, *S. nigra*, *S. pentandra*, *S. purpurea*, *S.* x *rubens*, and *S. viminalis* species and crosses, comprising different chemical composition, were clustered into five groups to accomplish preselection of candidate plants for bioactivity determination. Therefore, 28 *Salix* candidates were selected from each group and subsequent determination of the anti-inflammatory activity against PGE_2 release identified *S. pentandra* (PE1) as the most potent bark material. After solvent extraction of this plant using methanol, methanol/water (v/v, 70/30) and water, the bioactive methanol extract was applied to activity-guided fractionation using solid-phase extraction and (semi-)preparative high-performance liquid chromatography (HPLC). Subsequently, structure elucidation was performed by means of LC-MS/MS, 1D/2D-NMR, and CD-spectroscopy techniques. Thus, 2'-*O*-acetylsalicin (**I**), 3'-*O*- and 2'-*O*-acetylsalicortin (**II**, **III**), cinnamrutinose A (**IV**), 2',6'-*O*-diacetylsalicortin (**V**), lasiandrin (**VI**), and tremulacin (**VII**) were isolated and identified from SPE fractions F5, F6, and F7 (Figure 68). Precursor ion scan and information-dependent acquisition experiments of the methanol extract and fraction F5 showed plausible additional salicylates. Some of the detected compounds were not isolated by activity-guided fractionation since they were contained in non-bioactive fractions.
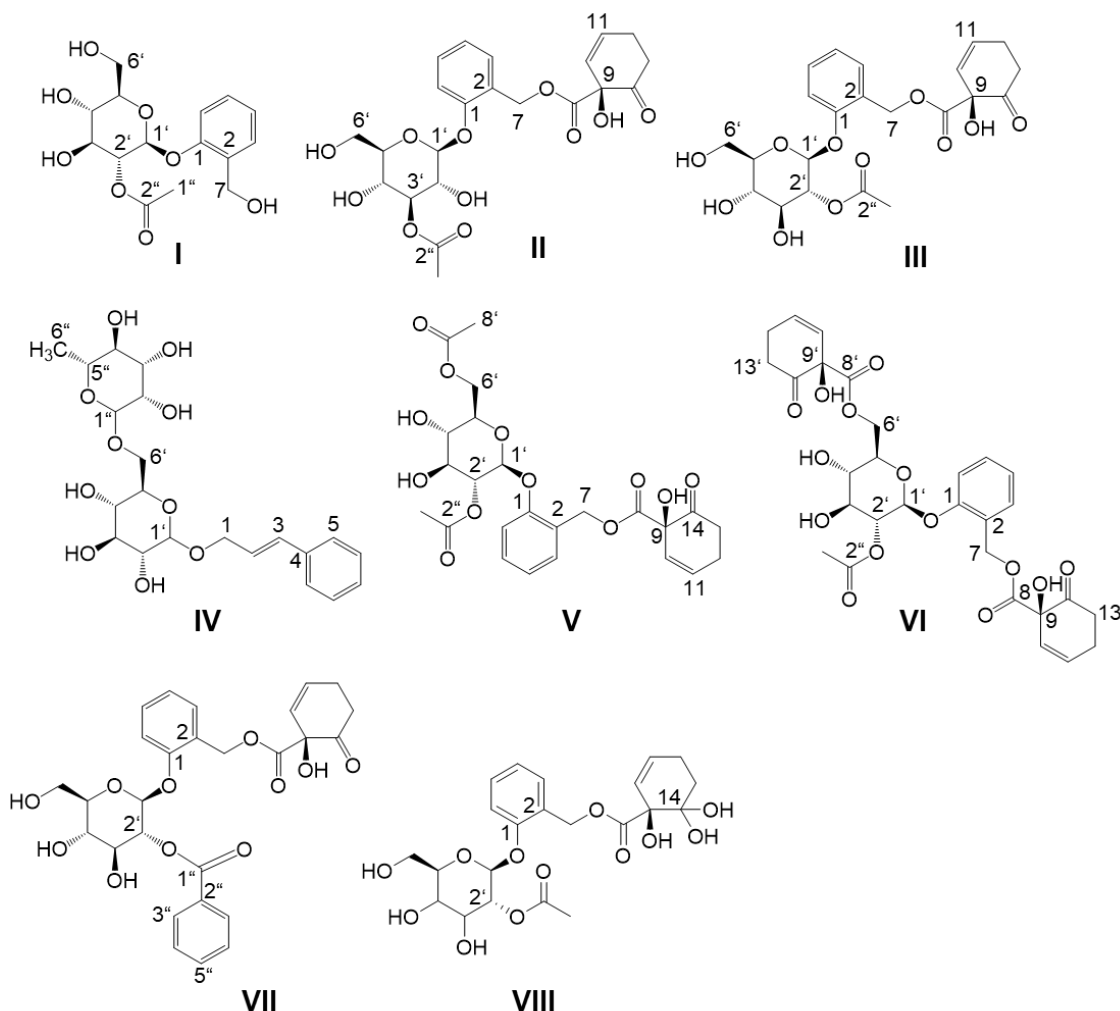
Figure 68: Chemical structures of compounds 2'-*O*-acetylsalicin (**I**), 3'-*O*- and 2'-*O*-acetylsalicortin (**II**, **III**), cinnamrutinose A (**IV**), 2',6'-*O*-diacetylsalicortin (**V**), lasiandrin (**VI**), tremulacin (**VII**), and *β*-D-glucopyranoside, 2-[[[(1-hydroxy-6,6-dihydroxy-2-cyclo-hexen-1-yl)dihydroxy]-oxy]methyl]phenyl, 2-acetate (**VIII**) from *S. pentandra* (PE1).

Sugar determination revealed *D*-glucose as part of the structures of **I**-**III** and **V**-**VII**, whereas **IV** contained *L*-rhamnose and *D*-glucose. Acetalization reaction was performed for subfraction 7-4-6 to protect the geminal diol group of novel *β*-D-glucopyranoside, 2-[[[(1-hydroxy-6,6-dihydroxy-2-cyclo-hexen-1-yl)dihydroxy]-oxy]methyl]phenyl, 2-acetate (**VIII**, Figure 68) and enabling structure elucidation. **VIII** contains a diol group at position C(14) in comparison to **II**, **III**, **V**, **VI**, and **VII**, which comprise of a carboxyl group at the same position of the HCH group.

Further, *S*-configured salicylates **II**, **III**, **V**, **VI**, and **VII**, exhibited anti-inflammatory potential against PGE$_2$ in contrast to **I** and **IV**. The potency may be explained due to the 1-hydroxy-6-oxo-2-cycohexenecarboxylate (HCH) moiety of the

salicylates, since it can degrade to bioactive catechol in cell culture conditions. Moreover, for the first time **III**, **IV**, and novel **VIII** were identified by LC-MS and 1D/2D-NMR in *S. pentandra* cortex. Even though **VI** was isolated from a less bioactive fraction F6, the compound showed higher efficiency against PGE_2 release in comparison to compounds **I-III**, which were isolated from the most bioactive fraction F5-5. Therefore, current standardization of medicinal *Salix* bark to salicin should be replaced by standardization to compounds containing HCH residues (e.g. **VI**), which are metabolized to catechol. Thus, bioactivity-guided fractionation and quantitation of the bioactive phytochemicals disproved the statement that polyphenols are responsible for the anti-inflammatory potential in previous studies.

Salicylates **I-III**, **V-VII**, salicin, saligenin, salicylic acid, and salicortin, and non-salicylate **IV** in bark extracts of 92 *Salix* species and crosses were quantified by means of a developed fast and sensitive LC-MS/MS method. Quantitative analysis revealed the highest content of bioactive **VI** in AL2xPE1_1 and PE1, and clustering showed an overall upregulation of **I-VI** in *S. pentandra and S. alba* species and crosses. The highest amount of **VI** in bioactive *S. pentandra* (PE1) among the 92 analyzed *Salix* species and crosses makes this species a possible candidate for future drug production. Moreover, saligenin, **II**, **IV**, and **VI** were quantified for the first time in *Salix* clones. New groups (A-J) were formed by a column scaled heatmap. Bioactive PE1 was compiled in group I as the only species, whereas *S. daphnoides* genotypes were grouping mainly in group C. High variety of the isolated compounds was detected in group D and I, which contained *S. pentandra* genotypes crosses with *S. alba* and *S. lasiandra*. In contrast, group F, G, and H containing *S. humboldtiana*, *S. lasiandra*, and *S. viminalis*, *S. nigra*, and a few *S. purpurea* species and crosses had the least amount of salicylate variety and content. This results showed that various *Salix* genotypes can have a different chemoprofile even if they belong to the same genus.

Further, it was possible to determine the IC_{50} values of **II**, **III**, **V**, **VI**, and **VII** for the first time, showing the half-maximal inhibitory potential of these compounds against PGE_2 release. The concentrations of salicortin, **III**, **V**, and **VI** in the anti-inflammatory bark extract PE1 were above the IC_{50} values, whereas the concentrations of **II** and **VII** were lower than the IC_{50}. This shows that the

concentration of salicortin, **III**, **V**, **VI** in the bark of the plant could confirm the bioactivity. The low concentration of salicin and salicylic acid, as well as the higher salicylate content in PE1 in contrast to non-bioactive *S. viminalis* x *S. viminalis* (*schwerinii* x *viminalis*) clone (VI4xVI3_2) containing mainly polyphenols, showed also the relevance of the salicylates for the phytopharmaceutical production in order to reduce inflammation.

After quantification, compound **VI**, showing the highest anti-inflammatory potential, accumulated in higher amounts in bioactive *S. pentandra* (PE1) among the 92 analyzed *Salix* species and crosses. This species could be a possible candidate for future drug production.

Finally, the present work could reveal that besides the investigation of the bioactivity, quantitative data of single phytochemicals were needed in order to verify the overall anti-inflammatory potential of willow bark. Based on these findings, new *Salix* species and crosses can be cultivated and bred by expressing high amounts of potent compounds in these plants. In this way, identified genotypes with high amounts of specific phytochemicals or composition of these, may be useful for medicinal purposes.

6 REFERENCES

Abreu, Ilka Nacif, Maria Ahnlund, Thomas Moritz, and Benedicte Riber Albrectsen. 2011. "UHPLC-ESI/TOFMS determination of salicylate-like phenolic gycosides in Populus tremula leaves." *Journal of chemical ecology* 37 (8):857-870. doi: 10.1007/s10886-011-9991-7.

Adelizzi, R. A. 1999. "COX-1 and COX-2 in health and disease." *J Am Osteopath Assoc* 99 (11 Suppl):S7-12.

Ahmed, Ajaz, Wajaht Shah, Seema Akbar, Mohammad Younis, and Dinesh Kumar. 2011. "A short chemical review on Salix Caprea commonly Known as Goat willow." *Int. J. Res. Phytochem. Pharmacol.* 1:17-20.

Aleixandre-Tudo, Jose Luis, and Wessel Du Toit. 2018. "The role of UV-visible spectroscopy for phenolic compounds quantification in winemaking." *Frontiers and new trends in the science of fermented food and beverages*:1-21.

Almenar-Queralt, A., A. Duperray, L. A. Miles, J. Felez, and D. C. Altieri. 1995. "Apical topography and modulation of ICAM-1 expression on activated endothelium." *The American journal of pathology* 147 (5):1278-1288.

Antoniadou, Kyriaki, Corinna Herz, Nguyen Phan Khoi Le, Verena Karolin Mittermeier-Kleßinger, Nadja Förster, Matthias Zander, Christian Ulrichs, Inga Mewis, Thomas Hofmann, Corinna Dawid, and Evelyn Lamy. 2021. "Identification of Salicylates in Willow Bark (Salix Cortex) for Targeting Peripheral Inflammation." *International Journal of Molecular Sciences* 22 (20):11138.

Argus, George W. 1997. "Infrageneric classification of Salix (Salicaceae) in the new world." *Systematic botany monographs*:1-121.

Aylott, Matthew J., E. Casella, I. Tubby, N. R. Street, P. Smith, and Gail Taylor. 2008. "Yield and spatial supply of bioenergy poplar and willow short-rotation coppice in the UK." *New Phytologist* 178 (2):358-370. doi: 10.1111/j.1469-8137.2008.02396.x.

Babicki, S., D. Arndt, A. Marcu, Y. Liang, J. R. Grant, A. Maciejewski, and D. S. Wishart. 2016. "Heatmapper: web-enabled heat mapping for all." *Nucleic Acids Res* 44 (W1):W147-53. doi: 10.1093/nar/gkw419.

Babst, Benjamin, Scott Harding, and Chung-Jui Tsai. 2010. "Biosynthesis of Phenolic Glycosides from Phenylpropanoid and Benzenoid Precursors in Populus." *Journal of chemical ecology* 36:286-97. doi: 10.1007/s10886-010-9757-7.

Bala, Manju, Cindy N. Chin, Asha T. Logan, Taneem Amin, Lawrence J. Marnett, Olivier Boutaud, and John A. Oates. 2008. "Acetylation of Prostaglandin H(2) Synthases by Aspirin is Inhibited by Redox Cycling of the Peroxidase." *Biochemical pharmacology* 75 (7):1472-1481. doi: 10.1016/j.bcp.2007.12.005.

Binder, M., and P. Zeiller. 1993. "[Antiphlogistic effect of salicylic acid and its derivatives]." *Fortschr Med* 111 (33):530-2.

Binns, W. W., G. Blunden, and D. L. Woods. 1968. "Distribution of leucoanthocyanidins, phenolic glycosides and imino-acids in leaves of Salix species." *Phytochemistry* 7 (9):1577-1581. doi: https://doi.org/10.1016/S0031-9422(00)88609-4.

Bonaterra, G. A., E. U. Heinrich, O. Kelber, D. Weiser, J. Metz, and R. Kinscherf. 2010. "Anti-inflammatory effects of the willow bark extract STW 33-I (Proaktiv(®)) in LPS-activated human monocytes and differentiated

macrophages." *Phytomedicine* 17 (14):1106-13. doi: 10.1016/j.phymed.2010.03.022.

Bosetti, C., S. Gallus, and C. La Vecchia. 2002. "Aspirin and cancer risk: an update to 2001." *Eur J Cancer Prev* 11 (6):535-42. doi: 10.1097/00008469-200212000-00005.

Bruch, Martha. 1996. *NMR spectroscopy techniques*: CRC Press.

Bryant, John P, Paul B Reichardt, and TP Clausen. 1992. "Chemically mediated interactions between woody plants and browsing mammals." *Rangeland Ecology & Management/Journal of Range Management Archives* 45 (1):18-24.

Bubner, Ben, A. Koehler, I. Zaspel, M. Zander, N. Förster, J. Gloger, C. Ulrichs, and V. Schneck. 2018. "Breeding of multipurpose willows on the basis of Salix daphnoides Vill., Salix purpurea L. and Salix viminalis L."

Bylesjö, Max, Mattias Rantalainen, Olivier Cloarec, Jeremy K Nicholson, Elaine Holmes, and Johan Trygg. 2006. "OPLS discriminant analysis: combining the strengths of PLS-DA and SIMCA classification." *Journal of Chemometrics: A Journal of the Chemometrics Society* 20 (8-10):341-351.

Chen, Jia-Hui, Hang Sun, Jun Wen, and Yong-Ping Yang. 2010. "Molecular Phylogeny of Salix L. (Salicaceae) Inferred from Three Chloroplast Datasets and Its Systematic Implications." *Taxon* 59 (1):29-37.

Chrubasik, S., E. Eisenberg, E. Balan, T. Weinberger, R. Luzzati, and C. Conradt. 2000. "Treatment of low back pain exacerbations with willow bark extract: a randomized double-blind study." *Am J Med* 109 (1):9-14. doi: 10.1016/s0002-9343(00)00442-3.

Clausen, Thomas P, John W Koller, and Paul B Reichardt. 1990. "Aglycone fragmentation accompanies β-glucosidase catalyzed hydrolysis of salicortin, a naturally-occurring phenol glycoside." *Tetrahedron letters* 31 (32):4537-4538.

Coudray, C., C. Mangournet, S. Bouhadjeb, H. Faure, and A. Favier. 1996. "Rapid high-performance liquid chromatographic assay for salicylic acid in plasma without solvent extraction." *J Chromatogr Sci* 34 (4):166-73. doi: 10.1093/chromsci/34.4.166.

Danten, D.; Ruckpaul K. 2006. "HSQC." In *Encyclopedic Reference of Genomics and Proteomics in Molecular Medicine*, 820-820. Berlin, Heidelberg: Springer Berlin Heidelberg.

de Graaf, Robin A. 2005. "Theoretical and experimental evaluation of broadband decoupling techniques for in vivo nuclear magnetic resonance spectroscopy." *Magnetic Resonance in Medicine: An Official Journal of the International Society for Magnetic Resonance in Medicine* 53 (6):1297-1306.

Decaestecker, T. N., S. R. Vande Casteele, P. E. Wallemacq, C. H. Van Peteghem, D. L. Defore, and J. F. Van Bocxlaer. 2004. "Information-dependent acquisition-mediated LC-MS/MS screening procedure with semiquantitative potential." *Anal Chem* 76 (21):6365-73. doi: 10.1021/ac0492315.

Dempsey, D'Maris Amick, and Daniel F. Klessig. 2017. "How does the multifaceted plant hormone salicylic acid combat disease in plants and are similar mechanisms utilized in humans?" *BMC Biology* 15 (1):23. doi: 10.1186/s12915-017-0364-8.

Deng, Chunhui, Xiangmin Zhang, Jie Zhang, Ji Qian, and Weimin Zhu. 2003. "Rapid Determination of Salicylic Acid in Plant Materials by Gas

Chromatography–Mass Spectrometry." *Chromatographia* 58 (3):225-229. doi: 10.1365/s10337-003-0041-7.

Deniau, MG, R Bonafos, M Chovelon, CE Parvaud, A Furet, C Bertrand, and PA Marchand. 2019. "Willow extract (Salix cortex), a basic substance of agronomical interests." *International Journal of Bio-resource and Stress Management* 10 (4):408-418.

Desborough, Michael J. R., and David M. Keeling. 2017. "The aspirin story – from willow to wonder drug." *British Journal of Haematology* 177 (5):674-683. doi: https://doi.org/10.1111/bjh.14520.

DeWitt, D. L., E. A. el-Harith, S. A. Kraemer, M. J. Andrews, E. F. Yao, R. L. Armstrong, and W. L. Smith. 1990. "The aspirin and heme-binding sites of ovine and murine prostaglandin endoperoxide synthases." *J Biol Chem* 265 (9):5192-8.

Dimitriou, Ioannis, Blas Mola-Yudego, Pär Aronsson, and Jan Eriksson. 2012. "Changes in Organic Carbon and Trace Elements in the Soil of Willow Short-Rotation Coppice Plantations." *BioEnergy Research* 5 (3):563-572. doi: 10.1007/s12155-012-9215-1.

Dissanayake, Amila A., Chuan-Rui Zhang, Mohamed K. A. Gaber, and Muraleedharan G. Nair. 2017. "Salicylic Glycosides in Salix mucronata with Antioxidant and Antiinflammatory Activities." *Natural Product Communications* 12 (11):1934578X1701201126. doi: 10.1177/1934578X1701201126.

Dötterl, Stefan, Ulrike Glück, Andreas Jürgens, Joseph Woodring, and Gregor Aas. 2014. "Floral reward, advertisement and attractiveness to honey bees in dioecious Salix caprea." *PloS one* 9 (3):e93421.

Dou, Jinze, Leonardo Galvis, Ulla Holopainen-Mantila, Mehedi Reza, Tarja Tamminen, and Tapani Vuorinen. 2016. "Morphology and Overall Chemical Characterization of Willow (Salix sp.) Inner Bark and Wood: Toward Controlled Deconstruction of Willow Biomass." *ACS Sustainable Chemistry & Engineering* 4 (7):3871-3876. doi: 10.1021/acssuschemeng.6b00641.

Dušek, Jiří, and Jan Květ. 2006. "Seasonal dynamics of dry weight, growth rate and root/shoot ratio in different aged seedlings of Salix caprea." *Biologia* 61:441-447. doi: 10.2478/s11756-006-0074-0.

Ekinci, D., M. Sentürk, and Öİ Küfrevioğlu. 2011. "Salicylic acid derivatives: synthesis, features and usage as therapeutic tools." *Expert Opin Ther Pat* 21 (12):1831-41. doi: 10.1517/13543776.2011.636354.

Ekinci, Deniz, Murat Şentürk, and Ömer İrfan Küfrevioğlu. 2011. "Salicylic acid derivatives: synthesis, features and usage as therapeutic tools." *Expert Opinion on Therapeutic Patents* 21 (12):1831-1841. doi: 10.1517/13543776.2011.636354.

El-Shazly, A., A. El-Sayed, and E. Fikrey. 2012. "Bioactive secondary metabolites from Salix tetrasperma Roxb." *Z Naturforsch C J Biosci* 67 (7-8):353-9. doi: 10.5560/znc.2012.67c0353.

Eliopoulos, Aristides G, Calin D Dumitru, Chun-Chi Wang, Jeonghee Cho, and Philip N Tsichlis. 2002. "Induction of COX-2 by LPS in macrophages is regulated by Tpl2-dependent CREB activation signals." *The EMBO journal* 21 (18):4831-4840.

Erickson, Richard L., Irwin A. Pearl, and Stephen F. Darling. 1970. "Populoside and grandidentoside from the bark of Populus grandidentata." *Phytochemistry* 9 (4):857-863. doi: https://doi.org/10.1016/S0031-9422(00)85193-6.

Ernst, E., and S. Chrubasik. 2000. "Phyto-anti-inflammatories. A systematic review of randomized, placebo-controlled, double-blind trials." *Rheum Dis Clin North Am* 26 (1):13-27, vii.

European Biomass Industry Association, EUBIA. n.d. "Short Rotation Plantations: Opportunities for efficient biomass production with the safe application of wastewater and sewage sludge." *European Commission BIOPROS research project*.

European Medicines Agency, EMA. 2017a. Assessment report on Salix [various species including S. purpurea L., S. daphnoides Vill., S. fragilis L.], cortex.

European Medicines Agency, EMA 2017b. "European Union herbal monograph on Salix [various species including S. purpurea L., S. daphnoides Vill., S. fragilis L.], cortex."9.

Faegri, Knut, and Leendert Van Der Pijl. 2013. *Principles of pollination ecology*: Elsevier.

Feistel, Felix. 2018. "Structural investigations of Salicaceae-derived salicylates and their metabolic transformation in the lepidopteran herbivore Cerura vinula."

Feistel, Felix, Christian Paetz, Sybille Lorenz, and Bernd Schneider. 2015. "The Absolute Configuration of Salicortin, HCH-Salicortin and Tremulacin from Populus trichocarpa × deltoides Beaupré." *Molecules* 20 (4):5566-5573.

Feistel, Felix, Christian Paetz, Riya C Menezes, Daniel Veit, and Bernd Schneider. 2018. "Acylated quinic acids are the main salicortin metabolites in the Lepidopteran specialist herbivore cerura vinula." *Journal of chemical ecology* 44 (5):497-509.

Fellenberg, C., O. Corea, L. H. Yan, F. Archinuk, E. M. Piirtola, H. Gordon, M. Reichelt, W. Brandt, J. Wulff, J. Ehlting, and C. Peter Constabel. 2020. "Discovery of salicyl benzoate UDP-glycosyltransferase, a central enzyme in poplar salicinoid phenolic glycoside biosynthesis." *Plant J* 102 (1):99-115. doi: 10.1111/tpj.14615.

Fellin, Marco, M Negri, G Macrì, B Bernardi, S Benalia, G Zimbalatti, and R Proto Andrea. 2016. "Electricity from Wood: A Wood Quality and Energy Efficiency Approach to Small Scale Pyro-gasification." *Procedia-Social and Behavioral Sciences* 223:783-790.

Fenning, Trevor. 2013. *Challenges and Opportunities for the World's Forests in the 21st Century*. Vol. 81: Springer.

Fiebich, Bernd, and Kurt Appel. 2003. "Anti-inflammatory effects of willow bark extract." *Clinical pharmacology and therapeutics* 74:96; author reply 96-7. doi: 10.1016/S0009-9236(03)00116-4.

Flower, Rod. 2003. "What are all the things that aspirin does?" *BMJ (Clinical research ed.)* 327 (7415):572-573. doi: 10.1136/bmj.327.7415.572.

Förster, N, C Ulrichs, M Zander, R Kätzel, and I Mewis. 2008. "Influence of the season on the salicylate and phenolic glycoside contents in the bark of Salix daphnoides, Salix pentandra, and Salix purpurea." *Journal of Applied Botany and Food Quality* 82 (1):99-102.

Förster, Nadja, Kyriaki Antoniadou, Matthias Zander, Sebastian Baur, Verena Karolin Mittermeier-Kleßinger, Corinna Dawid, Christian Ulrichs, and Inga Mewis. 2021. "Chemoprofiling as Breeding Tool for Pharmaceutical Use of Salix." *Frontiers in Plant Science* 12 (511). doi: 10.3389/fpls.2021.579820.

Förster, Nadja, Christian Ulrichs, Matthias Zander, Ralf Kätzel, and Inga Mewis. 2009. "Salicylatreiche Weiden für die Arzneimittelherstellung." *Gesunde Pflanzen* 61 (3-4):129-134.

Frank, Oliver, Johanna Karoline Kreissl, Andreas Daschner, and Thomas Hofmann. 2014. "Accurate Determination of Reference Materials and Natural Isolates by Means of Quantitative 1H NMR Spectroscopy." *Journal of Agricultural and Food Chemistry* 62 (12):2506-2515. doi: 10.1021/jf405529b.

Friebolin, Horst. 1991. *Basic one-and two-dimensional NMR spectroscopy*: VCH.

Füssel, Ulrike, Stefan Dötterl, Andreas Jürgens, and Gregor Aas. 2007. "Inter- and Intraspecific Variation in Floral Scent in the Genus Salix and its Implication for Pollination." *Journal of Chemical Ecology* 33 (4):749-765. doi: 10.1007/s10886-007-9257-6.

Gagnier, J. J., M. W. van Tulder, B. Berman, and C. Bombardier. 2007. "Herbal medicine for low back pain: a Cochrane review." *Spine (Phila Pa 1976)* 32 (1):82-92. doi: 10.1097/01.brs.0000249525.70011.fe.

Giménez-Bastida, Juan A., William E. Boeglin, Olivier Boutaud, Michael G. Malkowski, and Claus Schneider. 2019. "Residual cyclooxygenase activity of aspirin-acetylated COX-2 forms 15 R-prostaglandins that inhibit platelet aggregation." *FASEB journal : official publication of the Federation of American Societies for Experimental Biology* 33 (1):1033-1041. doi: 10.1096/fj.201801018R.

Golman, KOLE, Lars E Olsson, O Axelsson, S Mansson, Magnus Karlsson, and JS Petersson. 2003. "Molecular imaging using hyperpolarized 13C." *The British journal of radiology* 76 (suppl_2):S118-S127.

Gomes, João Victor Dutra, Corinna Herz, Simone Helmig, Nadja Förster, Inga Mewis, and Evelyn Lamy. 2021. "Drug-Drug Interaction Potential, Cytotoxicity, and Reactive Oxygen Species Production of Salix Cortex Extracts Using Human Hepatocyte-Like HepaRG Cells." *Frontiers in Pharmacology* 12. doi: 10.3389/fphar.2021.779801.

Gonnella, Nina C. 2020. *LC-NMR: Expanding the limits of structure elucidation*: CRC Press.

Grassin-Delyle, S., C. Abrial, H. Salvator, M. Brollo, E. Naline, and P. Devillier. 2020. "The Role of Toll-Like Receptors in the Production of Cytokines by Human Lung Macrophages." *Journal of Innate Immunity* 12 (1):63-73. doi: 10.1159/000494463.

Häikiö, Elina, Marika Makkonen, Riitta Julkunen-Tiitto, Jana Sitte, Vera Freiwald, T Silfver, Vivek Pandey, Egbert Beuker, Toini Holopainen, and Elina Oksanen. 2009. "Performance and secondary chemistry of two hybrid aspen (Populus tremula L. x Populus tremuloides Michx.) clones in long-term elevated ozone exposure." *Journal of chemical ecology* 35 (6):664-678.

Harris, Robin K, Edwin D Becker, Sonia M Cabral de Menezes, Robin Goodfellow, and Pierre Granger. 2002. "NMR nomenclature: nuclear spin properties and conventions for chemical shifts. IUPAC Recommendations 2001. International Union of Pure and Applied Chemistry. Physical Chemistry Division. Commission on Molecular Structure and Spectroscopy." *Magnetic Resonance in Chemistry* 40 (7):489-505.

Hathaway, R. L., and David Penny. 1975. "Root Strength in Some Populus and Salix Clones." *New Zealand Journal of Botany* 13 (3):333-344. doi: 10.1080/0028825X.1975.10430330.

Hawkey, C. J. 2001. "COX-1 and COX-2 inhibitors." *Best Pract Res Clin Gastroenterol* 15 (5):801-20. doi: 10.1053/bega.2001.0236.

Hedner, T., and B. Everts. 1998. "The early clinical history of salicylates in rheumatology and pain." *Clin Rheumatol* 17 (1):17-25. doi: 10.1007/bf01450953.

Heiska, Susanne, Olli-Pekka Tikkanen, Matti Rousi, and Riitta Julkunen-Tiitto. 2007. "Bark salicylates and condensed tannins reduce vole browsing amongst cultivated dark-leaved willows (Salix myrsinifolia)." *Chemoecology* 17 (4):245-253.

Hergert, H. L., and Otto Goldschmid. 1958. "Biogenesis of Heartwood and Bark Constituents. I. A. New Taxifolin Glucoside1." *The Journal of Organic Chemistry* 23 (5):700-704. doi: 10.1021/jo01099a015.

Hesse, Manfred, Herbert Meier, and Bernd Zeeh. 2005. *Spektroskopische Methoden in der organischen Chemie*: Georg Thieme Verlag.

Hesse, Manfred, Herbert Meier, Bernd Zeeh, M Hesse, H Meier, and B Zeeh. 2014. *Spectroscopic Methods in Organic Chemistry, 2007*: Georg Thieme Verlag.

Hon, David N-S, and Nobuo Shiraishi. 2000. *Wood and cellulosic chemistry, revised, and expanded*: CRC press.

Hou, J, Z Guo, H Liu, and T Yin. 2017. "Gender effects on Salix suchowensis Cheng ex Zhu. growth and wood properties as revealed by a full-sib pedigree." *Canadian journal of plant science* 97 (4):594-600.

Hou, Jing, Ning Ye, Defang Zhang, Yingnan Chen, Lecheng Fang, Xiaogang Dai, and Tongming Yin. 2015. "Different autosomes evolved into sex chromosomes in the sister genera of Salix and Populus." *Scientific reports* 5:9076.

Huang, Edward S., Lisa L. Strate, Wendy W. Ho, Salina S. Lee, and Andrew T. Chan. 2011. "Long Term Use of Aspirin and the Risk of Gastrointestinal Bleeding." *The American journal of medicine* 124 (5):426-433. doi: 10.1016/j.amjmed.2010.12.022.

Huremovic, Melita, Majda Srabovic, Benjamin Catovic, and Edina Huseinovic. 2016. "Crystallization and morphological characteristics of acetyl-salicylic acid (aspirin) synthesized from substrates of different source." 777:231-246.

i-flora. n.d. "Salix pentandra L.; Bay Willow."

Jack, D. B. 1997. "One hundred years of aspirin." *Lancet* 350 (9075):437-9. doi: 10.1016/s0140-6736(97)07087-6.

Jossang, Akino, Per Jossang, and Bernard Bodo. 1994. "Cinnamrutinoses A and B, glycosides of Populus tremula." *Phytochemistry* 35 (2):547-549.

Julkunen-Tiitto, R. 1985a. "Chemotaxonomical screening of phenolic glycosides in northern willow twigs by capillary gas chromatography." *Journal of Chromatography A* 324:129-139. doi: https://doi.org/10.1016/S0021-9673(01)81312-1.

Julkunen-Tiitto, Riitta. 1985b. "Phenolic constituents in the leaves of northern willows: methods for the analysis of certain phenolics." *Journal of Agricultural and Food Chemistry* 33 (2):213-217. doi: 10.1021/jf00062a013.

Julkunen-Tiitto, Riitta, and Beat Meier. 1992. "The enzymatic decomposition of salicin and its derivatives obtained from Salicaceae species." *Journal of natural products* 55 (9):1204-1212.

Julkunen-Tiitto, Riitta, and Sinikka Sorsa. 2001. "TESTING THE EFFECTS OF DRYING METHODS ON WILLOW FLAVONOIDS, TANNINS, AND SALICYLATES." *Journal of Chemical Ecology* 27 (4):779-789. doi: 10.1023/A:1010358120482.

Junttila, Olavi, and Åse Kaurin. 1990. "Environmental control of cold acclimation in Salix pentandra." *Scandinavian Journal of Forest Research* 5 (1-4):195-204. doi: 10.1080/02827589009382605.

Kacperska, Alina, and Leszek Kulesza. 1987. "Frost resistance of winter rape leaves as related to the changes in water potential and growth capability." *Physiologia Plantarum* 71 (4):483-488. doi: 10.1111/j.1399-3054.1987.tb02888.x.

Kam, P. C. A., and A. U-L. See. 2000. "Cyclo-oxygenase isoenzymes: physiological and pharmacological role." *Anaesthesia* 55 (5):442-449. doi: https://doi.org/10.1046/j.1365-2044.2000.01271.x.

Kammerer, B., R. Kahlich, C. Biegert, C. H. Gleiter, and L. Heide. 2005. "HPLC-MS/MS analysis of willow bark extracts contained in pharmaceutical preparations." *Phytochem Anal* 16 (6):470-8. doi: 10.1002/pca.873.

Karp, Angela. 2014. "Willows as a Source of Renewable Fuels and Diverse Products." *Challenges and opportunities for the World's forests*:617-641. doi: 10.1007/978-94-007-7076-8_27.

Karrenberg, S, J Kollmann, and PJ Edwards. 2002. "Pollen vectors and inflorescence morphology in four species of Salix." *Plant Systematics and Evolution* 235 (1-4):181-188.

Keefover-Ring, Ken, Maria Ahnlund, Ilka Nacif Abreu, Stefan Jansson, Thomas Moritz, and Benedicte Riber Albrectsen. 2014. "No Evidence of Geographical Structure of Salicinoid Chemotypes within Populus Tremula." *PLOS ONE* 9 (10):e107189. doi: 10.1371/journal.pone.0107189.

Keefover-Ring, Ken, Marcus Carlsson, and Benedicte Riber Albrectsen. 2014. "2′-(Z)-Cinnamoylsalicortin: A novel salicinoid isolated from Populus tremula." *Phytochemistry Letters* 7:212-216. doi: https://doi.org/10.1016/j.phytol.2013.11.012.

Kelly, S. M., T. J. Jess, and N. C. Price. 2005. "How to study proteins by circular dichroism." *Biochim Biophys Acta* 1751 (2):119-39. doi: 10.1016/j.bbapap.2005.06.005.

Khayyal, M. T., M. A. El-Ghazaly, D. M. Abdallah, S. N. Okpanyi, O. Kelber, and D. Weiser. 2005. "Mechanisms involved in the anti-inflammatory effect of a standardized willow bark extract." *Arzneimittelforschung* 55 (11):677-87. doi: 10.1055/s-0031-1296917.

Kim, Chung Sub, Lalita Subedi, Kyoung Jin Park, Sun Yeou Kim, Sang Un Choi, Ki Hyun Kim, and Kang Ro Lee. 2015. "Salicin derivatives from Salix glandulosa and their biological activities." *Fitoterapia* 106:147-152. doi: https://doi.org/10.1016/j.fitote.2015.08.013.

Klessig, Daniel F., Miaoying Tian, and Hyong Woo Choi. 2016. "Multiple Targets of Salicylic Acid and Its Derivatives in Plants and Animals." *Frontiers in Immunology* 7 (206). doi: 10.3389/fimmu.2016.00206.

Knuth, Susanne. 2013. "Pharmakologische und pharmakokinetische Untersuchungen zu Salicylalkoholderivaten aus Salicis cortex."

Knuth, Susanne, Rania M Abdelsalam, Mohamed T Khayyal, Frank Schweda, Jörg Heilmann, Martin Georg Kees, Georg Mair, Frieder Kees, and Guido Jürgenliemk. 2013. "Catechol conjugates are in vivo metabolites of Salicis cortex." *Planta medica* 79 (16):1489-1494.

Knuth, Susanne, Helmut Schübel, Martin Hellemann, and Guido Jürgenliemk. 2011. "Catechol, a bioactive degradation product of salicortin, reduces TNF-α induced ICAM-1 expression in human endothelial cells." *Planta medica* 77 (10):1024-1026.

Kulasekaran, Satish, Sergio Cerezo-Medina, Claudia Harflett, Charlotte Lomax, Femke de Jong, Amelie Rendour, Gianluca Ruvo, Steven J Hanley, Michael H Beale, and Jane L Ward. 2020. "A willow UDP-glycosyltransferase involved in salicinoid biosynthesis." *Journal of Experimental Botany*. doi: 10.1093/jxb/eraa562.

Kumari, Amita, Navneet Upadhyay, and Prem Khosla. 2016. "Gender specific variation of two phenolic glycosides (Populin and salicin) in populus ciliata and identification of a new compound (cinnamoyl-salicin)." *International Journal of Pharmacy and Phamaceutical Sciences* 8:156-162. doi: 10.22159/ijpps.2016v8i12.14843.

Kuzovkina, Yulia A., and Martin F. Quigley. 2005. "Willows Beyond Wetlands: Uses of Salix L. Species for Environmental Projects." *Water, Air, and Soil Pollution* 162 (1):183-204. doi: 10.1007/s11270-005-6272-5.

Kuzovkina, Yulia A., and Timothy A. Volk. 2009. "The characterization of willow (Salix L.) varieties for use in ecological engineering applications: Co-ordination of structure, function and autecology." *Ecological Engineering* 35 (8):1178-1189. doi: https://doi.org/10.1016/j.ecoleng.2009.03.010.

Lauron-Moreau, Aurélien, Frédéric E. Pitre, George W. Argus, Michel Labrecque, and Luc Brouillet. 2015. "Phylogenetic Relationships of American Willows (Salix L., Salicaceae)." *PLOS ONE* 10 (4):e0121965. doi: 10.1371/journal.pone.0121965.

Lautenschlager-Fleury, Dagmar, and Ernst Lautenschlager-Fleury. 1994a. "Allgemeines." In *Die Weiden von Mittel- und Nordeuropa: Bestimmungsschlüssel und Artbeschreibungen für die Gattung Salix L.*, 12-29. Basel: Birkhäuser Basel.

Lautenschlager-Fleury, Dagmar, and Ernst Lautenschlager-Fleury. 1994b. "Diagnosen der aufrechter Sträucher und Bäume." In *Die Weiden von Mittel- und Nordeuropa: Bestimmungsschlüssel und Artbeschreibungen für die Gattung Salix L.*, 57-125. Basel: Birkhäuser Basel.

Le, N. P. K., C. Herz, J. V. D. Gomes, N. Förster, K. Antoniadou, V. K. Mittermeier-Kleßinger, I. Mewis, C. Dawid, C. Ulrichs, and E. Lamy. 2021. "Comparative Anti-Inflammatory Effects of Salix Cortex Extracts and Acetylsalicylic Acid in SARS-CoV-2 Peptide and LPS-Activated Human In Vitro Systems." *Int J Mol Sci* 22 (13). doi: 10.3390/ijms22136766.

Lee, M., S. H. Lee, J. Kang, H. Yang, E. J. Jeong, H. P. Kim, Y. C. Kim, and S. H. Sung. 2013. "Salicortin-derivatives from Salix pseudo-lasiogyne twigs inhibit adipogenesis in 3T3-L1 cells via modulation of C/EBPα and SREBP1c dependent pathway." *Molecules* 18 (9):10484-96. doi: 10.3390/molecules180910484.

Lefevere, Hannes, Lander Bauters, and Godelieve Gheysen. 2020. "Salicylic acid biosynthesis in plants." *Frontiers in plant science* 11:338.

Lever, Jake, Martin Krzywinski, and Naomi Altman. 2017. "Principal component analysis." *Nature Methods* 14 (7):641-642. doi: 10.1038/nmeth.4346.

Levitt, Malcolm H. 2013. *Spin dynamics: basics of nuclear magnetic resonance*: John Wiley & Sons.

Lindegaard, KN, and JHA Barker. 1997. "Breeding willows for biomass." *Aspects of Applied Biology* 49:155-162.

Lloyd, David G., and C. J. Webb. 1977. "Secondary sex characters in plants." *The Botanical Review* 43 (2):177-216. doi: 10.1007/bf02860717.

Loll, Patrick J., Daniel Picot, and R. Michael Garavito. 1995. "The structural basis of aspirin activity inferred from the crystal structure of inactivated

prostaglandin H2 synthase." *Nature Structural Biology* 2 (8):637-643. doi: 10.1038/nsb0895-637.

Maclagan, T. 1876. "The treatment of acute rheumatism by salicin." *The Lancet* 107 (2741):383-384.

Mahdi, Jassem G. 2010. "Medicinal potential of willow: A chemical perspective of aspirin discovery." *Journal of Saudi Chemical Society* 14 (3):317-322. doi: https://doi.org/10.1016/j.jscs.2010.04.010.

Mahdi, Jassem G. 2014. "Biosynthesis and metabolism of β-d-salicin: A novel molecule that exerts biological function in humans and plants." *Biotechnology Reports* 4:73-79. doi: https://doi.org/10.1016/j.btre.2014.08.005.

Maistro, E. L., P. M. Terrazzas, F. F. Perazzo, I. O. M. Gaivão, Achf Sawaya, and P. C. P. Rosa. 2019. "Salix alba (white willow) medicinal plant presents genotoxic effects in human cultured leukocytes." *J Toxicol Environ Health A* 82 (23-24):1223-1234. doi: 10.1080/15287394.2019.1711476.

Maroon, Joseph C, Jeffrey W Bost, and Adara Maroon. 2010. "Natural anti-inflammatory agents for pain relief." *Surgical neurology international* 1.

Marson, Piero, and Giampiero Pasero. 2006. "The Italian contributions to the history of salicylates." *Reumatismo* 58 (1):66-75.

Marson, Piero, and Giampiero Pasero. 2008. "La scoperta del "sale amarissimo antifebbrile" del veronese Bartolommeo Rigatelli, ovvero le origini della farmacoeconomia." *Farmeconomia e percorsi terapeutici*.

Matyjaszczyk, Ewa; Schumann, Regina. 2018. "German Federal Institute for Risk assessment of white willow (Salix alba) in food." *EFSA Journal* 16 (S1):e16081. doi: 10.2903/j.efsa.2018.e16081.

McClure, Cynthia K. 1999. "Structural Chemistry Using NMR Spectroscopy, Organic Molecules."

Meier, Beat, Y Shao, R Julkunen-Tiitto, A Bettschart, and O Sticher. 1992. "A chemotaxonomic survey of phenolic compounds in Swiss willow species." *Proceedings of the Royal Society of Edinburgh, Section B: Biological Sciences* 98:229-232.

Mizuno, Mizuo, Masaya Kato, Chiemi Misu, Munekazu Iinuma, and Toshiyuki Tanaka. 1991. "Chaenomeloidin: A Phenolic Glucoside from Leaves of Salix chaenomeloides." *Journal of Natural Products* 54 (5):1447-1450. doi: 10.1021/np50077a042.

Mleczek, Mirosław, Iwona Rissmann, Paweł Rutkowski, Zygmunt Kaczmarek, and Piotr Golinski. 2009. "Accumulation of selected heavy metals by different genotypes of Salix." *Environmental and Experimental Botany* 66:289-296. doi: 10.1016/j.envexpbot.2009.02.010.

Morteau, O. 2000. "Prostaglandins and inflammation: the cyclooxygenase controversy." *Arch Immunol Ther Exp (Warsz)* 48 (6):473-80.

Mosser, David M, and Justin P Edwards. 2008. "Exploring the full spectrum of macrophage activation." *Nature reviews immunology* 8 (12):958.

Nahrstedt, A., M. Schmidt, R. Jäggi, J. Metz, and M. T. Khayyal. 2007. "Willow bark extract: the contribution of polyphenols to the overall effect." *Wien Med Wochenschr* 157 (13-14):348-51. doi: 10.1007/s10354-007-0437-3.

Nichols-Orians, Colin M., Robert S. Fritz, and Thomas P. Clausen. 1993. "The genetic basis for variation in the concentration of phenolic glycosides in Salix sericea: Clonal variation and sex-based differences." *Biochemical Systematics and Ecology* 21 (5):535-542. doi: https://doi.org/10.1016/0305-1978(93)90052-S.

Noleto-Dias, Clarice, Jane L. Ward, Alice Bellisai, Charlotte Lomax, and Michael H. Beale. 2018. "Salicin-7-sulfate: A new salicinoid from willow and implications for herbal medicine." *Fitoterapia* 127:166-172. doi: https://doi.org/10.1016/j.fitote.2018.02.009.

Noleto-Dias, Clarice, Yanqi Wu, Alice Bellisai, William Macalpine, Michael H. Beale, and Jane L. Ward. 2019. "Phenylalkanoid Glycosides (Non-Salicinoids) from Wood Chips of Salix triandra × dasyclados Hybrid Willow." *Molecules* 24 (6):1152.

Nosek, Radovan, Michal Holubcik, and Jozef Jandacka. 2016. "The impact of bark content of wood biomass on biofuel properties." *BioResources* 11 (1):44-53.

Oketch-Rabah, Hellen A, Robin J Marles, Scott A Jordan, and Tieraona Low Dog. 2019. "United States Pharmacopeia safety review of willow bark." *Planta medica* 85 (16):1192-1202.

Orians, CM, S Lower, RS Fritz, and BM Roche. 2003. "The effects of plant genetic variation and soil nutrients on secondary chemistry and growth in a shrubby willow, Salix sericea: patterns and constraints on the evolution of resistance traits." *Biochemical Systematics and Ecology* 31 (3):233-247.

Palo, R. Thomas. 1984. "Distribution of birch (Betula SPP.), willow (Salix SPP.), and poplar (Populus SPP.) secondary metabolites and their potential role as chemical defense against herbivores." *Journal of Chemical Ecology* 10 (3):499-520. doi: 10.1007/BF00988096.

Paré, Paul W., and James H. Tumlinson. 1999. "Plant Volatiles as a Defense against Insect Herbivores." *Plant Physiology* 121 (2):325-332. doi: 10.1104/pp.121.2.325.

Pasteels, Jacques M, Martine ROWELL-RAHIER, Jean Claude Braekman, and A Dupont. 1983. "Salicin from host plant as precursor of salicylaldehyde in defensive secretion of chrysomeline larvae." *Physiological Entomology* 8 (3):307-314.

Pearl, Irwin A., and Stephen F. Darling. 1968. "Studies on the barks of the family salicaceae—XX: Variations in the hot water extractives of populus balsamifera bark." *Phytochemistry* 7 (10):1855-1860. doi: https://doi.org/10.1016/S0031-9422(00)86659-5.

Pearl, Irwin A., and Stephen F. Darling. 1970a. "Phenolic extractives of Salix purpurea bark." *Phytochemistry* 9 (6):1277-1281. doi: https://doi.org/10.1016/S0031-9422(00)85319-4.

Pearl, Irwin A., and Stephen F. Darling. 1970b. "Purpurein, a new glucoside from the bark of Salix purpurea." *Phytochemistry* 9 (4):853-856. doi: https://doi.org/10.1016/S0031-9422(00)85192-4.

Pearl, Irwin A., and Stephen F. Darling. 1971. "Hot water phenolic extractives of the bark and leaves of diploid Populus tremuloides." *Phytochemistry* 10 (2):483-484. doi: https://doi.org/10.1016/S0031-9422(00)94089-5.

Pei, Ming Hao, and Alistair R McCracken. 2005. *Rust diseases of willow and poplar*: CABI.

Piria, R. 1838. "Sur des nouveaux produits extraits de la salicin." *CR Acad Sci* 6:620-624.

Pobłocka-Olech, Loretta, Anne-Marie van Nederkassel, Yvan Vander Heyden, Mirosława Krauze-Baranowska, Daniel Glód, and Tomasz Baczek. 2007. "Chromatographic analysis of salicylic compounds in different species of the genus Salix." *Journal of Separation Science* 30 (17):2958-2966. doi: https://doi.org/10.1002/jssc.200700137.

Protasiuk, E., and M. Olejnik. 2018. "Determination of Salicylic Acid in Feed Using LC-MS/MS." *J Vet Res* 62 (3):303-307. doi: 10.2478/jvetres-2018-0044.

Ramos, Patrícia AB, Catarina Moreirinha, Sara Silva, Eduardo M Costa, Mariana Veiga, Ezequiel Coscueta, Sónia AO Santos, Adelaide Almeida, M Manuela Pintado, and Carmen SR Freire. 2019. "The health-promoting potential of Salix spp. bark polar extracts: Key insights on phenolic composition and in vitro bioactivity and biocompatibility." *Antioxidants* 8 (12):609.

Reichardt, Paul B, Howard M Merken, Thomas P Clausen, and Jiejun Wu. 1992. "Phenolic glycosides from Salix lasiandra." *Journal of Natural Products* 55 (7):970-973.

Reichardt, PB, JP Bryant, BR Mattes, TP Clausen, FS Chapin, and M Meyer. 1990. "Winter chemical defense of Alaskan balsam poplar against snowshoe hares." *Journal of Chemical Ecology* 16 (6):1941-1959.

Reinhard, Karl, Donny L Hamilton, and Richard H Hevly. 1991. "Use of pollen concentration in paleopharmacology: coprolite evidence of medicinal plants."

Reynolds, W. F. 2017. "Chapter 29 - Natural Product Structure Elucidation by NMR Spectroscopy." In *Pharmacognosy*, edited by Simone Badal and Rupika Delgoda, 567-596. Boston: Academic Press.

Ricciotti, Emanuela, and Garret A. FitzGerald. 2011. "Prostaglandins and Inflammation." *Arteriosclerosis, thrombosis, and vascular biology* 31 (5):986-1000. doi: 10.1161/ATVBAHA.110.207449.

Ridker , Paul M., Mary Cushman , Meir J. Stampfer , Russell P. Tracy , and Charles H. Hennekens 1997. "Inflammation, Aspirin, and the Risk of Cardiovascular Disease in Apparently Healthy Men." *New England Journal of Medicine* 336 (14):973-979. doi: 10.1056/nejm199704033361401.

Rigatelli, Bartolommeo. 1824. "Terapeutica. Esito di alcuni sperimenti sul sale amarissimo del sig. Bartolomeo Rigatelli."

Rowell-Rahier, Martine, and Jacques M Pasteels. 1986. "Economics of chemical defense in Chrysomelinae." *Journal of Chemical Ecology* 12 (5):1189-1203.

Rubert-Nason, K. F., C. J. Hedman, L. M. Holeski, and R. L. Lindroth. 2014. "Determination of Salicinoids by Micro-high-performance Liquid Chromatography and Photodiode Array Detection." *Phytochemical Analysis* 25 (3):185-191. doi: https://doi.org/10.1002/pca.2485.

Ruuhola, T. M., and M. R. Julkunen-Tiitto. 2000. "Salicylates of intact Salix myrsinifolia plantlets do not undergo rapid metabolic turnover." *Plant physiology* 122 (3):895-905. doi: 10.1104/pp.122.3.895.

Ruuhola, Teija. 2001. "Dynamics of salicylates in willows and its relationship to herbivory."

Ruuhola, Teija, and Riitta Julkunen-Tiitto. 2003. "Trade-Off Between Synthesis of Salicylates and Growth of Micropropagated Salix pentandra." *Journal of Chemical Ecology* 29 (7):1565-1588. doi: 10.1023/A:1024266612585.

Ruuhola, Teija, Riitta Julkunen-Tiitto, and Pirjo Vainiotalo. 2003. "In Vitro Degradation of Willow Salicylates." *Journal of Chemical Ecology* 29:1083-1097. doi: 10.1023/A:1023821304656.

Schmid, B, B Tschirdewahn, I Kötter, I Günaydin, R Lüdtke, HK Selbmann, W Schaffner, and L Heide. 1998. "Analgesic effects of willow bark extract in osteoarthritis: results of a clinical double-blind trial." *Focus on Alternative*

and Complementary Therapies 3 (4):186-186. doi: https://doi.org/10.1111/j.2042-7166.1998.tb00927.x.

Schmid, B., I. Kötter, and L. Heide. 2001. "Pharmacokinetics of salicin after oral administration of a standardised willow bark extract." *Eur J Clin Pharmacol* 57 (5):387-91. doi: 10.1007/s002280100325.

Schmid, Christian, Corinna Dawid, Verena Peters, and Thomas Hofmann. 2018. "Saponins from European Licorice Roots (Glycyrrhiza glabra)." *Journal of Natural Products* 81 (8):1734-1744. doi: 10.1021/acs.jnatprod.8b00022.

Sciex. 2019. "Powerful Scan Modes of QTRAP® System Technology." accessed 08.09.2021. https://sciex.com/content/dam/SCIEX/pdf/tech-notes/all/QTRAP-Scan-Modes.pdf.

Shao, Y, MF Lahloub, B Meier, and O Sticher. 1989. "Isolation of phenolic compounds from the bark of Salix pentandra." *Planta Medica* 55 (07):617-618.

Shara, M., and S. J. Stohs. 2015. "Efficacy and Safety of White Willow Bark (Salix alba) Extracts." *Phytother Res* 29 (8):1112-6. doi: 10.1002/ptr.5377.

Sheetz, Michael P., and S. J. Singer. 1974. "Biological Membranes as Bilayer Couples. A Molecular Mechanism of Drug-Erythrocyte Interactions." *Proceedings of the National Academy of Sciences* 71 (11):4457-4461. doi: 10.1073/pnas.71.11.4457.

Shin, Soo-Joeng; Han, Sim-Hee 2014. "Investigation of solid energy potential of wood and bark obtained from four clones of a 2-year old goat willow." *Frontiers in Energy Research* 2:5. doi: https://doi.org/10.3389/fenrg.2014.00005.

Shivatare, Rakesh, Monali Phopase, Dheeraj Nagore, Sanjay Nipanikar, and Sohan Chitlange. 2014. "Development and Validation of HPLC Analytical Protocol for Quantification of Salicin from Salix alba L."

Sjöström, E. 1981. "Fundamentals and Applications of Wood Chemistry." *Wood chemistry, Academic Press Inc., New York*:223-245.

Smith, JB, and Al L Willis. 1971. "Aspirin selectively inhibits prostaglandin production in human platelets." *Nature New Biology* 231 (25):235-237.

Sneader, Walter. 2000. "The discovery of aspirin: a reappraisal." *BMJ : British Medical Journal* 321 (7276):1591-1594.

Solomons, T.W.G., C.B. Fryhle, and S.A. Snyder. 2016. *Organic Chemistry, 12th Edition*: Wiley.

Stewart, W. F., C. Kawas, M. Corrada, and E. J. Metter. 1997. "Risk of Alzheimer's disease and duration of NSAID use." *Neurology* 48 (3):626-32. doi: 10.1212/wnl.48.3.626.

Stone, Edward. 1763. "XXXII. An account of the success of the bark of the willow in the cure of agues. In a letter to the Right Honourable George Earl of Macclesfield, President of RS from the Rev. Mr. Edward Stone, of Chipping-Norton in Oxfordshire." *Philosophical Transactions* 53:195-200.

Straškraba, M. 1993. "Ecotechnology as a new means for environmental management." *Ecological Engineering* 2 (4):311-331. doi: https://doi.org/10.1016/0925-8574(93)90001-V.

Sun, Yen, Chang-Chun Lee, Wei-Chin Hung, Fang-Yu Chen, Ming-Tao Lee, and Huey W. Huang. 2008. "The bound states of amphipathic drugs in lipid bilayers: study of curcumin." *Biophysical journal* 95 (5):2318-2324. doi: 10.1529/biophysj.108.133736.

Šyc, Michal, Michael Pohořelý, Petra Kameníková, Jan Habart, Karel Svoboda, and Miroslav Punčochář. 2012. "Willow trees from heavy metals

phytoextraction as energy crops." *Biomass and Bioenergy* 37:106-113. doi: https://doi.org/10.1016/j.biombioe.2011.12.025.

Tahvanainen, J, R Julkunen-Tiitto, and J Kettunen. 1985. "Phenolic glycosides govern the food selection pattern of willow feeding leaf beetles." *Oecologia* 67 (1):52-56.

Tanaka, T., T. Nakashima, T. Ueda, K. Tomii, and I. Kouno. 2007. "Facile discrimination of aldose enantiomers by reversed-phase HPLC." *Chem Pharm Bull (Tokyo)* 55 (6):899-901. doi: 10.1248/cpb.55.899.

Thieme, H. 1964. "Zur Konstitution des Fragilins." *The Science of Nature* 51 (13):310-310.

Thieme, H. 1971. "Vorkommen und Verbreitung von Phenolglucosiden in der Familie der Salicaceen." *Poznan Inst Przemyslu Zielarskiego Biul.*

Todd, Alexander Robertus, and Robert Robinson. 1956. "Perspectives in organic chemistry."

Tollsten, Lars, and Jette T. Knudsen. 1992. "Floral scent in dioeciousSalix (Salicaceae)—a cue determining the pollination system?" *Plant Systematics and Evolution* 182 (3):229-237. doi: 10.1007/BF00939189.

Totland, O., and M. Sottocornola. 2001. "Pollen limitation of reproductive success in two sympatric alpine willows (Salicaceae) with contrasting pollination strategies." *Am J Bot* 88 (6):1011-5.

Tran, Hoai Thi Thu, Melinda-Rita Márton, Corinna Herz, Ronald Maul, Susanne Baldermann, Monika Schreiner, and Evelyn Lamy. 2016. "Nasturtium (Indian cress, Tropaeolum majus nanum) dually blocks the COX and LOX pathway in primary human immune cells." *Phytomedicine* 23 (6):611-620. doi: https://doi.org/10.1016/j.phymed.2016.02.025.

Uematsu, Satoshi, Makoto Matsumoto, Kiyoshi Takeda, and Shizuo Akira. 2002. "Lipopolysaccharide-dependent prostaglandin E2 production is regulated by the glutathione-dependent prostaglandin E2 synthase gene induced by the Toll-like receptor 4/MyD88/NF-IL6 pathway." *The Journal of Immunology* 168 (11):5811-5816.

Vane, J. R. 2000. "The fight against rheumatism: from willow bark to COX-1 sparing drugs." *J Physiol Pharmacol* 51 (4 Pt 1):573-86.

Vane, J. R., and R. M. Botting. 2003. "The mechanism of action of aspirin." *Thromb Res* 110 (5-6):255-8. doi: 10.1016/s0049-3848(03)00379-7.

Vollhardt, Kurt Peter C, and Neil Eric Schore. 1989. *Organische Chemie. Arbeitsbuch. Arbeitsbuch zu Vollhardt-Organische Chemie: Kommentare und Lösungen zu den Aufgaben*: VCH-Verlag-Ges.

Vroege, Peter W, and Paul Stelleman. 1990. "INSECT AND WIND POLLINATION IN SAUX REPENS L. AND SAUX CAPREA L." *Israel Journal of Plant Sciences* 39 (1-2):125-132.

Wei, W., K. Rena, and X. W. Yang. 2015. "New salicin derivatives from the leaves of Populus euphratica." *J Asian Nat Prod Res* 17 (5):491-6. doi: 10.1080/10286020.2015.1028920.

Wood, John N. 2015. "From plant extract to molecular panacea: a commentary on Stone (1763)'An account of the success of the bark of the willow in the cure of the agues'." *Philosophical Transactions of the Royal Society B: Biological Sciences* 370 (1666):20140317.

Woodson, Robert E., Robert W. Schery, and W. G. D'Arcy. 1978. "Flora of Panama. Part IV. Family 37. Salicaceae." *Annals of the Missouri Botanical Garden* 65 (1):1-4. doi: 10.2307/2395351.

Yang, H., S. H. Lee, S. H. Sung, J. Kim, and Y. C. Kim. 2013. "Neuroprotective compounds from Salix pseudo-lasiogyne twigs and their anti-amnesic

effects on scopolamine-induced memory deficit in mice." *Planta Med* 79 (1):78-82. doi: 10.1055/s-0032-1327949.

Zanger, M. 1972. "The determination of aromatic substitution patterns by nuclear magnetic resonance." *Organic Magnetic Resonance* 4 (1):1-25. doi: https://doi.org/10.1002/mrc.1270040102.

Zapesochnaya, G. G., V. A. Kurkin, V. B. Braslavskii, and N. V. Filatova. 2002. "Phenolic Compounds of Salix acutifolia Bark." *Chemistry of Natural Compounds* 38 (4):314-318. doi: 10.1023/A:1021661621628.

Zeiner, Michaela, and Iva Juranović Cindrić. 2017. "Review–trace determination of potentially toxic elements in (medicinal) plant materials." *Analytical Methods* 9 (10):1550-1574.

Zenk, MH. 1967. "Pathways of salicyl alcohol and salicin formation in Salix purpurea L." *Phytochemistry* 6 (2):245-252.

Zheng, L. T., G. M. Ryu, B. M. Kwon, W. H. Lee, and K. Suk. 2008. "Anti-inflammatory effects of catechols in lipopolysaccharide-stimulated microglia cells: inhibition of microglial neurotoxicity." *Eur J Pharmacol* 588 (1):106-13. doi: 10.1016/j.ejphar.2008.04.035.

Zhong, Zhifeng, Jing Han, Jizhou Zhang, Qing Xiao, Juan Hu, and Lidian Chen. 2018. "Pharmacological activities, mechanisms of action, and safety of salidroside in the central nervous system." *Drug design, development and therapy* 12:1479-1489. doi: 10.2147/DDDT.S160776.

Zhu, Jianjun, Stephen G Withers, Paul B Reichardt, Edward Treadwell, and Thomas P Clausen. 1998. "Salicortin: a repeat-attack new-mechanism-based Agrobacterium faecalis β-glucosidase inhibitor." *Biochemical Journal* 332 (2):367-371.

7 APPENDIX

Further explanations about chemical structures, statistical, spectroscopic NMR, and quantitative data were enclosed in the current Appendix section.

Table A1 shows the statistical data of the generated S-plots. Table A2 reveals the yield of each SPE fraction (F1-F11), the used mass in order to keep the natural concentrations of each fraction based on the S6 methanol extract for the bioactivity assay performed by UKF. The NMR data of the chemical structures of the isolated, structurally elucidated, and quantified compounds **I-VIII** are exhibited in Tables A3-A11. The concentrations and standard deviations of the compounds in 92 *Salix* species and crosses are displayed in Table A12. Table A13 exhibits the MRM transitions, as well as DP, CE, and CXP values of the analyzed polyphenols, which were obtained from the method developed by Tina Schmittnägel (Chair of Food Chemistry and Molecular Sensory Science).

Table A1: Statistical data generated between two groups of the obtained OPLS-DA models (Pareto scaling), and number of selected candidate markers extracted from the S-plots. GT: genotype, R2Y: total sum of explained variations in Y by the component, Q2: predictive ability.

group comparison	no. of *Salix* genotypes	OPLS-DA			S-plot	
		marked points	R2Y [%]	Q2 [%]	no. markers -1	no. markers 1
group 1 (-1) vs. group 2 (1)	23 vs. 26	92 vs. 104	99.19	99.14	21	17
group 1 (-1) vs. group 3 (1)	23 vs. 26	92 vs. 104	98.77	98.71	33	25
group 1 (-1) vs. group 4 (1)	23 vs. 16	92 vs. 63	99.18	98.77	21	23
group 2 (-1) vs. group 3 (1)	26 vs. 26	104 vs. 104	98.61	98.29	9	19
group 2 (-1) vs. group 4 (1)	26 vs. 16	104 vs. 63	98.98	98.73	10	21
group 3 (-1) vs. group 4 (1)	26 vs. 16	104 vs. 104	98.98	98.73	15	25

Table A2: S6 methanol extract yields after SPE fractionation and conversion of the yielded fraction amount in order to relate to the natural concentrations regarding the methanol extract. The concentrations (C) correspond to 10 mg/mL methanol extract (the volume (mL) of water was added by UKF after receiving the powder).

SPE fraction	yield [g/100g]	mg amount sent to UKF	water [mL]	C [mg/mL]
F1	6.26	10.50	16.78	0.626
F2	4.83	9.17	18.97	0.483
F3	8.85	7.42	8.39	0.885
F4	15.09	1.78	1.18	1.509
F5	26.59	14.49	5.45	2.659
F6	14.22	5.10	3.59	1.422
F7	3.07	2.63	8.56	0.307
F8	1.01	0.94	9.33	0.101
F9	0.16	1.00	62.99	0.016
F10	0.12	1.83	157.82	0.012
F11	0.32	8.15	253.76	0.032

Table A3: NMR data (500.13/125.77 MHz) of 2'-O-acetylsalicin (**I**) in methanol-d_4.

position	HSQC	δ_C [ppm]	δ_H [ppm]	multiplicity; J [Hz]
1	[C]	155.85	-	-
2	[C]	131.92	-	-
3	[CH]	128.90	7.38	m
4	[CH]	123.70	7.03	m
5	[CH]	129.47	7.21	m
6	[CH]	115.96	7.13	dd; 8.20, 1.05
7	[CH$_2$]	59.97	4.55	q; 15.46, 13.60 (overlap)
1'	[CH]	100.75	5.05	d; 8.05
2'	[CH]	75.07	5.03	dd: 8.01, 1.46
3'	[CH]	75.98	3.66	m
4'	[CH]	71.41	3.50	m
5'	[CH]	78.35	3.51	m
6'	[CH$_2$]	62.40	3.71	m
			3.91	m
1''	[CH$_3$]	21.02	2.14	s
2''	[C=O]	170.55	-	-

Table A4: NMR data (500.13/125.77 MHz) of 3'-*O*-acetylsalicortin (**II**) in acetone-*d₆*.

position	HSQC	δc [ppm]	δн [ppm]	multiplicity; *J* [Hz]
1	[C]	156.41	-	-
2	[C]	125.83	-	-
3	[CH]	130.10	7.33	m
4	[CH]	123.10	7.05	td; 7.50, 1.15
5	[CH]	130.66	7.31	m
6	[CH]	116.35	7.25	d; 7.84
7	[CH₂]	63.67	5.23	d; 12.80
			5.35	d; 12.80
8	[C=O]	170.86	-	-
9	[C]	78.83	-	-
10	[CH]	129.29	5.78	dt; 9.70, 1.70
11	[CH]	132.44	6.13	dt; 9.70, 3.80
12	[CH₂]	27.17	2.48-2.53	m
			2.64-2.71	m
13	[CH₂]	36.11	2.54-2.57	m
			2.83-2.90	m
14	[C=O]	206.21	-	-
1'	[CH]	102.03	5.11	d; 7.70
2'	[CH]	72.87	3.64	m
3'	[CH]	77.70	5.08	d; 9.30
4'	[CH]	69.36	3.66	m
5'	[CH]	78.46	3.63	m
6'	[CH₂]	62.19	3.74	dd; 11.35, 3.69
			3.89	dd; 11.39, 2.99
1''	[CH₃]	21.11	2.05	s
2''	[C=O]	170.79	-	-

Table A5: NMR data (500.13/125.77 MHz) of 2'-*O*-acetylsalicortin (**III**) in acetone-*d₆*.

position	HSQC	δ_C [ppm]	δ_H [ppm]	multiplicity; *J* [Hz]
1	[C]	155.88	-	-
2	[C]	125.94	-	-
3	[CH]	129.50	7.31	m
4	[CH]	123.36	7.05	td; 7.50, 1.08
5	[CH]	130.40	7.28	m
6	[CH]	116.49	7.21	d; 8.00
7	[CH₂]	63.08	5.18	d; 2.73 (overlap)
8	[C=O]	170.79	-	-
9	[C]	78.81	-	-
10	[CH]	129.30	5.80	dt; 9.78, 1.75
11	[CH]	132.43	6.14	dt; 9.82, 3.85
12	[CH₂]	27.20	2.49-2.54	m
			2.67-2.76	m
13	[CH₂]	36.09	2.59-2.66	m
			2.94-2.86	m
14	[C=O]	206.20	-	-
1'	[CH]	100.18	5.13	d; 7.16
2'	[CH]	74.39	5.02	dd; 8.08, 1.62
3'	[CH]	75.66	3.72	m
4'	[CH]	71.44	3.57	m
5'	[CH]	78.05	3.58	m
6'	[CH₂]	62.37	3.73	m
			3.91	m
1''	[CH₃]	21.02	2.07	s
2''	[C=O]	170.30	-	-

Table A6: NMR data (500.13/125.77 MHz) of cinnamrutinose A (**IV**) in acetonitrile-*d*₃.

position	HSQC	δ_C [ppm]	δ_H [ppm]	multiplicity; *J* [Hz]
1	[CH₂]	70.11	4.24	ddd; 12.83, 6.54, 1.44
			4.43	ddd; 12.80, 7.04, 1.52
2	[CH]	126.84	6.35	ddd; 16.14, 5.61
3	[CH]	133.01	6.69	dt; 15.89, 1.82
4	[C]	137.80	-	-
5	[CH]	127.41	7.44	d; 7.60
6	[CH]	129.67	7.35	m
7	[CH]	128.73	7.30	m
8	[CH]	129.67	7.35	m
9	[CH]	127.41	7.44	d; 7.60
1'	[CH]	102.85	4.31	d; 7.75
2'	[CH]	74.70	3.14	t; 8.10, 8.59
3'	[CH]	71.25	3.22	m
4'	[CH]	77.63	3.37	m
5'	[CH]	73.75	3.25	m
6'	[CH₂]	67.90	3.64	m
			3.88	dd; 11.46, 1.92
1"	[CH]	101.66	4.72	dd; 16.35, 1.03
2"	[CH]	71.74	3.78	dd; 3.78, 1.53
3"	[CH]	72.26	3.54	dd; 9.45, 3.63
4"	[CH]	76.34	3.29	m
5"	[CH]	69.07	3.59	m
6"	[CH₃]	18.10	1.21	d; 6.41

Table A7: NMR data (500.13/125.77 MHz) of 2',6'-*O*-diacetylsalicortin (**V**) in acetone-*d₆*.

position	HSQC	δ_C [ppm]	δ_H [ppm]	multiplicity; *J* [Hz]
1	[C]	155.78	-	-
2	[C]	126.10	-	-
3	[CH]	129.61	7.33	m
4	[CH]	123.56	7.06	td; 7.44, 1.12
5	[CH]	130.35	7.31	m
6	[CH]	116.62	7.22	dd; 8.78, 1.06
7	[CH₂]	63.07	5.13	d; 13.07 (overlap)
8	[C=O]	170.78	-	-
9	[C]	78.85	-	-
10	[CH]	129.31	5.80	dt; 9.81, 3.48
11	[CH]	132.41	6.14	dt; 9.67, 3.71
12	[CH₂]	27.20	2.48-2.53	m
			2.66-2.75	m
13	[CH₂]	36.06	2.54-2.58	m
			2.85-2.93	m
14	[C=O]	206.20	-	-
1'	[CH]	100.06	5.16	d; 7.16
2'	[CH]	74.26	5.06	dd; 8.33, 1.58
3'	[CH]	75.06	3.82	m
4'	[CH]	71.47	3.58	t; 9.31
5'	[CH]	75.50	3.77	t; 9.44
6'	[CH₂]	64.01	3.74	dd; 11.75, 2.30
			3.91	dd; 11.95, 6.24
7'	[C=O]	170.92	-	-
8'	[CH₃]	20.72	2.03	s
1"	[CH₃]	21.00	2.10	s
2"	[C=O]	170.27	-	-

Table A8: NMR data (600.13/150.90 MHz) of lasiandrin (**VI**) in acetone-d_6.

position	HSQC	δ_C [ppm]	δ_H [ppm]	multiplicity; J [Hz]
1	[C]	155.85	-	-
2	[C]	126.17	-	-
3	[CH]	130.61	7.37	m
4	[CH]	123.66	7.08	td; 7.42, 1.00
5	[CH]	129.55	7.32	dd; 7.78, 1.73
6	[CH]	116.80	7.22	d; 8.19
7	[CH$_2$]	62.17	5.18	d; 12.87 (overlap)
			5.12	d; 12.87
8	[C=O]	170.78	-	-
9	[C]	78.86	-	-
10	[CH]	129.30	5.80	dt; 9.80, 1.70
11	[CH]	132.43	6.14	dt; 9.81, 3.96
12	[CH$_2$]	27.20	2.46-2.54	m
			2.62-2.73	m
13	[CH$_2$]	36.07	2.53-2.59	m
			2.84-2.92	m
14	[C=O]	206.18	-	-
1'	[CH]	100.25	5.17	d; 8.19
2'	[CH]	74.41	5.02	dd; 8.10, 1.55
3'	[CH]	75.45	3.74	t; 9.45
4'	[CH]	71.39	3.52	t; 9.45
5'	[CH]	75.05	3.85	ddd; 6.90, 5.12, 2.04
6'	[CH$_2$]	65.76	4.27	dd; 11.80, 6.79
			4.64	dd; 11.82, 2.06
8'	[C=O]	170.78	-	-
9'	[C]	78.82	-	-
10'	[CH]	129.26	5.75	dt; 9.80, 1.79
11'	[CH]	132.35	6.09	dt; 9.93, 3.89
12'	[CH$_2$]	27.20	2.46-2.54	m
			2.62-2.73	m
13'	[CH$_2$]	36.07	2.53-2.59	m
			2.84-2.92	m
14'	[C=O]	206.18	-	-
1''	[CH$_3$]	21.01	2.08	s
2''	[C=O]	170.26	-	-

Table A9: NMR data (500.13/125.77 MHz) of tremulacin (**VII**) in dimethyl sulfoxide-d_6.

position	HSQC	δ_C [ppm]	δ_H [ppm]	multiplicity; J [Hz]
1	[C]	154.20	-	-
2	[C]	124.34	-	-
3	[CH]	127.94	7.13	dd; 7.70, 1.51
4	[CH]	122.30	7.00	td; 7.62, 1.00
5	[CH]	129.40	7.29	ddd; 7.97, 1.52
6	[CH]	115.05	7.18	d; 8.21
7	[CH$_2$]	61.40	4.80	d; 13.37
			4.95	d; 13.37
8	[C=O]	169.86	-	-
9	[C]	77.35	-	-
10	[CH]	128.66	5.66	dt: 9.90, 1.57
11	[CH]	131.56	6.07	dt; 9.81, 3.74
12	[CH$_2$]	25.85	2.39-2.46	m
			2.47-2.56	m (overlap)
13	[CH$_2$]	35.56	2.47-2.52	m (overlap)
			2.69-2.63	m
14	[C=O]	205.92	-	-
1'	[CH]	98.41	5.29	d; 8.13
2'	[CH]	73.79	5.05	dd; 8.08, 1.62
3'	[CH]	74.29	3.69	td; 5.49, 3.74
4'	[CH]	69.89	3.34	s
5'	[CH]	77.28	3.51	m
6'	[CH$_2$]	60.54	3.55	m
			3.76	dd; 10.68, 4.99
1"	[C=O]	165.10	-	-
2"	[C]	129.74	-	-
3"	[CH]	129.34	7.98	t; 7.94
4"	[CH]	128.68	7.52	m
5"	[CH]	133.38	7.65	m
6"	[CH]	128.68	7.52	t; 7.94
7"	[CH]	129.34	7.98	m

Table A10: NMR data (500.13/125.77 MHz) of diastereomer of **VIII** (compound B) in methanol-d_4.

position	HSQC	δ_C [ppm]	δ_H [ppm]	multiplicity; J [Hz]
1	[C]	156.06	-	-
2	[C]	126.72	-	-
3	[CH]	129.67	7.39	m
4	[CH]	123.82	7.04	dt; 7.07, 1.14
5	[CH]	130.39	7.30	m
6	[CH]	116.85	7.21	ddd; 1.23, 7.57
7	[CH$_2$]	63.13	5.11-5.18	m
8	[C=O]	171.58	-	-
9	[C]	86.75	-	-
10	[CH]	127.19	5.59	dd; 10.10, 2.75
11	[CH]	131.12	6.02	m
12	[CH$_2$]	23.31	1.98-2.06	m
			2.17-2.24	m
13	[CH$_2$]	33.19	1.93-2.00	m
			2.41-2.53	m
14	[C]	104.47	-	-
1'	[CH]	100.74	5.09	m
2'	[CH]	75.00	5.03	m
3'	[CH]	75.98	3.64-3.67	m
4'	[CH]	71.42	3.49	m
5'	[CH]	78.38	3.50	m
6'	[CH$_2$]	62.41	3.75	m
			3.94	m
1''	[CH$_3$]	21.10	2.15	s
2''	[C=O]	171.98	-	-

Table A11: NMR data (500.13/125.77 MHz) of diastereomer of **VIII** (compound C) in methanol-*d₄*.

position	HSQC	δ_C [ppm]	δ_H [ppm]	multiplicity; J [Hz]
1	[C]	156.06	-	-
2	[C]	126.72	-	-
3	[CH]	129.67	7.39	m
4	[CH]	123.82	7.04	dt; 7.07, 1.14
5	[CH]	130.39	7.30	m
6	[CH]	116.85	7.21	ddd; 1.23, 7.57
7	[CH$_2$]	63.13	5.11-5.18	m
8	[C=O]	173.02	-	-
9	[C]	77.33	-	-
10	[CH]	128.44	5.53	dt; 10.03, 2.01
11	[CH]	132.80	5.98	dt; 9.98, 3.62
12	[CH$_2$]	25.29	2.19-2.26	m
			2.33-3.39	m
13	[CH$_2$]	32.13	2.44-2.51	m
14	[C]	111.81	-	-
1'	[CH]	100.74	5.09	m
2'	[CH]	75.00	5.03	m
3'	[CH]	75.98	3.64-3.67	m
4'	[CH]	71.42	3.49	m
5'	[CH]	78.38	3.50	m
6'	[CH$_2$]	62.41	3.75	m
			3.94	m
1''	[CH$_3$]	21.10	2.15	s
2''	[C=O]	171.98	-	-

Table A12: Concentrations (µmol/g) and relative standard deviations (RSD in %) of 92 *Salix* species and crosses. **1**: salicin, **2**: saligenin, **3**: salicortin, **4**: salicylic acid, **I**: 2'-*O*-acetylsalicin, **II**: 3'-*O*-acetylsalicortin, **III**: 2'-*O*-acetylsalicortin, **IV**: cinnamrutinose A, **V**: 2',6'-*O*-diacetylsalicortin, **VI**: lasiandrin, **VII**: tremulacin, n.a.: not applicable/not detected.

Salix species or crosses	concentration [µmol/g] (RSD in %)										
	1	2	3	4	I	II	III	IV	V	VI	VII
LA1	6.01 (±4.85)	0.19 (±6.44)	24.77 (±4.56)	n.a.	0.74 (±15.19)	0.33 (±120.08)	12.76 (±4.07)	n.a.	n.a.	0.07 (±4.93)	12.81 (±1.59)
DA2xDA3_7	16.07 (±29.84)	0.27 (±13.67)	119.24 (±3.98)	0.003 (±141.42)	0.06 (±72.08)	n.a.	0.17 (±5.78)	n.a.	n.a.	n.a.	1.71 (±4.09)
VI5xVI2_2	0.38 (±25.25)	0.17 (±6.40)	6.94 (±3.56)	n.a.	n.a.	n.a.	n.a.	n.a.	n.a.	n.a.	0.14 (±8.45)
PE2xLA1_2	7.72 (±3.60)	0.23 (±15.56)	24.42 (±2.44)	n.a.	1.07 (±14.37)	n.a.	6.81 (±3.32)	n.a.	n.a.	3.21 (±3.57)	1.30 (±3.06)
AL3xAL4_2	9.52 (±4.47)	0.20 (±7.56)	32.10 (±2.31)	n.a.	0.15 (±34.79)	n.a.	1.79 (±2.43)	n.a.	n.a.	0.84 (±3.14)	0.09 (±7.75)
DA2xDA3_1	9.96 (±1.64)	0.27 (±15.71)	147.26 (±0.92)	n.a.	0.08 (±76.96)	n.a.	0.18 (±24.96)	n.a.	n.a.	n.a.	15.24 (±0.77)
PE2xAL5_1	5.54 (±4.95)	0.33 (±9.22)	19.18 (±8.78)	n.a.	5.05 (±12.62)	0.40 (±7.24)	41.72 (±3.58)	0.01 (±141.42)	n.a.	0.76 (±1.25)	0.90 (±5.28)
PE2	2.13 (±5.35)	0.38 (±11.67)	12.21 (±4.01)	n.a.	6.46 (±5.88)	0.03 (±71.46)	45.16 (±2.40)	n.a.	n.a.	3.21 (±3.59)	1.40 (±5.13)
DA3	6.16 (±4.51)	0.19 (±6.86)	53.62 (±1.80)	n.a.	0.03 (±141.42)	n.a.	0.03 (±86.80)	n.a.	n.a.	n.a.	5.56 (±2.02)
DA5xPU2_1	12.86 (±3.47)	0.25 (±15.92)	132.71 (±0.26)	n.a.	n.a.	n.a.	n.a.	n.a.	n.a.	n.a.	4.54 (±2.01)
AL5	2.54 (±7.52)	0.12 (±70.72)	15.44 (±2.67)	n.a.	0.21 (±24.63)	n.a.	3.62 (±4.87)	n.a.	n.a.	n.a.	0.21 (±2.69)
DA2xDA3_3	11.07 (±8.83)	0.25 (±8.24)	139.17 (±1.44)	0.002 (±141.42)	0.03 (±141.42)	n.a.	0.05 (±26.10)	n.a.	n.a.	n.a.	6.43 (±4.74)
VI5	0.16 (±42.03)	0.17 (±4.84)	4.10 (±7.00)	n.a.	n.a.	n.a.	n.a.	n.a.	n.a.	n.a.	0.01 (±40.46)
PE2xLA1_3	2.45 (±4.15)	0.23 (±9.12)	8.15 (±3.26)	n.a.	2.90 (±5.13)	0.24 (±48.86)	25.18 (±3.14)	0.15 (±31.03)	n.a.	0.32 (±13.67)	0.01 (±54.83)
VI5xVI2_1	n.a.	0.17 (±8.16)	0.35 (±12.90)	n.a.	0.03 (±141.42)	n.a.	n.a.	n.a.	n.a.	n.a.	n.a.

Salix species or crosses	1	2	3	4	I	II	III	IV	V	VI	VII
					concentration [µmol/g] (RSD in %)						
DA2xDA3_4	11.06 (±0.67)	0.32 (±5.89)	138.72 (±3.13)	n.a.	0.06 (±71.43)	n.a.	n.a.	n.a.	n.a.	n.a.	21.76 (±4.47)
DA2xDA3_5	13.01 (±9.02)	0.26 (±20.09)	146.54 (±2.82)	n.a.	0.08 (±81.24)	n.a.	0.25 (±4.83)	n.a.	n.a.	n.a.	13.93 (±1.08)
AL4	2.45 (±6.26)	0.24 (±16.26)	10.96 (±7.06)	n.a.	0.20 (±31.89)	n.a.	2.67 (±6.79)	n.a.	n.a.	n.a.	0.09 (±6.16)
AL3	7.77 (±10.03)	0.22 (±11.17)	30.16 (±4.66)	n.a.	0.46 (±16.36)	n.a.	7.65 (±8.80)	n.a.	n.a.	3.83 (±7.14)	2.27 (±7.30)
DA2	12.44 (±3.78)	0.27 (±7.86)	167.38 (±3.04)	n.a.	n.a.	n.a.	n.a.	n.a.	n.a.	n.a.	15.34 (±3.58)
PE2xAL5_4	1.46 (±10.82)	0.28 (±31.75)	9.88 (±3.27)	n.a.	3.65 (±15.06)	0.55 (±12.08)	34.02 (±6.03)	n.a.	n.a.	0.45 (±11.13)	0.69 (±10.17)
DA2xDA3_2	13.76 (±21.72)	0.24 (±22.45)	144.70 (±4.11)	n.a.	n.a.	n.a.	0.24 (±25.48)	n.a.	n.a.	n.a.	11.44 (±4.42)
VI5xVI2_4	n.a.	0.19 (±1.54)	0.45 (±3.42)	n.a.	n.a.	n.a.	n.a.	n.a.	n.a.	n.a.	n.a.
PE2xLA1_1	2.77 (±4.15)	0.33 (±12.34)	7.71 (±0.84)	n.a.	7.23 (±6.45)	0.18 (±16.73)	40.77 (±1.96)	n.a.	n.a.	2.11 (±4.86)	0.02 (±33.83)
DA2xDA3_6	11.21 (±23.25)	0.23 (±5.68)	158.92 (±0.80)	n.a.	0.06 (±71.56)	n.a.	0.24 (±7.09)	n.a.	n.a.	n.a.	18.40 (±2.87)
PE2xAL5_3	5.67 (±2.51)	0.42 (±8.60)	19.00 (±5.21)	n.a.	11.91 (±8.62)	0.51 (±12.01)	60.75 (±5.87)	3.08 (±11.05)	n.a.	13.09 (±5.05)	3.24 (±7.15)
AL3xAL4_1	8.81 (±4.14)	0.23 (±20.20)	40.40 (±7.02)	n.a.	0.58 (±14.42)	n.a.	7.73 (±4.18)	n.a.	n.a.	2.73 (±4.30)	1.40 (±8.98)
DA2xDA3_8	14.05 (±4.80)	0.25 (±15.81)	147.65 (±0.28)	n.a.	0.05 (±100.00)	n.a.	0.09 (±15.78)	n.a.	n.a.	n.a.	10.60 (±1.30)
DA5	13.70 (±3.28)	0.34 (±11.96)	155.31 (±3.06)	n.a.	n.a.	n.a.	0.24 (±6.28)	n.a.	n.a.	n.a.	9.05 (±1.55)

Salix species or crosses	concentration [µmol/g] (RSD in %)										
	1	2	3	4	I	II	III	IV	V	VI	VII
PE2xAL5_2	13.30 (±0.00)	0.12 (±70.87)	50.37 (±3.58)	n.a.	2.00 (±19.28)	0.02 (±141.42)	19.17 (±4.01)	n.a.	n.a.	5.15 (±5.41)	7.12 (±2.72)
DA5xPU2_2	10.79 (±1.66)	0.25 (±18.16)	109.57 (±1.77)	n.a.	0.07 (±70.84)	n.a.	0.18 (±12.29)	n.a.	n.a.	n.a.	7.76 (±4.36)
VI5xVI2_3	0.20 (±36.72)	0.18 (±3.89)	8.33 (±6.28)	n.a.	0.03 (±141.42)	n.a.	n.a.	n.a.	n.a.	n.a.	0.19 (±6.53)
DA6	10.12 (±3.96)	0.23 (±7.79)	107.52 (±2.63)	0.08 (±16.48)	0.03 (±141.42)	n.a.	0.06 (±53.54)	n.a.	n.a.	n.a.	4.19 (±1.98)
HU1xPU1_3	7.14 (±2.28)	0.22 (±11.09)	67.12 (±4.21)	n.a.	0.03 (±141.42)	n.a.	n.a.	n.a.	n.a.	n.a.	1.88 (±3.70)
PU3xDA6_5	7.87 (±2.80)	0.27 (±15.85)	105.22 (±3.14)	n.a.	0.05 (±70.71)	n.a.	n.a.	n.a.	n.a.	n.a.	1.73 (±2.66)
PU3xDA6_3	9.82 (±2.55)	0.23 (±2.67)	82.10 (±0.68)	n.a.	0.03 (±141.42)	n.a.	0.005 (±141.42)	n.a.	n.a.	n.a.	3.54 (±2.42)
PU3xDA6_4	8.65 (±8.56)	0.20 (±5.45)	102.74 (±4.79)	n.a.	n.a.	n.a.	0.03 (±10.44)	n.a.	n.a.	n.a.	5.67 (±3.78)
HU1xPU1_2	12.68 (±4.09)	0.23 (±6.06)	74.74 (±2.38)	n.a.	0.03 (±141.42)	n.a.	n.a.	n.a.	n.a.	n.a.	0.18 (±3.10)
HU1xPU1_1	2.70 (±13.43)	0.12 (±70.72)	46.22 (±6.28)	n.a.	n.a.	n.a.	n.a.	n.a.	n.a.	n.a.	3.24 (±3.97)
HU1xVI6_1	4.78 (±4.97)	0.24 (±9.76)	18.13 (±0.74)	n.a.	0.03 (±141.42)	n.a.	n.a.	n.a.	n.a.	n.a.	0.26 (±2.93)
SN1	1.05 (±4.28)	0.21 (±1.52)	1.86 (±10.16)	n.a.	n.a.	n.a.	n.a.	n.a.	n.a.	n.a.	0.38 (±5.12)
VI6	1.82 (±7.79)	0.20 (±6.01)	12.59 (±5.00)	n.a.	n.a.	n.a.	n.a.	n.a.	n.a.	n.a.	0.06 (±11.18)
HU1xVI6_2	3.69 (±4.33)	0.12 (±71.06)	8.49 (±2.96)	n.a.	n.a.	n.a.	n.a.	n.a.	n.a.	n.a.	0.15 (±6.01)

Salix species or crosses	concentration [µmol/g] (RSD in %)										
	1	2	3	4	I	II	III	IV	V	VI	VII
VI2	0.02 (±84.74)	0.18 (±10.96)	2.53 (±6.26)	n.a.	n.a.	n.a.	n.a.	n.a.	n.a.	n.a.	0.02 (±28.72)
PU4xVI2_2	1.63 (±3.37)	0.20 (±13.26)	14.99 (±2.46)	n.a.	n.a.	n.a.	n.a.	n.a.	n.a.	n.a.	0.08 (±1.34)
PU3xPU2_1	5.53 (±2.51)	0.21 (±6.65)	78.65 (±2.56)	n.a.	n.a.	n.a.	n.a.	n.a.	n.a.	n.a.	10.77 (±4.02)
PU1	6.67 (±2.64)	0.23 (±11.00)	99.90 (±3.40)	n.a.	n.a.	n.a.	n.a.	n.a.	n.a.	n.a.	17.00 (±2.78)
PU3xPU2_3	6.59 (±3.31)	0.19 (±9.12)	66.43 (±0.21)	n.a.	0.03 (±141.42)	n.a.	n.a.	n.a.	n.a.	n.a.	1.35 (±8.90)
PU3	9.90 (±2.97)	0.19 (±4.58)	51.90 (±2.57)	n.a.	n.a.	n.a.	n.a.	0.03 (±45.00)	n.a.	n.a.	2.66 (±2.68)
PU2	7.31 (±2.87)	0.23 (±8.76)	82.97 (±3.10)	n.a.	n.a.	n.a.	n.a.	n.a.	n.a.	n.a.	8.29 (±0.83)
PU3xDA6_1	7.57 (±3.81)	0.21 (±4.90)	69.09 (±5.55)	0.10 (±4.59)	n.a.	n.a.	n.a.	n.a.	n.a.	n.a.	0.37 (±1.62)
PU3xPU2_2	6.20 (±5.27)	0.21 (±9.81)	67.98 (±3.10)	n.a.	n.a.	n.a.	n.a.	n.a.	n.a.	n.a.	7.67 (±1.21)
PU4xVI2_1	2.39 (±9.25)	0.12 (±70.81)	37.82 (±0.72)	n.a.	n.a.	n.a.	n.a.	n.a.	n.a.	n.a.	0.58 (±2.36)
PU3xVI3_1	5.23 (±3.62)	0.24 (±14.79)	22.99 (±1.68)	n.a.	0.61 (±21.09)	0.02 (±77.17)	10.27 (±2.86)	n.a.	n.a.	2.42 (±3.19)	2.51 (±4.65)
PU3xDA6_2	10.52 (±2.62)	0.24 (±0.42)	102.95 (±1.75)	0.15 (±2.30)	0.06 (±71.34)	n.a.	n.a.	n.a.	n.a.	n.a.	2.75 (±2.22)
PU4	8.27 (±20.95)	0.19 (±14.70)	78.41 (±16.54)	0.01 (±141.42)	n.a.	n.a.	n.a.	n.a.	n.a.	n.a.	6.28 (±34.34)
PU3xVI3_2	1.51 (±11.69)	0.23 (±13.00)	43.63 (±3.83)	n.a.	1.02 (±2.00)	0.06 (±74.96)	19.32 (±9.49)	n.a.	n.a.	0.002 (±141.42)	6.26 (±5.33)

Salix species or crosses	concentration [μmol/g] (RSD in %)										
	1	2	3	4	I	II	III	IV	V	VI	VII
SN1xPE1	0.57 (±13.60)	0.18 (±0.52)	10.92 (±4.68)	n.a.	0.29 (±6.67)	0.02 (±100.00)	4.59 (±3.24)	n.a.	n.a.	n.a.	0.36 (±1.63)
HU1	4.15 (±10.43)	0.14 (±70.91)	17.04 (±7.20)	n.a.	n.a.	n.a.	n.a.	n.a.	n.a.	n.a.	0.01 (±29.35)
(DA2xDA3)xVI2_2	20.94 (±23.68)	0.31 (±24.88)	267.40 (±21.69)	0.02 (±105.32)	0.03 (±141.42)	n.a.	0.55 (±21.12)	n.a.	n.a.	n.a.	25.30 (±22.06)
VI1xDA1_3	0.34 (±11.30)	0.17 (±5.93)	1.18 (±2.77)	0.18 (±4.76)	n.a.	n.a.	n.a.	n.a.	n.a.	n.a.	0.003 (±34.28)
(DA2xDA3)xVI2_3	17.49 (±16.36)	0.17 (±71.41)	226.38 (±16.63)	n.a.	0.03 (±141.42)	n.a.	0.30 (±11.41)	n.a.	n.a.	n.a.	17.04 (±13.36)
DA4	10.64 (±7.73)	0.14 (±71.00)	136.71 (±3.13)	0.16 (±9.28)	n.a.	n.a.	0.08 (±40.85)	n.a.	n.a.	n.a.	5.53 (±8.27)
AL2xPE1_1	5.60 (±16.34)	0.56 (±19.18)	9.22 (±13.45)	n.a.	22.58 (±8.33)	0.28 (±94.69)	78.36 (±9.22)	n.a.	0.49 (±14.43)	18.06 (±7.43)	0.26 (±12.38)
(HU1xPU1)xDA4_1	6.46 (±8.29)	0.21 (±10.88)	88.51 (±15.15)	0.002 (±141.42)	0.08 (±70.72)	n.a.	n.a.	n.a.	n.a.	n.a.	2.68 (±6.58)
VI1xDA1_9	8.80 (±6.11)	0.22 (±9.96)	92.56 (±6.19)	0.23 (±13.58)	n.a.	n.a.	n.a.	n.a.	n.a.	n.a.	0.17 (±3.53)
VI3_h	0.22 (±6.51)	0.20 (±3.11)	1.57 (±22.31)	n.a.	0.03 (±141.42)	n.a.	0.09 (±41.96)	n.a.	n.a.	n.a.	0.08 (±11.60)
VI1xDA1_2	0.01 (±141.42)	0.16 (±2.47)	0.61 (±12.90)	n.a.	n.a.	n.a.	n.a.	n.a.	n.a.	n.a.	n.a.
PE1	2.13 (±5.02)	0.72 (±4.80)	7.82 (±12.18)	n.a.	25.06 (±7.05)	0.07 (±141.42)	118.27 (±3.55)	1.18 (±4.07)	18.04 (±11.10)	14.56 (±3.86)	n.a.
VI4	n.a.	0.18 (±7.72)	0.28 (±2.30)	n.a.	0.03 (±141.42)	n.a.	n.a.	n.a.	n.a.	n.a.	2.04 (±2.59)
VI1xDA1_8	2.15 (±5.72)	0.17 (±3.43)	7.81 (±5.61)	n.a.	n.a.	n.a.	n.a.	n.a.	n.a.	n.a.	0.03 (±1.44)

Salix species or crosses	concentration [µmol/g] (RSD in %)										
	1	2	3	4	I	II	III	IV	V	VI	VII
(HU1xPU1)xDA4_2	8.10 (±13.38)	0.22 (±5.93)	105.66 (±12.71)	0.36 (±20.05)	n.a.	n.a.	n.a.	n.a.	n.a.	n.a.	0.06 (±16.92)
VI1xDA1_1	8.36 (±6.22)	0.24 (±12.88)	103.45 (±6.94)	n.a.	n.a.	n.a.	0.16 (±7.89)	n.a.	n.a.	n.a.	7.85 (±2.88)
VI1xDA1_7	0.00 (±0.00)	0.06 (±141.42)	0.13 (±28.42)	n.a.	n.a.	n.a.	n.a.	n.a.	n.a.	n.a.	n.a.
VI4xVI3_2	0.52 (±31.24)	0.20 (±3.63)	0.41 (±41.70)	n.a.	n.a.	n.a.	0.41 (±20.16)	n.a.	n.a.	0.08 (±58.02)	0.01 (±73.53)
(DA2xDA3)xVI2_5	13.00 (±7.76)	0.24 (±9.98)	134.56 (±8.97)	n.a.	0.05 (±141.42)	n.a.	0.13 (±9.35)	n.a.	n.a.	n.a.	6.29 (±8.34)
DA2xDA3	27.08 (±10.06)	0.23 (±11.83)	151.53 (±8.17)	n.a.	n.a.	n.a.	0.16 (±6.00)	n.a.	n.a.	n.a.	11.63 (±5.02)
DA1	13.70 (±4.31)	0.25 (±7.18)	134.36 (±5.36)	n.a.	0.09 (±74.50)	n.a.	n.a.	n.a.	n.a.	n.a.	14.45 (±7.32)
AL2	3.53 (±12.22)	0.21 (±18.31)	22.10 (±12.45)	n.a.	0.50 (±4.62)	n.a.	8.12 (±14.37)	n.a.	n.a.	0.08 (±18.57)	0.37 (±16.02)
(HU1xPU1)xDA4_3	12.90 (±13.54)	0.34 (±10.68)	117.50 (±13.43)	0.02 (±101.61)	0.13 (±33.67)	n.a.	0.14 (±56.49)	n.a.	n.a.	0.004 (±141.42)	14.24 (±8.92)
AL1_h	1.92 (±13.55)	0.28 (±18.32)	17.94 (±11.26)	n.a.	1.05 (±16.55)	n.a.	17.90 (±6.48)	n.a.	n.a.	2.15 (±5.80)	3.47 (±6.62)
HU1xPU1	5.38 (±3.72)	0.18 (±6.97)	36.84 (±2.69)	n.a.	0.04 (±141.42)	n.a.	n.a.	n.a.	n.a.	n.a.	0.86 (±5.59)
VI1xDA1_4	0.60 (±13.41)	0.19 (±3.67)	1.35 (±12.88)	n.a.	n.a.	n.a.	n.a.	n.a.	n.a.	n.a.	n.a.
AL2xAL1_1	5.86 (±7.51)	0.20 (±19.00)	32.48 (±6.48)	n.a.	0.12 (±5.47)	n.a.	1.44 (±9.55)	n.a.	n.a.	0.06 (±25.44)	0.47 (±10.64)
VI4xVI3_1	n.a.	0.17 (±7.13)	0.15 (±12.77)	n.a.	n.a.	n.a.	n.a.	n.a.	n.a.	n.a.	n.a.

Salix species or crosses	concentration [µmol/g] (RSD in %)										
	1	2	3	4	I	II	III	IV	V	VI	VII
AL2xPE1_2	5.56 (±5.42)	0.23 (±70.89)	9.15 (±4.23)	0.05 (±8.60)	6.95 (±1.29)	0.06 (±141.42)	60.03 (±0.84)	n.a.	2.09 (±4.80)	14.16 (±8.00)	0.88 (±6.07)
AL2xAL1_2	4.57 (±5.68)	0.26 (±3.22)	28.86 (±3.46)	n.a.	0.83 (±33.87)	0.02 (±100.00)	10.11 (±1.92)	n.a.	n.a.	0.40 (±3.63)	0.48 (±1.68)
VI1xDA1_6	0.38 (±37.79)	0.11 (±70.71)	5.61 (±4.15)	n.a.	0.04 (±141.42)	n.a.	n.a.	n.a.	n.a.	n.a.	0.01 (±25.62)
(DA2xDA3)xVI2_1	12.03 (±5.10)	0.15 (±71.05)	143.16 (±4.30)	n.a.	0.05 (±141.42)	n.a.	0.49 (±6.35)	n.a.	n.a.	n.a.	14.28 (±6.20)
(DA2xDA3)xVI2_4	14.95 (±21.89)	0.32 (±15.98)	150.97 (±6.21)	n.a.	0.09 (±73.79)	n.a.	0.38 (±17.55)	n.a.	n.a.	n.a.	16.11 (±6.76)
VI1	3.86 (±17.67)	0.25 (±8.32)	13.34 (±9.63)	n.a.	0.04 (±141.42)	n.a.	n.a.	n.a.	n.a.	n.a.	0.08 (±24.07)
VI1xDA1_5	1.32 (±2.66)	0.19 (±7.54)	8.17 (±8.60)	n.a.	0.03 (±141.42)	n.a.	n.a.	n.a.	n.a.	n.a.	0.03 (±30.70)

Table A13: Quantifier and qualifier mass transitions (*m/z*, Da) of polyphenols. DP: declustering potential, CE: collision energy, and CXP: collision cell exit potential. Data obtained from Tina Schmittnägel (Chair of Food Chemistry and Molecular Sensory Science).

compound	Q1 mass [Da]	Q3 mass [Da]	DP [V]	EP [V]	CE [V]	CXP [V]
p-hydroxybenzaldehyde	120.9	92.0	-15	-10	-34	-13
	120.9	64.9	-15	-10	-32	-7
p-hydroxybenzoic acid	136.9	65.0	-20	-10	-40	-9
	136.9	75.0	-20	-10	-44	-11
	136.9	39.0	-20	-10	-50	-5
vanillin	150.9	136.0	-10	-10	-18	-15
	150.9	92.0	-10	-10	-26	-11
gentisic acid	152.9	107.9	-30	-10	-28	-13
	152.9	80.9	-30	-10	-24	-9
2,4-dihydroxybenzoic acid	152.9	109.0	-30	-10	-18	-13
	152.9	64.9	-30	-10	-22	-9
o-coumaric acid	162.9	92.9	-5	-10	-36	-11
	162.9	65.0	-5	-10	-46	-9
p-coumaric acid	162.9	116.9	-35	-10	-42	-13
	162.9	92.0	-35	-10	-50	-11
vanillic acid	166.9	151.9	-25	-10	-18	-17
	166.9	107.9	-25	-10	-26	-13
gallic acid	168.9	69.0	-55	-10	-28	-9
	168.9	51.1	-55	-10	-40	-7
caffeic acid	178.9	134.5	-45	-10	-32	-15
	178.9	107.0	-45	-10	-30	-11
dihydrocaffeic acid	181.0	108.9	-50	-10	-20	-13
	181.0	59.0	-50	-10	-20	-9
methyl gallate	182.9	123.9	-50	-10	-28	-13
	182.9	77.9	-50	-10	-40	-11
ethyl p-coumarate	191.0	118.0	-50	-10	-24	-13
	191.0	161.9	-50	-10	-20	-17
ferulic acid	192.9	134.0	-25	-10	-22	-15
	192.9	177.9	-25	-10	-16	-21
syringic acid	196.9	181.9	-25	-10	-18	-19
	196.9	94.9	-25	-10	-38	-11
ethyl gallate	196.9	167.9	-75	-10	-20	-19
	196.9	105.9	-75	-10	-38	-11
sinapinaldehyde	207.0	191.9	-25	-10	-18	-21
	207.0	148.9	-25	-10	-32	-15
ethyl caffeate	207.0	177.9	-75	-10	-22	-21
	207.0	89.0	-75	-10	-58	-13
ethyl ferulate	221.0	206.0	-25	-10	-20	-19
	221.0	133.0	-25	-10	-34	-9
sinapinic acid	223.0	208.0	-25	-10	-18	-19
	223.0	164.0	-25	-10	-20	-17
(*E*)-resveratrol	227.0	185.0	-105	-10	-26	-17
	227.0	143.0	-105	-10	-34	-17
(*Z*)-resveratrol	227.0	185.1	-20	-10	-24	-9
	227.0	143.0	-20	-10	-32	-33
oxyresveratrol	243.0	225.1	-90	-10	-20	-25
	243.0	175.0	-90	-10	-24	-1
(*E*)-piceatannol	243.1	158.8	-105	-10	-34	-17
	243.1	173.0	-105	-10	-32	-21
(*E*)-pterostilbene	255.0	239.9	-70	-10	-26	-15
	255.0	168.9	-70	-10	-50	-17
	255.0	223.9	-70	-10	-38	-21
genistein	268.8	132.8	-10	-10	-36	-13
	268.8	224.2	-10	-10	-34	-27
apigenin	269.0	117.0	-110	-10	-44	-13
	269.0	149.0	-110	-10	-32	-17
naringenin	270.8	151.2	-35	-10	-24	-17
	270.8	119.0	-35	-10	-34	-11
luteolin	284.9	133.1	-15	-10	-44	-7
	284.9	151.0	-15	-10	-36	-21
	284.9	175.0	-15	-10	-36	-11

compound	Q1 mass [Da]	Q3 mass [Da]	DP [V]	EP [V]	CE [V]	CXP [V]
kaempferol	284.9	187.0	-130	-10	-38	-21
	284.9	117.0	-130	-10	-52	-13
eriodictyol	287.0	135.0	-30	-10	-34	-15
	287.0	64.9	-30	-10	-52	-29
(+)-catechin	289.0	205.0	-105	-10	-24	-23
	289.0	108.9	-105	-10	-32	-13
	289.0	122.9	-105	-10	-38	-15
(-)-epicatechin	289.0	205.0	-115	-10	-24	-15
	289.0	108.9	-115	-10	-32	-13
ellagic acid	300.9	283.9	-155	-10	-40	-31
	300.9	144.9	-155	-10	-50	-17
quercetin	300.9	150.9	-95	-10	-28	-17
	300.9	178.9	-95	-10	-24	-13
(+-)-hesperetin	301.0	286.0	-30	-10	-24	-25
	301.0	135.9	-30	-10	-38	-23
(+)-taxifolin	303.0	285.0	-50	-10	-16	-25
	303.0	125.0	-50	-10	-26	-13
(-)-epigallocatechin	305.0	124.9	-70	-10	-28	-13
	305.0	167.0	-70	-10	-26	-15
(-)-gallocatechin	305.0	124.9	-45	-10	-28	-15
	305.0	167.0	-45	-10	-26	-13
isorhamnetin	314.9	299.9	-45	-10	-30	-33
	314.9	150.9	-45	-10	-38	-17
myricetin	316.9	150.9	-110	-10	-30	-15
	316.9	136.9	-110	-10	-32	-19
syringetin	345.0	314.9	-90	-10	-34	-35
	345.0	286.9	-90	-10	-44	-33
chlorogenic acid	353.0	93.0	-35	-10	-56	-11
	353.0	135.0	-35	-10	-44	-19
astringin	405.0	242.9	-145	-10	-26	-21
	405.0	159.0	-145	-10	-60	-9
	405.0	200.9	-145	-10	-48	-17
(-)-epicatechin gallate	440.9	168.8	-70	-10	-22	-7
	440.9	289.1	-70	-10	-24	-23
(-)-catechin gallate	441.0	168.9	-40	-10	-24	-11
	441.0	124.9	-40	-10	-52	-13
kaempferol-3-*O*-glucoside	447.0	283.9	-125	-10	-36	-33
	447.0	227.0	-125	-10	-58	-25
quercitrin	447.0	300.9	-95	-10	-30	-35
	447.0	271.0	-95	-10	-54	-23
(-)-gallocatechin gallate	456.9	168.8	-5	-10	-20	-11
	456.9	125.0	-5	-10	-54	-11
	456.9	124.5	-5	-10	-80	-11
(-)-epigallocatechin gallate	456.9	168.9	-55	-10	-22	-13
	456.9	125.0	-55	-10	-54	-13
quercetin-3-*O*-glucoside	462.9	301.0	-110	-10	-30	-35
	462.9	254.9	-110	-10	-54	-29
quercetin-3-*O*-galactoside	463.0	299.9	-60	-10	-36	-35
	463.0	270.9	-60	-10	-56	-31
taxifolin-3-*O*-glucoside	465.0	282.9	-110	-10	-18	-21
	465.0	180.9	-110	-10	-14	-15
	465.0	136.9	-110	-10	-20	-19
quercetin-3-*O*-glucuronide	476.9	178.9	-85	-10	-42	-17
	476.9	121.0	-85	-10	-56	-13
isorhamnetin-3-*O*-glucoside	477.0	270.9	-10	-10	-50	-31
	477.0	285.0	-10	-10	-48	-33
myricetin-3-*O*-glucoside	479.0	270.7	-195	-10	-50	-27
	479.0	259.0	-195	-10	-64	-29
syringetin-3-*O*-glucoside	507.0	272.9	-135	-10	-48	-31
	507.0	300.9	-135	-10	-48	-35
procyanidin A1	574.9	449.1	-160	-10	-30	-17
	574.9	284.9	-160	-10	-32	-33
	574.9	288.9	-160	-10	-30	-35
procyanidin A1	574.9	449.1	-160	-10	-30	-17
	574.9	284.9	-160	-10	-32	-33
	574.9	288.9	-160	-10	-30	-35

compound	Q1 mass [Da]	Q3 mass [Da]	DP [V]	EP [V]	CE [V]	CXP [V]
procyanidin A2	574.9	284.9	-155	-10	-36	-33
	574.9	449.0	-155	-10	-28	-15
procyanidin B3	576.9	425.0	-45	-10	-22	-27
	576.9	288.9	-45	-10	-34	-25
procyanidin B1	577.0	288.9	-65	-10	-32	-33
	577.0	407.0	-65	-10	-30	-15
procyanidin B2	577.0	407.0	-55	-10	-30	-15
	577.0	289.0	-55	-10	-32	-31
rutin	609.0	299.9	-175	-10	-50	-33
	609.0	270.9	-175	-10	-68	-31
procyanidin C1	865.1	407.0	-210	-10	-52	-13
	865.1	288.9	-210	-10	-50	-33
picein	296.9	134.9	-5	-10	-16	-9
	296.9	92.0	-5	-10	-72	-7
eriodictyol-7-glycoside	449.0	286.7	-120	-10	-26	-49
	449.0	150.9	-120	-10	-36	-17